

Carbon dynamics resulting from paddy management  
under different climatic conditions in different soil types

Dissertation  
zur Erlangung des Doktorgrades  
der Mathematisch-Naturwissenschaftlichen Fakultät  
der Christian-Albrechts-Universität  
zu Kiel

Vorgelegt von  
Erwin Prastowo

Kiel, 2018

Erstachter Gutachter : Prof. Dr. Ingmar Unkel  
Zweiter Gutachter : Prof. Dr. Hans-Rudolf Bork  
Tag der mündlichen Prüfung : 19.10.2018  
Zum Druck genehmigt : 19.10.2018

---

Gez. Prof. Dr. rer. nat. Frank Kempken, Dekan

## Acknowledgements

It's my honor to engrave this acknowledgement to convey my gratefulness to persons who have helped me through this research work.

I am deeply grateful to Prof. P. M. Grootes, who has provided me the opportunity to do my PhD at the Institute for Ecosystem Research, Kiel University. His advice, guidance, immense knowledge, and care shown throughout the course of the project are so appreciated.

I would like also to express my gratitude and special thanks to Prof. Ingmar Unkel, my academic supervisor, for his advice, guidance, motivation, enthusiasm, care and immense knowledge throughout PhD works.

Furthermore, I would like to thank the German Research Foundation (DFG) for financial support of the Research Initiative FOR 995. I would like to acknowledge Prof. Hans-Rudolf Bork, as the second reviewer of this thesis, for help and support, the Director of Indonesian Coffee and Cocoa Research Institute and Dr. Sri Rahayu Utami who supporting me to do my PhD at the University of Kiel.

Also, I would like to extend my sincere thanks to all of you who provided me part of scientific data, foremost Prof. Marie-José Nadeau, and Dr. Angelika Kölbl. I would like also to thank Prof. Wiebke Kirleis for providing me some facilities in her Laboratory. A special thanks goes to Dr. Pauline Winkler for sharing her data.

I would like to thank to Dr. habil Stefan Dreibrodt for laboratory guidance and knowledge-sharing, Britta Witt for administrative issues, and Sophia Dazert, Markus Schütz and Mathias Bahns for laboratory assistance. I would like to acknowledge Svetlana Khamnueva, Clemens von Scheffer, Thomas Birndorfer, and Joana Seguin for constructive discussions during the Environmental History and Archives group meeting.

Last, but not least, my special thanks to my wife, friend, and colleague, Rina Arimarsetiowati, for everything she sacrificed. Her constant support have enabled me to obtain this degree. She inspired me to move forward by her encouragement and extreme patience.

And finally, I am so grateful to both my parent for their unconditional love, blessing, inspiration, moral support and prayer during my study.

Any omission from this list is only overlooked, and it does not constitute a lack of gratitude.

# Table of contents

Table of contents .....	I
List of Tables .....	V
List of Figures .....	VI
Summary.....	VIII
Zusammenfassung .....	IX
1. Introduction .....	1
1.1. Soil radiocarbon ( <sup>14</sup> C) dynamics .....	3
1.1.1. Origin of radiocarbon in the soil .....	3
1.1.2. Depth distribution of <sup>14</sup> C in the soil column .....	4
1.2. Study of carbon dynamics in the soil using <sup>14</sup> C as a natural tracer .....	5
1.2.1. Principle of <sup>14</sup> C dating of soil organic carbon .....	5
1.2.2. <sup>14</sup> C as a tracer in soil carbon studies .....	7
1.3. Humic substances and age heterogeneity of organic carbon.....	8
1.4. Characteristics of paddy soils.....	9
2. Materials and methods .....	11
2.1. Site description .....	11
2.1.1. Sampling year 2012.....	12
2.1.1.1. Site 1 - Ploso Lor, Ngawi, East Java .....	12
2.1.1.2. Site 2 - Jasinga, Bogor, West Java .....	13
2.1.1.3. Site 3 - Perbawati, Sukabumi, West Java .....	13
2.1.2. Sampling year 2016.....	16
2.1.2.1. Site 1 - Randusongo, Ngawi, East Java .....	16
2.1.2.2. Site 2 - Gerih, Ngawi, East Java .....	16
2.1.2.3. Site 3 - Pojok, Ngawi, East Java .....	16
2.1.2.4. Site 4 - Danguk, Ngawi, East Java .....	17
2.1.2.5. Site 5 - Ploso Lor, Ngawi, East Java .....	17
2.1.2.6. Site 6 - Bobol, Bojonegoro, East Java .....	17
2.2. Soil sampling .....	18
2.3. Sample preparation .....	23
2.3.1. Wet sieving.....	23
2.3.2. Acid-alkali-acid (AAA) treatment .....	24
2.3.3. Ultrasonication.....	25
2.4. Sample analysis .....	30
2.4.1. Grain size analysis .....	30
2.4.2. X-ray fluorescence (XRF) .....	31
2.4.3. Total, organic, and inorganic carbon and nitrogen.....	32

2.4.4. $^{13}\text{C}$ solid state nuclear magnetic resonance ( $^{13}\text{C}$ -NMR).....	33
2.4.5. Accelerator mass spectrometry (AMS) .....	34
2.4.5.1. Sample pre-treatment .....	35
2.4.5.2. Preparation of graphite targets .....	35
2.4.5.3. $^{14}\text{C}$ AMS measurement (system at NTNU, Trondheim, Norway) .....	36
2.4.5.4. Calculation of $^{14}\text{C}$ data .....	37
2.4.5.5. Correction for isotopic fractionation .....	39
2.4.5.6. Correction for background.....	39
2.4.5.7. Measurement uncertainty .....	40
2.4.5.8. Calculation of the conventional radiocarbon age and the calendar age.....	40
3. Characteristics of tropical soils in the research area .....	42
3.1. Grain size distribution .....	42
3.2. Soil reaction (pH) and alkalinity (EC).....	46
3.3. Elemental compositions.....	48
3.4. Organic matter characteristics.....	52
Conclusions .....	58
4. Origins, distributions and isotopic compositions of soil organic carbon .....	59
4.1. Litter carbon inputs.....	60
4.1.1. Amount of litter input.....	60
4.1.2. Litter $^{14}\text{C}$ content.....	65
4.2. Depth distribution of total organic carbon .....	66
4.3. Carbon isotopic compositions ( $\delta^{13}\text{C}$ and $^{14}\text{C}$ ).....	69
4.3.1. Depth distribution of $\delta^{13}\text{C}$ .....	69
4.3.2. Depth distribution of $^{14}\text{C}$ .....	72
4.3.2.1. $^{14}\text{C}$ in different soil types .....	72
4.3.2.2. $^{14}\text{C}$ in the bulk and organic fractions .....	78
4.3.2.3. $^{14}\text{C}$ in the particle size fractions.....	80
Conclusions .....	83
5. Modelling carbon dynamics in agriculture soil in different soil types under different climate conditions .....	85
5.1. Introduction .....	85
5.2. Model formulation .....	86
5.2.1. Soil organic carbon transformation .....	86
5.2.1.1. Carbon inputs ( $C_{(i)}$ ) .....	86
5.2.1.2. Carbon decomposition ( $C_{(o)}$ ) .....	88
5.2.2. Depth-transport of soil organic carbon .....	95
5.2.3. Conceptual model .....	96
5.3. Finite element method .....	97
5.4. Model validation .....	102

5.5. Result and discussion .....	102
5.5.1. TOC-model ( $TOC_M$ ) .....	103
5.5.2. Radiocarbon-model ( $R_M$ ) .....	107
5.6. Conclusions .....	107
6. Synthesis .....	109
6.1. Field variability controls of soil organic carbon dynamics .....	109
6.2. Plant litter control to carbon refreshments .....	111
Conclusions .....	111
References.....	113
Appendix 2.1. Farm questionnaires .....	i
Appendix 2.2. Distribution of P, $E_o$ and $E_{To}$ in some research areas .....	viii
Appendix 2.3. Soil profile descriptions of 2016 field campaign.....	ix
Appendix 2.4. Weight proportion of concretions .....	xx
Appendix 2.5. Some important mineral content in concretions .....	xxi
Appendix 2.6. Mineral enrichment in PL samples .....	xxii
Appendix 2.7. Elemental composition of some soil inorganic fractions from point samples .....	xxiii
Appendix 2.8. Elemental composition of 2012 bulk soil samples .....	xxiv
Appendix 3.1. Grain size composition, TOC (%), pH ( $H_2O$ ) and EC of point samples .....	xxvii
Appendix 3.2. Data from analysis of bulk samples used for PCA (excl. EC) .....	xxxiii
Appendix 3.3. Data used for principal component analysis .....	xxxvii
Appendix 3.4. $^{13}C$ NMR integral of samples .....	xxxviii
Appendix 4.1. Model of depth distribution of litter .....	xl
Appendix 4.2. Total organic carbon content according to landuse.....	xli
Appendix 4.3. TOC and TIC (%) in Vertisol (PL) .....	xlii
Appendix 4.4. Radiocarbon content according to landuses. ....	xliii
Appendix 4.5. Plant remains collected from soil profiles. ....	xlvi
Appendix 4.6. TOC, TON, $\Delta^{14}C$ , and $\delta^{13}C$ content of selected bulk soil, humic, fulvic, and conc. HCl extracted samples (only for PL samples).....	xlviii

Appendix 5.1. Model litter distribution in the soil columns. ....	liii
Appendix 5.2. Temperature sensitivity coefficient. ....	liv
Appendix 5.3. Soil moisture sensitivity coefficient. ....	lv
Appendix 5.4. Soil oxygen coefficient. ....	lvi
Appendix 5.5. Soil carbon storage coefficient. ....	lvii
Appendix 5.6. Soil carbon transformation-PL. ....	lviii
Appendix 5.7. Soil carbon transformation-PBW. ....	lix
Appendix 5.8. Soil carbon transformation-JSG. ....	lx
Appendix 5.9. FEM modelling MATLAB script. ....	lxi

## List of Tables

Table. 2.1. General information of research area of 2012 field campaign.....	12
Table. 2.2. General information of research area of 2016 field campaign.....	17
Table. 3.1. Loadings of first two principal components grain size compositions .....	44
Table. 3.2. Coefficient of variation (%) of depth soil texture, pH, EC and elemental compositions in the soil columns.....	47
Table. 3.3. Loadings of first three principal components elemental compositions, TOC, TON, and pH .....	49
Table. 3.4. Integral of the <sup>13</sup> C NMR chemical shift regions of humic.....	54
Table. 3.5. Loadings of first four principal components of grain size composition, TOC, TON, and chemical structures and molecular composition of humic .....	57
Table. 4.1. Characteristics of e-folding depth of root distribution at different soil profiles (D = interval depth) .....	62
Table. 4.2. Carbon turnover time in different landuses .....	64
Table. 4.3. Organic carbon content and isotopic composition of collected macrofossils at different depths.....	66
Table. 4.4. Organic carbon and isotopic composition in the soil particle size fractions.....	81
Table. 5.1. General parameters used in model.....	90
Table. 5.2. Specific parameters used in model .....	91
Table. 5.3. The efficiency of model (EF).....	102
Table. 5.4. Estimated parameter of models .....	103

## List of Figures

Figure. 1.1. Radiocarbon, $^{14}\text{C}$ , production and distribution into the soil.....	4
Figure. 1.2. (a) World map of atmospheric bomb $^{14}\text{C}$ zones; (b) Summer atmospheric $^{14}\text{C}$ curves for different zones (Hua et al., 2013).....	6
Figure. 2.1. Map of research areas (a) relative global positions (b) Cixi, China (c) Perbawati-Sukabumi and Jasinga-Bogor, West Java, and (d) Ploso Lor-Ngawi, East Java, Indonesia, with display of geological and topographical conditions in c) and d). .....	14
Figure. 2.2. Soil profiles from the 2012 and 2016 field campaigns in Ploso Lor, PL.....	19
Figure. 2.3. Soil profiles from the 2012 field campaign in Jasinga, JSG .....	20
Figure. 2.4. Soil profiles from the 2012 field campaign in Perbawati, PBW .....	20
Figure. 2.5. Soil profiles from the 2016 field campaign in Randusongo, Rds .....	21
Figure. 2.6. Soil profiles from the 2016 field campaign in Gerih, Grh .....	21
Figure. 2.7. Soil profiles from the 2016 field campaign in Pojok, Pjk .....	22
Figure. 2.8. Soil profiles from the 2016 field campaign in Danguk, Dgk.....	22
Figure. 2.9. Soil profiles from the 2016 field campaign in Bobol, Bbl.....	23
Figure. 2.10. Regression of calculated $P_o$ and displayed $P_e$ after simulation.....	27
Figure. 2.11. Soil particle sedimentation of JSG-Alisol sample .....	29
Figure. 2.12. The illustration of XRF Niton XL3t ( <a href="https://www.dal.ca/">https://www.dal.ca/</a> ) .....	32
Figure. 2.13. Layout of the AMS system in NTNU laboratory, Trondheim (Klein et al., 2006).....	37
Figure. 3.1. Loadings of 6 classes soil fractions defined by PC1 and PC2. Data set from point samples (Appendix 3.1). Markers with dotted and solid border are topsoil (< 30 cm depth) and subsoil (>30 cm depth) .....	43
Figure. 3.2. Loadings of elemental compositions, TOC, TON, and pH ( $\text{H}_2\text{O}$ ) defined by PC1 and PC2 (a), PC1 and PC3 (b), and PC2 and PC3 (c). Markers with white and black border are top soils (0-25 cm depth), and subsoils (below 25 cm depth). Data set from bulk samples with removing the outliers (Appendix 3.2). .....	51
Figure. 3.3. Solid state $^{13}\text{C}$ nuclear magnetic resonance spectra of top soil humic samples of P and NP. ....	53
Figure. 3.4. Loadings of grain size composition, TOC, TON, and chemical structures and molecular composition of the top soil humic defined by factor 1 and factor 2 (a), factor 1 and factor 3 (b), and factor 1 and factor 4. Data set from point samples (Appendix 3.3). .....	55
Figure. 3.5. Predicted molecular compositions of organic carbon from top soil humic samples (ca. 20 cm depth) of P and NP.....	56
Figure. 4.1. Some collected subsoil plant remains for $^{14}\text{C}$ dating, i.e. (a) and (b), leaves and dark roots from PBW-P and -NP; (c) and (d), leaves and dark-light roots from JSG-P and -NP; (e) and (f), light leaf fragments and dark roots from PL-P and -NP. ....	60

Figure. 4.2. Normalized carbon concentrations of plant remains collected from 2 cm thick layers in PL, JSG, and PBW as a function of depth, with an exponential curve defining its depth-distribution, and organic carbon content of the soils. ....	63
Figure. 4.3. Total bulk organic carbon in relation to $\Delta^{14}\text{C}$ (sample 2012). The vertical dotted lines indicate an atmospheric $\Delta^{14}\text{CO}_2$ level in 2012 ( $\sim 31\text{‰}$ ). ....	68
Figure. 4.4. The signals of $\delta^{13}\text{C}$ in relation to $\Delta^{14}\text{C}$ in the soil layers. Grey and green shading represents $\delta^{13}\text{C}$ range for $\text{C}_3$ and $\text{C}_4$ crop types according to Ehleringer (1991). Vertical dotted lines indicate atmospheric level of $\Delta^{14}\text{CO}_2$ in 2012 ( $\sim 31\text{‰}$ ) and in 2016 ( $\sim 9\text{‰}$ ) (Hammer and Levin, 2017; Levin et al., 2013). ....	71
Figure. 4.5. Depth distribution of TOC and $\delta^{13}\text{C}$ obtained from bulk, humic (hmc), humin (hmn), and conc. HCl extracted (only for PL) 2012 samples. Open marks in PL-NP represent samples from the garden plot. Grey and green shading represents $\delta^{13}\text{C}$ range for $\text{C}_3$ and $\text{C}_4$ crop types according to Ehleringer (1991). ....	73
Figure. 4.6. Depth distribution of $\Delta^{14}\text{C}$ and $\delta^{13}\text{C}$ obtained from humic (hmc) and humin (hmn) 2016 samples. Grey and green shading represents $\delta^{13}\text{C}$ range for $\text{C}_3$ and $\text{C}_4$ crop types according to Ehleringer (1991). Horizontal dotted lines indicate atmospheric level of $\Delta^{14}\text{CO}_2$ in 2016 ( $\sim 9\text{‰}$ ) (Hammer and Levin, 2017; Levin et al., 2013). ....	74
Figure. 4.7. Depth distribution of TOC and $\Delta^{14}\text{C}$ obtained from bulk, humic (hmc), humin (hmn), and conc. HCl extracted (only for PL) samples. Open marks in PL-NP represent samples from the garden plot. Horizontal dotted lines indicate atmospheric level of $\Delta^{14}\text{CO}_2$ in 2012 ( $\sim 31\text{‰}$ ) (Hammer and Levin, 2017; Levin et al., 2013). ....	76
Figure. 5.1. Conceptual of soil carbon dynamics model (1a = topsoil litter at $z=0$ cm depth; 1b = subsoil litter at $z=20$ cm depth; 2 = desorption; 3 = adsorption; 4a = lateral diffusion; 4b = vertical diffusion; 5a = lateral convection; 5b = vertical convection; (i) = organic carbon transformation, (ii) = organic carbon transport). ....	95
Figure. 5.2. Simulated depth distribution of TOC and organic fractions in different soil types and crop managements (Obs: data measured, Bulk: total organic fractions, FOM: active fractions, IOM: passive fractions, SOM: slow fractions). ....	104
Figure. 5.3. Simulated depth distribution of $^{14}\text{C}$ activity in different soil types and crop managements. ....	106
Figure. 6.1. Field variability controls the dynamics of soil carbon in the study areas .....	110

## Summary

In the global carbon cycle, soil carbon may play an important role to control the balance among different reservoirs as the climate issues may have been a big concern nowadays. In the smaller scale in the soil, carbon affects many processes, e.g. physics, chemistry, biology, and pedology that constantly occurred in the soils. Study of soil carbon dynamics was performed to reveal the effect of crop management practices, i.e. crop types, annual crop rotations, in combination with different environmental conditions, i.e. topography, hydrology, and climate condition, and to evaluate the  $^{14}\text{C}$  concentration and residence time of carbon in different organic matter and soil mineral fractions of different tropical soil types (Andosol, Alisol, Vertisol, Regosol, Cambisol, Fluvisol). Totally 17 sites were selected under both P and NP. Profile observations were made in each soil types in 8 different sites, i.e. PBW, Jasinga (JSG), Ploso lor (PL), Randusongo (Rds), Gerih (Grh), Pojok (Pjk), Danguk (Dgk) and Bobol (Bbl), and samples were taken at small interval depth, i.e. 2-3 samples per horizons, with excluding the top layers (0-20 cm depth). Identified plant remains at depth was collected for carbon dating. The  $^{14}\text{C}$ -AMS together with  $\delta^{13}\text{C}$  signatures were used as natural tracer to study depth carbon dynamics together with routine soil analysis to understand the important soil processes that occurred in specific area. The depth distributions of  $^{14}\text{C}$  demonstrate a typical decreasing concentrations with depths except in PBW profile. Similar to total organic carbon distribution, the less gradient  $^{14}\text{C}$  depth in the PL profiles suggests a subsoil carbon enrichment may be existed. Profiles of JSG show the most regularity of  $^{14}\text{C}$  depth distributions as a result of homogeneity profile compositions. Conversely, PBW profiles show the most irregularity of  $^{14}\text{C}$  depth distributions which is attributable to the variety in the parent material origins, and carbon contamination from different atmospheric origins. It is suggested that field variability, i.e. profile layer compositions, play an important role in controlling the carbon distribution at depth. The inconsistent variation of  $^{14}\text{C}$  content in different fractions (bulk, humic, humin, clay) suggested as the results from both difference in the depth interval of samples, and efficiency of extractants in relation to the different the organo-mineral complexation mechanism posed in different soil types. Carbon enrichment in the humin, suggested as due to acid-alkali-insoluble fine organic remains, showed to happen in NP sites of both PL and JSG. The higher  $^{14}\text{C}$  concentration associated with high quantity of plant residues imply an important role of crop managements (crop types, annual crop rotations) to the refreshment of soil carbon. Clay fractions regardless layer depth do not always associate with older carbon. Clay fractions extracted from subsoils shows consistently older than from the top clays. The radiocarbon dating of clay samples may show the association with humin, with slight variety over different soil types. In this study, no clear trends were observed between soil size fractions and  $^{14}\text{C}$  content as possibly the result of the variety of carbon compositions in relation to specific fractions. A model was attempted to explain the depth-distribution of total organic carbon, and  $^{14}\text{C}$  with transport parameters, i.e. diffusion  $D$  and convection  $v$ , vary among different soil types indicating a different mechanisms responsible for the movement of subsoil carbon. However, the application of this model may be limited to homogeneous soil columns.

## Zusammenfassung

In der Bilanz der unterschiedlichen Reservoirs des globalen Kohlenstoffkreislaufs kann Bodenkohlenstoff eine wichtige Rolle spielen und damit in den aktuell Besorgnis erregenden Klimaprozessen. Auf kleinerer Skala, insbesondere im Boden, beeinflusst Kohlenstoff viele physische, chemische, biologische und pedologische Prozesse, die dort ablaufen. Vorliegende Studie untersucht die Dynamik des Kohlenstoffs im Boden, um die Auswirkung verschiedener landwirtschaftlicher Anbaumethoden (z.B. Pflanzentyp und Fruchtwechsel) im Zusammenhang mit unterschiedlichen Umweltbedingungen wie Topographie, Hydrologie und Klima zu beschreiben. Ferner wird anhand des  $^{14}\text{C}$ -Gehalts die Verweildauer des Kohlenstoffs in organischen Substanzen und in (organo-)mineralischen Bodenfraktionen in sechs verschiedenen tropischen Bodentypen (Andosol, Alisol, Vertisol, Regosol, Cambisol, und Fluvisol) untersucht. Insgesamt wurden 17 Profile, je zur Hälfte unter Reisanbau (P) und ohne Reisanbau (NP), an 8 Standorten für die Untersuchungen ausgewählt: Perbawati (PBW), Jasinga (JSG), Ploso Lor (PL), Randusogno (Rds), Gerih (GrH), Pojok (Pjk), Danguk (Dgk) und Bobol (Bbl). Mit Ausnahme des Oberbodens (je nach Boden etwa die obersten 20 cm) wurden in jedem Bodenhorizont des Unterbodens 2-3 Proben in geringen Abständen entnommen. Identifizierbare Pflanzenreste im Unterboden wurden zur  $^{14}\text{C}$ -Datierung gesammelt. Der über Beschleunigermassenspektrometrie (AMS) bestimmte  $^{14}\text{C}$ -Gehalt und die  $\delta^{13}\text{C}$  Signatur wurden als natürlicher Tracer benutzt, um der Kohlenstoffdynamik im Unterboden nachzugehen und, in Kombination mit standardmäßigen Bodenanalysen, daraus ein besseres Verständnis der lokal wichtigen Bodenprozesse zu gewinnen. Der  $^{14}\text{C}$ -Gehalt des organischen Bodenmaterials nimmt mit zunehmender Tiefe generell ab, mit Ausnahme des Perbawati Profils (PBW). Sowohl die Verteilung des organischen Gesamtkohlenstoffgehalts (TOC) als auch der niedrigere  $^{14}\text{C}$ -Tiefengradient in den Profilen von Ploso Lor (PL) deuten auf eine Anreicherung von Kohlenstoff im Unterboden hin. Die Jasinga Profile (JSG) zeigen aufgrund des insgesamt sehr homogenen Bodenprofils die gleichmäßigste  $^{14}\text{C}$ -Verteilung über die Tiefe. Die Perbawati Profile (PBW) hingegen zeigen die stärksten Unregelmäßigkeiten in der  $^{14}\text{C}$ -Tiefenverteilung. Dies ist wahrscheinlich der Variabilität des Ausgangsmaterials sowie Kohlenstoffkontamination mit unterschiedlicher atmosphärischer Herkunft zuzuschreiben. Es gibt Hinweise, dass die Variabilität im Gelände, d.h. die Zusammensetzung der Bodenhorizonte, eine wichtige Rolle bei der Kohlenstoffverteilung im Unterboden spielt. Die Streuung der  $^{14}\text{C}$ -Gehalte in unterschiedlichen Fraktionen (Gesamtkohlenstoff, Humine, Huminsäure, Ton) resultiert möglicherweise sowohl aus Unterschieden in den Beprobungsintervallen, 2-cm versus Gesamtschichtproben, als auch aus einer unterschiedlichen Effizienz der chemischen Extraktion der organo-mineralen Komplexe aus den verschiedenen Bodentypen. Kohlenstoffanreicherung in der Huminfraction, möglicherweise als feine, in Säure und Lauge unlösliche organische Reste, wurde in den NP Profilen von Ploso Lor and Jasinga gefunden. Der Zusammenhang zwischen einer höheren  $^{14}\text{C}$  Konzentration und einer höheren Zahl an Pflanzenresten deutet auf eine wichtige Rolle der Anbauplanung (Pflanzenart und jährliche Fruchtwechsel) bei der Erneuerung des organischen Bodenkohlenstoffs hin. Die Tonfraktion enthält, unabhängig von der Tiefe, nicht immer den älteren Kohlenstoff. Der Kohlenstoff im mit Säure und Lauge extrahierten Ton im Unterboden datiert konsistent älter als der mit Ton assoziierte Kohlenstoff im Oberboden. Die  $^{14}\text{C}$ -Datierung von Tonproben deutet auf eine Huminfraction mit geringen Variationen zwischen unterschiedlichen Bodentypen hin. In vorliegender Studie wurde kein klarer Zusammenhang zwischen KorngröÙefraction und  $^{14}\text{C}$ -Gehalt gefunden, möglicherweise wegen der großen Variabilität der organischen Zusammensetzung in den unterschiedlichen Fraktionen. Es wurde ein Modell zur Erklärung der Tiefenverteilung des gesamten organischen Kohlenstoffs und der  $^{14}\text{C}$  Transportparameter herangezogen. Die Diffusion  $D$  und Konvektion  $v$  variieren zwischen unterschiedlichen Bodentypen, dies deutet auf verschiedene Mechanismen hin, die für den Kohlenstoff im Unterboden verantwortlich sind. Das Modell muss zunächst jedoch auf homogene Böden beschränkt angewendet werden.



# Chapter 1

## 1. Introduction

In the global carbon cycle, the variety in abundance and composition of soil carbon affects many processes (Batjes, 1996), i.e. the agronomic yield and use efficiency of added input, for instance fertilizer, irrigation water, and so on (Lal, 2011), CO<sub>2</sub> emissions (Davidson et al., 2000; Schlesinger and Andrews, 2000), and silicate weathering (Goudie and Viles, 2012). Soil is an important reservoir for carbon and soil carbon cycling, can act either as a source or a sink of atmospheric CO<sub>2</sub> (Lal, 2004), that is highly dependent on landuse (Detwiler, 1986), crop management, e.g. soil tillage, crop rotation (Wood and Edwards, 1992), and climate change (Davidson and Janssens, 2006). Furthermore, soil carbon accounts for 2 - 3 times the amount in the atmosphere, i.e. 1500-2000 PgC in the top meter (Houghton, 2007), which gives rise to concern with respect to feedback to a global warming (Houghton et al., 1998).

In this study, the attention was given to subsoil carbon. The subsoil is characterized by providing ca. 60% of the total carbon stocked in the soil column, and typically increasing <sup>14</sup>C ages with depth, as a result of the increase in the microbial inaccessibility of carbon associated with organomineral complexes and the limited supply of fresh carbon from the top. Nevertheless, subsoil carbon is likely to be refreshed by young carbon (Baisden and Parfitt, 2007; Gleixner, 2013; Rethemeyer et al., 2004a; Rumpel and Kögel-Knabner, 2011). Carbon inputs, in the context of origin and composition, and soil processes are both dynamic and varying across environmental conditions, such as parent material, topography, hydrology, and climate, and the extent to which their variations influence subsoil carbon is not clear yet. Furthermore, the specific conditions created in the paddy soils due to alternating drying-flooding (section 1.4) give rise to speculations about their effect on subsoil carbon dynamics. Paddy management effects on mineral and element transformations, and pedogenesis have been confirmed widely (Kögel-Knabner et al., 2010; Kölbl et al., 2014; Nishimura et al., 2008; Nishio et al., 1994; Ono, 1989; Wassmann et al., 2000), yet some results indicated that their effect may be mainly limited to the top layers (Bräuer et al., 2013b; Wissing et al., 2014).

As an open system, soil organic matter receives new carbon through photosynthesis and organism death, and removes older carbon via microbial decomposition (Schoor et al., 2016a). Therefore, soil organic carbon defines the wide range of timescales from minutes to millennia which is difficult to quantify. Radiocarbon provides a tool to determine this dynamics of carbon in spite of the complexity of soil system (section 1.2). The use of <sup>14</sup>C enables us to trace carbon mobility through soil components, e.g. organomineral complexes (Anderson and Paul, 1984), organic matter fractions (Bräuer et al., 2013a, 2013b), dissolved organic carbon (Gandois et al., 2014; Hagedorn et al., 2015), soil respiration (Gaudinski et al., 2000), and microbial metabolism (Rethemeyer et al., 2004a). While  $\delta^{13}\text{C}$  may provide additional information of plant material origins (Balesdent et al., 1990, 1987; Nissenbaum and Schallinger, 1974). So an elaborate interpretation of these carbon isotope signals in combination with an understanding of soil processes may elucidate the dynamics of soil carbon.

The study was part of Research Unit FOR995, “Biogeochemistry of Paddy Soil Evolution” supported by the Deutsche Forschungsgemeinschaft (DFG, the German Research Foundation). The research project aimed at documenting the effect of soil redox conditions over long periods on the evolution of soil mineralogy and soil organic matter properties and their interactions during pedogenesis. The program brought together the expertise of working groups with different background to jointly elaborate research outcomes and derive new insights by applying new analytical techniques. After a first phase in China, the project decided on Indonesia as research area for the second phase. Indonesia, one of the main rice producers in the world, offers areas with a variety of (volcanic) soil types, subject to different tropical climatic regions, for comparison with the Chinese subtropical results.

The main objective of this study was:

- a) To reconstruct carbon dynamics in different tropical subsoils under different crop management practices, i.e. crop types, annual crop rotations, and environmental conditions, i.e. topography, hydrology, and climate. Due to the high field variabilities, a direct comparison of factors, like soil type, crop management, and environmental conditions, to quantify their effects on carbon dynamics is not possible statistically. Therefore, field observations in combination with laboratory analysis were used to elucidate the carbon dynamics in the soil columns due to the influence of research factors.
- b) To study the dynamics and infiltrations of  $^{14}\text{C}$  through different soil organic matter fractions, i.e. humic and humin, and mineral fractions, i.e. sands, silts, and clay.

## 1.1. Soil radiocarbon ( $^{14}\text{C}$ ) dynamics

### 1.1.1. Origin of radiocarbon in the soil

Carbon atoms occur in three distinct isotope forms,  $^{12}\text{C}$ ,  $^{13}\text{C}$ , and  $^{14}\text{C}$ , which account for, respectively, 99%, 1%, and only one part in million million of modern carbon (Bowman, 1990). These carbon isotopes are chemically similar but differ physically due to a different number of neutrons in the nucleus (6, 7, and 8 for  $^{12}\text{C}$ ,  $^{13}\text{C}$ , and  $^{14}\text{C}$ , respectively). The mass difference among carbon isotopes brings about differences in reaction rates and bond strength (Schuur et al., 2016b), that provide fractionation in chemical and physical processes and result in a variability of their distribution in different carbon compounds. The stable carbon isotopes,  $^{12}\text{C}$  and  $^{13}\text{C}$  are neither produced nor decay, just fractionated. The radioactive  $^{14}\text{C}$  is, in addition, produced in the atmosphere, distributed, and decays over time (Gillespie, 1984; Goh, 1991; Trumbore, 2009).

Radiocarbon is cosmogenic (Fig. 1.1), i.e. generated in the atmosphere by cosmic radiation, mainly in the lower stratosphere (Taylor and Bar-Yosef, 2014). The cosmic rays with high-energy charged particles, hydrogen ( $^1_1\text{H}$ ) and helium ( $^4_2\text{He}$ ) nuclei, are deflected by the magnetic fields of sun and earth. They collide with the nuclei of atmospheric gas molecules to produce spallation products, including energetic free neutrons ( $n$ ) that, furthermore, lose their energy due to collisions with atmospheric particles. Reaction of a slow (thermal) neutron with a nitrogen nucleus,  $^{14}_7\text{N}$ , produces  $^{14}_6\text{C}$  while liberating a proton ( $p$ ).



Via hydroxyl radicals, OH, in the atmosphere, the atoms of  $^{14}\text{C}$  will be converted to  $^{14}\text{CO}$ , and additionally to  $^{14}\text{CO}_2$ . Ultimately,  $^{14}\text{CO}_2$  is distributed throughout the earth's atmosphere by winds. Radiocarbon decays with a half-life  $5730 \pm 40$  years (Godwin, 1962) by releasing a negatively charged beta particle/electron ( $\beta^-$ ) and an electron antineutrino ( $\bar{\nu}_e$ ).



Radiocarbon decays continuously, but its concentration in plant tissue only starts to decrease when it no longer takes part in terrestrial-atmosphere carbon exchange (is "dead"). As long as there is exchange, the deficit of  $^{14}\text{C}$  atoms will be compensated by the supply of new  $^{14}\text{C}$  atoms, continuously created in the upper atmosphere.

The cycle of carbon in the soil starts from plant photosynthesis to fix atmospheric  $\text{CO}_2$  (Craig, 1953). Subsequently, it plays a role in many physiological processes, i.e. respiration/energy, growth, reproduction, and maintenance of fungal symbionts (Schuur et al., 2016b). Active plants liberate some carbon into the rhizosphere through root exudates, i.e. rhizodeposition (Kuz'yakov and Domanski, 2000). Further carbon is delivered to the soil system through the decay of their anatomical parts, i.e. shoots or roots, after plants are dead.

During litter decomposition, microbes assimilate/resynthesize fresh/old carbon to support their growth with higher efficiency for easily decomposable compounds, e.g. amino acids, carbohydrates, and proteins, and lower for recalcitrant materials, e.g. lignin, plant-derived lipids, and so on. When the microbes are dead, assimilated carbon is released back into soil,

and with stabilization may occur as attachment on the surface of clay minerals, i.e. organomineral complexation or physical protection within fine pores (Mikutta et al., 2006). The remaining soluble and non-stabilized carbon may be subject to recycling and leaching.

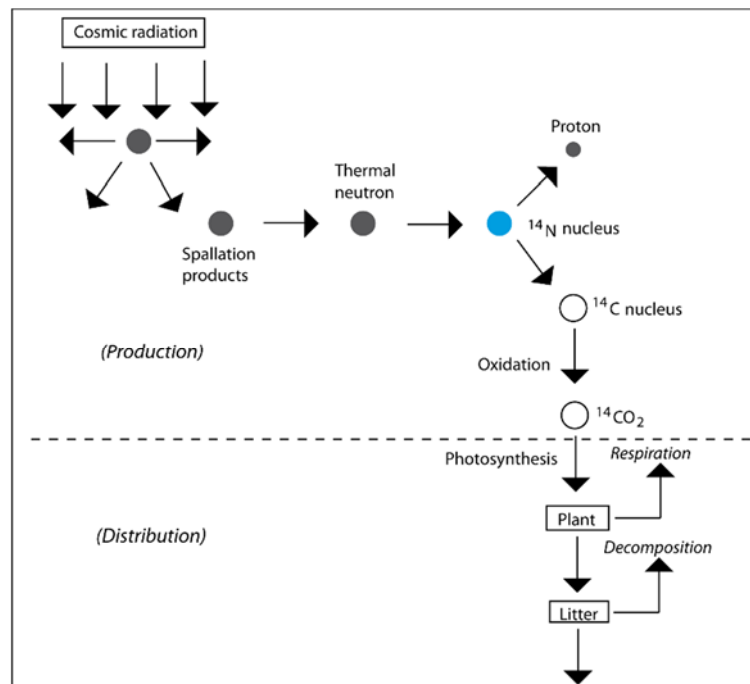


Figure. 1.1. Radiocarbon,  $^{14}\text{C}$ , production and distribution into the soil.<sup>1</sup>

### 1.1.2. Depth distribution of $^{14}\text{C}$ in the soil column

$^{14}\text{C}$  can be introduced into the subsoil column through several processes, e.g. directly in plant roots (Baisden and Parfitt, 2007; Bräuer et al., 2013a), and released exudates from roots (Hütsch et al., 2002; Pausch et al., 2013), and as dissolved organic matter moving down the soil column (Gandois et al., 2014; Hagedorn et al., 2015). The introduction of young carbon into the subsoil may be observed in the consistently higher  $^{14}\text{C}$  content in the humic fraction than in the humin samples from depth (Rethemeyer et al., 2005).

Soil organisms, i.e. earthworms, termites, ants, and arthropods (Rumpel and Kögel-Knabner, 2011) may play a role in getting carbon into soil depth, by the so-called bioturbation. This is a random process, by which carbon transport comes with the random motion of soil organisms and microbial biomass. As microbes use carbon for energy, their preferences for carbon sources are independent of soil depth (Kramer and Gleixner, 2008; Rethemeyer et al., 2005, 2004b).

A response of carbon mobility to pedogenic processes may depend on the specific soil types. For instance, in high-smectitic soils, i.e. Vertisol, the process called pedoturbation may play a role in the context of subsoil carbon re-distribution. In such soils, the active seasonal shrinkage during dry seasons and swelling during wet seasons, mix carbon from the top down, following material fallen from the top and the wall of cracks, and carbon from the subsoil up, as the swelling soil expands (Birkeland, 1999). Prominent cracks with highly variable dimensions were obviously observed on the surface after shrinking (Bandyopadhyay et al., 2003). This

<sup>1</sup> Modified from Taylor and Bar-Yosef, 2014

way, fresh plant residues from the top can be transported down immediately (Bräuer et al., 2013a).

## 1.2. Study of carbon dynamics in the soil using $^{14}\text{C}$ as a natural tracer

### 1.2.1. Principle of $^{14}\text{C}$ dating of soil organic carbon

The application of the carbon isotopes  $^{14}\text{C}$ , for soil organic matter studies rests basically on its distinctive character providing a natural “clock” (Bowman, 1990; Gillespie, 1984; Taylor and Bar-Yosef, 2014). Being radioactive, the percentage decrease in the number of  $^{14}\text{C}$  atoms per unit time is constant for all carbon-holding materials. If the concentrations of  $^{14}\text{C}$  both at initial time,  $t_0$ , and after elapsed time,  $t_1$ , are known and designated  $^{14}\text{C}_0$  and  $^{14}\text{C}_1$ , respectively, the decay time  $t_1 - t_0$  can be calculated from the exponential decay law, provided we have a closed system. The decay of  $^{14}\text{C}$  is a first-order reaction. Applying a decay constant ( $\lambda$ ) to relate concentration of  $^{14}\text{C}$  and elapsed time ( $t$ ).

$$\frac{\partial C}{\partial t} = -\lambda C \quad (1.3)$$

The above differential equation, (1.3), can be solved analytically resulting in the following formula:

$$C(t) = e^{-\lambda t + c} \quad (1.4)$$

The constant ( $c$ ) can be obtained by assuming that at initial condition,  $t=0$ , the concentration of  $^{14}\text{C}$  is  $C_0$ . Then the equation becomes:

$$\begin{aligned} C(t) &= C(0)e^{-\lambda t} \\ C(t) &= C_0 e^{-\lambda t} \end{aligned} \quad (1.5)$$

Where  $C(t)$  is the number of  $^{14}\text{C}$  atoms remaining after time  $t$  (yr),  $C_0$  is the initial number of  $^{14}\text{C}$  atoms, and  $\lambda$  is decay constant ( $\text{yr}^{-1}$ ) which corresponds to the mean-life ( $\tau$ ), having a negative sign means a decay process. In radiocarbon dating, the term  $\lambda$  is related to the half-life ( $T_{1/2}$ ) via the equation below (Bowman, 1990):

$$T_{1/2} = 0.693\tau \quad (1.6)$$

The accepted value for the half-life of radiocarbon,  $T_{1/2}$ , is  $5730 \pm 40$  years (Godwin, 1962), but so-called “conventional radiocarbon ages” are calculated with the Libby half-life of 5568 years, which is 2.83% smaller (Stuiver and Polach, 1977). To calculate a radiocarbon age  $t$ :

$$\begin{aligned} t &= -\frac{1}{\lambda} \ln\left(\frac{C(t)}{C_0}\right) \\ t &= -8033 \ln\left(\frac{C(t)}{C_0}\right) \end{aligned} \quad (1.7)$$

In the formula above,  $t$  is the radiocarbon age;  $C(t)$  is the measured  $^{14}\text{C}/^{12}\text{C}$  ratio of the sample; while  $C_0$  is its original ratio at  $t_0$ . Since  $C_0$  cannot be measured directly, it is assumed that  $C_0$  corresponded with the atmospheric  $^{14}\text{C}$  concentration at  $t_0$  and a standard “modern atmosphere” has been defined having a  $^{14}\text{C}$  concentration 95% of that of the oxalic acid standard (Ox I) in 1950. Due to carbon isotope fractionation (Craig, 1953), and variation in  $^{14}\text{CO}_2$  atmospheric levels (Gillespie, 1984), the subsequent correction of isotope fractionation and calendar years calibration are needed (section 2.4.5).

For radiocarbon dating several general assumptions have to be met before a measured  $^{14}\text{C}$  concentration  $C(t)$  can be translated into an age  $t$ , namely:

1. The production of  $^{14}\text{C}$  has been constant for more than  $10^5$  years.
2. The carbon exchange between the carbon reservoirs (atmosphere, biosphere, and ocean) is rapid compared to the half-life of  $^{14}\text{C}$ , and the reservoirs are well-mixed.
3. Carbon isotope ratios in samples are in equilibrium with their surrounding before the carbon exchange ceases.
4. After the death of the organisms or deposition of carbonates no carbon exchange takes place (closed system-assumption).
5.  $^{14}\text{C}$  decays at a constant rate, not influenced by its chemical or physical surroundings.

Human activities temporarily significantly increased atmospheric  $^{14}\text{C}$  production, violating assumption no. 1. For soil carbon studies assumptions no. 2 and no. 3 are not relevant. Soils are, however, open systems violating the assumptions no. 4. The last assumption, no. 5, is valid. Therefore, this makes it difficult to define a meaningful soil carbon age by measuring the  $^{14}\text{C}$  concentration of the mixture of organic compounds that typically makes up a soil carbon sample.

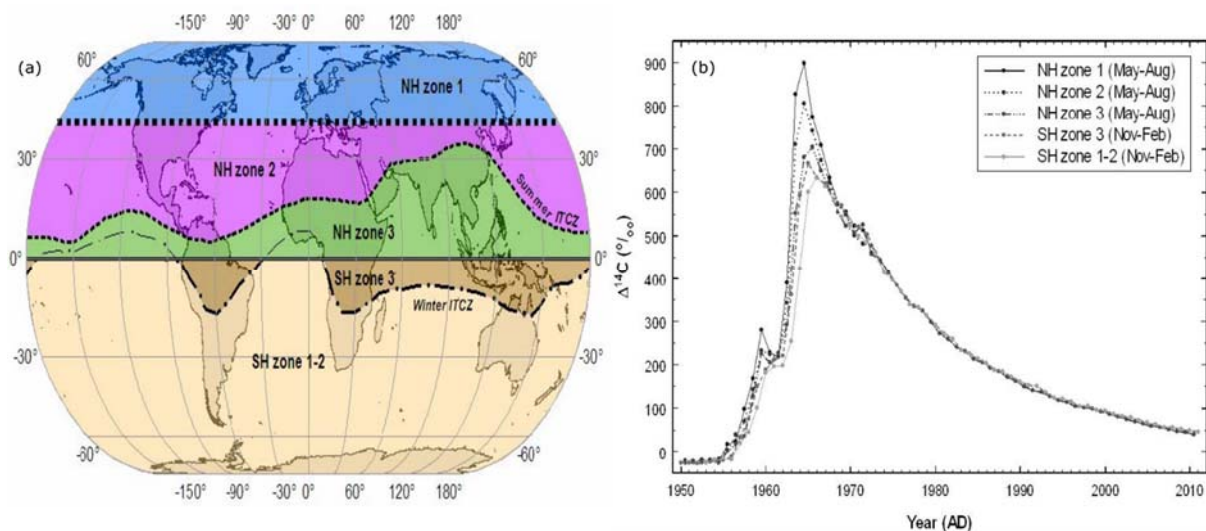


Figure. 1.2. (a) World map of atmospheric bomb  $^{14}\text{C}$  zones; (b) Summer atmospheric  $^{14}\text{C}$  curves for different zones (Hua et al., 2013).

The amount of  $^{14}\text{C}$  added into the soil through plant photosynthesis changed over time following the atmospheric  $^{14}\text{CO}_2$  level (Fig. 1.2). Since there is isotope fractionation during plant photosynthesis (Craig, 1953), the original  $^{14}\text{C}$  concentration would be slightly different in plant-derived organic residues (Trumbore et al., 2016), but never higher than that of

atmospheric CO<sub>2</sub> of the same year. The effect of human activity on the atmospheric <sup>14</sup>C level has been recognized in the industrial or Suess effect (Bowman, 1990; Suess, 1965), and the Bomb effect (Hua et al., 2013; Reimer et al., 2004). The first effect occurs since around 1850 as result the burning of fossil fuels, i.e. coal, oil, and natural gas, containing no <sup>14</sup>C. The mixture of <sup>14</sup>C-free fossil-derived CO<sub>2</sub> with the natural level of <sup>14</sup>CO<sub>2</sub> results in a depressed <sup>14</sup>C/<sup>12</sup>C ratio. The second effect has been observed from 1955 onwards (Fig. 1.2), when thermonuclear weapons tests released large amounts of <sup>14</sup>C to the atmosphere which resulted in an increase in the <sup>14</sup>C/<sup>12</sup>C ratio. Between 1955 and 1963, when the atmospheric test ban treaty was signed, the level of atmospheric <sup>14</sup>CO<sub>2</sub> and, thus, of <sup>14</sup>C distributed to the terrestrial environment almost doubled reaching the maximum at ca. 200 pMC in late summer 1963. Since then the atmospheric <sup>14</sup>C concentrations are gradually decreasing through exchange with and uptake by the ocean and the biosphere and the continued use of fossil fuel.

### 1.2.2. <sup>14</sup>C as a tracer in soil carbon studies

The use of <sup>14</sup>C as a dating tool is extensive in archaeology (Bowman, 1990; Gillespie, 1984; Taylor and Bar-Yosef, 2014). Although its potential for dating is limited in soil science, it is a useful tracer tool in the context of soil organic matter study (Schuur et al., 2016a; Trumbore, 2009). Radiocarbon enables us to trace the mobility of carbon atoms from the atmosphere through different organic matter fractions and soil minerals (Anderson and Paul, 1984; Rethemeyer et al., 2004a; Torn et al., 1997; Wang et al., 1996), with a few to thousand years turnover times (Harrison et al., 1993). In this respect the atmospheric bomb <sup>14</sup>C spike is especially useful.

Models of soil organic matter dynamics usually take into account three different fractions according to their turnover times (Schuur et al., 2016a), (i) decomposable/fast/active pools, with a 1-2 years residence time (ii) structural/intermediate/passive pools, with decadal-scale residence time, and (iii) a resistant/slow pool, exhibiting hundreds to thousands of years residence time. Therefore, a single turnover time of a bulk soil sample is obviously inadequate. To extract information on soil organic matter fractions, they need to be isolated by chemical or physical approaches. The chemical preparation includes the simple acid-alkali-acid treatment (section 2.3.2), commonly used in radiocarbon dating (Goh, 1991; Grootes et al., 2004). Physical fractionation based on particle size (section 2.3.3), is one approach to study organomineral complexes (Christensen, 2001; Morra et al., 1991; Schmidt et al., 1999).

To study turnover times of soil organic carbon, either on bulk or on fractionated samples, two different time-scales are used. The first is based on natural atmospheric <sup>14</sup>C that reflects the slow turnover of organic matter, stabilized by soil matrix or chemical soil processes, and resides in the soils long enough for radioactive decay to occur. The natural <sup>14</sup>C age, equal to an “apparent mean residence time” of carbon under steady state conditions, presumes a closed, homogeneous organic pool with a single decay rate. The second uses the so-called “bomb <sup>14</sup>C” disequilibrium, derived from atmospheric testing of nuclear weapons back in the late 1950s, early 1960s. The bomb <sup>14</sup>C method is an advanced tool to study fast cycling organic carbon on time scales of years to decades. Like natural <sup>14</sup>C, bomb <sup>14</sup>C enters soil organic matter through plant residues that were formed in equilibrium with the contemporaneous atmospheric <sup>14</sup>CO<sub>2</sub>. The measured <sup>14</sup>C concentration of the soil carbon or soil fraction is thus the weighted average of the year-by-year inputs, each with its individual <sup>14</sup>C concentration,

remaining in the carbon pool at the time of sampling. The calculation of true carbon turnover times thus requires extensive input modelling. The availability of archived pre-bomb- $^{14}\text{C}$  soil samples, which directly document the incorporation into soil organic matter over a certain period (Bowman, 1990; Gillespie, 1984; Schuur et al., 2016a; Trumbore, 2009) is thereby helpful. Although bomb  $^{14}\text{C}$  thus makes it difficult to quantify turnover times, it amplifies the  $^{14}\text{C}$  differences between different organic compounds and fractions, and provides a valuable tracer to study input and soil carbon processes.

### 1.3. Humic substances and age heterogeneity of organic carbon

Organic carbon pools in the soil consist of living organisms, organic residues (undecayed and partially decayed) and humus (Essington, 2005). Humus is always designated as soil organic matter, and discussed in this section. In a modern concept, humus can be distinguished, based on its complexity, as humic substances (HS) and non-humic substances (nHS) (Saiz-Jimenez, 1996; Stevenson, 1994). The first designates the component of soil humus resulting from incomplete mineralization (Zech et al., 1997), which is slowly decomposable, less preferable for microbial degradation, has a macromolecular size, undergoes chemical structure modifications, and has already lost chemical characteristics of its precursors (Hayes and Himes, 1986; Saiz-Jimenez, 1996; Wilson et al., 1986). HS are transformed substances consisting of large/complex structures with high molecular weight, and highly heterogeneous molecules (MacCarthy, 2001). The nHS represent more identifiable chemical structures, and low molecular weights, e.g. amino acids, carbohydrates, fats, waxes, resins, and low molecular weight organic acids (Tipping, 2004). The two groups are not easily separated since humus may bind covalently some carbohydrates, and contain most of the biochemical compound synthesized by soil organisms (Stevenson, 1994).

In the radiocarbon dating protocol, humic substances collected during pre-treatment of samples are part of decontaminations prior to analysis (Goh, 1991; Grootes, 1977; Grootes et al., 2004). They are separated based on their solubility in water into three fractions. The first comprises both alkali- and acid-soluble fulvic acids, the second alkali-soluble and acid-insoluble humic acids, and the third both alkali- and acid-insoluble humic substances, the residue of alkali humin (Essington, 2005). Humic acids and humin are associated with the solid part of soils, while fulvic acids are more mobile soil components. In the humin fraction, humic acids bound to clay minerals can also be present (Stevenson, 1994). The separation of these organic fractions by acid-alkali-acid treatment will be discussed along with sample preparation (section 2.3.2).

The isolation of organic samples into different fractions makes it possible to trace the amount of  $^{14}\text{C}$  infiltration (Trumbore et al., 1989). Furthermore, to investigate soil carbon heterogeneity, one can compare  $^{14}\text{C}$  content of bulk samples with that of physically or chemically separated organic sample fractions (Schuur et al., 2016a). The level of heterogeneity of organic samples is highly dependent on the dominant carbon in existence. As for example from a previous study, a high-level of old carbon contaminants, in an industrial environment, may influence typical modern top soil carbon to exhibit a strong old carbon signal (Rethemeyer et al., 2004a).

#### 1.4. Characteristics of paddy soils

Wetlands, of which paddy soils are an important agriculture example, often present alternating anoxic-oxic conditions as result of seasonal crop rotations, i.e. artificial flooding during rice cultivation, and drained during non-rice. Oxic-anoxic alternation may change the original soil properties (Kögel-Knabner et al., 2010), as a result of some processes, mainly in the surface layer, for instance decalcification and mineral transformations (Kölbl et al., 2014; Winkler et al., 2016; Wissing et al., 2013), and organic carbon accumulation (Wissing et al., 2011).

During rice growing, the water infiltration may bring along carbon and minerals that potentially influence subsoil carbon. Dissolved organic matter, with a majority of fresh and modern carbon (Gandois et al., 2014; Kalbitz et al., 2003), may enrich older subsoil carbon depending on the hydraulic properties of the soil, i.e. soil texture, hydraulic conductivity, and the duration of submergence. The leaching of top soil carbon below the plough layer has been reported (Maie et al., 2004a). The translocation of minerals, for instance Fe, may result in the change of the carbon composition in the subsoil, as associated with organic matter stabilization (Kögel-Knabner et al., 2010). The increase in the total pedogenetic Fe oxides in the subsoil of a 50-yr paddy soil profile compared to the neighboring non paddy soil corresponded with the significant drop of carbon age (Bräuer et al., 2013b; Kölbl et al., 2014).

Paddy soils are widely postulated to accumulate organic matter in the top layers (Kögel-Knabner et al., 2010). The litter inputs exceed the decomposition rate under anoxic conditions (Reddy and DeLaune, 2008) with smaller free energy for the reactions (Kirk, 2004), which may be responsible for this accumulation. Subtropical paddy soils may have accumulated organic carbon (Wissing et al., 2011), yet tropical paddy soils were shown to produce less organic carbon in top layers compared to the nearby non paddy (Winkler et al., 2016). Their results pointed out that the initial organic carbon content and quantity of organic inputs should be taken into account.

To summarize this section, some points are presented as the main framework of this thesis as the following:

- The research aims at documenting the effect of soil redox conditions over long periods on the evolution of soil mineralogy and soil organic matter properties and their interactions during pedogenesis.
- The effect of management (P and NP, seasonal crop rotations), soil types (Vertisol, Alisol, Andosol, Regosol, Cambisol, Fluvisol), topography conditions (section 2.1), and climate on subsoil carbon and carbon dynamics will be evaluated.
- The highlights of organic inputs produced in each research site, as a result of different crop managements, are predicted through plant remains obtained from wet sieving (section 2.3.1), and with additional carbon dating for some deep samples to reveal their origins (section 4.1).
- The nature of soils (parent materials, and the important soil processes) are characterized, both vertically in the soil column and laterally in different sites, by analysis of grain size and elemental compositions (section 3.1; section 3.2), as well as other routine soil analyses, i.e. pH, EC, to provide a further guidance in understanding the dynamics of both total organic carbon and  $^{14}\text{C}$ .

- The influence of climate conditions is approached by the mineralization rate of top soil organic matter indicated from the majority of organic compound occurred (section 3.3).
- The carbon age in organic fractions (humic acid, humin) will be compared to that of bulk samples to see the level of heterogeneity.
- The origin of carbon in the context of plant materials and crop managements will be evaluated through the  $\delta^{13}\text{C}$  signal (section. 4.3.1).
- The association of carbon composition with size of soil particles will be studied by physical fractionation (section 2.3.3) to accomplish the chemical fractionation (humic acid, humin) of samples, prepared for radiocarbon dating. The carbon ages revealed in the fractions obtained from both techniques are compared to see the potential of similarity in terms of compositions. Radiocarbon and  $\delta^{13}\text{C}$  infiltrations through soil fractions will be evaluated.
- The observations will be complemented by testing a steady-state simple finite element model formulation. A single formula will attempt to explain organic carbon and  $^{14}\text{C}$  transformation (section 5.2.1), and their depth-distribution (section 5.2) in the specific soil types, considering: i) climate variables, i.e temperature and precipitation, ii) some important micro-environment variables to expose anoxic conditions, i.e. soil moisture and oxygen availability (section 5.1), iii) variation of litter quantity in the specific crop management (section 5.2.1.1), and iv) soil profile characteristics through transport parameters, i.e. diffusion and convection (section 5.2.2). obtained from both techniques are compared to see the potential of similarity in terms of compositions. Radiocarbon and  $\delta^{13}\text{C}$  infiltrations through soil fractions will be evaluated.
- The study will be improved by testing a climate variable, i.e temperature, and with incorporation of some important micro-environment variables to expose anoxic condition, i.e. soil moisture and oxygen availability (section 5.1); variation of litter quantity in the specific crop management (section 5.2.1.1); and with combination to soil profile characteristics through transport parameters, i.e. diffusion and convection (section 5.2.2), in a steady-state simple model formulation. A single formula will attempt to explain organic carbon and  $^{14}\text{C}$  transformation (section 5.2.1), and their depth-distribution (section 5.2) in the specific soil types.

## Chapter 2

### 2. Materials and methods

#### 2.1. Site description

This study was performed as part of Research Unit FOR 995, “Biogeochemistry of Paddy Soil Evolution” of the *Deutsche Forschungsgemeinschaft* (DFG, the German Research Foundation) carried out in China and Indonesia (Bräuer et al., 2013b; Kögel-Knabner et al., 2010). While reports of earlier studies in China have been published elsewhere e.g. Bräuer et al., (2013a), Bräuer et al (2013b), Kölbl et al., (2014), Wissing et al., (2011) and Wissing et al., (2013), this study will address tropical environments in Indonesia, aimed at generally improving the understanding of the cycling and storage of organic matter (OM) and the role of hydrologically and microbially mediated redox processes. The areas under study cover variations in soil parent materials, topography, climatic conditions and crop managements (Table 2.1; Table 2.2).

The multiple areas studied were located in West and East Java (Fig. 2.1). Sampling plots required that the typical existing developed soils must be in agreement with landscape and geomorphology conditions. Furthermore, different constraints were taken into account, i.e. duration and history of rice paddies with corresponding dry crops as the backgrounds, and the area likeness. Both paddy soils (P) and non-paddy soils (NP) plots were selected close each other to keep parent material heterogeneity at a minimum, taking into account the landscape similarity.

Two field campaigns were carried out in 2012 and 2016 by digging representative soil pits to perform a morphological observation of soil profiles and to sample corresponding soil layers (section 2.2). Three sites were chosen in the first campaign, i.e. Perbawati (PBW) and Jasinga (JSG) in West Java, and Ploso lor (PL) in East Java (section 2.1.1). In the latter campaign, additional sampling was intended to resolve some research questions raised after 2012 sample analysis results from the East Java sites became available. First, regarding the current snapshots of  $^{14}\text{C}$  profile in PL: Does fact that the organic carbon input in the  $\text{C}_4$  sugarcane plot, as NP site, (Table 2.1) is physiologically larger than in the neighbouring  $\text{C}_3$  rice paddies (Prastowo et al., 2017), contribute to the new  $^{14}\text{C}$  level in the soil columns?. Second, does the physiographical position of the Ngawi PL plots, in between volcanic Lawu and Kendeng ridge containing marine sediment (Fig. 2.1), determine the extent to which these two parent materials influence the existing mineral compositions as well as  $^{14}\text{C}$  in the soils?.

Therefore, the second field campaign in 2016 sampled at three different altitudes on both the Mt. Lawu, i.e. Randusongo (Rds), Gerih (Grh), and Pojok (Pjk), and the Kendeng ridge slopes, i.e. Danguk (Dgk), Ploso Lor garden plot (PLG), and Bobol (Bbl) (Fig. 2.1). The sites of which the altitude is highest at both Mt. Lawu and Kendeng ridge slope are presumably in close association with the origin of the soil materials, while the sites situated at the lowest altitudes, in the alluvial plain, may pose more heterogeneity of materials deposited from various origins. This approach also provides the background to identify the prominent source of sedimented minerals in the profiles.

The information dealing with agronomic practices, i.e. fertilizer, water irrigation, cropping rotation, disease protection, rice variety, and yields, as well as the history of land were obtained through direct interview with the farmowner in 2012 (Dieterich, 2012) and in 2016 (Appendix 2.1). The regional settings in the context of physical environment and crop management of the research areas of sampling year 2012 and 2016 will be discussed below.

### 2.1.1. Sampling year 2012

A joint sampling by the FOR 995 research group was carried out in February until March 2012 during the early stage of plant growth. The initial sampling organization covered three replications at both P and NP, i.e. mainsite at the centre, and subsite 1/subsite 2 from the immediate vicinity (Dieterich, 2012; Winkler et al., 2016), but for this study the samples were measured out only from one profile in each fieldcrop respectively, i.e. mainsite (P/NP) in PL, mainsite (P) and subsite 1 (NP) in JSG, and subsite 2 (P) and mainsite (NP) in PBW. The profile morphology and agronomic history of study areas has been discussed (Dieterich, 2012; Winkler et al., 2016). The additional important characteristics of the study sites will be discussed in the below subsections.

Table. 2.1. General information of research area of 2012 field campaign.

Site	Alt (m asl)	Parent material	Soil order	Prec (mm y <sup>-1</sup> )	T (°C) <sup>2</sup>	Annual crop rotation
PL-P	79	Alluvial-andesitic volcanic materials-marl	Vertisol	2756±1288	27 <sup>3</sup>	P-P-Tobacco
	80	Alluvial-andesitic volcanic materials-marl	Vertisol	2756±1288	27	Sugarcane
PL-NP						
JSG-P	240	Andesitic tuff	Alisol	2880±990	25.5 – 26	P-P-Maize
JSG-NP	236	Andesitic tuff	Alisol	2880±990	25.5 – 26	Cassava /Chili/Talas
PBW-P	871	Colluvial fan deposit, breccia	Andosol	3455±1170	20.4 – 21.8	P-P-Bok Choi
PBW-NP	981	Colluvial fan deposit, breccia	Andosol	3455±1170	20.4 – 21.8	Maize-Cassava

(with PL= Ploso Lor; JSG= Jasinga; PBW = Perbawati; P = paddy, NP = non paddy; Alt=Altitude; Prec = precipitation (mean±std); T = temperature).

#### 2.1.1.1. Site 1 - Ploso Lor, Ngawi, East Java

This site is situated on a stagnant old alluvial plain associated with quaternary and tertiary deposits. This area is bordered by the Kendeng ridge to the northeast and Madiun river to the southwest (Fig. 2.1). Physiographically, it is part of the longitudinal central depression zone of Java island (van Bemmelen, 1949). The alluvial plain lays over the Lidah formation which is claystone with local intercalations by sandstone and limestone, and with marl material of the Mundu formation underlying it (Fig. 2.1).

The alluvial materials originate from the ash deposits of nearby volcanoes (Mt. Lawu, Mt. Ngliman), and from the upper hills, i.e. Kendeng ridge, from which eroded materials are

<sup>2</sup> Source of climate data 2001 - 2010: Indonesian Agency for Meteorology, Climatology and Geophysics.

<sup>3</sup> Amien et al (1996).

transported down through small rivers, i.e. Bangon and Lusungwatu. A previous report has also confirmed Kendeng ridge as the most likely origin of parent materials to the soils developed in this area (Dames, 1955). He called it margalite soils to designate a soil, derived from limestones, marls and volcanic tuffs, with black-grey colour, loamy-heavy clay texture and a capacity to swelling and drying. The influence of volcanic-derived materials on the development and characteristics of soils in these areas has been reported through the finding of some andesitic-derived heavy minerals, i.e. hornblende, opaque, amphibole, augite, hypersthene, and andesine (Prasetyo, 2007; Prasetyo et al., 2007). The high alkalinity environment with soil pH (H<sub>2</sub>O) up to 8.5 (Fig. 2.2) has provided evidence of alkaline-derived materials.

The climate data show an annual wet-dry cycle with 4 consecutive dry months from June to September with < 60 mm precipitation (Appendix 2.2). During these months the average of evaporation as determined by pan experiments is 120 to 200 mm per month, which is higher than the average precipitation, ranging from 1 to 50 mm per month. Consequently, during those months, the more drought-tolerant crop tobacco substitutes for rice in the farms (Table 2.1). As wet months (precipitation > evaporation) occur between mid October and mid May, i.e. 7 months, all year-round (Appendix 2.2) this area is agroclimatically defined as subhumid (Juo and Franzluebbbers, 2003). The irrigation water is obtained through a pumping system from the shallow water-table at ca. 1.2 m depth.

#### 2.1.1.2. Site 2 - Jasinga, Bogor, West Java

Physiographically the area belongs to the Bogor Zone (van Bemmelen, 1949), which is an anticlinorium of strongly folded neogene strata with many intrusions of magma-derived rocks for instance hyp-abysal volcanic necks, stocks, and bosses. These complex belts extend from Rangkasbitung to the west to Bumiaju to the east in Central Java.

The soil is developed on terraced mid-slopes on the Bojongmanik formation of aged miocene, characterized by the presence of sandstone, pumiceous tuff, marl with molluscs, limestone, claystone with bituminous clay and lignite intercalations and resin fragments (Fig. 2.1). The presence of andesitic volcanic materials and glassy tuff were noticed in the profiles during field observation (Dieterich, 2012).

From the period of 2001 to 2010, dry months with precipitation < 60 mm regularly occur in July – September (Appendix 2.2) with a recorded longest period for two consecutive months in 2006. Yet, wet months with precipitation greater than the potential evapotranspiration happen throughout the year (Appendix 2.2), to allow for this area to be defined humid (Juo and Franzluebbbers, 2003). To support the rice farm with irrigation water, a canal irrigation has been established.

#### 2.1.1.3. Site 3 - Perbawati, Sukabumi, West Java

The area is situated on the southwest terraced upper-slopes of Gede volcano, which is physiographically a quaternary volcano (van Bemmelen, 1949). The soil has developed from a colluvial fan deposit (lahar) and tuffaceous breccia, mostly highly-weathered (Fig. 2.1). The fan deposit has more than 50 m thickness with an age older than ca. 43.500 yr BP pointed out from wood-incorporated dating (Belousov et al., 2015).

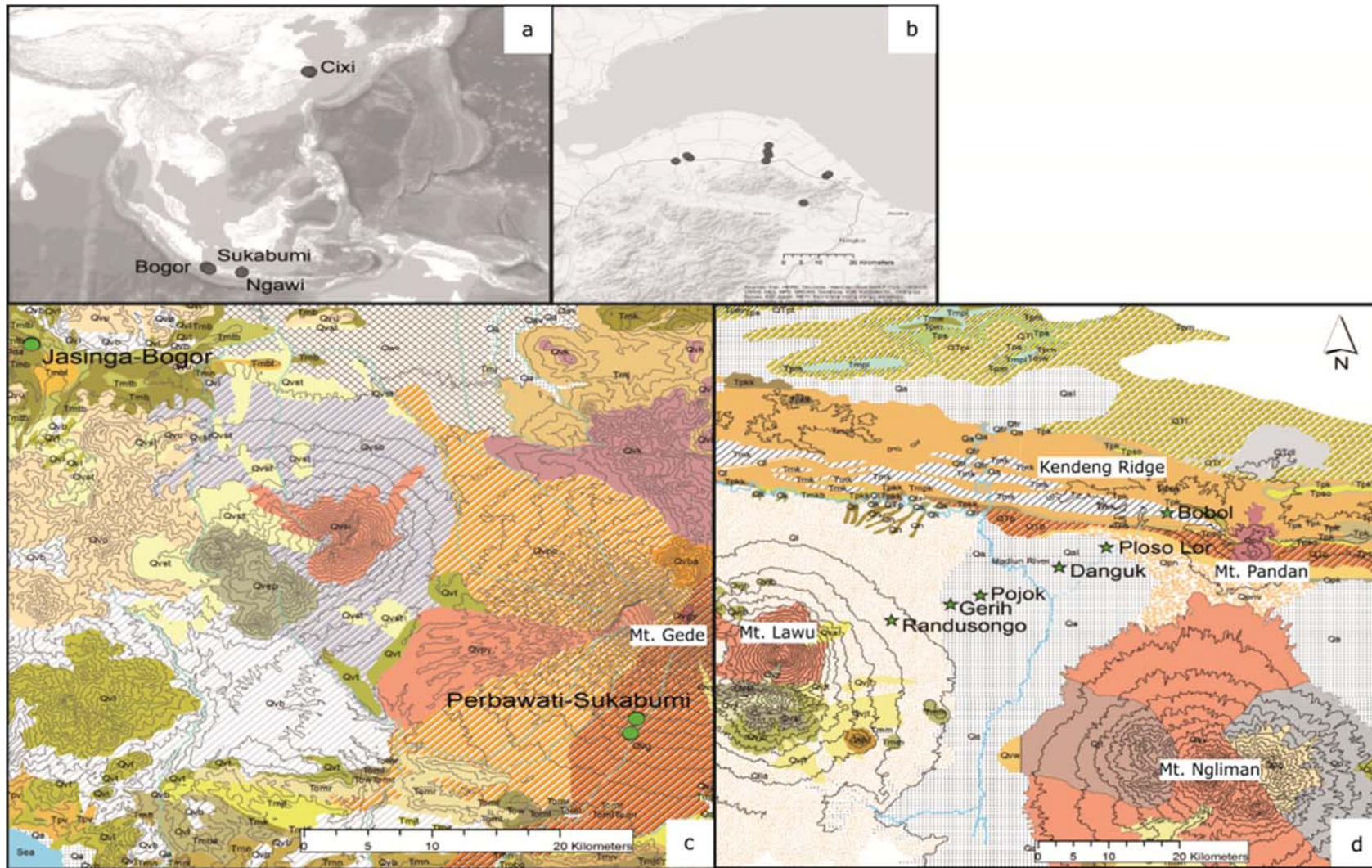


Figure. 2.1. Map of research areas (a) relative global positions (b) Cixi, China (c) Perbawati-Sukabumi and Jasinga-Bogor, West Java, and (d) Ploso Lor-Ngawi, East Java, Indonesia, with display of geological and topographical conditions in c) and d).

## Description of geology symbols<sup>4</sup> in Figure 2.1:

### (c) Sukabumi and Bogor, West Java

*Qa=Alluvium; Qav=Alluvium fans; Tmbe=Bentang formation; Tmn=Nyalindung formation; Tmnl=Limestone member of the Nyalindung formation; Tmle=Lengkong formation; Tmbo=Bojonglopang formation; Tmjv=Jampang formation; Tmjc=Cikarang member of Jampang formation; Tmjt=Tuff and Breccia member of Jampang formation; Tomr=Rajamandala formation; Toml=Limestone member of Rajamandala formation; Toba=Batuasih formation; Tow=Walat formation; Tmtb=Tuff and Breccia; Tmb=Bojongmanik formation; Tmbl=Limestone member of Bojongmanik formation; Tmcb=Breccia member of Cantayan formation; Tmk=Klapanunggal formation; Tmj=Jatiluhur formation; Qvep=Gunung Endut-Prabakti lava; Qvsl=lava flow, basaltic andesite with piroxene; Qvsb=lahar, tuffaceous breccia and lapili, basaltic andesite in composition, mostly strongly weathered; Qvst=sandy pumiceous tuff; Qvpy=younger deposits, andesite lahar; Qvpo=older deposits, lahar and lava, andesitic basalt with oligoclase-andesine labradorite, olivine, pyroxene, and hornblende; Qvgy=youngest lava flow; Qvg=tuffaceous breccia and lahar, andesite with oligoclase-andesine, pyroxene and abundant hornblende, trachytic texture, mostly high weathered; Qvgl=lava flow, basaltic andesite in composition; Qvba=basalt lava flow of Mt. Gegerbentang; Qvk=breccia and lava of Mt. Kencana and Mt. Limo; Qvu=undifferentiated volcanic rocks; Qvb=volcanic breccia; Qvl=volcanic lava; Qvt=tuff; Tpv=breccia, pumiceous tuff breccia, lava flows and tuffaceous sandstone; Tpb=breccia lava flow, tuffaceous sandstone and conglomerate, andesitic-basaltic in composition; a=andesite with oligoclase-andesine, augite, hypersthene, and hornblende; da=dacite, qd=quartz diorite; ha=hornblende andesite; dp=diorite porphy.*

### (d) Ngawi, East Java

*Qal=alluvium; Qpm=Notopuro formation; Qpv=Pandan breccia; Qia=intrusive rocks; Qpk=Kabuh formation; QTI=Lidah formation; QTP=Pucangan formation; QTdl=Dander member of Lidah formation; Tps=Selorejo formation; TpsO=Sonde formation; Tpk=Klitik formation; Tpm=Mundu formation; Tpp=Paciran formation; TpkA=Atasangin member of Kalibeng formation; Tmpk=Kalibeng formation; Tml=Ledok formation; Tmw=Wonoculu formation; Tmk=Kerek formation; Tmb=Bulu formation; Tmn=Ngrayong formation; Tmt=Tawun formation; Qa=Alluvial deposits; Qtr=terrace deposits; Ql=Lawu deposits; Qn=Notopuro formation; Qk=Kabuh formation; Qp=Pucangan formation; QTpt=Tambakromo formation; Tpkk=Klitik member of Kalibeng formation; Tmkb=Banyak member of Kalibeng formation; Tmpl=Ledok formation; Tmw=Wonocolo formation; Tmm=Madura formation; Tmn=Ngrayong formation; Tmt=Tawun formation; Qav=Argokalangan morphocet; Qas=Sedudo morphonit; Qp=Pawonsewu morphocet; Qpg=Gajahmungkur morphonit; Qppr=Parangandesite intrusive; Qpp=Punjul andesite intrusive; Qj=Patukbanteng-Jeding morphocet; Qjt=Tanjungsari morphonit; Qjn=Ngebel morphonit; Qjd=Dangean morphonit=Dangean morphonit; Qjk=Klotok morphonit; Qpmv=Notopuro formation; Qpk=Kabuh formation; TmwL=Wonosari formation; Tmw=Wuni formation; Tmj=Jaten formation; Tomm=Mandalika formation; Tomi=intrusive rocks.*

The heavy mineral composition of sand fractions of the parent materials demonstrate the high-abundance of augite, hypersthene and labradorite, which is an indication of intermediate (andesitic-basaltic) volcanic materials (Wibisono et al., 2016).

---

<sup>4</sup> Source of geology information: Geology map of Bojonegoro, 1508-5, 1:100.000; Geology map of Bogor, 1209-1, 1:100.000; Geology map of Ngawi, 1508-4, 1:100.000; Geology map of Ponorogo, 1508-1, 1:100.000 – Geological Research and Development Centre, Geological Agency of Indonesia.

Dry months (< 60 mm) usually take place in June/July to August/September; the longest period of 3 months occurred in 2006. This area is agroclimatically classified into humid region (Juo and Franzluebbers, 2003) as the precipitation is greater than the potential evapotranspiration all year-round (Appendix 2.2). Water for ricefields is distributed from an irrigation canal.

### 2.1.2. Sampling year 2016

The field campaign was carried out from 20-24 July 2016 just before or right in the early stage of rice growing season, i.e. during land flooding. The study covers three main landforms, i.e. volcanic region, alluvial plain, and ridge area. The six chosen sites, following a toposequence of the area, include Randusongo (Rds), Gerih (Grh), and Pojok (Pjk) on the Mt. Lawu slope, and Danguk (Dgk), Ploso Lor (PL), and Bobol (Bbl) on the Kendeng ridge side (Fig. 2.1, and Table. 2.2). In each site, at both P and the neighbouring NP, one soil pit was dug out for profile morphology observation (Appendix 2.3) and layer sampling. The information of agronomic practices and history of lands were obtained from personal communication to the landowner (Appendix 2.1). The general additional descriptions of study plots are as follows:

#### 2.1.2.1. Site 1 - Randusongo, Ngawi, East Java.

Located at the lower slope of Mt. Lawu, the soil is derived from a lahar consisting of various sizes of andesite, and basalt mixing with tuff volcanic. The existence of coarse materials in the field, i.e. gravels, stones, and boulders, suggests lahar-derived materials as a complementary of ash-volcanic deposits. A non-active old river to the north, through which the lahar was most likely transported to this area, borders the rice plot.

In the P site, water seepage in the profile measured a pH slightly neutral at 6.5. Water is irrigated to this farm through an established canal system. The NP site, located close to a convex bend of a non-active meandering river, ca. 400 m from the P site to the west, has a shallow solum<sup>5</sup>, ca. 25 cm thickness, with a minimum soil profile development. The water seepage pH in the profile measured at 6.3. Being dryland, irrigation water is just from rain.

#### 2.1.2.2. Site 2 - Gerih, Ngawi, East Java

The area is a floodplain at the footslope of Mt. Lawu. The fluvial materials may have been deposited by Bemu river to the west, which is topographically situated higher than the village level.

The intensive rice cultivation, 3 times per year without an extra of dry crops, has been made possible in this area by the high availability of irrigation water, supplied to farms by an established canal system. Measured water seepage pH in P profile was 6.8, which was slightly more alkaline than for the upper plot in Rds.

#### 2.1.2.3. Site 3 - Pojok, Ngawi, East Java

The chosen plots were on a toe slope of Mt. Lawu on the active alluvial plain. The flat area continuously receives deposits from the Madiun river which is only ca. 200 m to the north. The water seepage pH was alkaline at ca. 7.6 pointing out the subsoil alkaline environment down to ca. 1.5 m depth. Due to the high availability of water for irrigation, rice paddies are intensively cultivated three times per year. The field has been rice paddies since 1960 with a

---

<sup>5</sup> Surface and subsoil layers above the parent material.

break period between 2009 and 2014 for sugarcane. The neighbouring NP plot was a small garden covered by bamboo (Table 2.2), dissected by a small creek from the ricefield.

Table. 2.2. General information of research area of 2016 field campaign.

Site	Alt (m asl)	Parent material	Soil order	Prec (mm y <sup>-1</sup> )	T (°C) <sup>6</sup>	Annual crop rotation
Rds-P	197	Andesitic-basaltic tuff	Regosol	3215 <sup>7</sup>	25.1	P-P-Soybean
Rds-NP	204	Andesitic-basaltic tuff	Regosol	3215	25.1	Teak plantation
Grh-P	81	Andesitic-basaltic alluvium	Cambisol	3215	25.8	P-P-P
Grh-NP	81	Andesitic-basaltic alluvium	Cambisol	3215	25.8	Teak plantation
Pjk-P	51	Andesitic-basaltic alluvium	Fluvisol	NA	25.9	P-P-P
Pjk-NP	51	Andesitic-basaltic alluvium	Fluvisol	NA	25.9	Bamboo garden
Dgk-P	63	Andesitic-basaltic alluvium	Fluvisol	NA	25.9	P-P-P
Dgk-NP	63	Andesitic-basaltic alluvium	Fluvisol	NA	25.9	Banana garden
PL-NP	79	Alluvial-andesitic volcanic materials-marl	Vertisol	2756±1288	27	Garden plot
Bbl-P	152	Colluvium w. sandstone, claystone, volcanic tuff	Regosol	NA	25.4	P-P-soybean
Bbl-NP	152	Colluvium w. sandstone, claystone, volcanic tuff	Regosol	NA	25.4	Garden plot

(with Rds = Randusongo; Grh= Gerih; Pjk = Pojok; Dgk=Danguk; PL=Ploso Lor; Bbl=Bobol; P = paddy; NP = non paddy; Alt = Altitude; Prec = precipitation (mean±std); T = temperature; NA = not available).

#### 2.1.2.4. Site 4 - Danguk, Ngawi, East Java

These plots are situated on the toe slope of Kendeng ridge on a non-active meander alluvial plain. Madiun river cut through the Ngawi alluvial plain right in the middle and separates this area from the Pjk site (Fig. 2.1). As it is lying at ca. 10 m higher altitude than Pjk, the fluvic materials from the upper hills are most likely deposited through Bangon and Lusungwatu rivers. Rice is cultivated intensively 3 times per year as facilitated by a well-established canal irrigation system from the Sangiran dam. The water seepage in the pit from NP plot measured pH at ca. 7.

#### 2.1.2.5. Site 5 - Ploso Lor, Ngawi, East Java

Located on the toe slope of Kendeng ridge on a non-active meander alluvial plain, this was the study area sampled in 2012 (section 2.1.1.1). In 2016 the samples were only taken from a mixed garden plot for comparison with the results obtained from the 2012 sugarcane plot. Measured pH of water seepage was 7, which is similar to Dgk's plot from 15 m lower altitude in the same slope. Wild grasses, shrubs, and banana cover the area which is ca. 200 m away from the 2012 sugarcane plot.

#### 2.1.2.6. Site 6 - Bobol, Bojonegoro, East Java

The plots are situated on the agriculture terraced slopes on the valley zone of the Kendeng anticlinorium, at the lower slope of Mt. Pandan to the southeast which is the highest level of the ridge. Soil developed on the Kerek formation originated from colluvium containing sandstone, claystone, and volcanic tuff (Fig. 2.1). The sediment that fills up the valey is most

<sup>6</sup> Estimated from Braak formula, mean annual T = 26.3 – 0.61\*altitude (hm).

<sup>7</sup> Data 2016 from Statistics Bureau of Ngawi.

likely derived from eroded deposits of hills to the east and to the south, as this area is relatively higher than the closest non-active river to the west.

Agriculture in this area is rainfed. The pH of water seepage in the profile of P site measured ca. 7.3 which is higher than on the lower Kendeng ridge slopes (Dgk and PL) confirming the increase in the alkalinity through slope gradient. The shallow solum of the ricefield, with only ca. 27 cm thickness, overlies a sedimentary rock, i.e. claystone (Appendix 2.3).

## 2.2. Soil sampling

A pit for each plot was excavated down to ca. 1 m depth with lateral dimension approximately 1 m by 1 m. Soil morphology in the profiles was characterized according to FAO criteria (FAO, 2006). The horizons were specified based on soil characteristics in the layers, i.e. structure, fingering texture, colour, or their compactness. In addition, the physical environment in which the pit observations were carried out was also identified ((Dieterich, 2012); Appendix 2.3).

The top layers (Ap/Ah horizons) were mostly removed from examination based on the earlier findings in Chinese paddy soil (Bräuer et al., 2013a, 2013b). This layer is heavily disturbed and mixed due to normal agricultural practices. Moreover, in this layer the young to old carbon proportion is consistently high, so the concentration of  $^{14}\text{C}$  is always close to the recent atmospheric  $\text{CO}_2$ . On the other hand, in the subsoil, a stable environment with more homogeneous soil column, organic composition is reported as being more decayed in which the ratio of young to old carbon drops with increasing depth. By looking at the subsoil carbon, this study puts the attention more to the soil processes related to subsoil carbon enrichments.

Samples were selected from subsoil horizons by dividing each main horizon mostly into top, middle, and bottom sections. Some thinner horizons were subject to limited discretization into only one or two sections. This way, not only inter-horizons carbon distributions can be observed, but also variations within a single main horizon. This detailed sampling may be advantageous to see any trend between carbon variation and layer composition.

Soil samples covering 1 - 2 cm depth intervals were taken for two categories, i.e. small and large samples. The small samples of ca. 250 - 450 g of air-dried soil were measured out for analysis of pH, C/N, element compositions, grain size, soil fractionation, and carbon isotopic compositions ( $^{13}\text{C}$ ,  $^{14}\text{C}$ ). Large samples, amounting to ca. 5 kg of air-dried soil, were collected for plant/mineral remains identification. The large sampling requires that the 1 - 2 cm point sampling be extended laterally to reach the desired sample size. In the second field campaign in 2016 (section 2.1.2), water seepage in the soil pits was collected into 1000 ml glass bottles.

The pH were measured, and the remaining water samples were freeze-dried in the laboratory in the Department of Soil, Brawijaya University, Malang, East Java to prevent any biochemical changes during transport to Kiel. The air-dried soil samples in polyethylene bags were stored in a container with constant temperature  $4^\circ\text{C}$  to slow-down any microbial related biochemical processes until the laboratory analysis was performed.

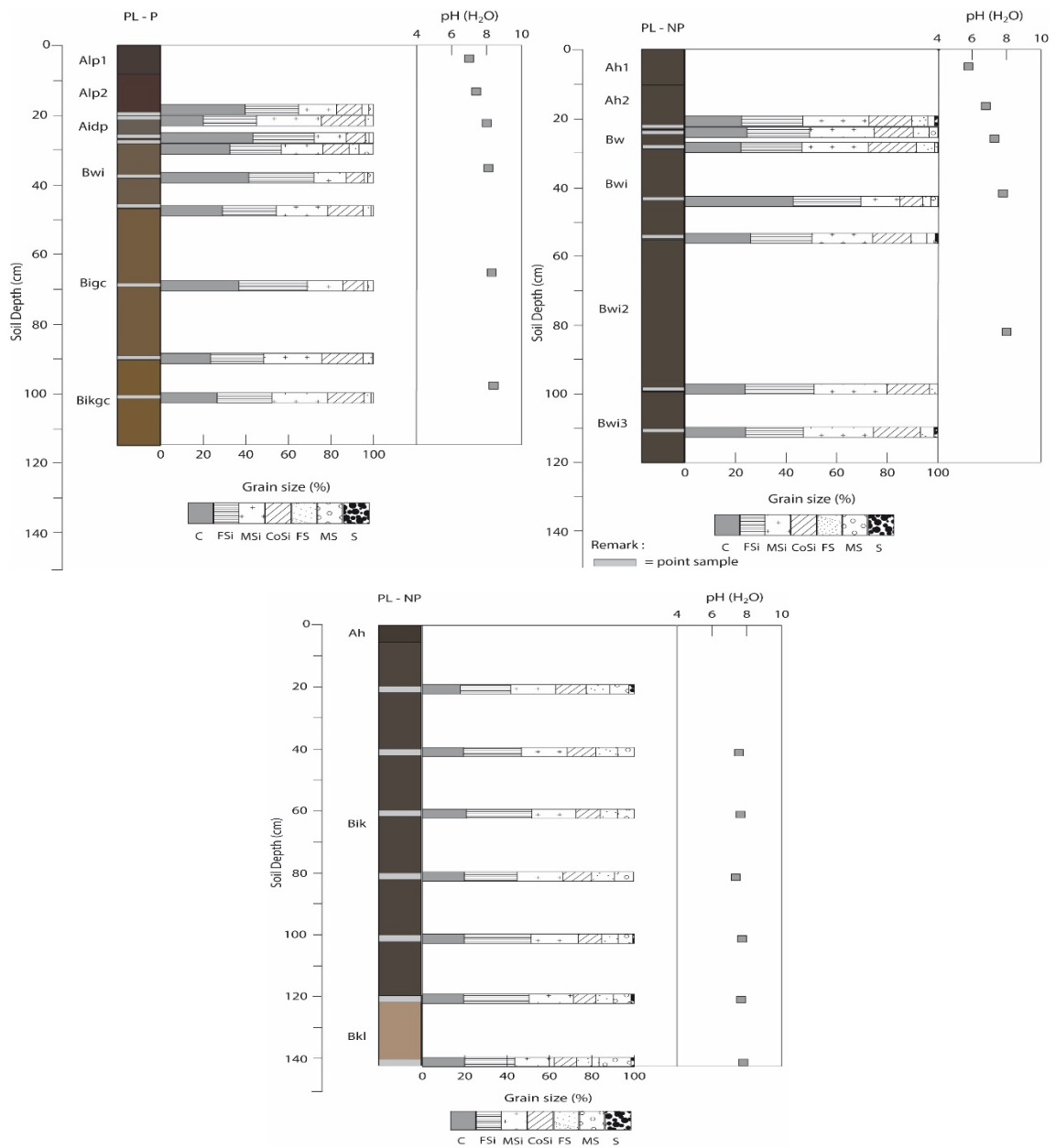


Figure. 2.2. Soil profiles from the 2012 and 2016 field campaigns in Ploso Lor, PL.<sup>8</sup>

<sup>8</sup> (P = Paddy, NP = Non Paddy-Sugarcane, top right; 2016 Garden plot, bottom) with point samples (grey bars) and soil horizon symbols (A/B represent master horizons; l=capillary fringe mottling, p=ploughing or other human disturbance, d=dense layer, g=stagnic condition, c=concretions or nodules, w=development of structure/colour, h=accumulation of organic matter, i=slickenside, k=accumulation of pedogenetic carbonates).

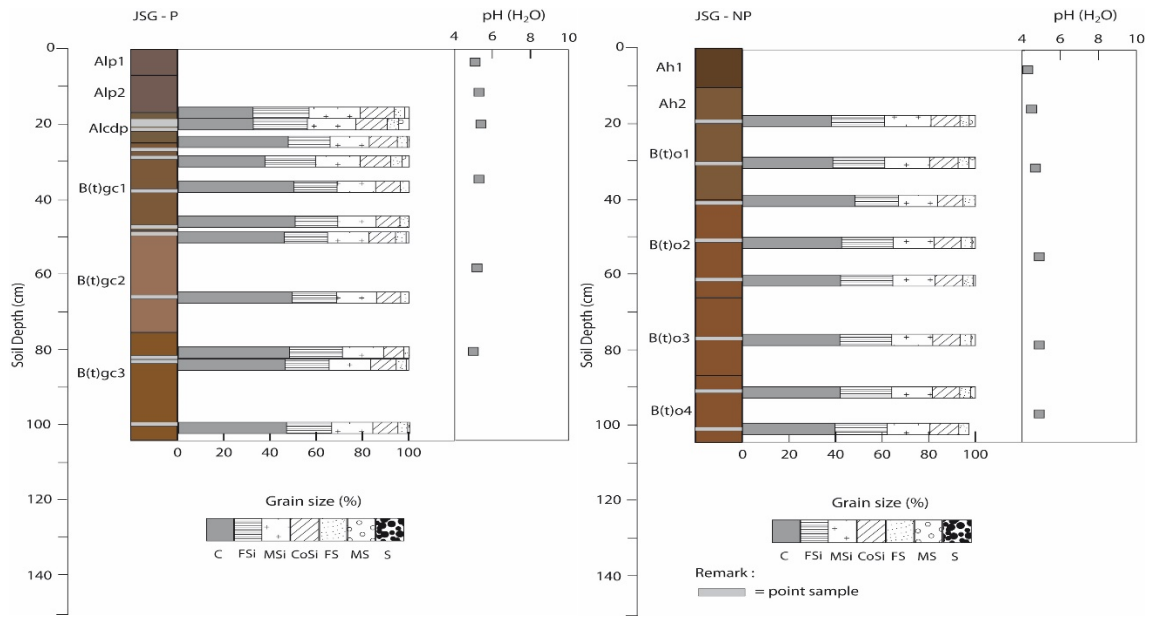


Figure. 2.3. Soil profiles from the 2012 field campaign in Jasinga, JSG.<sup>9</sup>

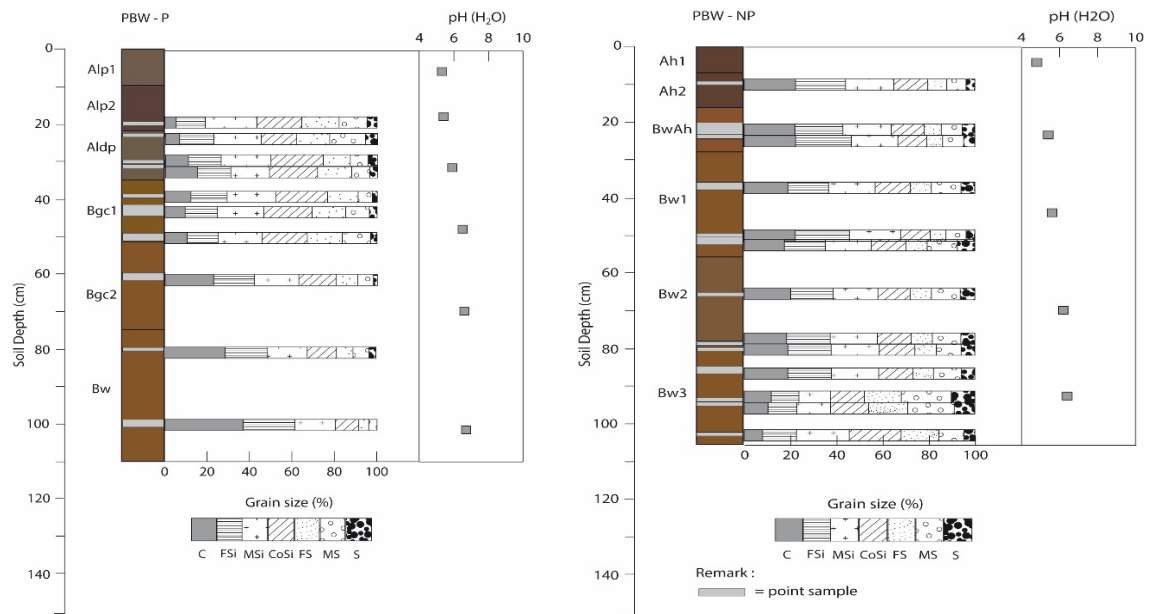


Figure. 2.4. Soil profiles from the 2012 field campaign in Perbawati, PBW.<sup>10</sup>

<sup>9</sup>(P = Paddy, NP = Non Paddy) with point samples (grey bars) and horizon symbols (A/B represent master horizons; l=capillary fringe mottling, p=ploughing or other human disturbance, d=dense layer, g=stagnic condition, c=concretions or nodules, w=development of structure/colour, h=accumulation of organic matter, t=illuvial accumulation of silicate clay, o= residual accumulation of sesquioxide).

<sup>10</sup>(P = Paddy, NP = Non Paddy) with point samples (grey bars) and horizon symbols (A/B represent master horizons; l=capillary fringe mottling, p=ploughing or other human disturbance, d=dense layer, g=stagnic condition, c=concretions or nodules, w=development of structure/colour, h=accumulation of organic matter).

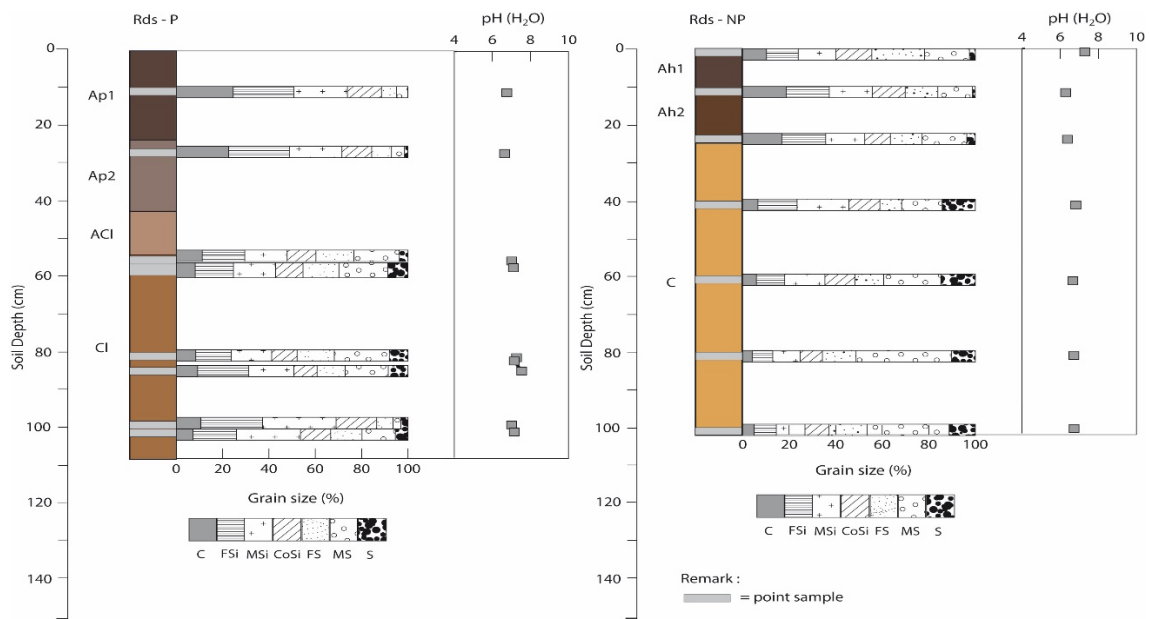


Figure. 2.5. Soil profiles from the 2016 field campaign in Randusongo, Rds.<sup>11</sup>

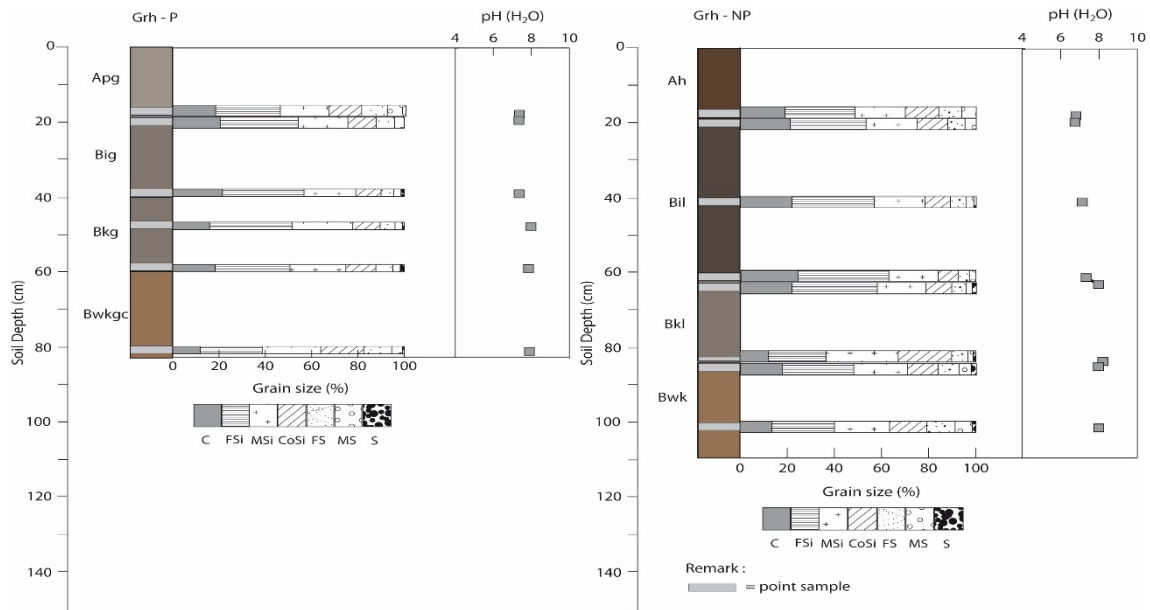


Figure. 2.6. Soil profiles from the 2016 field campaign in Gerih, Grh.<sup>12</sup>

<sup>11</sup> (P = Paddy, NP = Non-Paddy) with point samples (grey bars) and horizon symbols (A/B/C represent master horizons; l=capillary fringe mottling, p=ploughing or other human disturbance, h=accumulation of organic matter).

<sup>12</sup> (P = Paddy, NP = Non Paddy) with point samples (grey bars) and horizon symbols (A/B represent master horizons; l=capillary fringe mottling, p=ploughing or other human disturbance, c=concretions or nodules, w=development of structure/colour, h=accumulation of organic matter, i=slickenside, k=accumulation of pedogenetic carbonates).

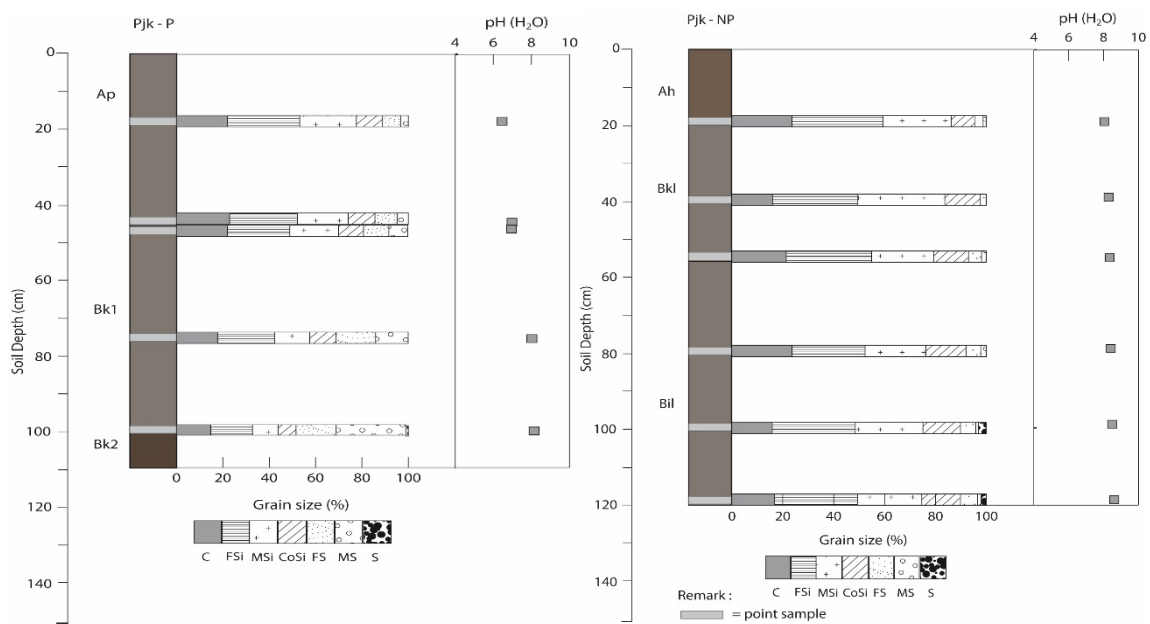


Figure. 2.7. Soil profiles from the 2016 field campaign in Pojok, Pjk.<sup>13</sup>

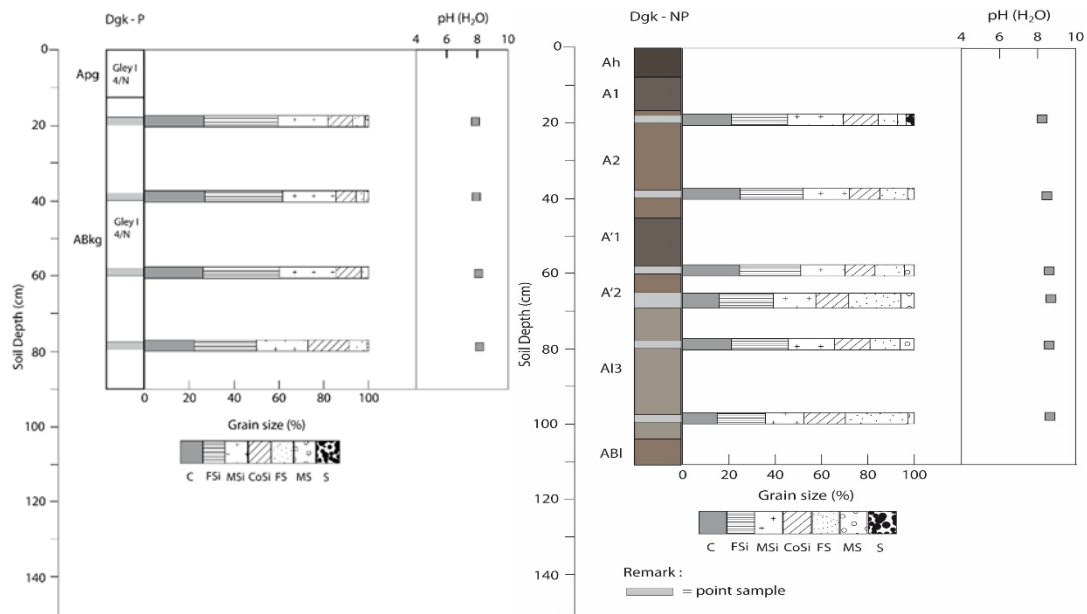


Figure. 2.8. Soil profiles from the 2016 field campaign in Danguk, Dgk.<sup>14</sup>

<sup>13</sup>(P = Paddy, NP = Non Paddy) with point samples (grey bars) and horizon symbols (A/B represent master horizons; l=capillary fringe mottling, p=ploughing or other human disturbance, h=accumulation of organic matter, i=slickenside, k=accumulation of pedogenetic carbonates).

<sup>14</sup>(P = Paddy, NP = Non Paddy) with point samples (grey bars) and horizon symbols (A/B represent master horizons; l=capillary fringe mottling, p=ploughing or other human disturbance, d=dense layer, g=stagnic condition, h=accumulation of organic matter, i=slickenside, k=accumulation of pedogenetic carbonates). The corresponding RGB colour for Dgk-P munsell colour is not available.

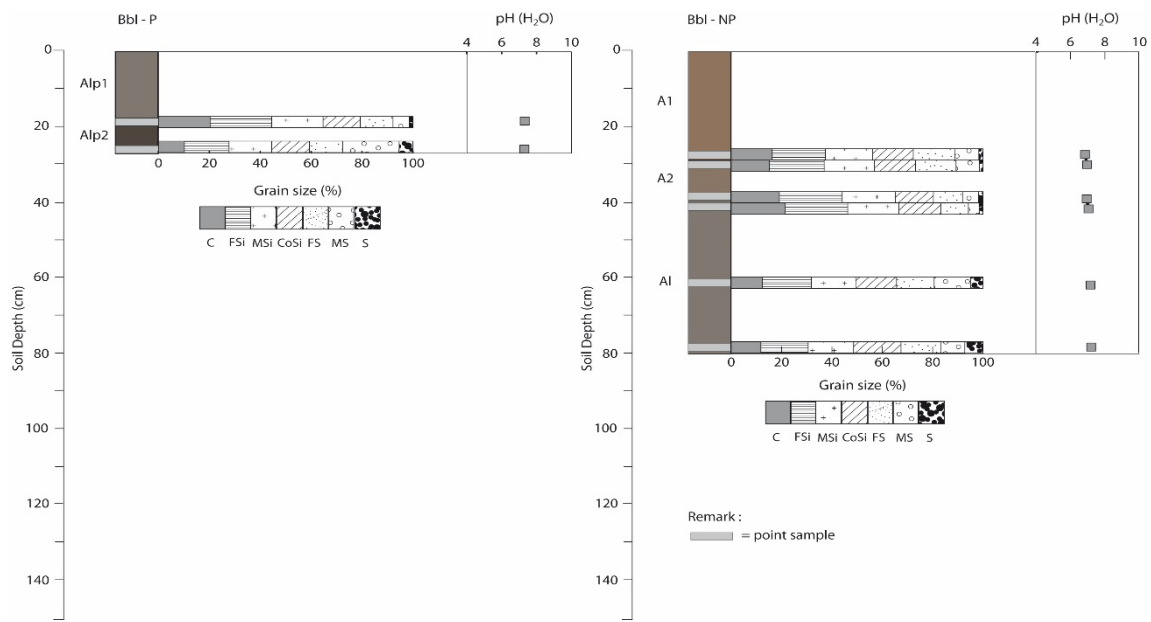


Figure. 2.9. Soil profiles from the 2016 field campaign in Bobol, Bbl.<sup>15</sup>

### 2.3. Sample preparation

Sample preparations prior to laboratory analysis include wet sieving to collect plant and mineral remains; acid-alkali-acid treatment to remove carbon-containing contaminants from <sup>14</sup>C samples and extract the concomitant organic matter fractions (alkali-soluble humic acids, and acid/alkali-insoluble humins), and ultrasonication to isolate soil mineral-associated carbon fractions. Details will be discussed in the following.

#### 2.3.1. Wet sieving

Soils contain varying components, both organic, i.e. plant derived residues (macrofossils), and non-organic, i.e. concretions, and nodules. They are glued together and to the soil matrix which brings difficulties in terms of individual sorting. By dispersing the air-dried soil matrix in water, called wet sieving, various soil particles can be extracted more easily on appropriate sieves. The wet sieving for 2012 air dried samples was done in the Institute for Ecosystem Research, Kiel University. Sieving for 2016 wet soil samples was performed in the Soil Physics Laboratory, Department of Soil, Brawijaya University.

The large, either air-dried or fresh samples, ca. 5 kg, collected from the field were soaked overnight in demineralized water in 10 liter buckets to facilitate washing and sieving the next day. On a double stack of 2 and 0.37 mm sieves, a high-pressure water sprayer was employed to break up the aggregates and remove  $\phi < 0.37$  mm sized particles by repeated spraying-decanting until no more residue is left. The retained plant remains, i.e. seeds, roots, and leaves, as well as mineral concretions on the surface of the sieves were collected, and oven-

<sup>15</sup>(P = Paddy, NP = Non Paddy) with point samples (grey bars) and horizon symbols (A/B represent master horizons; l=capillary fringe mottling, p=ploughing or other human disturbance).

dried at 60°C until a constant-weight was obtained. The distribution of plant remains collected in different soil types as a function of depth will be discussed later (section 4.1). Mineral concretions, generated in some soil layers, data is presented in the Appendix 2.4.

Microscopic observation was used to identify and separate the plant remains by their colour, i.e. light versus dark material, and by physical appearance, i.e. roots, fragment of leaves, charcoal. Dating these materials requires subsequent acid-alkali-acid treatment (section 2.3.2), and will be discussed in the section 4.1.

The mineral contents of some concretions were assessed by XRF scanning both on the surface and nucleus of individual sample (section 2.4.2). For average values, some concretions were ground prior to scanning. The important mineral contents of some collected concretions are presented in the Appendix 2.5 and 2.6.

### 2.3.2. Acid-alkali-acid (AAA) treatment

Traditional chemical cleaning of plant material and soil for radiocarbon dating using the AAA treatment splits organic matter into three different fractions based on their relative stability, i.e. acid-soluble fulvic acids, alkali-soluble humic acids, and acid/alkali-insoluble humins (in plants mostly cellulose). The most stable soil organic matter fractions are the humins, which results from the strong clay and fine-silt-sized protection which is prominent in clayey soils. The less stable fraction, fulvic acids, is water-soluble and mobile, and always contains young organic carbon. When dissolved, it can multilaterally move in the subsoil to mix with older and stabilized carbon, and increase the average <sup>14</sup>C concentration, which gives rise to age falsification. In this view, fulvic acids are contaminant and thus removed in this preparation.

The protocol of AAA treatment will be summarized from a paper elsewhere (Grootes et al., 2004). Air-dried soil samples, ca. 2 g, were extracted with 20 ml of 1% HCl to get rid of water and acid soluble contaminants, i.e. carbonates and fulvic acids. Carbonates can also be a serious contaminant, as they contain carbon with a history and <sup>14</sup>C concentration potentially different from that of the organic carbon. Their presence in the samples, therefore, could change the measured radiocarbon age (Rapp and Hill, 2006).

The solid residue after acid extraction was separated from the acid extract by centrifugation. To get rid of the excess acids and any dissolved contaminants, the solid residue was repeatedly washed with distilled water until the pH of the wash-water increased to 3-4. The solid was then extracted with 1% NaOH in a waterbath at 60°C for 4 hours. Thus, the extractable humic substances, humic acids, will be dissolved from the soil samples. High speed centrifugation (Thermo Scientific Heraeus 3S-R), i.e. 4600 rpm, which is equal to 4550 g<sup>16</sup>, for 10 minutes, was applied to separate the alkali-soluble humic substances from the solid humin fraction. The humic acid fraction was precipitated from the alkali extract by acidification with concentrated HCl until the pH of the solution < 1. The next day, centrifugation was again used to separate the solid humic acids from the acid-soluble fraction. Humic acids were washed repeatedly with distilled water until pH increases to 3-4.

---

<sup>16</sup> Relative centrifugal force (G-force) =  $1.12 \times R \times (\text{RPM}/1000)^2$ , with R = radius of rotation (mm); 192 mm for bucket type TTH 750.

The humin fraction after alkali extraction was washed in sequence using distilled water to drop the pH from ca. 12 to ca. 10. To remove atmospheric CO<sub>2</sub>, potentially introduced during the alkali treatment, the humin samples were acidified with 1% HCl until the pH of the solution is below 1. Then the same repeated distilled-water-washing was done to produce a pH of solution 3-4. Both humic acid and humin fractions are ready for further analysis after oven/freeze-drying for ca. 3 days.

### 2.3.3. Ultrasonication

Instead of chemical fractionation, the use of ultrasonication may be advantageous to isolate soil mineral-associated carbon fractions, and trace carbon infiltration. It does not significantly affect the subsequent isolated fractions by any chemical inputs and pH alteration (Christensen, 2001; Oorts et al., 2005). This technique breaks-up the inter-aggregate attractive forces because the bubbles created by the cavitation process of the ultrasonicator produce a certain stress on the soil-water suspension (Raine and So, 1994; Zhu et al., 2009). By setting up the dispersion energy within the acceptable range, the ultrasonication will keep mineral-associated carbon destruction at minimum. Excessive dispersion energy, may cause undesirable soil fraction mass distribution, while too low energy will not break the soil aggregate bonds (Poeplau and Don, 2014).

The acceptable dispersion energies have been obtained by monitoring the yields of particle size fractions from a given energy. The optimum energy could be determined where changes in yields level off, and by calibrating against yields obtained from standard textural analysis (Morra et al., 1991; Schmidt et al., 1999). Furthermore, the dispersion energy applied should minimize the re-distribution of organic matter during the ultrasonication (Amelung et al., 1998). Based on these criteria, a dispersion energy of 60 Jml<sup>-1</sup>, as the minimum, and energies of 440 Jml<sup>-1</sup> (Amelung et al., 1998), 1500 Jg<sup>-1</sup> (Oorts et al., 2005), or 450-500 Jml<sup>-1</sup> as the maximum, have been considered acceptable. The first dispersion energy (the minimum) is sufficient to isolate secondary organomineral complexes which relates to the aggregate structure of soils (macro-,  $\phi > 250 \mu\text{m}$ , and microaggregates,  $\phi < 250 \mu\text{m}$ ), while the latter complete dispersion (the maximum) isolates the primary organo-mineral complexes which relate to the primary structure of soils (clay-,  $\phi < 2 \mu\text{m}$ , silt-,  $\phi 2\text{-}20 \mu\text{m}$ , and sand-sized,  $\phi 20\text{-}2000 \mu\text{m}$ ).

Therefore, it can be concluded that the first dispersion retains the sand associated organic matter, and subsequent additional energy breaks-up the secondary organic matter complexes into smaller fractions (primary organic matter complexes), which gives rise to the increase in clay sized organic matter complex abundance in the suspension (Schmidt et al., 1999).

Ultrasonicators are now available in a variety of commercial brands. They have different default output power, generated by, for instance, different probe diameters used, so that an interlaboratory comparison is quite difficult to carry out. To cope with this problem, the standardization of ultrasonication protocols is urgently needed (Morra et al., 1991). One well-known and widely accepted method is by measuring the ultrasonic output power calorimetrically (North, 1976).

In this study, the ultrasonicator type operated was Labsonic U (Braun Melsungen, Germany) with a 19 mm diameter titanium probe. First of all, the ultrasonicator was calibrated according to North (1976), as below:

$$P_o = \frac{m_w c_w \Delta T}{t} + H \quad (2.1)$$

With:

- $P_o$  : the output power (W)  
 $m_w$  : the mass of water (g) in the calorimeter  
 $c_w$  : specific heat capacity of water ( $4.18 \text{ J.g}^{-1}.\text{K}^{-1}$ )  
 $\Delta T$  : the difference of temperature, final temperature ( $T_1$ ) – initial temperature ( $T_0$ )  
 $t$  : sonication time (s)  
 $H$  : energy loss by conduction ( $\text{J.s}^{-1}$ ).  $H$  value is negligible since a Dewar vessel with a plastic cover was used.

To calibrate the displayed power in the instrument ( $P_e$ ),  $m_w$ ,  $\Delta T$ , and  $t$  data were collected in the laboratory using a Dewar flask. The specific heat capacity of Dewar flask is estimated through calorimetry. The equilibrium condition of boiled and cool water temperature (at room temperature) in the same Dewar flask were recorded. The calculation is presented in eq. (2.2).

$$\begin{aligned} m_{dewar} * \Delta t_{dewar} * C_{dewar} &= m_{water} * \Delta t_{water} * C_{water} \\ 300 * (100 - 25.6) * C_{dewar} &= 200 * (25.6 - 20.8) * 4.18 \\ C_{dewar} &= 0.179 \text{ J.g}^{-1}.\text{°C}^{-1} \text{ or } 0.179 \text{ J.g}^{-1}.\text{K}^{-1} \end{aligned} \quad (2.2)$$

With:

- $m_{dewar}$  = mass of Dewar (g)  
 $\Delta T_{dewar}$  = the temperature change of Dewar flask;  $T_0 = 100^\circ\text{C}$ , and  $T_1 = 25.6^\circ\text{C}$   
 $C_{dewar}$  = heat capacity of Dewar in contact with water ( $\text{J.g}^{-1}.\text{°C}^{-1}$ )  
 $m_{water}$  = mass of water (g)  
 $\Delta T_{water}$  = the temperature change of water;  $T_0 = 20.8^\circ\text{C}$ , and  $T_1 = 25.6^\circ\text{C}$

The heat capacity of the Dewar flask is ca. 4% of the heat capacity of water, i.e.  $4.18 \text{ J.g}^{-1}.\text{K}^{-1}$ , therefore it can be neglected.

A constant volume of 200 ml of distilled water in a 250 ml Dewar vessel was used, the nominal power  $P_e$  and  $t$  were varied. The initial water temperature was recorded ( $T_0$ ) using a digital thermometer. In the sound-enclosure, the Dewar vessel was adjusted so that the tip of the ultrasonic probe immersed 15 mm into the water. The  $P_e$  settings used in this calibration were 100, 120, 150, 180, 200, 225, and 250 watt (maximum point) with a duration  $t$  of 60, 120, and 180 seconds. Every single measurement was performed threefold. Since  $m_w$  was constant at 200 ml, the measured variables  $\Delta T$ , calculated from  $T_1$  and  $T_0$ , and  $t$  allow the calculation of the real output power  $P_o$ . In between runs, a minimum 15 minute break was allocated to allow the probe to cool down.

A simple regression model was implemented to relate  $P_e$  and  $P_o$  (Fig. 2.11).

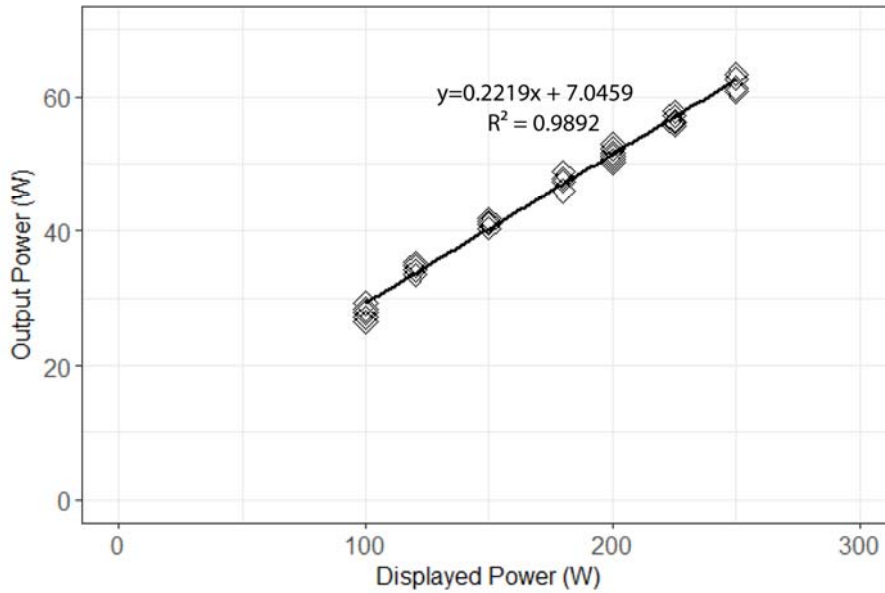


Figure. 2.10. Regression of calculated  $P_o$  and displayed  $P_e$  after simulation.

Using a calibrated output power of the instrument, subsequent sample dispersion was performed. A displayed power of 200 watt was chosen, which corresponds to ca. 50 watt calorimetrically, used as a fixed energy throughout the course of ultrasonication. Samples were dispersed to isolate four different size fractions, i.e. 250-2000  $\mu\text{m}$  (macroaggregates); 63-250  $\mu\text{m}$  (free microaggregates); <20  $\mu\text{m}$  (medium-fine silt + clay-with associated organic matter); and < 2  $\mu\text{m}$  (clay-with associated organic matter). The first two fractions were obtained by wet-sieving, while the remaining silt and clay fractions were extracted by the pipette method (will be discussed at the end of this section).

The first sonication applied the dispersion energy at 60  $\text{J}\cdot\text{ml}^{-1}$  to collect macroaggregates, while the second at 440  $\text{J}\cdot\text{ml}^{-1}$  followed to complete dispersion to isolate primary organo-mineral complexes. To keep the ratio of soil:water at 1:5, in the current work, 30 g of air-dried samples were used together with 150 ml of distilled water. The time required for sonication is calculated using the equation below:

$$E = \frac{Pt}{V} \quad (2.3)$$

With:

- E : energy required for sonication ( $\text{J}\cdot\text{ml}^{-1}$ ); which is 60 and 440  $\text{J}\cdot\text{ml}^{-1}$
- P : output power (W); which was 50 watt
- t : time (s)
- V : volume of suspension (ml)
- : volume of water + volume of soil sample
- : 150 ml + 30 g/2.65  $\text{g}\cdot\text{cm}^{-3}$  (density of quartz)
- : 150 ml + 11.32  $\text{cm}^3$  (1  $\text{cm}^3$  equal to 1 ml)
- : 161.32 ml

Therefore, the operational times for ultrasonication were 3 minutes, 7 seconds, and 23 minutes, 39 seconds for 60 and 440 J/ml, respectively. Prior to ultrasonication, the soil samples were soaked overnight using distilled water in a 300 ml beaker glass. During dispersion, the energy released by the probe will increase the temperature of the suspension. This may change the biochemistry of organic matter in the sample, i.e. enzymatic composition, microbial biomass, or soil respiration. Therefore, the temperature was kept below 35°C by surrounding the 300 ml beaker glass with ice cubes in a 1000 ml beaker glass.

After first dispersion at 60 J.ml<sup>-1</sup>, the suspension was poured into stacked 250 and 2000 µm sieves. The samples used for analysis were obtained after laboratory preparation, φ<2000 µm, therefore no soil materials were remaining on the surface of the 2000 µm sieve. The particles retained on the surface of the 250 µm sieves were collected and oven-dried, while the material that passed through the sieve, as a suspension, was taken back into a 300 ml beaker glass. In the same way, the second ultrasonication at 440 J.ml<sup>-1</sup> was operated at soil/water ratio of 1:10 (Amelung et al., 1998) from the initial sample weight, and ended up sieving the free microaggregates on 63 µm sieves. The particles on the surface of the sieves were collected and oven-dried, while the φ<63 µm suspension was poured back into the beaker glass before a transfer into a 1 L glass cylinder for sedimentation. The oven-drying of both micro- and macro-aggregate fractions was at 40°C until a constant weight was obtained.

The use of a sedimentation technique to collect silt + clay and clay fractions is based on the relative settling velocity of particles in water. Applying Stokes' law, the velocity of a spherical particle settling under gravity in a fluid of given density ρ and viscosity η is proportional to the square of the particle's radius (Hillel, 2004). The gravitationally falling particles in water will encounter frictional resistance proportional to the radius of particles, and viscosity of water. The gravitational force can be formulated as:

$$F_g = \frac{4}{3}\pi r^3(\rho_s - \rho_w)g \quad (2.4)$$

With:

$\frac{4}{3}\pi r^3$  : volume of spherical particles, with r = equivalent radius of the particle (cm)

$\rho_s$  : density of the spherical particles (g.cm<sup>-3</sup>)

$\rho_w$  : density of water (g.cm<sup>-3</sup>)

Frictional force can be formulated as follows:

$$F_f = 6\pi\eta r v \quad (2.5)$$

With:

6π : constant for sphere

η : viscosity of water at specific temperature (g.cm<sup>-1</sup>.s<sup>-1</sup>)

r : radius of particle (cm)

v : particle settling's speed (cm.s<sup>-1</sup>)

Assuming the two forces are equal, the following formula is obtained for the particle settling speed:

$$v = \frac{2(\rho_s - \rho_w)}{9\eta} gr^2 \quad (2.6)$$

$$= \frac{1}{18} \frac{(\rho_s - \rho_w)}{\eta} gd^2 \quad (2.7)$$

Therefore, the time  $t$  needed for the particle to settle down through a vertical distance  $h$  is:

$$t = \frac{18h\eta}{(\rho_s - \rho_w)gd^2} \quad (2.8)$$



Figure. 2.11. Soil particle sedimentation of JSG-Alisol sample.

According to Hillel (2004), the use of Stoke's law to measure particle sizes of soil samples makes the following some assumptions:

1. The particles are not affected by random motion of the fluid molecules
2. The particles are rigid, spherical and smooth
3. All particle have the same density
4. The suspension is dilute enough so particles settle independently
5. Fluid flow around the particles is laminar (slow enough to avoid onset of turbulence)

For soil particles, the sedimentation technique provides only approximate results. Soil particles are highly-heterogeneous since they are neither spherical nor smooth and have various densities. Clays are platy, and subject to random motion when they settle down in

water. Furthermore, in non-destructive preparation, the existence of organomineral complexes may have an influence on the density and shape of soil particles.

As discussed before, the  $\phi < 63 \mu\text{m}$  fractions after wet sieving were transferred into a 1 L cylinder to collect for silt and clay-sized fractions. The time required to settle-down fractions at a particular depth and temperature was calculated from eq. 2.8. For example, 10:31':19" was required to withdraw  $\phi < 2 \mu\text{m}$  fractions and 00:06':10" for 20  $\mu\text{m}$  fractions. The settling times were calculated at a transfer depth of 15 cm (bottom mouth of outlet) of the 1 L volume Atterberg cylinder (Fig. 2.11) at 23°C. When particular fractions are collected from the outlet, all particles smaller than these sizes will be included. For example, withdrawing of  $\phi < 20 \mu\text{m}$  soil particles allows for  $\phi < 6$  to 2  $\mu\text{m}$  fractions in the samples, and so on.

First, the  $< 20 \mu\text{m}$  fraction was collected and transferred into a pre-weighed aluminium dish. Then the cylinder was re-filled with distilled water up to the mark and shaken repeatedly before the following smaller fractions were withdrawn. The suspension collected covered a volume approximately equal to half of the transfer depth (Fig. 2.11) which was considered to be sufficient for AMS-<sup>14</sup>C analysis in terms of sample size. Because in this study the sedimentation did not collect individual fractions completely, a residual bulk soil that contains parts of  $\phi < 63 \mu\text{m}$  fractions was present at the bottom of cylinder after the last clay withdrawal. This bulk was collected together with the other fractions. A water sample was collected after the last transfer from the clay fraction by centrifuging ca. 150 ml of suspension, and eliminating the solid part. The isolated solid fractions and water sample were oven-dried at 40°C and freeze-dried respectively.

Considering the calculated recovered fractions were only ca. 30-80% of the initial weight, then to study the mass balance of carbon is actually not appropriate. Consequently, these samples were prepared to investigate the signal of <sup>13</sup>C and <sup>14</sup>C infiltrated in different class soil fractions (section 4.3.2.3). Different to the bulk samples, the isolated individual fractions were without an AAA treatment prior to AMS-<sup>14</sup>C analysis.

## 2.4. Sample analysis

The association between the mineral matrix and associated organic material in soils depends not only on the organics, but also on the size and properties of the mineral particles. Therefore, the grain size distribution and elemental composition of the mineral fraction of the soil samples were analysed to complement the carbon analysis.

### 2.4.1. Grain size analysis

Grain size analysis is one way to study the extent of soil weathering. In the soil column, the variation of grain size could be an indicator of the pedogenic and the geological history of the soil and associated geomorphic surfaces (Birkeland, 1999). This variation may control the distribution of total carbon which is a function of clay-, and fine-sized fractions.

In the current study, the grain-size distribution of samples was quantitatively analysed by a Mastersizer (Hydro 2000G). Prior to measurement the standard preparation for soil texture

analysis was employed (van Reeuwijk, 2002), i.e. elimination of carbonates (Ca-carbonate, dolomite, limestone), organic matter destruction, and dispersion. It is preferable to remove carbonates at the first step, otherwise oxidation of organic matter may produce oxalic acid that can give rise to the neo-formation of calcium oxalate.

To get rid of carbonates, 1% HCl was used to extract samples for overnight. For carbonate rich samples, a strong reaction will start immediately, along with bubble production as CO<sub>2</sub> starts to evolve. To accelerate the reactions, samples were heated in a waterbath at 60°C for 4 hours, and subsequently placed out on the bench overnight to get the reaction completed. The final solutions, when bubbles no more appeared, ended up with a variety of colours depending on soil types, i.e. milky/reddish/yellowish/brownish. The loosening of aggregates due to carbonate elimination has made the soil structure swollen.

Organic matter destruction requires a strong oxidizer like concentrated H<sub>2</sub>O<sub>2</sub> by which organic components will be removed as CO<sub>2</sub>. During extraction, mainly for samples with a high organic content, strong effervescence may appear, with subsequent discolouration of the supernatant. As for the previous working step, a waterbath at 60°C was used for the reaction until the solution remained colourless and no more effervescence could be observed. This required ca. 2-4 repetitions of 10 ml H<sub>2</sub>O<sub>2</sub> each.

After carbonates and organic matter were eliminated, the solid mineral residue was separated from the suspension by centrifugation. The excess of H<sub>2</sub>O<sub>2</sub> in the residue was removed by repeatedly washing with distilled water. Furthermore, a 0.5 ml dispersing solution with 0.5 M Na<sub>4</sub>P<sub>2</sub>O<sub>7</sub> was added to the solids before they were shaken on a mechanical shaker for ca. 16 hours. This way, sand, silt, and clay particles are expected to be completely broken apart, which subsequently facilitates the laser scanning in the Mastersizer.

#### 2.4.2. X-ray fluorescence (XRF)

The elemental composition data in this study was obtained through ICP-OES analysis for bulk samples (source primary data: Pauline Winkler, pers. comm; Appendix 3.2; Fig.2.2 to Fig. 2.4) and portable XRF scanning for concretions and selected soil fractions (Appendix 2.5; Appendix 2.7). Elemental composition by ICP-OES has been discussed elsewhere (Winkler et al., 2016), and this section will briefly summarize the principle of portable XRF used in this study.

The use of portable XRF is a non-destructive and non-invasive technique. This is widely applied for archaeological samples, e.g. ceramics, glass, pottery, and other mineral fragments, that require an undisturbed condition of the sample for further analysis. In this study an energy-dispersive type portable XRF (Niton XL3t) was applied.

X-rays from the source in the instrument scan the sample with high energy, higher than the atom's K or L inner-shell binding energy. This causes the inner electrons to be ejected with a kinetic energy,  $E-\phi$ , which is the energy difference between the incident radiation,  $E$ , and the binding energy,  $\phi$ , of the electron in the atom. The ejection of electrons out of the inner shells creates empty spaces that will be filled by electrons from one of the atom's higher energy

orbital shells while releasing a characteristic fluorescent x-ray (Conklin, 2005). The x-ray photons emitted from each heavy element are unique as proportional to the binding energies  $\phi$  of the element. This specific energy allows us to identify the source atoms.



Figure. 2.12. The illustration of XRF Niton XL3t (<https://www.dal.ca/>).

Air-dried samples were powdered mechanically using a grind-mill (Fritsch) to homogenize the size of particles to  $< 60 \mu\text{m}$  (Dreibrodt et al., 2017). Because XRF only scans the surface of samples, homogenized samples yield results that are more representative. The powdered samples were placed in XRF polyethylene cups with XRF thin film covers on one end. Tubes were placed upside down on the XRF test-stand, and the incoming X-ray beam from the bottom penetrates through the thin film cover. For selected Fe-Mn concretions, measurements were made at the surface, of the nucleus and on powdered samples to get the mean values. To get an idea of uncertainty, scanning was set internally to 10 replicates. Results with more than 10% uncertainty are considered statistically questionable.

Elemental compositions provide supporting data for grain-size distributions, because various elements have a different affinity to different mineral fractions. Therefore their abundance ratios can be used as an indicator of the uniformity of parent materials. The grain-size distributions were indicated through Rb/Zr ratio, since rubidium is bound strongly to clay minerals, while zirconium is associated to medium to coarse silt (Heymann et al., 2013; Kylander et al., 2011). Similarly, the Ti/Zr ratio, even though it does not always successfully reveal lithologic discontinuities (Ahr et al., 2012), helps to test the difference in the origin of parent material (Buurman, 2004; Chapman and Horn, 1968).

#### 2.4.3. Total, organic, and inorganic carbon and nitrogen

Total carbon and nitrogen were determined based on dry combustion via elemental analyzer (EuroEA 3000) for bulk samples, and by a muffle furnace in the system of Accelerator Mass Spectrometry (AMS), for organic fraction samples. The use of an elemental analyzer (EA) requires a bit specific sample preparation, while the use of the combustion technique requires the same preparation as radiocarbon analysis.

The application of EA reduces the size of samples to ca. 30 mg rather than the cumbersome size for different classical methods, for instance 5 g for the chemical Walkley and Black (van Reeuwijk, 2002), and 10 g for the loss-on-ignition method (Faithfull, 2002). In addition, total carbon and nitrogen are measured simultaneously, which improves the efficiency. Dry combustion of samples at high temperature, ca. 900°C, produces the elemental gases, that are separated in a chromatographic column for further detection using a high-sensitivity thermal conductivity detector. On the other hand, the use of the dry combustion system in AMS requires a muffle furnace at 900°C for 4 hours, and the total CO<sub>2</sub> evolved from the sample can be assumed as total organic carbon given that carbonates have been removed prior to combustion.

The preparation of samples for dry combustion by chemical treatments has been discussed in the section 2.3.2. For EA analysis, the total C/N can be measured directly on ground  $\phi < 2$  mm bulk sample. Organic C/N is obtained by removing carbonates from the samples prior to measurement with HCl. Therefore, inorganic C/N is the difference between total C/N and organic C/N. Carbonate elimination is needed especially on neutral to alkaline, pH 7.5-8.5, samples from the PL Vertisol. On the other hand, for acid Alisol and Andosol samples with pH range 4-6, total organic C/N is assumed to be equal to total C/N since carbonates are instable in this pH range.

Inorganic nitrogen, i.e. NO<sub>3</sub><sup>-</sup>, NH<sub>4</sub><sup>+</sup> accounts for less than 10% of the total nitrogen in the soil. Of these two, nitrates are the dominant inorganic form of nitrogen in an oxidized environment. Yet, nitrates are water-soluble, and consequently their availability in the soil highly depends on soil moisture conditions. Meanwhile ammonium, if present in the soil, is associated with clay minerals, otherwise nitrification converts immediately into nitrate under aerobic conditions. Results of EA analysis suggest that these inorganic elements have not been present in some samples. The HCl-pretreatment did not result in a lower total N content. Based on this assumption, therefore, organic matter-derived nitrogen may be similar to total nitrogen.

#### 2.4.4. <sup>13</sup>C solid state nuclear magnetic resonance (<sup>13</sup>C-NMR)

For the characterization of soil organic matter, solid state <sup>13</sup>C-NMR spectroscopy (Bruker Biospin DSX 200 NMR spectrometer, Rheinstetten, Germany, Soil sciences TH München), with cross-polarization magic-angle spinning (CPMAS) (Kölbl and Kögel-Knabner, 2004; Wissing et al., 2013) was applied. Using this technique has the potential to characterize soil organic matter from both bulk and size-fractionated samples without any extraction prior to analysis (Stevenson, 1994). Yet, the samples used in this study were acid-insoluble humic acids to overcome the problems that come up in the absence of hydrofluoric acid (HF) treatment, i.e. long acquisition times, low resolution, and low signal to noise ratios of the spectra (Kögel-Knabner, 1997). The HF treatment, applied to eliminate the soil mineral fraction, results in highly pure organic carbon, especially connected with the low organic carbon content of soil samples.

Details of the solid state CPMAS <sup>13</sup>C-NMR technique used in this analysis have been discussed by Kölbl and Kögel-Knabner (2004), and Wissing et al (2011). Spectra were integrated for 6 chemical shift regions, i.e. 0-45 ppm (alkyl-C), 45-95 ppm (N-alkyl/methoxyl, O-alkyl), 95-110

ppm (O<sub>2</sub>-alkyl), 110-145 ppm (aromatic), 145-160 ppm (O-aromatic), and 160-220 ppm (carboxyl-C).

The spectra regions resulting from CPMAS <sup>13</sup>C-NMR do not provide any information regarding the molecular composition of organic matter. An approach to predict molecular components from <sup>13</sup>C NMR spectra has been reported (Ahmad et al., 2006; Nelson et al., 1999; Nelson and Baldock, 2005). The following paragraph will summarize the principle of CPMAS <sup>13</sup>C-NMR based on these references.

The NMR spectra and N:C ratios of samples are translated by comparing them with the NMR spectra and N:C ratios of chosen components that are produced in highest abundance by 1) plants, i.e. cellulose, hemicellulose, protein, lignin, cutin, and suberin, 2) microorganisms, i.e. protein derived from structural components and enzyme, 3) chitin derived from amino-sugars, 4) polymer produced by fungi and soil fauna, 5) structural and muco-polysaccharides, and 6) aliphatic membrane components. All these compounds have neither characteristic solid-state <sup>13</sup>C NMR spectra nor characteristic N:C ratios. To cope with this problem, they are grouped into six components as their representative, i.e. carbohydrate (cellulose, muco-polysaccharides, and smaller molecular weight saccharides), protein (proteins, peptides, and amino acids), lignin, aliphatic (cutin, suberin, and aliphatic membrane components), carbonyl (uronic acids in the carbohydrate component, and fatty acids in the aliphatic component), and charcoal. The distribution C in spectral regions and molar N:C ratios of these components are summarized in Nelson and Baldock (2005).

To calculate a model spectral distribution for a sample, the amount of each component should be estimated by solving these equations:

$$\begin{aligned}
 a + b + c + d + e + f &= 1 & (2.9) \\
 a(n_A) + b(n_B) + c(n_C) + d(n_D) + e(n_E) + f(n_F) &= n_{sample} \\
 a(\alpha_A) + b(\alpha_B) + c(\alpha_C) + d(\alpha_D) + e(\alpha_E) + f(\alpha_F) &= \alpha_{sample} \\
 a(\beta_A) + b(\beta_B) + c(\beta_C) + d(\beta_D) + e(\beta_E) + f(\beta_F) &= \beta_{sample} \\
 a(\gamma_A) + b(\gamma_B) + c(\gamma_C) + d(\gamma_D) + e(\gamma_E) + f(\gamma_F) &= \gamma_{sample} \\
 a(\delta_A) + b(\delta_B) + c(\delta_C) + d(\delta_D) + e(\delta_E) + f(\delta_F) &= \delta_{sample}
 \end{aligned}$$

In the equations above, a, b, c, d, e, and f are the proportions of component A (carbohydrate), B (protein), C (lignin), D (aliphatic components), E (carbonyl) and F (char) in the model. *n* equals to N:C ratio for specified component and sample, i.e. *n<sub>A</sub>* equals to N:C ratio of component A. *α*, *β*, *γ*, and *δ* are the proportion of carbon in the specified component and sample to represent the chemical shift regions of 45 to -10, 95 to 60, 210 to 165 and 145 to 110 ppm. The chemical shift is expressed in ppm, obtained from the absolute resonance frequency of the sample and standard reference compound,  $\frac{\nu_{sample} - \nu_{ref}}{\nu_{ref}}$ . The numerator is usually expressed in hertz, and the denominator in megahertz.

#### 2.4.5. Accelerator mass spectrometry (AMS)

The most noticeable strong point of AMS <sup>14</sup>C measurements over conventional techniques, e.g. proportional gas or liquid scintillation counter, is an about 10,000 times higher sensitivity. This is the result of the direct mass spectrometric detection of all <sup>14</sup>C atoms rather than only

those that decay during measurement through  $\beta^-$  particles emitted during that decay. The  $^{14}\text{C}$   $\beta$ -detection has a limitation related to the fairly low maximum  $\beta$  energy of ca. 0.156 MeV (Taylor and Bar-Yosef, 2014), if compared to different elements, e.g.  $^{36}\text{Cl}$  0.709 MeV, or  $^{85}\text{Kr}$  0.687 MeV. The high sensitivity of AMS  $^{14}\text{C}$  is advantageous, because the size of samples required is small, typically a factor of 1000 smaller (Bowman, 1990), which means that a small object that would be destroyed by conventional dating, still can be sampled. In addition, since each sample measurement requires less than an hour instead of several days, AMS can potentially obtain a year-round high sample throughput.

AMS combines the capabilities of conventional mass spectrometry with a particle accelerator to improve its detection limit for isotopic ratios which are in nature below  $10^{-10}$  for some cosmogenic isotopes, e.g.  $^{10}\text{Be}$ ,  $^{26}\text{Al}$ ,  $^{36}\text{Cl}$ , and  $^{14}\text{C}$  (Steinhof, 2016). The particle accelerator speeds up ionized particles in a beam line and separates ions of mass 12, 13, and 14 by passing them through electric and magnetic fields. This electrostatic system also deals with discrimination against unwanted isobars, which are in the case of radiocarbon mostly the mass-14 interfering molecular fragments  $^{13}\text{CH}$  and  $^{12}\text{CH}_2$ , and the nitrogen isotope  $^{14}\text{N}$ , which does not form a stable negative ion. A tandem electrostatic accelerator is equipped with a terminal stripper for charge-exchange to remove interferences (positive ions) by dissociating isobaric molecular ions (Steinhof, 2016; Taylor and Bar-Yosef, 2014; Tuniz et al., 1998), and raise the ion energy to levels suitable for  $^{14}\text{C}$  identification.

#### 2.4.5.1. Sample pre-treatment

Samples are first subjected to pre-treatment, before running in AMS, to get rid of the contaminations. The presence of foreign carbon may influence the measured  $^{14}\text{C}/^{12}\text{C}$  ratio, so it differs from that of the original material. The level of contamination that could be tolerated is very low, less than 0.1‰ (Grootes, 1977).

In principle, decontamination is performed in two ways, i.e. physical and chemical treatments. The physical treatments include the removal of visible plant remains, e.g. roots, rootlets, with the assistance of a microscope. The chemical preparation of samples, in principle, removes contaminants like calcium carbonate, limestone, and fulvic acids, by acid-alkali-acid treatments (section 2.3.2).

#### 2.4.5.2. Preparation of graphite targets

To obtain high purity carbon, suitable for AMS measurement, the pretreated samples are combusted to  $\text{CO}_2$  in an evacuated sealed quartz ampoule with  $\text{CuO}$  in a muffle oven at  $900^\circ\text{C}$  for 4 hours. The  $\text{CO}_2$  is then graphitized using the Fe/Zn method (Nadeau et al., 2015), which eliminates hydrogen in the reactions. Two reactions are going on, first  $\text{CO}_2$  is reduced to  $\text{CO}$  over hot Zn, at ca.  $500^\circ\text{C}$ , and second the resulting  $\text{CO}$  is converted to graphite over the iron catalyst at ca.  $700^\circ\text{C}$  (Slota et al., 1987). Iron also acts as a thermal conductor and as a binder that facilitates the physical handling of the final product (Taylor and Bar-Yosef, 2014).

The powder of graphite-Fe is then pressed into stainless steel target holders using a Cu pin (Nadeau et al., 2015), to improve the uniformity of the targets and to ease target preparation. The target holders are then fixed in the target wheel, and subsequently placed in the ion source of an AMS instrument.

#### 2.4.5.3. $^{14}\text{C}$ AMS measurement (system at NTNU, Trondheim, Norway)

The AMS facility used in NTNU, Trondheim, Norway, will be briefly discussed to summarize from the reports of Klein et al (2006) and Nadeau et al (2015).

The ion source in this system is the SO 110 hybrid with a 50 target carousel. Target holders from the wheel are placed in the ion source where the metal ionizer is heated to more than  $1000^{\circ}\text{C}$  to support the thermal process of ionizing cesium (Cs) vapor, fed into it, to  $\text{Cs}^+$  ions (Steinhof, 2016). The  $\text{Cs}^+$  ions are accelerated and focused on the graphite target by a 7 kV potential difference. When they hit the target, typically at -35 kV, they eject atoms and ions from its surface, a process called sputtering. This generates a beam of negatively charged ions, consisting of  $^{12}\text{C}$ ,  $^{13}\text{C}$ , and  $^{14}\text{C}$ , and other elemental and molecular ions that is accelerated towards ground potential and extracted from the ion source with 35 keV energy. This suppresses  $^{14}\text{N}$ , as this isobar of  $^{14}\text{C}$  does not form stable negative ion.

The ion source connects to the accelerator through the injector which mass-analyses the injected ions from the source in a  $90^{\circ}$  magnet, since all ions with the same charge have now been accelerated by the same potential difference and gained the same energy. The purpose of the injector is, as a traditional mass spectrometer, to ensure that only ions of the correct mass and charge are injected into the accelerator (Hellborg and Skog, 2008). Heavier ions are bent less than lighter ones because of higher momentum. The three carbon ions have to be injected into the accelerator. All ions in the source are accelerated by the same potential and obtained the same energy (for the same charge ions), therefore the momentum-based separation depends on the different masses. The energy should be adjusted to allow the carbon ions to enter the accelerator. The potential of the bouncer can rapidly be switched up and down, so the potential difference between the target and the bouncer, and thus the energy of the ions can be adjusted. The  $^{12}\text{C}^-$  and  $^{13}\text{C}^-$  beams are  $10^{12}$  and  $10^{10}$  times stronger than the  $^{14}\text{C}$  beam and need to be measured only briefly, while  $^{14}\text{C}$  needs to be measured long to improve statistics. Therefore,  $^{12}\text{C}$  and  $^{13}\text{C}$  are injected sequentially for only very short periods, followed by a much longer  $^{14}\text{C}$  injection. To obtain quasi-simultaneous readings on all three isotopes, the magnetic field (bouncer) cycles the sequence of 3 isotopes 100 times per second (100 Hz).

The negative ions of carbon subsequently enter the tandem accelerator, a 1 MV Tandetron™ with a solid state power supply. In the tandem accelerator, the ionized particles are accelerated twice. First, the negative ions towards the central positive terminal due to the attraction of different ion charges, and second, the positive ions, produced passing through the stripper, away from it due to the repulsion of the same ion charges. The charge-exchange device in the high-voltage terminal, in this case the argon (Ar) gas stripper canal, removes electrons from the ions by interaction with the argon stripper gas, producing carbon with various positive charge states ( $\text{C}^{++}$  used), and breaking-up molecular isobars. In this, the molecular ions are eliminated because they are not stable in positive charge state. After stripping, the positively charged carbon ions are accelerated back to ground potential in the high energy part of accelerator.

From the accelerator, the ion beam is connected to the detector through the high-energy (HE) analysis system. Due to the higher energy of the ions after the accelerator and stripper, the

magnetic and electric fields in the HE analysis have to be stronger than those in the injector (Steinhof, 2016). The HE analysis with a 90° analyzer magnet has a function as a filter, at which the focused ion beam separates carbon into its three isotopes according to momentum, and eliminates other ions. The ion beams containing positively charged  $^{12}\text{C}$  and  $^{13}\text{C}$  are bent more than  $^{14}\text{C}$ , and are collected and measured in Faraday cups, while  $^{14}\text{C}$  is allowed to continue on towards the gas ionization chamber for counting.

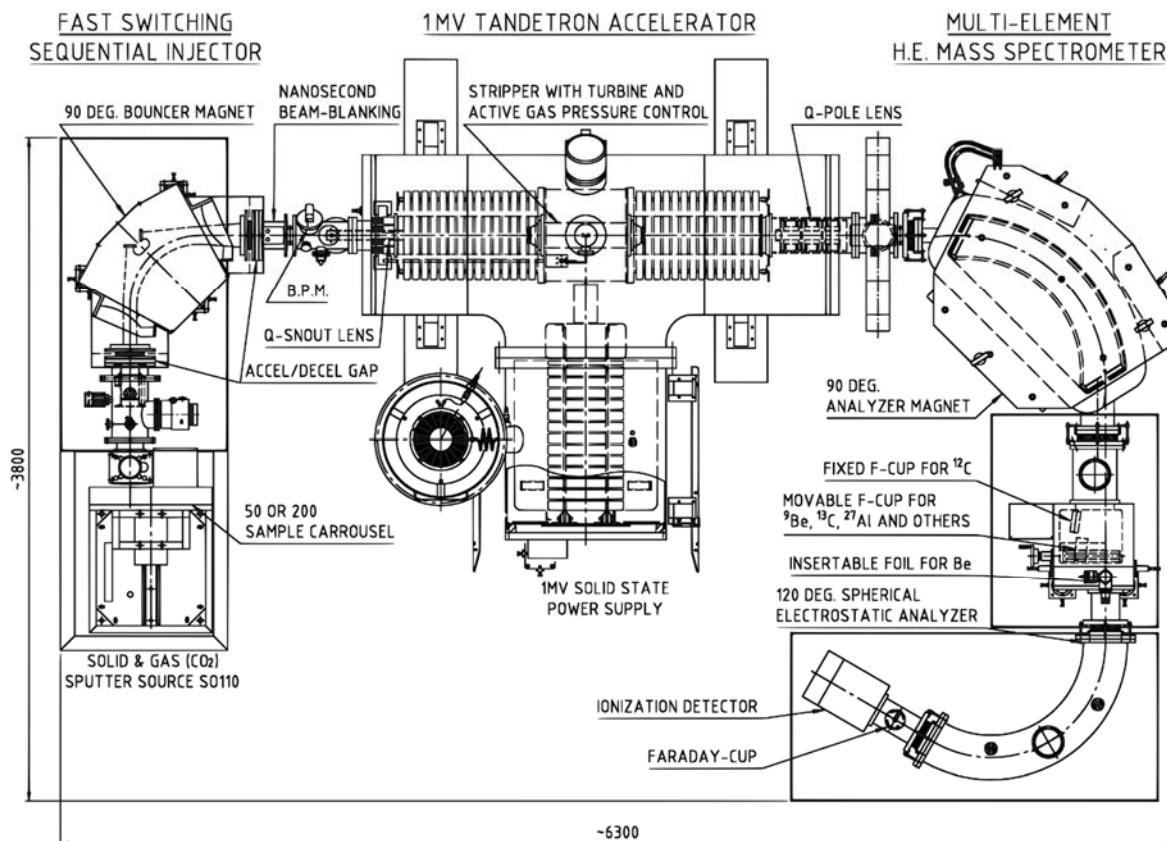


Figure. 2.13. Layout of the AMS system in NTNU laboratory, Trondheim (Klein et al., 2006).

The ionization gas used is isobutane, in which free electrons are produced as energetic ions travel through it. The ions lose their energy until they are stopped completely. The difference in the energy loss distribution along their track in the detector is used to tell apart the same mass and similar energy particles. This requires the two-anode system and the use of energy loss per track unit ( $dE/dx$ ) and total energy to identify  $^{14}\text{C}$  and eliminate background. The particle count rate, and the Faraday cup currents are used to calculate a ratio of  $\frac{^{14}\text{C}}{^{12}\text{C}}$  and  $\frac{^{13}\text{C}}{^{12}\text{C}}$  for samples and standard.

#### 2.4.5.4. Calculation of $^{14}\text{C}$ data

The calculation of a  $^{14}\text{C}$  concentration requires three separate measurements, i.e.  $\frac{^{14}\text{C}}{^{12}\text{C}}$  ratios of the sample for which a  $^{14}\text{C}$  decay age is desired; for the modern standard to define  $t = 0$  on the  $^{14}\text{C}$  timescale; and for the background to determine the contribution to the measured sample activity of “dead carbon” materials (Gillespie, 1984; Taylor and Bar-Yosef, 2014).

The measurement of  $\frac{^{14}\text{C}}{^{12}\text{C}}$  ratios has been discussed in the previous sections. The determination of  $^{14}\text{C}$  is made relative to a standard of known  $^{14}\text{C}$  concentration. The first modern radiocarbon standard was distributed by the National Institute of Standards and Technology (NIST), Gaithersburg, Maryland, USA, oxalic acid I ( $\text{C}_2\text{H}_2\text{O}_4$ ) or Ox-I, made from 1955 sugar beets (Stenström et al., 2011). Ninety-five percent of the activity of Ox-I, with a  $^{14}\text{C}$  isotope ratio of 105.26 pMC measured in the year 1950 and normalized to  $-19\text{‰}$   $\delta^{13}\text{C}$ , is equal to the measured  $^{14}\text{C}$  activity of 1890 wood, decay-corrected to 1950, and normalized to  $-25\text{‰}$   $\delta^{13}\text{C}$ , and is used to define a zero  $^{14}\text{C}$  age (Stuiver and Polach, 1977; Trumbore et al., 2016), by convention the Modern Standard. Having a  $\frac{^{14}\text{C}}{^{12}\text{C}}$  of 100 pMC (100 percent of the Modern Carbon Standard) defines the modern standard atmosphere. 1890 wood was selected as the standard of radiocarbon to represent pre-suess effect atmospheric  $^{14}\text{CO}_2$ .

By the late 1970s, the supply of the original oxalic acid had become depleted (Taylor and Bar-Yosef, 2014), and no longer commercially available. A substitute standard was prepared, oxalic acid II or Ox II (Mann, 1983), made from 1977 French beet molasses, with an isotope ratio of 134.07 pMC at  $-25\text{‰}$   $\delta^{13}\text{C}$ , distributed by the International Atomic Energy Agency (IAEA), Vienna, Austria. The isotope ratio of new-to-old Ox standard normalized to  $\delta^{13}\text{C}$ , defined as a conversion factor, has been used to correct Ox II to that of Ox I standard. The conversion factor is  $1.2736 \pm 0.0004$  (Mann, 1983), and adjusted to 1890 wood  $0.95/1.2736 = 0.7459$ .

The formula to calculate  $^{14}\text{C}$  concentration in percent modern carbon (pMC) is the following:

$$pMC = \frac{(R_{sample*})}{(R_{ox*})} * 100 \quad (2.10)$$

With:

$$R_{sample*} = R_{sample} \left[ \frac{\left(1 - \frac{25}{1000}\right)}{\left(1 + \frac{\delta^{13}\text{C}}{1000}\right)} \right]^2 \quad (2.11)$$

For Ox I standard, normalized to  $-19\text{‰}$   $\delta^{13}\text{C}$ :

$$R_{ox*} = 0.95 R_{ox\ I} \left[ \frac{\left(1 - \frac{19}{1000}\right)}{\left(1 + \frac{\delta^{13}\text{C}}{1000}\right)} \right]^2 \quad (2.12)$$

For Ox II standard, normalized to  $-25\text{‰}$   $\delta^{13}\text{C}$ :

$$R_{ox*} = 0.7459 R_{ox\ II} \left[ \frac{\left(1 - \frac{25}{1000}\right)}{\left(1 + \frac{\delta^{13}\text{C}}{1000}\right)} \right]^2 \quad (2.13)$$

Where  $R_{sample}$  is the  $\frac{^{14}\text{C}}{^{12}\text{C}}$  ratio of the sample,  $R_{ox}$  is the oxalic acid standard, and  $R_{sample*}$  and  $R_{ox*}$  are the respective values corrected for isotopic fractionation.

To express the absolute amount of  $^{14}\text{C}$ , the formula used as below (Trumbore et al., 2016):

$$\Delta^{14}C(\text{‰}) = \left[ \frac{\left(\frac{^{14}C}{^{12}C}\right)_{\text{sample}, -25}}{\left(\frac{^{14}C}{^{12}C}\right)_{\text{OxI}, -19} \exp\left(\frac{y-1950}{8267}\right)} - 1 \right] \times 1000 \quad (2.14)$$

#### 2.4.5.5. Correction for isotopic fractionation

Mass dependent isotopic fractionations come about naturally in the environment and in the laboratory and affect radiocarbon concentration. In the environment, for instance, the assimilation of CO<sub>2</sub> by plants or CO<sub>2</sub> exchange between the air and surface water, and in the laboratory, e.g. incomplete combustion or reduction (Mook and van der Plicht, 1999; Steinhof, 2016; Stenström et al., 2011). In any biological pathway, the lighter carbon isotopes are preferentially taken up (Bowman, 1990), because the heavier isotopes move slower. Therefore, the isotopes are subject to relative enrichment or depletion due to the different isotope reaction rates. The changes in the stable isotopic ratio,  $\frac{^{13}C}{^{12}C}$ , during the formation of the sample to be dated, give rise to a change in  $\frac{^{14}C}{^{12}C}$  ratio of about twice the magnitude (for simplification) reflecting the mass difference (Gillespie, 1984).

In order to eliminate fractionation effects to make inter-laboratory comparisons of different materials possible, conventionally, <sup>14</sup>C results of samples are normalized to a δ<sup>13</sup>C of -25‰ relative to PDB. Furthermore, the results of the oxalic acid standard are corrected to a δ<sup>13</sup>C of -19‰ PDB for Ox I and to δ<sup>13</sup>C of -25‰ PDB for Ox II (Mann, 1983; Mook and van der Plicht, 1999). The  $\frac{^{13}C}{^{12}C}$  ratio of the sample and the oxalic acid standard, which are measured by AMS simultaneously with the  $\frac{^{14}C}{^{12}C}$  ratio, are used for the correction. The value of <sup>13</sup>C of sample (s) and standard (r) are calculated as following:

$$\delta^{13}C(\text{‰}) = \left[ \frac{\left(\frac{^{13}C}{^{12}C}\right)_s - \left(\frac{^{13}C}{^{12}C}\right)_r}{\left(\frac{^{13}C}{^{12}C}\right)_r} \right] * 1000 \quad (2.15)$$

With:

$\left(\frac{^{13}C}{^{12}C}\right)_s$  is the measured stable isotope ratio of the sample, and  $\left(\frac{^{13}C}{^{12}C}\right)_r$  is the measured stable isotope ratio of the reference which is a Cretaceous carbonate, *Belemnita Americana* from the Pee Dee formation of South Carolina, known as PDB.

#### 2.4.5.6. Correction for background

The contribution of non-sample <sup>14</sup>C to routine sample <sup>14</sup>C concentration activity is estimated from a process blank. A process blank to determine the contamination introduced during sample processing is obtained by a sample of <sup>14</sup>C-free anthracite. Anthracite is a geological sample with infinite age and should contain no <sup>14</sup>C. The correction introduced by subtracting

the blank from the  $\delta^{13}\text{C}$  corrected  $^{14}\text{C}$  sample data, depends on the size of the  $\text{CO}_2$  sample obtained during the combustion or hydrolization processes, and on the age of the samples.

Two chemical graphite powders, i.e. a synthetic graphite with a  $^{14}\text{C}$  content equivalent to a  $^{14}\text{C}$  age of 50,000 years BP (0.2 pMC), and a natural based graphite with almost no inherent  $^{14}\text{C}$ , are used to test the machine background in Trondheim (Nadeau et al., 2015). The latter shows the stability of  $^{14}\text{C}$  measurement as well, with limited sensitivity due to its old age.

In the NTNU, Trondheim AMS laboratory, no machine blank is applied as the system is exceptionally clean and this effect is included in the measurement of the process blanks.

#### 2.4.5.7. Measurement uncertainty

The statistical uncertainty of  $^{14}\text{C}$  results is estimated based on the scatter of measurements of samples, Ox-standards, and backgrounds as well as on Poisson statistics (Stuiver and Polach, 1977). The uncertainty of measurements is described by a Gaussian probability function. The separate measurements are not expected to deviate from a true value by more than one standard deviation or one sigma ( $\pm 1\sigma$ ), which implies a 68.3 % probability that the true value lies between the  $+1\sigma$  and  $-1\sigma$  limits around the measured value.

#### 2.4.5.8. Calculation of the conventional radiocarbon age and the calendar age

The mathematical formulation for the calculation a  $^{14}\text{C}$  age (t) in years has been discussed in section 1.2.1, based on some assumptions outlined by Stuiver and Polach (1977). The final formula can be expressed as the following equation:

$$t = -8033 * \ln\left(\frac{R_{sample*}}{R_{Ox*}}\right) \quad (2.16)$$

With:

t : radiocarbon age (years before present, BP, where present is 1950 AD, as 0 years BP)

8033 : mean-life of  $^{14}\text{C}$  based on the original Libby half-life of 5568 years.

$R_{sample*}$ : the  $\frac{^{14}\text{C}}{^{12}\text{C}}$  ratio of the sample corrected for isotope fractionation (eq. 2.11)

$R_{Ox*}$ : the  $\frac{^{14}\text{C}}{^{12}\text{C}}$  ratio of the modern oxalic acid standard corrected for isotope fractionation (eq. 2.12, 2.13)

The equations above are based on some assumptions that were discussed in the section 1.2.1. The mean life of 8033 yr implies that 1% deviation will result in a variation of ca. 80 radiocarbon years. The radiocarbon years calculated are, actually, not equal to real time calendar years. The reason is that a) the Libby half-life of 5568 yr is too short;  $5730 \pm 40$  yr has been agreed upon as the recommended value (Godwin, 1962), and b) the concentration of atmospheric  $^{14}\text{CO}_2$  fluctuates through time as a results of changes in the production rate and in the global carbon cycle (Reimer et al., 2013). Therefore, in order to get the corresponding calendar years, the results in radiocarbon years are corrected using a calibration curve that relates the  $^{14}\text{C}$  age to the calender age obtained from known-age samples, e.g. from dendrochronology. By convention, the reported form of calendar age range usually

corresponds to  $\pm 1\sigma$  of  $^{14}\text{C}$  age. To cite calibrated radiocarbon dating results, the terms of cal BC, cal AD or even cal BP are recommended.

## Chapter 3

### 3. Characteristics of tropical soils in the research area

Soil properties have been suggested to influence deep carbon more than climate (Mathieu et al., 2015). Among of them, two factors, i.e. soil texture and mineral composition, pose important contributions in the context of their strong physical association to carbon dynamics (Feller and Beare, 1997; Han et al., 2016). They may explain the variability in carbon sorption exerted in different soil types (Mayes et al., 2011), and profile layers (Kothwala et al., 2008), dynamics to microbial accessibility (Gleixner, 2013), and dissolved organic carbon related enrichment (Gandois et al., 2014; Hagedorn et al., 2015). Therefore, it is suggested that the balance between input and output of carbon allows for several soil processes to make up the existing concentration of carbon.

To take into account these soil type-related processes, which are the key for soil carbon dynamics, this chapter will discuss some important soil characteristics in the study areas, i.e. grain size (section 3.1), soil reaction (pH) and salinity (EC) (section 3.2) and mineral compositions (section 3.3), to provide a framework for understanding soil carbon dynamics. In addition, the chemical structure of organic matter from top layers will also be discussed (section 3.4), since soil organic matter structure may provide insights in the context of plant litter compositions in combination with environmental condition, e.g. soil types, climatic factors (temperature and precipitation).

The climatic condition of the study areas will be summarized in this introduction. As lying around 6° N to 11° S and 95° to 141° E (Fig. 2.1), Indonesia generally has two main climate types, i.e. humid tropical, for example in Sumatera and Kalimantan, and monsoon in Java with a tendency to be flat all year-round (Tan, 2008). The annual seasons, i.e. the wet season between November and March, and the dry season between April and October, are driven by Australia and Asia continents.

The primary data collected from local meteorology stations nearby shows that in Perbawati, Sukabumi, the mean annual temperature ranged from 20.4 to 21.8 °C with rainfall from 2300 to 4600 mm/year (data 2001-2010), while Jasinga, Bogor, has a mean annual temperature within the range of 25.5 to 26 °C with annual precipitation from 1890 to 3900 mm/year (data 2001-2010), and in Ploso Lor, Ngawi, East Java, the mean annual temperature (data 1973-1992) is a bit higher at 26.6 °C (Amien et al., 1996) with precipitation ranged from 1470 to 4040 mm/year (data 2006-2014). Grouping the region using Schmidt-Fergusson classification based on precipitation data, by comparing the averaged dry months (< 60 mm) over wet months (>100 mm) to get the quotient value Q (Tan, 2008), results in two distinguished climatic zones, i.e. zone A (Sukabumi and Bogor) with Q = 10.78% and 9.57% respectively, and zone C (Ngawi) with Q = 59.38%. These indicate that zone A is a wet region, while zone C is a monsoon region with more sharp dry seasons (Appendix 2.2).

#### 3.1. Grain size distribution

Parent materials play a crucial role in the soil formation in Indonesia (Tan, 2008), and in the inherited soil characteristics. They influence grain size variability through inheritance,

mechanical weathering, deposition, and neof ormation of clay (Birkeland, 1999), pointing to soil forming processes that take place in the soil column.

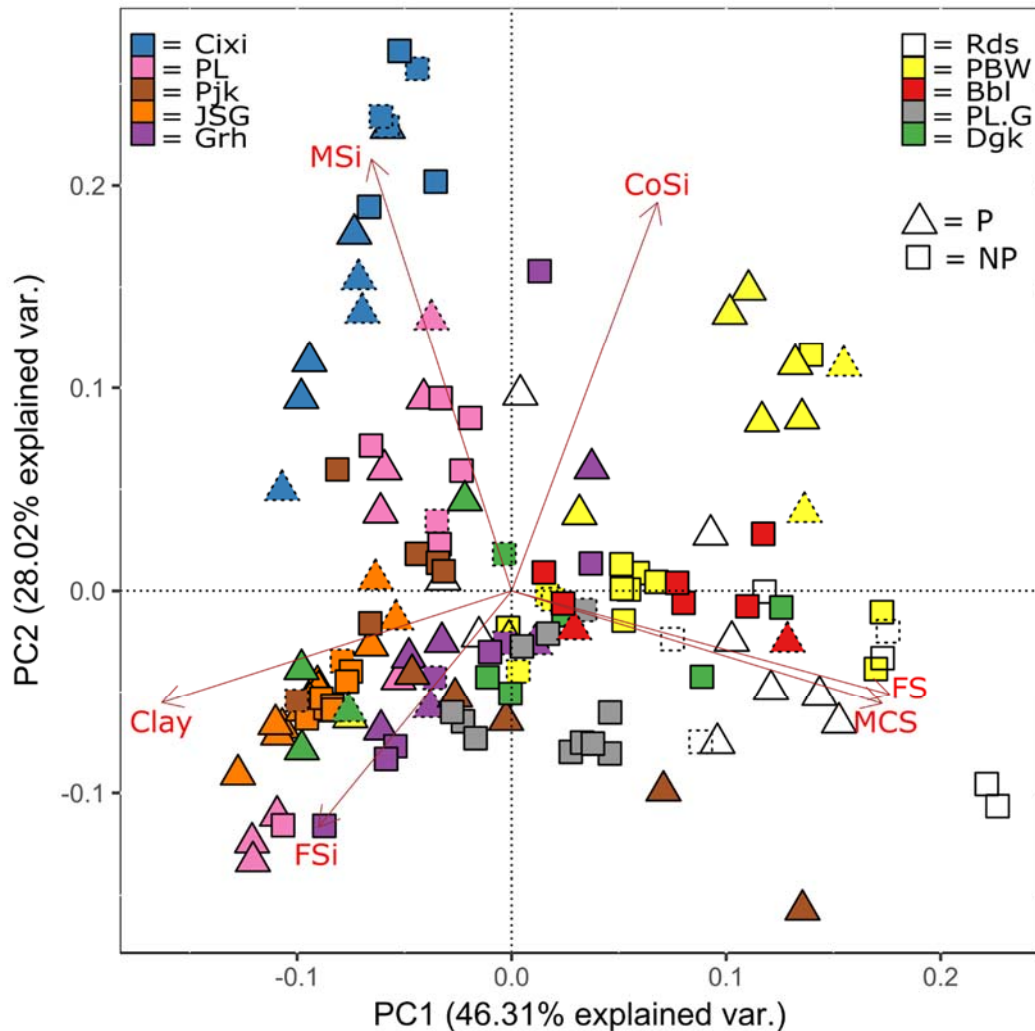


Figure. 3.1. Loadings of 6 classes soil fractions defined by PC1 and PC2. Data set from point samples (Appendix 3.1). Markers with dotted and solid border are topsoil (< 30 cm depth) and subsoil (>30 cm depth).

Due to the high complexity of soil properties, grain size composition will be presented according to parent material composition as a framework to make discussion simpler. They are grouped into four types, namely, extrusive igneous rocks (PBW, Rds) – type 1, i.e. volcanic ash, lahar; intrusive with combination extrusive igneous rocks (JSG) – type 2, sedimentary rocks (Bbl) – type 3, and alluvial materials (PL, Dgk, Pjk, Grh, Cixi) – type 4. As situated in different landforms with different inherent mineral compositions, each profile may pose a different regularity in view of the distribution of mineral soil particles.

Grain size compositions were analysed in the laboratory as discussed in the preceding Chapter (section 2.4.1). To facilitate data interpretation, principal component analysis (PCA) was

performed (using package PRCOMP in R Studio 1.1.414). It is a multivariate statistical method with central aim of reducing the dimensionality of data set while retaining as much of the original variation as possible (Buurman et al., 2008; Everitt and Hothorn, 2011). To get strong correlations among variables, in this analysis the significant factors with eigenvalues that exceed one are retained (McKillup and Dyar, 2010). The PCA of grain size data shows the two principal components, PC1 and PC2, account for 74% of total variation in the original variables (Fig. 3.1; Table 3.1). Clay and sand fractions explain most of the grain size composition in the study area (Table 3.1).

Type 1 (PBW, Rds) is characterized by grain size compositions shifted towards sand fractions, to the right of plot space (Fig. 3.1). They exhibit the most irregularity as a function of depth, which is typical of volcanic regions (Dames, 1955). Coefficient of variation (CV) shows values of up to ca. 60% for depth clay distribution, and of up to ca. 40% for depth sand in the soil columns (Table 3.2). As situated on the upper to middle slope of volcanoes the influence of frequent deposition and reworking of volcanic materials (ashes, lahar) may have existed.

From the plot (Fig. 3.1), grain size compositions in PBW are clustered toward in between sand and coarse silt fractions at one hand, and toward more fine fractions, i.e. fine- and medium + coarse fractions, fine silt, clay on the other hand. The difference in grain size compositions pose a difference in parent material composition in two locations observed, i.e. P and NP sites. The coarser soil fractions may have related to the P site (Appendix 3.1; Fig. 2.4) which is situated at ca. 100 m lower altitude than NP. In the profile of PBW-P, the increase in clay content below 30 cm depth has shifted the textural class from silt loam into silty clay loam with concomitant mineral composition (section 3.2) and carbon origin (section 4) changes (Appendix 3.1; Fig. 2.4). This layer inhomogeneity can be explained as the different origin of volcanic materials. In the neighbouring profile in NP site, the grain size composition at depth (below 30 cm) is characterized by the increase in sand particles without any effect to textural class changes, i.e. silt loam at throughout soil column.

Table. 3.1. Loadings of first two principal components grain size compositions.

	PC1 (46.31%)	PC2 (28.02%)
Clay	-0.50	-0.17
Fine silt	-0.28	-0.36
Medium silt	-0.20	0.66
Coarse silt	0.21	0.59
Fine sand	0.55	-0.16
Medium+coarse sand	0.53	-0.17

Rds plot (Fig. 3.1) shows a single cluster of values, this points out a similarity in grain size compositions of P and NP profile. Some layers may occur at the factor space towards silt fractions (P site), while other layers are clustered around sands (NP site) (Appendix 3.1). The significant increase of sand fractions below 50 cm (P) and 25 cm (NP) depth (Fig. 2.5; Appendix 3.1) brings about the changes in textural class from silt loam into loam, and into sandy loam respectively. The high sand fractions amount to 30-40% at depth is related to the high abundance of undecomposed coarse volcanic materials.

Type 2 (JSG), is characterized by grain size compositions explained by clay, and fine silt (Fig. 3.1) with a regular depth pattern (Fig. 2.3), which leads to some indications that they have developed on stable environment with homogeneous parent material. In-situ weathering may be more pronounced than the addition from deposited materials which is made possible by flat topography conditions. As clustered together (Fig. 3.1), JSG-P and -NP may have similar grain size compositions. The distribution of clay with CV values of < 15% indicates a low variability throughout profiles, while for sand has a CV of ~11% in NP and ca. 36% in P (Table 3.2). JSG records the highest clay content within the range 37.58 – 48.84% (Fig. 2.3; Appendix 3.1), and all categorized as silty clay.

In type 3 (Bbl), grain size composition can be explained at the factor space close to sand fractions (Fig. 3.1). Both P and NP occur at the space around type 1 to indicate their similarity in the compositions. The CV close to ca. 30% for depth clay and sand fractions may show a quite high in profile variability (Table 3.2). Different to type 1, grain size compositions in Bbl may depend on two origins, i.e. in-situ weathering of sedimentary rocks at the bottom, and ex-situ materials deposited at the top layers from eroded surrounding upper hills, or fly ash from nearby volcanoes. The effect of volcanic ash may be minimized considering the distance of location to the closest volcanos, i.e. Mt. Pandan (897 m) ca. 20 km to the southeast (no records of eruption was found), and Mt. Lawu (3265 m) ca. 60 km to the southwest (last eruption 1885). The dominant sandstone-derived soil particles add up to the increase of sand contents at bottom layers up to ca. 40%. These increases have shifted silt loam at the top layers into loam in P site, yet it does not affect all silt loam texture in NP site.

In type 4 (Grh, Pjk, Dgk, PL, Cixi), situated at lower slope the soil particles are mostly alluvial. Coefficient of variation may indicate less variability of clay (CV ca.  $\leq 20$ ) but with more variability for sand (CV up to ca. 50%) throughout profiles. At ca. 70 - 80 m a.s.l with better drainage condition, i.e. Grh, and PL, soil structure has been developed as revealed during observations. Going down to the lower level at river banks (50 – 60 m a.s.l), i.e. Pjk, and Dgk, the weathering intensity may slow down with structure-less profile composition as influenced by active deposition of fluvic materials. Cixi is an exception, though just standing at 5 m a.s.l nearby the sea, the structure development in the profile is promoted (Kölbl et al., 2014).

All these areas in type 4, except in Cixi which is mostly towards medium silt, plot in multiple directions in factor spaces (Fig. 3.1), mostly to the left correspond to clay, fine-, and medium silt fractions. In Cixi, the dominance of silty clay loams means that additional fine-sized particles come from mechanical weathering. A slight difference in grain size compositions between P and NP sites may have occurred (Fig. 3.1; Appendix 3.1). In PL, the most texture class of layers are silt loam with exception in the top soil of the P site (Appendix 3.1), of which the clay content is higher and classified as silty clay loam. The grain size compositions between P and NP are partly similar as pointed out from the plot at the space towards medium- and fine-silt (Fig. 3.1). The garden plot in PL site (PL.G-NP) shows a bit different grain size composition to the neighbouring P and NP sites. The coarser soil fractions in PL.G-NP may be related more to the field variability than agriculture effect in P and NP sites.

Standing at approximately the same altitude ca. 80 m a.s.l on different slopes, both PL and Grh pose different grain size compositions. Grh at the Mt. Lawu slope (Fig. 2.1), shows quite

coarser than PL. Plots of Grh are located at the centre mostly towards fine silt (Fig. 3.1), and characterized by homogeneity in the profile composition with silt loam as texture classes (Appendix 3.1).

In Pjk and Dgk, irregular fluvial patterns of up and down of grain size compositions are observed in the soil columns (Fig. 2.7; Fig. 2.8). The classified silt loam exists throughout profiles with exception below 98 cm depth in Pjk-P at which sand contents increased significantly to make up a loam textural class (Appendix 3.1). Grain size compositions vary between sites as some scatter from left to the right in the factor space, and some clusters mostly to clay variable (Fig. 3.1). Similarly, Dgk shows some plots scattered from centre of plot to the right, towards sand fractions, and some mostly to the left, around clay, fine-, and medium silt (Fig. 3.1).

### 3.2. Soil reaction (pH) and alkalinity (EC)

Principal component analysis shows a strong relationship between soil pH (H<sub>2</sub>O) and parent material (PC1 in Table 3.3; Fig. 3.2). The pH is higher in the soil of Ngawi, East Java, study sites, mainly in the alluvial plain of the lower slope of Mt. Lawu (Grh and Pjk), and Kendeng ridge (Dgk, PL, and Bbl) than in the soil of Bogor and Sukabumi, West Java (JSG and PBW). This high pH may indicate either the alkaline origin of parent materials or the accumulation of highly soluble basic minerals through leaching from the upper slopes (Fig. 2.2 to 2.9; Appendix 3.1; Appendix 3.2). The variability of soil pH in the soil columns are quite low with CV below ca. 10% across soil types (Table 3.2).

In the East Java sites, data show pH values of  $7.07 \pm 0.25$  (P) and  $6.70 \pm 0.30$  (NP) in Rds,  $7.63 \pm 0.28$  (P) and  $7.52 \pm 0.55$  (NP) in Grh profiles,  $7.31 \pm 0.66$  (P) and  $8.37 \pm 0.17$  (NP) in Pjk profiles,  $8.01 \pm 0.11$  (P) and  $8.55 \pm 0.15$  (NP) in Dgk profiles,  $7.3 \pm 0.81$  (P),  $7.9 \pm 0.38$  (NP) and  $7.75 \pm 0.19$  (G) in PL profiles, and  $7.31 \pm 0.01$  (P) and  $7.03 \pm 0.13$  (NP) in Bbl profiles. These data may suggest the presence of a high amount of basic cations, i.e. Na, Mg, K, and Ca in the soil as XRF analysis for PL samples (P and NP) has confirmed (Appendix 3.1; Appendix 3.2).

For West Java profiles, soil pH values were  $5.50 \pm 0.54$  (P) and  $6.10 \pm 0.65$  (NP) in PBW profiles and  $4.90 \pm 0.59$  (P) and  $5.20 \pm 0.12$  (NP) in JSG profiles. This low pH may associate with the strong presence of Al, Fe, Ti and Zr in the soil as indicated by principal component analysis (Fig. 3.2). In JSG with Alisol of high abundance of kaolinite (Winkler et al., 2016), the presence of all these minerals may indicate a high level of soil weathering. Under oxic condition, all these minerals are typically residual after the leaching away of soluble part of minerals (Birkeland, 1999).

In the Ngawi study areas, the lateral flow of basic cations may follow a toposequence as pH values increase above 8 at foot-slopes (Pjk of Mt. Lawu slope and Dgk of Kendeng ridge slope). Soil pH tends to increase with depth corresponding with the carbonate accumulation in the profiles (Appendix 2.3). The carbonate bound to minerals in the profiles shows as greyish-greenish spots in the alluvial subsoil, e.g. in PL (G), with pH values higher than the corresponding darker sample from the same depth.

Table. 3.2. Coefficient of variation<sup>17</sup> (%) of depth soil texture, pH, EC and elemental compositions in the soil columns.

Site	Soil texture			pH (H <sub>2</sub> O)	EC	Si	Al	Fe	Mn	Ti	Zr	Na	Mg	K	Ca
	Clay	Silt	Sand												
PL-P	24.1	13.2	40.7	11.03	31.72	1.22	2.31	3.62	6.47	3.33	7.67	6.38	7.04	5.57	4.51
PL-NP	25.5	9.9	31.5	4.85	36.59	0.69	1.32	1.79	10.85	5.83	4.18	4.22	2.43	1.87	2.25
PL-G	6.64	7.55	22.01	2.51	58.43	nd									
JSG-P	14.73	9.93	36.17	12.1	124.16	7.06	10.91	13.44	43.93	5.31	3.44	26.91	24.81	28.77	42.88
JSG-NP	7.09	4.67	11.06	2.28	36.08	1.82	5.88	5.56	18.38	3.35	2.78	25.01	19.28	28.22	45.07
PBW-P	61.8	6.2	32.4	9.81	97.03	5.22	9.69	36.25	47.32	10.09	9.52	9.82	9.31	7.62	15.83
PBW-NP	25.9	10.1	29.8	10.62	53.3	18.67	12.73	22.58	21.3	19.06	15.09	13.79	12.56	17.08	23.2
Rds-P	50.41	16.98	42.43	3.54	15.39	nd									
Rds-NP	56.72	18.85	25.91	4.5	67.24	nd									
Grh-P	17.64	4.68	24.45	3.68	19.6	nd									
Grh-NP	21.2	5.51	30.01	7.28	40.97	nd									
Pjk-P	15.7	19.14	54.62	9.01	41.1	nd									
Pjk-NP	17.66	5.51	41.76	2.05	9.45	nd									
Dgk-P	7.66	2.38	32.02	1.35	12.24	nd									
Dgk-NP	18.85	4.68	28.98	1.8	15.8	nd									
Bbl-P	33.07	9.07	32.38	0.14	9.21	nd									
Bbl-NP	21.6	5.24	24.12	1.79	33.59	nd									

<sup>17</sup> Coefficient of variation (CV) defines scatter of the data points around the average without removal of any trends with depth.

Corresponding to soil pH, the electrical conductivity (EC) exhibits higher values in the East than in the West Java study sites (Appendix 3.1). EC shows a higher depth variability up to more than 100% as in JSG-P (Table 3.2). The significant increase in EC at plow layers may result from agricultural inputs, for instance manure and mineral fertilizer, while at depth it may be related to the accumulation of salts. An analysis ( $N=111$ ,  $P\leq 0.01$ ) shows a significant correlation between EC and Na ( $r=0.48$ ), Mg ( $r=0.63$ ), K ( $r=0.56$ ), and Ca ( $r=0.67$ ).

In East Java, data show EC values of  $31.89\pm 4.91$  (P) and  $54\pm 36.31$  (NP) in Rds,  $136.37\pm 26.79$  (P) and  $83.63\pm 34.26$  (NP) in Grh profiles,  $89.40\pm 36.74$  (P) and  $115.67\pm 10.93$  (NP) in Pjk profiles,  $346.25\pm 42.39$  (P) and  $233.83\pm 36.94$  (NP) in Dgk profiles,  $234.8\pm 74.48$  (P),  $396.30\pm 144.97$  (NP) and  $524.90\pm 58.43$  (G) in PL profiles, and  $76\pm 7$  (P) and  $52.17\pm 17.53$  (NP) in Bbl profiles (Appendix 3.1). Data suggest the lower EC values at Rds and Bbl than at the lower slopes (alluvial soils).

For West Java profiles, soil EC values were  $73.5\pm 71.34$  (P) and  $133.4\pm 71.12$  (NP) in PBW profiles and  $124.3\pm 154.33$  (P) and  $40.4\pm 14.59$  (NP) in JSG profiles. The effect of agricultural practices to the EC may be observed in P as the variability is significantly high both in PBW and JSG.

In the Ngawi toposequence, the EC was higher in the soils on Kendeng ridge slope than on Mt. Lawu slopes. These two slopes are separated by the Madiun river going north to the Solo river at the west of Ngawi. At the bottom of slopes, EC values reach  $400\ \mu\text{S}/\text{cm}$  in Dgk, while at comparable level of Mt. Lawu slope at Pjk the EC was up to  $130\ \mu\text{S}/\text{cm}$ . In addition, at around 150 cm depth in PL-G profile, EC shows an increase up to ca.  $1000\ \mu\text{S}/\text{cm}$  (~50 times lower than sea water EC level). These may have supported the idea of the influence of marine sediment derived from the Kendeng ridge formation on the soil development on this slope. Strong signals of salts were not identified from sedimentary Bbl samples which developed on the “Kerek” formation at the top of ridge. The source of black clays, which is supposed to be marine clays, is “Putjangan” formation at the bottom of the ridge (van Bemmelen, 1949).

### 3.3. Elemental compositions

Soil elemental compositions, either released from in-situ or ex-situ parent materials, determine the type of clay formed under environmental regulations, e.g. climate (Birkeland, 1999). As discussed earlier in this Chapter, clays play a crucial role for soil physical carbon stabilization. Their associations can enhance carbon storage through sorption or occlusion within aggregates (Han et al., 2016; Kögel-Knabner et al., 2010), and control the accessibility to microbial decomposition (Gleixner, 2013). The balance (input/output) of carbon distributed in the soil columns however determines the concentration of both total carbon and radiocarbon (Chapter 4).

Elemental composition data obtained from laboratory analysis (section 2.4.2) is further evaluated using principal component analysis as preceding discussion (section 3.1). Three extracted factors (PC1, PC2, and PC3) account for 89.41% of the total variation in the original variables (Table 3.3) after two outliers were eliminated. The remaining variation, ca. 10.59%, is attributable to random variation as a result of field variability and analytical errors (Buurman et al., 2008). With the outliers eliminated the principal component analysis gave a total

variation for three factors of 86.90% which is not significantly different from the post-elimination (robust).

PC1 points to a positive association of Ca, Mg, pH (H<sub>2</sub>O), Na, K, and Si, and a negative of Ti, Al, Fe, Zr (Table 3.3; Fig. 3.2). As corresponds to bases minerals, PC1 is likely interpretable as parent material composition. PC2 > ± 0.3 loadings are explained by TOC, TON, and P which is obviously the signature of soil organic matter (Fig. 3.2). Since all these variables exist at the PBW plots with a strong character of volcanic soils (Winkler et al., 2016), their high values may be related to the high fixation capacity of the soil. PC3 with > ± 0.3 loadings allows for positive correlation between Si and Zr, and negative association of Mn, Fe, and Al (Table 3.2), and reflects parent material compositions. The variables of Mn, Fe, and Al, are in factor space towards PBW (Fig. 3.2). The strong association of these variables in volcanic soils (PBW) may point out the level of crystallinity of clay minerals.

As discussed before, two groups exist in the space defined by PC1 and PC2 (Fig. 3.2). The first group consist of base minerals (called type A for simplicity), i.e. Ca, Mg, Na, K, and Si. These plot to the right in mutual dependence with pH (H<sub>2</sub>O). The second group exists to the left of plot, in opposite direction to pH (H<sub>2</sub>O), with a number of acid mineral members, i.e. Ti, Al, Zr, and Fe (called type B). In the middle of the plot, with some individual values close to type B, is PBW (Fig. 3.2). Individual values in P site that are more away from type B may show a different parent material composition, while some individual values in NP site that closer can be considered more similar to type B.

Table. 3.3. Loadings of first three principal components elemental compositions, TOC, TON, and pH.

	PC1 (54.17%)	PC2 (23.42%)	PC3 (11.82%)
Si	0.28	-0.09	0.37
Al	-0.26	0.07	-0.47
Fe	-0.21	-0.23	-0.48
Mn	0.19	-0.11	-0.49
P	-0.12	0.49	-0.14
Ti	-0.31	-0.21	0.11
Zr	-0.25	-0.27	0.29
Na	0.33	0.17	-0.08
Mg	0.34	-0.01	-0.08
K	0.33	0.14	-0.12
Ca	0.35	-0.01	0.03
TOC	-0.11	0.50	0.09
TON	-0.13	0.49	0.08
pH (H <sub>2</sub> O)	0.33	-0.10	-0.10

Given that PC1 is explained by parent material compositions, it is assumed that pH (H<sub>2</sub>O) dependence of type A and type B groups is associated with soil parent material. Strong bases character of type A parent materials, which was reported as marl (Prasetyo, 2007), in combination with poor drainage conditions and low leaching capacity may have created a specific environment that promotes the alkalinity. The high amount of Ca at 2-3% in the profiles, with corresponding Ca/Mg ratio 2-3, indicate this. As comparison, in the more acid

condition with volcanic materials as dominant parent rocks, e.g. P site in PBW, the content of Ca is less than 1% and Ca/Mg ratios mostly < 1, except in PBW-P where Ca/Mg can reach up to 2.7. As developed on an alluvial plain, Ca-rich materials must have been deposited from the hills to the north (section 2.1.1.1). The large effect of basic parent material on soil properties may be noticed through the high correlation of variables Ca, Mg, Na, K, and Si in PC1 (Table 3.2). The smectites have been reported as majority clay minerals in this environment (Winkler et al., 2016).

Type B mineral compositions show a dominance of volcanic derived materials, which is considered as intermediate type materials (Wibisono et al., 2016). The soil pH (H<sub>2</sub>O) is opposite to type A, which means that most basic cations, e.g. Ca, Mg, Na, K, likely have been leached. The pronounced acid cations as result of intensive leaching may indicate good drainage conditions. In this more weathered condition, the dominance of a kaolinitic clay type has been reported (Winkler et al., 2016).

As mentioned before, the P site of PBW is associated to type A nor B, and can be considered having a different parent material origin. Soil in the NP site at 110 m higher than this point shows more development as it poses a similarity with profiles at JSG on lower slope ca. 240 m a.s.l.

Consequently, the soil development in this climatic region (zone A-Schmidt-Fergusson) may go from PBW-NP site toward the left to JSG. The promoted acid minerals, with concomitant high soil acidity, in type B may thus point out their relation to soil development. In other words, soils in JSG are weathered at higher level.

From PCA plot (Fig. 3.2), top and subsoil individual values at PL overlap partly in factor space grouped according to the landuse (P, and NP), close to pH variable defined to PC1. As increasing with depth, subsoil pH may not be influenced by agricultural practices (Fig. 2.2). The less strong signal of pH in top layers (Fig. 3.2) is likely the result of acidification after fertilization, e.g. urea. The enrichment of subsoil Ca in all profiles is possibly partly contributed by shallow groundwater (Tan, 2008), which is at ca. 100 cm depth. It is suggested that intensive capillarity exists during dry periods. Groundwater pH measured at ca. 7 (section 2.1.2.5) may indicate a considerable amount of soluble salts.

In the JSG site, different from other soils, the columns are characterized by Ti contents generally exceeding 1% all over the layers. Landuse-based grouping the individual samples in the PCA plots shows a similarity of variables, as they are clustered nearby, toward Al (for top layers), and Ti and Zr (for sub layers) in Fig. 3.2a, and towards Ti and Zr for both top- and subsoil in Fig. 3.2b. As both minerals are insoluble, however, their existence in the layers is typically for nearby mineral sources (Birkeland, 1999). This indicates the similarity of parent materials of the two sites, in accord with the position of the NP sites immediately adjacent to the paddies.

The negative correlation of Ti to PC1 means that it remains in the soil when most of salt minerals, that occurred to the right of the PC1 plot (type A), have been leached away. On the other hand, Zr defines most of PC3 scores and associates with top layers especially in the JSG-P site.

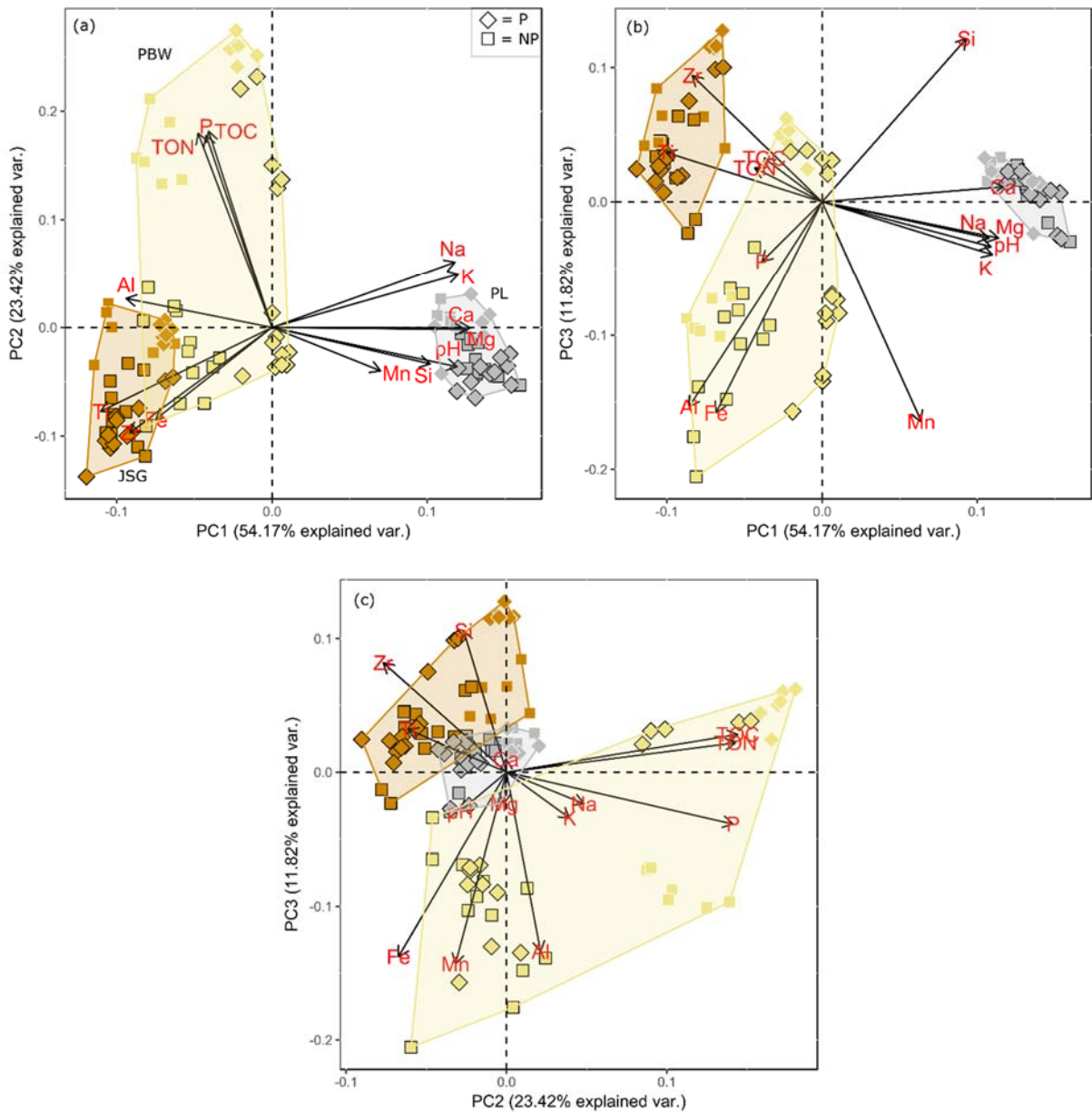


Figure 3.2. Loadings of elemental compositions, TOC, TON, and pH (H<sub>2</sub>O) defined by PC1 and PC2 (a), PC1 and PC3 (b), and PC2 and PC3 (c). Markers with white and black border are top soils (0-25 cm depth), and subsoils (below 25 cm depth). Data set from bulk samples with removing the outliers (Appendix 3.2).

Being associated with medium to coarse silt (Heymann et al., 2013; Kylander et al., 2011), the high abundance of Zr at top layers may be related to grain size composition (Fig. 2.3).

Soils in PBW are characterized by high soil organic matter stocks as defined to PC2 in the top layers. The two sites (P, NP) are characterized as non-overlapped, and clearly separated at the factor space in PC1 (Fig. 3.2). In addition, there is a clear separation between upper- and deep layers of P and NP in PC2, and of P in PC3. It is suggested that field variability may explain this variation as they are situated in different altitude (Table. 2.1). Instead, subsoil layer compositions of NP are more similar to soil in JSG for some minerals, i.e. Al, Ti, Fe, and Zr (Fig. 3.2a). The layer composition heterogeneity, both spatially and temporally, are typical in the region such as volcanoes (Dames, 1955). To PC3 loadings, Al, Fe, and Mn define the most variability. Individual samples of NP site occur towards Al and Fe, while samples of P sites exist mostly close to Mn. Amorphous clay minerals are in high abundance in this region (Winkler et al., 2016).

As discussed earlier (section 3.1), grain size compositions are slightly different between above and below ca. 35 cm depth in P column. Below it clay is a bit higher, and has different organic carbon composition (Chapter 4). The  $^{14}\text{C}$  content of humic acids at ca. 35 cm depth,  $111 \pm 0.36$  pMC, shows an atmospheric origin different from the 2012  $^{14}\text{CO}_2$  level which is 103 pMC. This may indicate that this layer, bottom of second puddle layer, was in direct contact with atmosphere in the past. Its properties and those of the immediately underlying “second puddle layer” differ substantially from those of the profile below 35 cm and suggest a profile discontinuity.

The higher clay content in old layers (below 35 cm depth) corresponds to important increases in Fe, Mn, Ti, and pH (>6), and decreases in Si, P and Ca contents (Appendix 3.2). From this point, it is quite clear that the two layers have a different origin of materials since the residual element like Ti tends to be retained in the layer. Assuming that the point at ca. 35 cm depth of new layer is 0 cm depth of old layer, thus the significant increase in Fe and Mn at ca. 5 – 20 cm depth of old layer (Fig. 2.4; Appendix 3.2) may be the results of alternating oxic-anoxic processes that happened in the past since these cations are mobile in the reduced condition.

In contrast to PL, the negative relation of Ca with pH in this site indicates a different origin of Ca. Some primary minerals identified, e.g. augite and labradorite (Wibisono et al., 2016), are potential sources for Ca in the soils. The higher Ca content in the new layer’s parent material (above 35 cm depth) than the old layer (Fig. 2.4; Appendix 3.2) is related to the nature of parent rock composition, as field information did not indicate any important Ca inputs due to agricultural practices (Dieterich, 2012). The new layer is observed to be more silicious than the old layer with special attention to 0 – 22 cm depth in which Si/Ti ratios are up to 35, significantly higher than any other old layers (< 28). The high ratios on top soil may be related to external input of Si, e.g. agricultural practices.

### 3.4. Organic matter characteristics

Soil organic matter responds differently to any environment conditions, mainly, in view of high variation in the quality of litter inputs and soil types. Litter inputs determine their variation in terms of chemical compositions (Kögel-Knabner, 1997), while soil types pose specific conditions typical of parent material and environment, i.e. climate conditions and topography,

on which the weathering takes place. In this discussion, the study area will be characterized through structure identification of organic compounds making use of  $^{13}\text{C}$ -NMR spectral analysis. The advantage of this tool is that it allows us to examine decomposition related chemical changes of soil organic matter (Baldock et al., 1997; Preston et al., 2009). As described earlier (section 2.4.4),  $^{13}\text{C}$  NMR analysis was performed in TUM, Munich by analysing humic acid samples.

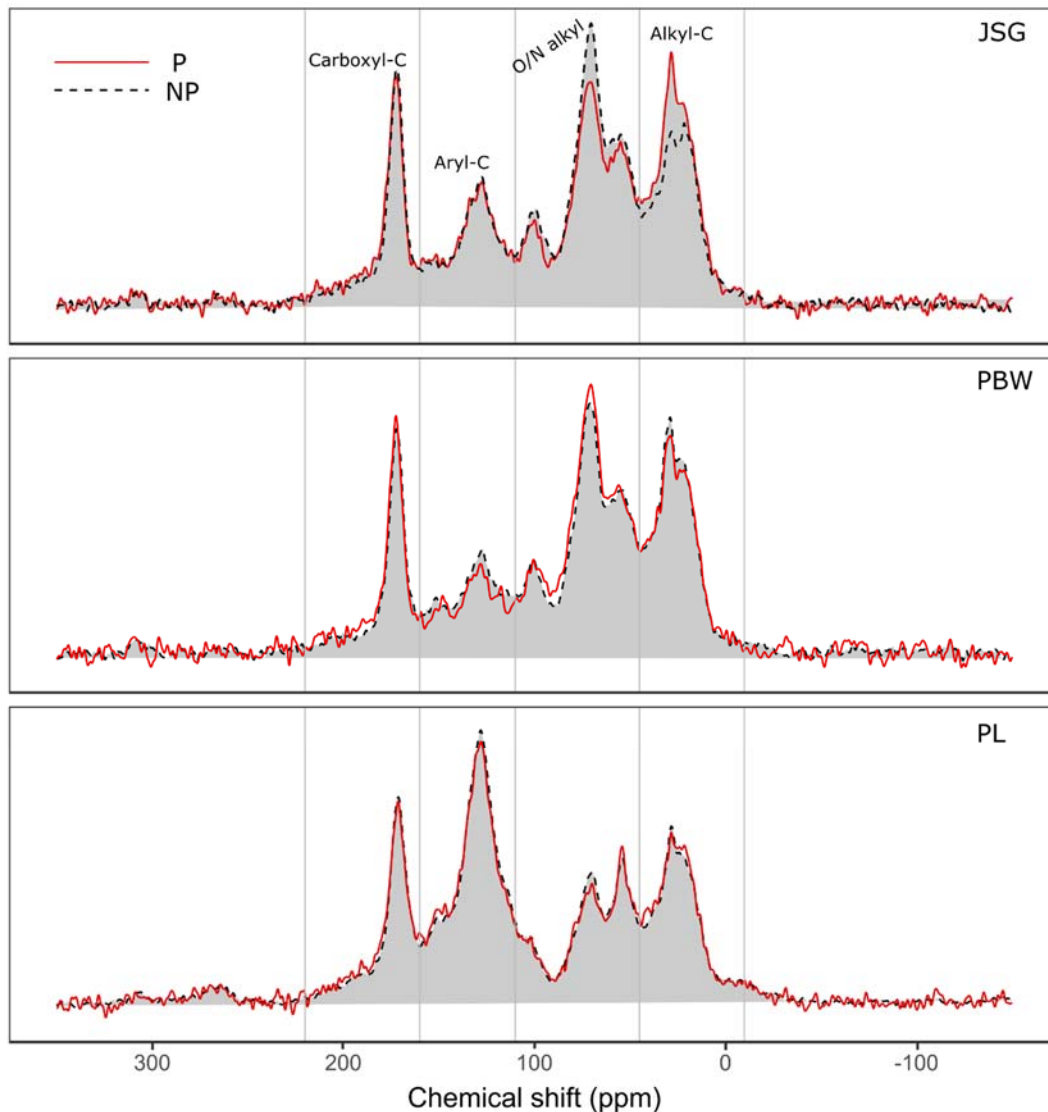


Figure. 3.3. Solid state  $^{13}\text{C}$  nuclear magnetic resonance spectra of top soil humic samples of P and NP.

Similar to grouping for mineral compositions (section 3.2), two types of specific organic structures are identified as type A (PL), and type B (PBW, JSG). In the principal component analysis plot defined to PC 1 and PC2, the first type mostly occurred at the space to the left, while the second type close to the middle of plot towards to the right. In the type A, soils at PL, are characterized by a high proportion of aryl-C identified as aromatic components. It exists at frequency of 110 – 160 ppm defined by broad resonances, and accounts for ca. 35% of total components. Aryl-C associates with char (Fig. 3.4), which is poorly degradable. In type B, the

structure of organic compounds are characterized by high proportion of O-alkyl-C occurred at frequency 45 – 110 ppm, and accounts for ca. 40% of total component in the spectral regions (Fig. 3.3). This compound associates with carbohydrate (Fig. 3.4), which is more easily degradable.

Alkyl-C compounds tend to be more resistant in the soil than O-alkyl-C, so their ratios get higher along the decomposition stage. The high proportion of O-alkyl-C compared to alkyl-C in type B samples may thus indicate that the decomposition of organic matter is still in progress (Table 3.3). On the other hand, higher levels of decomposition in type A samples were observed since the difference between O-alkyl-C and alkyl-C is getting smaller (Table 3.3). It is suggested that the difference in these decomposition stages may be strongly driven by soil type as well as climatic condition. The <sup>13</sup>C-NMR spectra may reflect the large quality heterogeneity of organic inputs as result of different field agricultural management and seasonal crop rotations (Table 2.1), therefore samples obtained from P and NP plots are not comparable to study the effect of plant litter inputs.

Table. 3.4. Integral of the <sup>13</sup>C NMR chemical shift regions of humic.

Site	alkyl-C (0-45 ppm)	Spectral region (integration)				carboxyl-C (160-220 ppm)	$\frac{\text{Alkyl - C}}{\text{O alkyl - C}}$	$\frac{\text{Aryl - C}}{\text{O alkyl - C}}$
		N- alkyl/meth oxyl, O- alkyl (45- 95 ppm)	O <sub>2</sub> -alkyl (95-110 ppm)	Aromatic (110-145 ppm)	O- aromatic (145-160 ppm)			
		O alkyl-C (45-110 ppm)	aryl-C (110-160 ppm)					
JSG-P	28.82	32.51	4.89	13.68	3.29	16.81	0.77	0.45
		37.4		16.97				
JSG-NP	24.38	37.3	5.65	13.78	3.02	15.87	0.57	0.39
		42.95		16.8				
PBW-P	27.28	37.59	5.5	10.34	3.08	16.21	0.63	0.31
		43.09		13.42				
PBW-NP	27.98	35.34	5.58	12.28	3.5	15.32	0.68	0.39
		40.92		15.78				
PL-P	22.55	21.1	4.34	28.62	6.19	17.2	0.89	1.37
		25.44		34.81				
PL-NP	22.04	21.52	4.54	29.71	5.77	16.42	0.85	1.36
		26.06		35.48				

The type A samples rich in both alkyl-C and aryl-C relative to O-alkyl-C (Fig. 3.3) can also be derived from external inputs, as high abundance of char materials associated with black carbon was reported in this area, ca. 17 – 19 t.ha<sup>-1</sup> (Lehndorff et al., 2016).

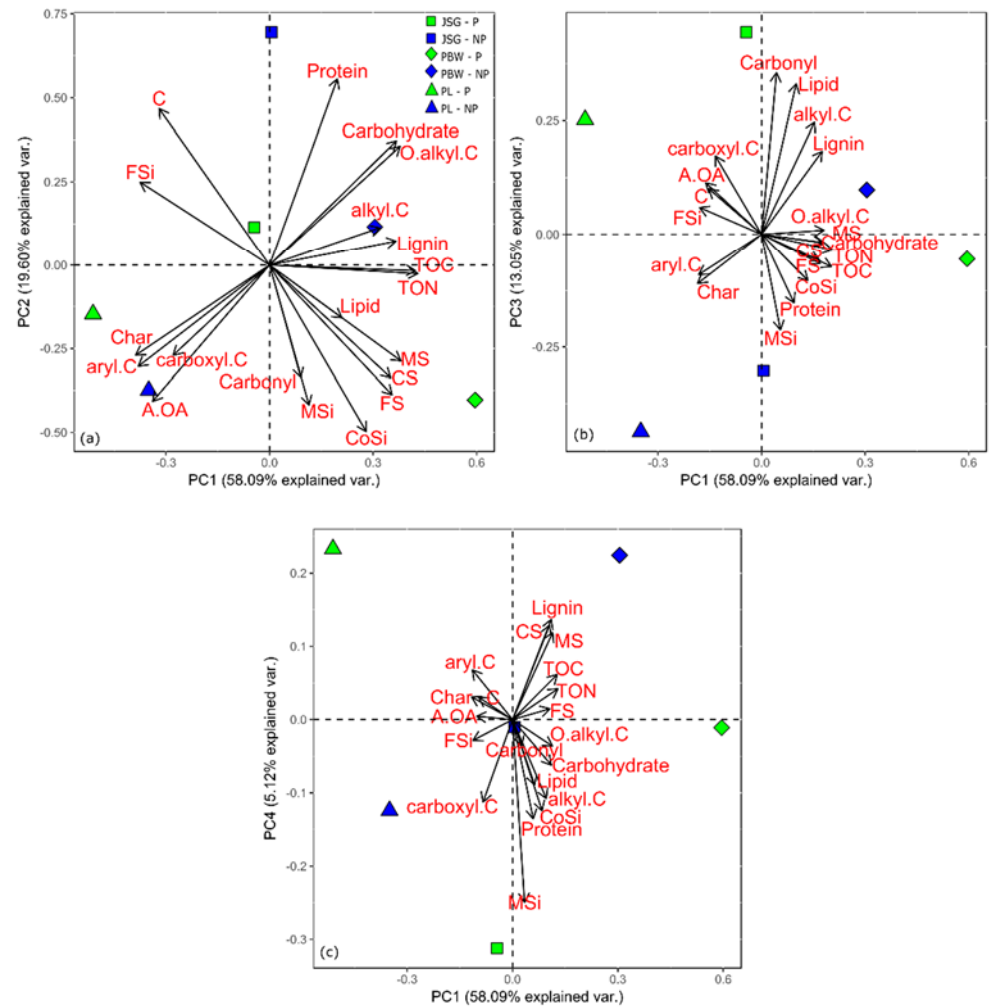


Figure 3.4. Loadings of grain size composition, TOC, TON, and chemical structures and molecular composition of the top soil humic defined by factor 1 and factor 2 (a), factor 1 and factor 3 (b), and factor 1 and factor 4. Data set from point samples (Appendix 3.3).

As the samples were obtained from the bottom of plow layers, ca. 20 cm depth, the presence of char materials may be expected from the burnt plant residues applied, a common traditional practice to improve soil fertility. But this may not fully be true, since the widespread application of this practice in West Java sites (Dieterich, 2012), did not affect our type B samples (Fig. 3.3).

In type B organic samples, the signal shows a similar spectrum but with difference in the intensities for P samples (Fig. 3.3). The higher O-alkyl-C with concomitant lower alkyl-C and aryl-C in PBW may indicate the more degradable origin of plant materials which is associated with carbohydrate (Fig. 3.5). Special attention may be given to the type of rotating dry crops where maize is in JSG and vegetable in PBW, i.e. bok-choi. The slight difference in mineral compositions between P and NP sites in PBW (section 3.2) is not observed to significantly affect organic matter structures.

As discussed before, the effect of crop management, P and NP, could not be seen clearly in this study. The  $^{13}\text{C}$ -NMR spectra of humic from P and NP plots are insignificantly different (Fig.3.3). Yet in JSG samples, the difference in the context of specific spectral regions is quite pronounced as ca. 15% deviations of O/N-alkyl and alkyl-C integrals were observed. It resonates quite low in the O/N-alkyl regions (45 – 95 ppm) but slightly higher in the alkyl-C regions (0 – 45 ppm) for the P sample. The difference in the relative signal intensity may indicate either the alteration of original chemical structure or the presence of different sources of organic residues. Principal component analysis shows that NP sample occurs close to protein while P sample close to lignin both in the space defined by PC2 (Fig. 3.4). This result points out the difference in quality of organic compounds.

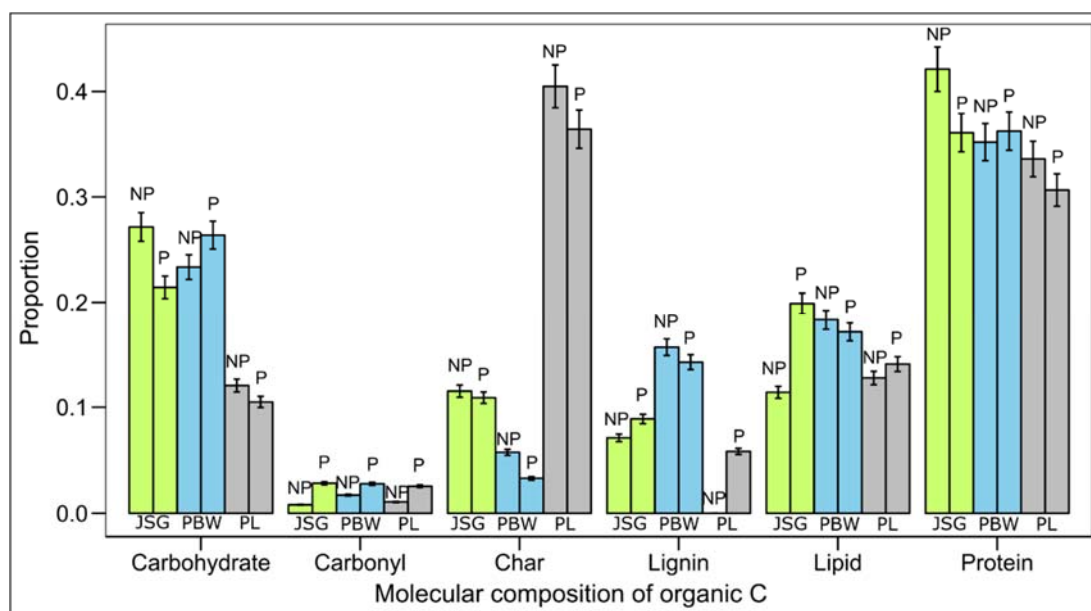


Figure. 3.5. Predicted molecular compositions of organic carbon from top soil humic samples (ca. 20 cm depth) of P and NP.

The prediction of proportions of soil C contributed at the molecular scale used a mixing model (section 2.4.4). It reveals more aromatic for type A samples as their main components, i.e. lignin, lipid, char, account for > 50% out of total components (Fig. 3.5). The high protein

content with concomitant char signal is not expected since both fractions are typically not in mutual dependence. It means that aliphatic compounds will be depleted with decomposition stage leaving the aromatic compounds behind. It is suggested that the presence of a strong char signal is related to older carbon that was preserved in the clay, as carbon dating of humic samples showed lower concentration in type A than type B samples (Chapter 4). The preservation of carbon in smectitic soils is related to protection through clay surfaces (Saggar et al., 1997). Conversely, type B samples are characterized by rich in aliphatic components, i.e. carbohydrate, protein, carbonyl, account for » 60% out of total components. The higher aliphatic compounds correspond with a lower level of refractory components.

The carbonyl components, i.e, uronic and fatty acids, are consistently higher in P plots (Fig. 3.5). This may indicate the relation with rice as most dominant crop during growing period. Conversely, the higher amount of char materials in NP plots may be connected to the absence of flooding condition. As flooding during rice paddies is able to leach down organic materials from plow layers (Maie et al., 2004b).

Table. 3.5. Loadings of first four principal components of grain size composition, TOC, TON, and chemical structures and molecular composition of humic.

	PC1 (58.09%)	PC2 (19.60%)	PC3 (13.05%)	PC4 (5.12%)
Alkyl-C	0.22	0.08	0.35	-0.24
O alkyl-C	0.26	0.24	0.013	-0.08
Aryl-C	-0.26	-0.21	-0.13	0.15
Carboxyl-C	-0.19	-0.18	0.24	-0.25
A/OA	-0.23	-0.28	0.16	0.01
TOC	0.29	-0.11	-0.10	0.14
TON	0.29	-0.02	-0.05	0.09
Clay	-0.22	0.32	0.14	0.07
Fine silt	-0.25	0.17	0.08	-0.06
Medium silt	0.08	-0.28	-0.30	-0.56
Coarse silt	0.19	-0.33	-0.14	-0.28
Fine sand	0.24	-0.26	-0.09	0.03
Medium sand	0.26	-0.19	-0.03	0.27
Coarse sand	0.24	-0.23	-0.08	0.29
Carbohydrate	0.25	0.25	-0.02	-0.14
Protein	0.13	0.38	-0.22	-0.30
Lignin	0.25	0.05	0.26	0.31
Lipid	0.14	-0.11	0.47	-0.20
Carbonyl	0.06	-0.22	0.50	-0.08
Char	-0.26	-0.18	-0.16	0.07

Principal component analysis shows the positive relation of TOC, TON, carbohydrate, lignin, and sand fractions as defined to PC1 (Fig. 3.4; Table 3.4). These variables are connected to PBW samples (Fig. 3.4; Fig. 3.5; section 3.2), and may be interpretable as the association of organic matter to amorphous clay minerals, that is dominant in this soil (Winkler et al., 2016). Atypical negative correlation of TOC to char (Table 3.4) may be explained as the more

aromatic signal obtained from humic than bulk soil organic matter. The association of char with clay and fine silt indicates the presence of carbon preservation that supports the above discussion.

Defining to PC2, protein associates with clay occurred at the space close to JSG, and more related to NP site (Fig. 3.4). As negatively correlated to A/O-A ratio (Table 3.4), the high abundance of protein may be related to the new input from plant residues. In the negative relation to PC2, carbonyl has a mutual dependence with more coarse (larger than medium silt) than fine fractions. Carbonyl and lipid explain most of the variation in PC3, existed at the space close to P site in JSG (Fig. 3.4).

## Conclusions

Research areas are characterized by topographical, and environmental controls (climate, hydrology) on grain size, soil pH and elemental compositions. On the middle to high altitude, volcanic environment, (PBW, Rds; type 1) the coarse fractions are dominant. Similarly, soils developed on the combination from in-situ and ex-situ parent materials (Bbl; type 3) pose a depth-variability with coarse fractions as the dominant texture. On the more stable environment, i.e. gentle slopes with homogeneous profile compositions, (JSG, type 2), the depth-grain size compositions are more stable, and dominated by clay fractions. Down to alluvial plains (Cixi, Grh, Pjk, Dgk, PL; type 4), soils develop from fluvial materials, and fine fractions are dominant.

Two strong characteristics of the environment, based on mineral compositions, are type A, i.e. PL site, that developed on an alluvial plain with basic parent material, and poor drainage condition and exhibits a high alkalinity; and type B, i.e. JSG and PBW site, formed on higher slopes with more acidic parent material, and good drainage condition posing a more acid environment. In the subsequent implications they may have created a specific soil properties and processes both laterally and vertically in the soil columns, e.g. mineralogy compositions, and carbon fixing capacity.

Grain size and mineral compositions show a high heterogeneity of soil profile in PBW, mainly in P site. Different layer compositions pose different origins of parent material typical of volcanic environment. Similarly, heterogeneity of soil compositions in Rds and Bbl were also observed based on merely grain size compositions data. Conversely, profiles of JSG and PL exhibit more homogeneity soil compositions.

Soil type-environment associates with plant litter to affect the chemical compositions of soil organic matter typical for the region. Similar to mineral composition distributions, the two types, i.e. type A (PL) and type B (JSG and PBW) are separated based on the chemical structure of organic matter. In the first type in the monsoon region of smectitic soils, organic matter is characterized by the high amount of aryl-C associated with char, which is poorly degradable. The use of humic fractions as sample for measurement may, however, affect the stronger char signal obtained from this analysis. Therefore, the strong signal of char may have posed a different way with the total organic carbon content. In the second type in wet region of allophanic and kaolinitic soils, the structure of organic compounds is dominated by O-alkyl-C associates with carbohydrate, which is more easily degradable.

## Chapter 4

### 4. Origins, distributions and isotopic compositions of soil organic carbon

Parent material characteristics, i.e. grain size and mineral compositions, have been shown to considerably contribute to the soil properties and processes, and influence soil organic matter structure in the study area (Chapter 3). This Chapter will elaborate the previous insights with further discussions in the context of subsoil carbon by putting together data on litter inputs, total organic carbon, and isotopic compositions ( $\delta^{13}\text{C}$ ,  $^{14}\text{C}$ ). The main attention is on the soil carbon in relation to plant residue inputs, environmental conditions (topography, climate), and soil characteristics. For comparison, data available from the earlier project in Cixi's subtropical soils are presented with environmental background discussed elsewhere (Bräuer et al., 2013b, 2013a), as well as data from the 2016 field campaign on the Mt. Lawu – Kendeng ridge slopes (section 2.1.2).

Plant residues, i.e. surface litter, roots, root exudates, are the main carbon inputs into the ground (Balesdent and Balabane, 1996; Rumpel and Kögel-Knabner, 2011). The importance of their contribution to subsoil carbon may be estimated by comparing it with the total soil organic carbon stock (Hulugalle et al., 2009), which depends on landuses and climate (Lugo et al., 1986). In combination with soil processes, the  $^{14}\text{C}$  ages of plant residues at depth may elucidate a way and origin of carbon inputs (Bräuer et al., 2013a), since typically most of fresh carbon accumulates on the ground surface.

Different environmental conditions, i.e. climate and topography, shape parent materials into specific soil properties, with differences in clay mineralogy compositions (Winkler et al., 2016). The important role of soil minerals in the carbon storage capacity of soils has been discussed (Han et al., 2016; Mikutta et al., 2006, 2005). As important to carbon preservation (Torn et al., 1997), the clay mineralogy composition will be related to organic fractions by making use of  $^{14}\text{C}$  for dating. The inaccessibility of carbon for enrichment and microbial decomposition due to, e.g. mineral complexation and aggregate occlusion (Mikutta et al., 2006), leads to carbon preservation with constant  $^{14}\text{C}$  decay. This means that the extreme levels of soil  $^{14}\text{C}$  concentration, either much higher or lower concentration than the current atmospheric composition, may be associated with preservation. This will come up to suggest a sample with  $^{14}\text{C}$  concentration above that of the current atmosphere originated at a time of different, higher, atmospheric  $^{14}\text{C}$  compositions.

The isotopic compositions of soil organic carbon ( $\delta^{13}\text{C}$ ,  $^{14}\text{C}$ ) may vary with the origin and history of the organic input. The isotopic composition of plant materials best reflects the photosynthetic pathway, atmospheric conditions, and environment at the time and place of photosynthesis (Warren and Meredith, 1998). Plants with the  $\text{C}_3$ - (Calvin cycle) and  $\text{C}_4$ - (Hatch-Slack) photosynthetic pathways fractionate  $^{13}\text{C}$  differently relative to  $^{12}\text{C}$  during photosynthesis (O'Leary, 1981).  $\text{C}_3$  plants fractionate carbon with  $\delta^{13}\text{C}$  values close to -28‰, range -21 to 35‰, while  $\text{C}_4$  plants have values enriched in  $^{13}\text{C}$  to around -14‰, range -10 to -

14‰ (Ehleringer, 1991; O’Leary, 1988). Therefore, by tracing  $\delta^{13}\text{C}$  signatures the origin of plant residue inputs at depth may be revealed (Balesdent et al., 1987).

The apparent age of organic carbon in the soil is estimated by  $^{14}\text{C}$  dating. Given the high age-heterogeneity nature of soil organic matter (Rethemeyer et al., 2004a), the isolation of carbon samples into single fractions to trace the  $^{14}\text{C}$  infiltration and organic carbon transformation, and to quantify the heterogeneity may be useful (Trumbore et al., 1996). To test the level of heterogeneity,  $^{14}\text{C}$  concentrations of fractions obtained from AAA treatments, i.e. humic and humin (section 2.3.2), and grain size fractionation are compared to those of bulk samples. As fresh carbon has a  $^{14}\text{C}$  concentration always close to the contemporaneous atmospheric level, the chemical complexity of compounds may not contribute to the resulting signatures (Gleixner, 2013).

#### 4.1. Litter carbon inputs

##### 4.1.1. Amount of litter input

Plant remains as a function of depth were collected from samples of ca. 5 kg of air-dried subsoil by wet sieving (section 2.3.1) to quantify litter and root inputs. The original data of plant remains are presented in Appendix 4.5. To avoid the strong disturbance and high plant contributions of the top soil, sampling started near the topsoil-subsoil transition around 20 cm depth. Plant remains are greatly varied in terms of their appearance with different colors and shapes, ranging from full size to fragmented materials, e.g. leaves, roots, with old-dark to light fresh-looking (Fig. 4.1).



Figure. 4.1. Some collected subsoil plant remains for  $^{14}\text{C}$  dating, i.e. (a) and (b), leaves and dark roots from PBW-P and -NP; (c) and (d), leaves and dark-light roots from JSG-P and -NP; (e) and (f), light leaf fragments and dark roots from PL-P and -NP.

By taking into account the bulk density of layers, the quantity of plant remains as a function of depth can be normalized to  $\text{g cm}^{-3}$ . It highly depends on crop management (Fig. 4.2). The monoculture  $C_4$  crops, i.e. sugarcane in PL-NP and maize in PBW-NP (Table 2.1), may have contributed more biomass than  $C_3$  crops do. The difference in quantity of biomass between these two crops may be related to the physiology of the plants, as  $C_4$  crops produce more than double the annual biomass of  $C_3$  crops due to their higher water-, nitrogen- and radiation-use efficiency (Sage and Zhu, 2011), and their minimizing of carbon loss by 30 – 50% by suppressing photorespiration (Bhagwat, 2005). The positive effects of  $C_4$ -maize and -sugarcane in the context of increasing both residual biomass and soil organic carbon have been reported elsewhere (Tavares et al., 2015; Tirado-Corbalá et al., 2015; Wood and Edwards, 1992).

The depth-distribution of plant residues may be fitted with an exponential model ((Jackson et al., 1996); Appendix 4.1), using a formula  $Y = 1 - \mu^z$ , with  $Y$  = cumulative root fraction (0-1),  $z$  = soil depth (cm), and  $\mu$  = fitting parameter of depth coefficient. Results show  $\mu$  values to vary with different soil types, i.e. 0.91 (PL-P), 0.93 (PL-NP), 0.96 (JSG-P), 0.96 (JSG-NP), 0.93 (PBW-P), and 0.85 (PBW-NP). In JSG with assumed amount of litter input at the top not significantly different between P and NP (Table 4.1), the  $\mu$  is the same. In general, the higher constant  $\mu$  indicates the more carbon distributed with soil depth.

The most plant residues were found in the top sample at ca. 20 cm depth. They account for more than 50% of the total plant remains throughout the soil column. Below this depth the quantity of residues drop significantly with increasing depth. The organic residue inputs, predicted by extrapolating the fitting curve to the surface, are consistently higher in the NP fields than in the P (Fig. 4.2), as mostly NP plots cultivate  $C_4$  crops. The gap is reduced in JSG (Appendix 4.1), as  $C_4$ -maize is used as a rotating crop for rice during dry seasons (Table. 2.1).

The e-folding depth of root distribution (Table 4.1) shows to vary among soil types and crop management. The increase in the 25 cm interval depth is followed by a constant percentage decrease of root carbon at ca. 10% in PL-P and PBW-NP. While in the remaining profiles, its percentage decrease with interval depth is constantly with different factor.

By assuming the carbon content in the plant tissues as presented in Table 4.3, the plant residues can be expressed as carbon inputs (Fig. 4.2). The estimated carbon derived from roots, as indicated by plant remains, account for ca.  $\leq 1\%$  out of total organic carbon stock (Fig. 4.2). By assuming the annual input of carbon using data from some reference, it is suggested that the turnover time under different landuses shows to vary in different sites (Table 4.2). The rapid carbon turnover time ( $<10$  yr) is likely resulted from the higher carbon input in land subject to agricultural practices, as carbon inputs are not only from plant litter but also from different source, e.g. manure. Under the same P management with estimated input ca.  $0.626 \text{ kg C m}^{-2} \text{ yr}^{-1}$ , the turnover time of carbon is higher in PBW than the other sites. This suggests a higher organic carbon stock capacity in PBW supporting the result of PCA as already discussed in section 3.3.

Table. 4.1. Characteristics of e-folding depth of root distribution at different soil profiles (D = interval depth).

D (cm)	Log (D)	Site											
		PL-P		PL-NP		JSG-P		JSG-NP		PBW-P		PBW-NP	
		C root (g cm <sup>-3</sup> )	log (C root) (-)	C root (g cm <sup>-3</sup> )	log (C root) (-)	C root (g cm <sup>-3</sup> )	log (C root) (-)	C root (g cm <sup>-3</sup> )	log (C root) (-)	C root (g cm <sup>-3</sup> )	log (C root) (-)	C root (g cm <sup>-3</sup> )	log (C root) (-)
0	nd	0.000500	-3.301030	0.000800	-3.096910	0.000300	-3.522879	0.000300	-3.522879	0.000200	-3.698970	0.000400	-3.397940
25	1.40	0.000050	-4.299907	0.000174	-3.759209	0.000046	-4.337181	0.000105	-3.978888	0.000051	-4.296125	0.000036	-4.440247
50	1.70	0.000005	-5.298785	0.000038	-4.421508	0.000007	-5.151483	0.000037	-4.434897	0.000013	-4.893280	0.000003	-5.482554
75	1.88	0.000001	-6.297662	0.000008	-5.083807	0.000001	-5.965785	0.000013	-4.890906	0.000003	-5.490435	0.000000	-6.524860
100	2.00	0.000000	-7.296539	0.000002	-5.746106	0.000000	-6.780087	0.000004	-5.346916	0.000001	-6.087590	0.000000	-7.567167

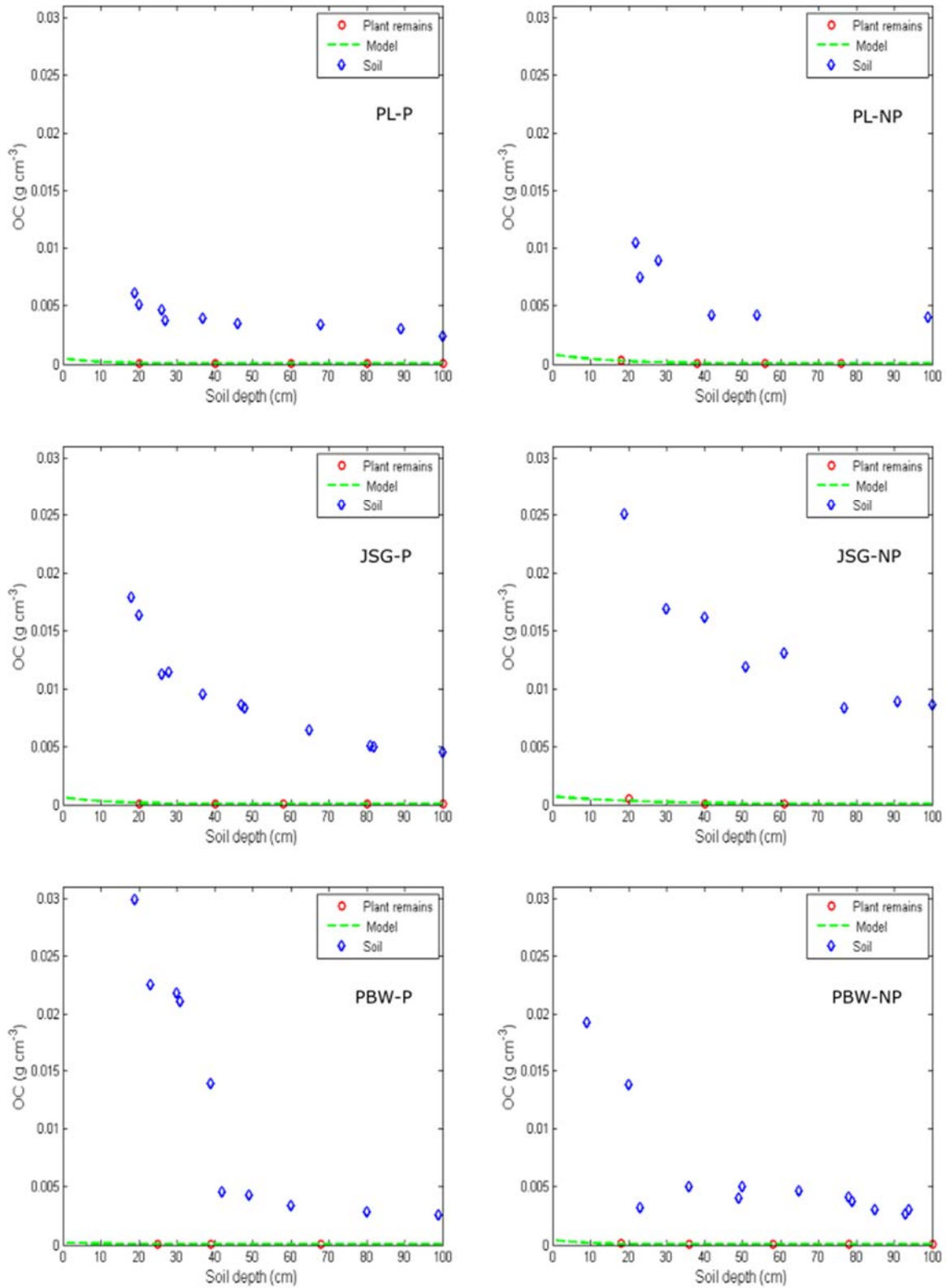


Figure. 4.2. Normalized carbon concentrations of plant remains collected from 2 cm thick layers in PL, JSG, and PBW as a function of depth, with an exponential curve defining its depth-distribution, and organic carbon content of the soils.

Table. 4.2. Carbon turnover time in different landuses.

Site	Crop types	Input of C (kg m <sup>-2</sup> yr <sup>-1</sup> )	Amount of C in the soil (kg m <sup>-2</sup> )	Carbon turnover (yr)
PL-P	Rice (twice yr <sup>-1</sup> )	0.6000 <sup>a</sup>		
	Tobacco	0.0003 <sup>d</sup>		
	Manure (once yr <sup>-1</sup> )	0.1200 <sup>a</sup>		
	Total	0.7203	1.20	1.67
PL-NP	Sugarcane	4.0000 <sup>b</sup>		
	Manure (once yr <sup>-1</sup> )	0.1200 <sup>a</sup>		
	Total	4.1200	1.36	0.33
JSG-P	Rice (twice yr <sup>-1</sup> )	0.6000 <sup>a</sup>		
	Maize	0.4000 <sup>c</sup>		
	Manure (once yr <sup>-1</sup> )	0.1200 <sup>a</sup>		
	Total	1.1200	1.18	1.05
JSG-NP	Cassava	0.0700 <sup>c</sup>		
	Manure (once yr <sup>-1</sup> )	0.2400 <sup>a</sup>		
	Total	0.3100	1.88	6.06
PBW-P	Rice (twice yr <sup>-1</sup> )	0.6000 <sup>a</sup>		
	Manure (once yr <sup>-1</sup> )	0.1200 <sup>a</sup>		
	Bok Choy	0.2000		
	Total	0.9200	2.33	2.53
PBW-NP	Maize	0.4000 <sup>c</sup>		
	Manure (once yr <sup>-1</sup> )	0.1200 <sup>a</sup>		
	Cassava	0.0700 <sup>c</sup>		
	Total	0.5200	1.53	2.94

<sup>a</sup>(Prastowo et al., 2013)

<sup>b</sup>(Tirado-Corbalá et al., 2015)

<sup>c</sup>(Shirato et al., 2005)

<sup>d</sup>(Beyaert and Voroney, 2011)

<sup>e</sup>(Liang et al., 2014)

Under paddy management, carbon input derived from root, manure, and straw may account for ca. 38%, 16% and 29% of seasonal total input (Prastowo et al., 2013). Additional carbon input may be expected from irrigation water. Weeds are also important contributor for carbon in rice field (Kimura et al., 2004).

The variation of carbon stocks in different soil types (Fig. 4.2) may indicate their inherent storing capacity. Results indicate the higher carbon preserving capacity in PBW, since the gap of TOC-soil to C-plant is the biggest compared to other soil types (Fig. 4.2). The high carbon stock capacity in PBW, which has allophanic soils (Winkler et al., 2016), is probably associated with the formation of Al/Fe-humus complexes (Matus et al., 2014; Takahashi and Dahlgren, 2016), and wet climate (Trumbore, 2009).

The low amount of soil carbon stored in PL, compared to JSG, with corresponding high residue inputs (Fig. 4.2; Appendix 4.1), e.g. in the sugarcane field, is theoretically in a disagreement, considering the higher adsorption capacity of smectite than kaolinite (Singh et al., 2016). In view of the climatic data (Table 2.1; Chapter 3), this low carbon stored may result from a higher organic matter mineralization rate. With a mean annual temperature of 27° C (Amien et al., 1996), and subject to 3-4 consecutive dry months (rainfall < 60 mm) opening up soil cracks, a high intensity of organic matter decomposition may be favoured in this area. Temperature sensitivity of soil organic matter mineralization has also been discussed elsewhere (Benbi et al., 2014; Davidson and Janssens, 2006; Lützow and Kögel-knabner, 2009).

The high organic matter mineralization rate in PL has been indicated previously (section 3.3) by the lower proportion of labile organic fractions, e.g. carbohydrate and protein, with concomitant higher  $\frac{\text{Alkyl-C}}{\text{O alkyl-C}}$  ratios than in the organic matter samples from other sites (Fig. 3.5; Table 3.3).

#### 4.1.2. Litter <sup>14</sup>C content

As shown in Fig. (4.1), plant remains collected at depth vary in colours, i.e. light versus dark. This led to the question if there could be a correlation with the radiocarbon age. However, the results in Table. (4.2) show no correlation between them. The dark roots do not necessarily reflect a high degree of decomposition and old material, as the materials collected from PBW-NP, JSG-NP, and PL-NP showed  $\Delta^{14}\text{C}$  concentrations above current atmospheric composition (in 2012) ca. 31‰ (Levin et al., 2013). The colours may also prove the crop species in combination with  $\delta^{13}\text{C}$  signals. The dark roots in the PL-NP sugarcane field may be recognized as young sugarcane roots by  $\delta^{13}\text{C}$  values enriched towards -15‰ (Table 4.2).

Conversely, light coloured plant remains are not always fresh material as light leaf fragments collected from JSG-P Alisol at ca. 100 cm depth showed a  $\Delta^{14}\text{C}$  concentration -371‰ (Table. 4.2). The low <sup>14</sup>C content means that this residue may have been either protected from microbial attack or posed a chemical structure that is not easily degradable.

The <sup>14</sup>C content of most residues, higher than the 2012 atmospheric <sup>14</sup>C level (Table 4.2), indicates the different origin of carbon fixed to grow their structures. As plant material collected is already dead, they could derive from years earlier than 2012 (sampling year), e.g.

2000's, with higher levels of  $^{14}\text{CO}_2$  (Hua et al., 2013; Levin et al., 2013). Yet, the carbon signature in the plant materials is not necessarily derived from carbon fixed in the current year since plants can develop new structure using carbon fixed in the previous 1-2 years (Gaudinski et al., 2001). It means that for biennial crop like sugarcane, the higher plant residue  $^{14}\text{C}$  signal can be derived from previous years.

Table. 4.3. Organic carbon content and isotopic composition of collected macrofossils at different depths.

Site	Crop type	Plant remains	Depth (cm)	TOC* (%)	$\Delta^{14}\text{C}$ (‰)	$\delta^{13}\text{C}$ (‰)**
PBW	Maize	Dark roots	78-83	44	$50.1 \pm 2$	$-27.54 \pm 0.46$
PBW	Paddy	Light leaf	98-102	46	$30.2 \pm 0.8$	$-28.35 \pm 0.66$
JSG	Paddy	Light roots	100	53	$45.2 \pm 2$	$-32.35 \pm 0.28$
JSG	Paddy	Light leaf fragments	100	64	$-402.5 \pm 1$	$-28.94 \pm 0.43$
JSG	Cassava	Dark roots	100-104	46	$42.2 \pm 2$	$-29.72 \pm 1.70$
JSG	Cassava	Light roots	100-104	47	$43.1 \pm 1$	$-26.62 \pm 1.59$
JSG	Cassava	Charcoal	80-84	64	$-268.5 \pm 2$	$-28.15 \pm 0.56$
PL	Paddy	Light leaf fragments	80-85	44	$36.2 \pm 1$	$-23.61 \pm 1.84$
PL	Sugarcane	Dark roots	110-115	47	$54.1 \pm 2$	$-15.85 \pm 1.73$
PL	Sugarcane	Dark roots	110-115	48	$40.2 \pm 2$	$-11.12 \pm 1.40$

\*Carbon content calculated from  $\text{CO}_2$  yield in combustion of  $^{14}\text{C}$  sample

\*\* $\delta^{13}\text{C}$  calculated from AMS measurement

Modern plant residues observed at depth (Table 4.3) may indicate direct distributions from the root zones (ca. 0-20 cm depth). Depth translocations may be facilitated by irrigation water/rainfall that transports the light materials preferentially through holes created by root activities, or by soil animal burrows, e.g. earthworms, termites, ants, and anthropods. In the smectitic soils in PL, depth translocation may also be accelerated by pedoturbation, which is an alternating process of shrinking and swelling of soil in response to drying and wetting. Roots are predominantly placed in fine shrinkage cracks and between slickensides (Nicoullaud et al., 1994), so they penetrate more easily to depth.

The plant fragments in deep layers indicate another way of carbon inputs into the soil. The extent of roots distributed into subsoils may be dependent on the crop types (Rumpel and Kögel-Knabner, 2011), and the deeper root zones may result in more roots distributed at greater depth. although root residues may mostly exist in the immediate vicinity of the rhizosphere. Yet, the use of  $^{14}\text{C}$  dating in this study has proven that modern roots may penetrate well below the classical root zones, down to ca. 100 cm depth, as found earlier in the study in Cixi rice paddies (Bräuer et al., 2013a).

#### 4.2. Depth distribution of total organic carbon

Total organic carbon (TOC) stored throughout the soil columns (2012 samples) varies within the range (min to max) 0.25 to 0.55% in PL-P, 0.36 to 0.952% in PL-NP, 0.55 to 1.57% in JSG-

P, 0.78 to 2.24% in JSG-NP, 0.33 to 3.69% in PBW-P, and 0.41 to 3.12% in PBW-NP (Appendix 3.1). Concentrations drop with increasing depth, which suggests a typical highest carbon stock near the soil surface is derived from plant litter and agricultural inputs, e.g. manure. The coefficient of variation in the soil columns shows high values in PBW ca. 78% at P and NP. The scattered distribution of depth-TOC with significant difference of its concentration between top and subsoil are responsible for this high variability. In the JSG, CV values are lower, i.e. 34% (P) and 38% (NP). The lowest value shows in PL-P with CV ca. 22%, increasing in NP with CV ca. 37% as a result of the increase in the plant litter, i.e. sugarcane, near the ground surface.

Generally, depth TOC content is higher in NP than in P profiles (Appendix 4.2). The presumable association of TOC with plant litter inputs has been discussed in section 4.1.1. Analysis shows a poor correlation of TOC with clay fraction (N=58,  $P \leq 0.025$ ,  $r = -0.24$ ). By excluding PBW samples in the analysis, the correlation is getting significantly better with  $r = 0.26$  (N=35,  $P \leq 0.20$ ). This suggest that the higher TOC content in PBW soils (Fig. 4.5; Fig. 4.7) is not related to clay fraction. Scatter plots (Fig. 4.5; Fig. 4.7) show a better correlation of TOC with  $\Delta^{14}\text{C}$  than with  $\delta^{13}\text{C}$ .

As indicated above, the variability of TOC in PL mainly P site is lower than in the other profiles. The TOC depth gradient is less steep, which indicates less heterogeneity in profile compositions (Fig. 2.2; section 3.1; section 3.2). Beside due to the low carbon input at the top, this greater homogeneity may also be contributed by the high abundance of expandable clay in the soil column that causes argili-pedoturbation (Dell'Abate et al., 2002). In the dry seasons, shrinkage creates deep fissures in which carbon both on the surface and on the fissure wall may be introduced at depth (Birkeland, 1999). On wet season's swelling, subsoil carbon may move randomly through aggregate's force actions. In this way, soil in the column will mix resulting in reduced carbon depth gradients.

The profiles of PBW, with high variability of depth-TOC distribution, indicate a discontinuity in carbon concentration at 30-40 cm depth at P and ca. 20 cm at NP (Fig. 4.2; Appendix 4.2). Grain size and elemental compositions (Fig. 2.4; section 3.1; section 3.2), in combination with the  $^{14}\text{C}$  signal (section 4.3.2), indicate the discontinuity may reflect a change in the parent material, overlying new layers containing fresh carbon on older layers with older carbon content at PBW-P (section 3.2). Therefore, the profile distribution of carbon may be related to the sequence of parent materials deposited. Differently, in the more homogeneous NP profile, atypical depth of carbon may appear as a result of crop type as indicated by  $\delta^{13}\text{C}$  signal (Fig. 4.5). It is suggested that before  $\text{C}_4$ -maize as current crop,  $\text{C}_3$  crops were originally planted. The smaller carbon contribution below 20 cm depth is likely  $\text{C}_3$ -derived materials as having a similar trend with TOC.

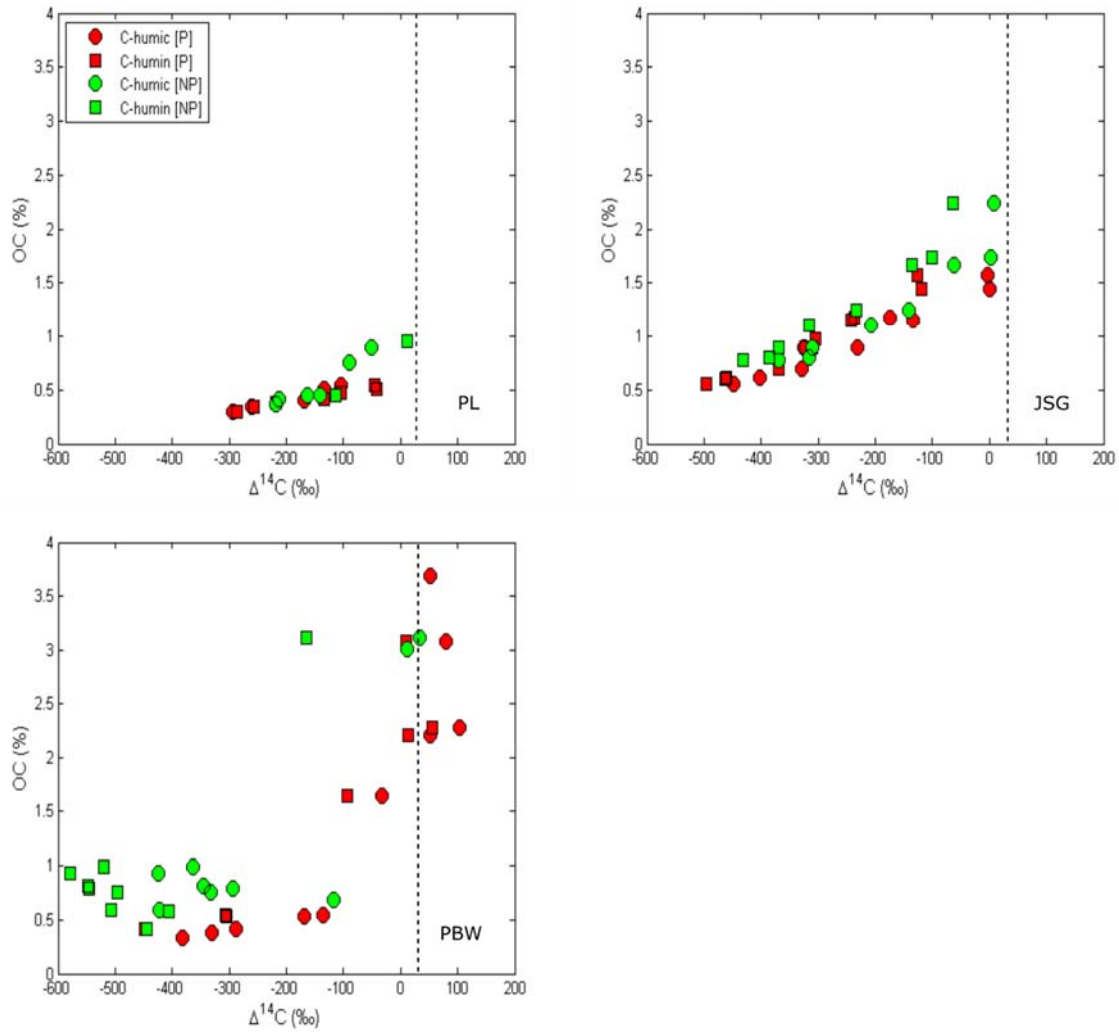


Figure. 4.3. Total bulk organic carbon in relation to  $\Delta^{14}\text{C}$  (sample 2012). The vertical dotted lines indicate an atmospheric  $\Delta^{14}\text{CO}_2$  level in 2012 ( $\sim 31\text{‰}$ ).

The carbon accumulation related to the anoxic environment created during rice cultivation as widely hypothesized (Kögel-Knabner et al., 2010), is not clearly observed in this study (Fig. 4.2) of the subsoil, and in top soil samples (Winkler et al., 2016). The dry season crop rotation may explain this situation. Dry periods in between rice paddy cultivation have been held responsible for the reduced amount of easily decomposable organic matter (Nishio et al., 1994), related to the production of  $\text{CO}_2$  contributing to an important loss of carbon (Nishimura et al., 2008). In addition, re-wetting the dried paddy soils may promote mineralization (Ono, 1989), which means that the quantity of soil carbon can be expected to be diminished during the initial stage of rice seasons after the dry period. Furthermore, as discussed previously (section 4.1), the consistently higher amount of total carbon stored mostly in the NP may suggest a relation to plant debris.

In contrast, 50 years and more paddy management in Cixi, China have been shown to increase soil organic carbon in the top layers to values similar to those at our sites without a clear increase in the subsoil (Bräuer et al., 2013a). With vegetable as a background with low biomass production, the input of carbon in the rice field can be expected to be higher. In these

soils, the initial organic carbon contents in the parent materials (tidal flat) were low (Bräuer et al., 2013b) so that the accumulation of carbon along crop managements may be observed. Therefore, it is suggested that crop types/managements may have played an important role in storing carbon in the soil (section 4.1), under similar climatic conditions, topography and soil types in Cixi.

Samples with high organic carbon are consistently associated with high  $^{14}\text{C}$  content (Fig. 4.3), which means that young carbon must have accounted for most of the bulk organic carbon. These carbon materials mostly occur in the top layers where plant residues accumulate. Conversely, samples with low total organic carbon content exhibit low  $^{14}\text{C}$  contents, which indicates a high proportion of old carbon. Data shows that these samples are typically from deep layers. The preserved organic carbon in the deep layer samples may be related to the interaction with Fe/clay minerals (Eusterhues et al., 2007, 2005).

The scatter in the PBW TOC- $^{14}\text{C}$  plots is stronger than the other sites (Fig. 4.3), as also indicated by high CV values. The relation of organic carbon and  $\Delta^{14}\text{C}$  is more linear in PL and JSG. The  $^{14}\text{C}$  values above those of the 2012 atmosphere mostly in PBW-P may indicate an earlier origin of the carbon. The older carbon is shown to be dominated by organic materials derived from NP site.

Generally, the carbon content is higher in the humins than humic acids (Appendix 3.1). Humin contains organic carbon up to 1.16% (of soil weight) in JSG-P 18 cm depth sample, and down to 0.01% (of soil weight) in Rds-NP 60 cm depth sample. While humic contains organic carbon up to 0.23% (of soil weight) in 89 cm depth PL-P sample, and down to 0.01% (of soil weight) in 110 cm depth PL-NP sample and 80 cm depth Rds-P sample.

Both the humic acids and the humins show consistently more organic carbon in the top soil than in the subsoil which is related to higher bulk TOC content. In top soil sample (0-20 cm depth), PBW humin sample, with low content of crystalline clay (<25%) but with high TOC (ca. 3-4%), contains less carbon than JSG humin sample, with higher content of crystalline clay (>40%) but with low TOC in the bulk soil (ca. 2%). As soil carbon is bound to clay, it is suggested that clay in the humin may also be responsible for the content of carbon.

In clayey soils, i.e. PL and JSG, the humin fraction accounts for most of the isolated soil organic carbon with proportion > 30% of TOC. Yet in the PBW with lower crystalline clay content, the proportion of carbon in the humin decreases to below 30% of TOC. The exception is a sample from 89 cm depth of PL-P with higher proportion of carbon in the humic ca. 77% of TOC. This may indicate a higher aromaticity of organic compound in the humic sample as discussed in section 3.4.

### 4.3. Carbon isotopic compositions ( $\delta^{13}\text{C}$ and $^{14}\text{C}$ )

#### 4.3.1. Depth distribution of $\delta^{13}\text{C}$

The  $\delta^{13}\text{C}$  values in the study areas range from  $\text{C}_3$  to  $\text{C}_4$  photosynthetic pathway (Appendix 4.6; Fig. 4.4; Fig. 4.5; Fig. 4.6). However, the depth-distribution of  $\delta^{13}\text{C}$ , in combination with  $\Delta^{14}\text{C}$  values shows various plant material origins with different time of carbon deposit (Fig. 4.4). The  $\delta^{13}\text{C}$  signals indicate  $\text{C}_3$  type as a majority crop mainly in agricultural fields (Fig. 4.4). The

signals obtained may not be only an indication of in-situ crop types but also of the agricultural inputs, e.g. manure and irrigation water that are widely applied during field management.

As field management practices include seasonal crop rotations (Table 2.1), i.e. dry crops in a dry season, soil  $^{13}\text{C}$  may be enriched or depleted in  $^{13}\text{C}$  as a result of carbon mixing. As for example, in Fig. (4.4) the Ploso Lor, diagram shows for recent times ( $\Delta^{14}\text{C} > -50\text{‰}$ ) rice  $\text{C}_3$  values in the paddy and sugarcane  $\text{C}_4$  values in the non paddy field, while below  $-50\text{‰}$ , deeper in the subsoil, the  $\text{C}_3$  and  $\text{C}_4$  carbon may have mixed. This indicates intensive crop rotations in the past. Crop rotation was actually observed during the 2016 re-sampling as rice was growing on the 2012 sugarcane field.

While in nature  $\text{C}_3$  and  $\text{C}_4$  crops exhibit a different range of  $\delta^{13}\text{C}$  values, with the mean difference of the two approximately  $14\text{‰}$  (Boutton, 1991), the presence of intermediate  $\delta^{13}\text{C}$  values ( $-14$  to  $-21\text{‰}$ ), may demonstrate the existence of transitional  $\text{C}_3$ - $\text{C}_4$  intermediate photosynthetic crops, or the mixing of soil organic carbon. An example of this crop type is observed in the JSG field with dry crop cassava.

By relating the concentration of  $\delta^{13}\text{C}$  and  $^{14}\text{C}$  from the same samples (Appendix 4.6), the youngest carbon in each sites show existed to the right of plots (Fig. 4.4), and similarly regardless the crop types. The values are all modern, i.e. close to or even slightly above the 2012 and 2016 atmosphere (Fig. 4.7 and Fig. 4.8) as typically expected from the top layers, which means that there is no specific condition of crop types contributed to the  $^{14}\text{C}$  input but atmospheric compositions. Conversely, the oldest carbon assigned as preserved shows varying from site to site. The lowest carbon concentration in the study areas was almost  $-800\text{‰}$  at ca. 80 cm depth of P profile in Rds with  $\text{C}_3$  rice/soybean as current crop. As  $^{14}\text{C}$  signal indicates a pre-bomb period, this result demonstrate a majority and long history of the use  $\text{C}_3$  crops in this site.

The  $\delta^{13}\text{C}$  results of the humic and humin fractions, obtained from AAA extraction for  $^{14}\text{C}$  AMS, are shown in Fig. 4.5 and Fig. 4.6. To compare the results, bulk samples were prepared for running the same measurements. For PL samples, conc. HCl extraction were also performed as comparative samples.

The PL samples from P and NP (sugarcane and garden plot) sites show  $\delta^{13}\text{C}$  values of humic, humin and bulk samples that range from  $-15$  to  $-30\text{‰}$  (Fig. 4.5). They cover all of the wide range of  $\delta^{13}\text{C}$  signals for  $\text{C}_3$ ,  $\text{C}_4$ , and  $\text{C}_3$ - $\text{C}_4$  intermediate crops. Therefore, it is interpretable that crop rotations among different photosynthetic pathway may have occurred through agriculture history of the land. The garden plot exhibits  $\delta^{13}\text{C}$  signals more similar to P than to NP which means that  $\text{C}_3$ -type carbon inputs may be dominant.

The effect of maize ( $\text{C}_4$ ) as rotating crop in rice paddies of JSG is not evident in the  $\delta^{13}\text{C}$  signals (Fig. 4.5). These are depleted in the range of  $-20$  to  $-30\text{‰}$  as a result of carbon mixing with rice ( $\text{C}_3$ ) which was planted more intensively. In the neighbouring NP site the  $\delta^{13}\text{C}$  signals go from  $-15$  to  $-30\text{‰}$  throughout soil columns. Carbon enriched at ca. 100 cm depth suggests a presence of  $\text{C}_4$ -type carbon input in the past before 1950.

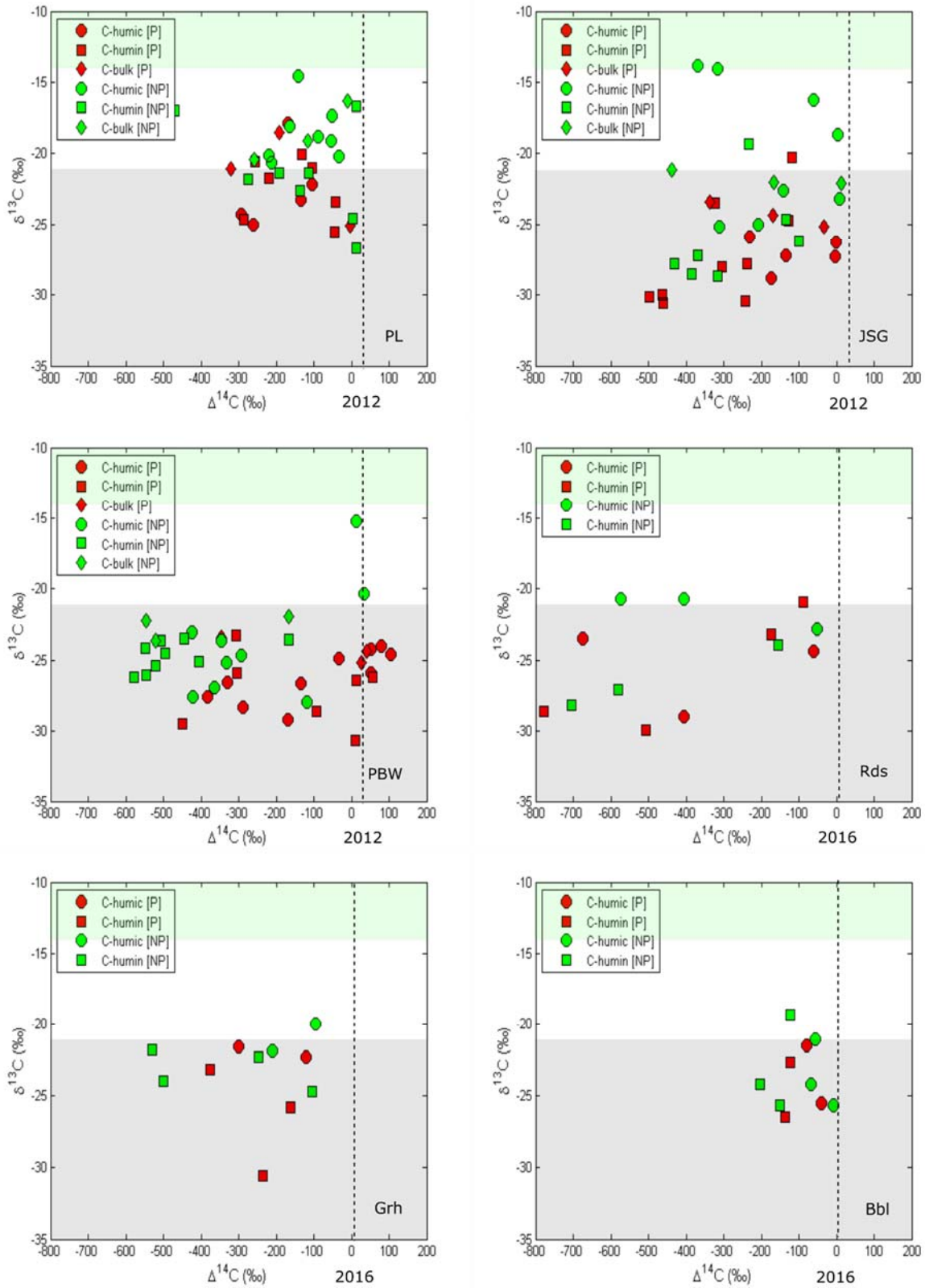


Figure. 4.4. The signals of  $\delta^{13}\text{C}$  in relation to  $\Delta^{14}\text{C}$  in the soil layers. Grey and green shading represents  $\delta^{13}\text{C}$  range for  $\text{C}_3$  and  $\text{C}_4$  crop types according to Ehleringer (1991). Vertical dotted lines indicate atmospheric level of  $\Delta^{14}\text{CO}_2$  in 2012 ( $\sim 31\text{‰}$ ) and in 2016 ( $\sim 9\text{‰}$ ) (Hammer and Levin, 2017; Levin et al., 2013).

The transition values between C<sub>3</sub> and C<sub>4</sub> may be contributed by cassava as a dry land crop cultivated in this site. As NP site does not represent a large scale and an intensive of agricultural area, therefore a representative conclusion may not be able to drawn.

At PBW the samples from the P site show a limited range of  $\delta^{13}\text{C}$  values throughout the soil column, ca. -22 to -30‰, which are slightly homogeneous from the long history of agriculture. It may be because Bok Choi as a rotating crop (Table 2.1) has the same signals as rice as C<sub>3</sub> crops. In the NP site, strong signals of maize as current crop, ca. -15‰, show only in the layers close to ground surface. However, for deeper layers they are depleted up to ca. -27‰ towards C<sub>3</sub>-plant signals. This is evidence a crop variation preceding current maize.

The samples from the 2016 study, showed C<sub>3</sub> type as dominant crops in the fields (Fig. 4.6). Carbon enrichment is likely appeared to shift  $\delta^{13}\text{C}$  down to -20‰, even from a monoculture rice field (three period of rice annually) like in Grh. This may indicate a different origin of some of the carbon, for instance from weeds, manure or irrigation water. The NP sites occupied by annual crops (Rds, Grh) show a depleted  $\delta^{13}\text{C}$  signals towards C<sub>3</sub> type.

In general, organic matter fractionation may result in inconsistent variations in the  $\delta^{13}\text{C}$  signals compared to bulk samples.  $\delta^{13}\text{C}$ -bulks as mean values subject either to be enriched or depleted depending on the original carbon. As  $\delta^{13}\text{C}$  values reflect not only the crop types but also specific plant organs (O'Leary, 1981). For example, stems and roots are 1‰ enriched in  $\delta^{13}\text{C}$  than leaves in tomato (Park and Epstein, 1960), and seeds are generally up to 10‰ more positive than leaves (O'Leary, 1981). Therefore, the average variation in  $\delta^{13}\text{C}$  of humic and humin fractions may also retain characteristics of their carbon origins. However, the extent to which the similarity between organic fractions to bulk samples isotopically were not clear. No single organic fractions is isotopically consistently close to the plant material signatures in each site (Table 4.2). It indicates that carbon enrichment/depletion can take place in both organic fractions. Earlier research suggested fulvic acids (not recovered in this study) as fraction isotopically close to the plant materials (Nissenbaum and Schallinger, 1974).

#### 4.3.2. Depth distribution of <sup>14</sup>C

##### 4.3.2.1. <sup>14</sup>C in different soil types

A gradual drop of <sup>14</sup>C content in different fractions, i.e. humic, humin, and bulk samples with increasing depth, with exception of the highly heterogeneous profiles in PBW and Rds (Fig. 4.7; Fig. 4.8), demonstrates a typical <sup>14</sup>C profile (Bräuer et al., 2013b; Rethemeyer et al., 2005). In combination with both vertical and lateral variability in the soil properties, i.e. grain size and mineral compositions, discussed in the preceding chapter (section 3.1; section 3.2), the depth distribution shows typical patterns according to the important processes active in the soil types. These will be discussed in this section.

Generally, the concentration of  $\Delta^{14}\text{C}$  typically decreases gradually with increasing soil depth, with exception PBW and Rds profiles (Fig. 4.6; Fig. 4.7; Appendix 4.6). In these two volcanic soils, the variability of depth- $\Delta^{14}\text{C}$  is higher due to the more heterogeneity of profile composition as a result of different origin and properties of soil parent materials (section 3.1; section 3.3).

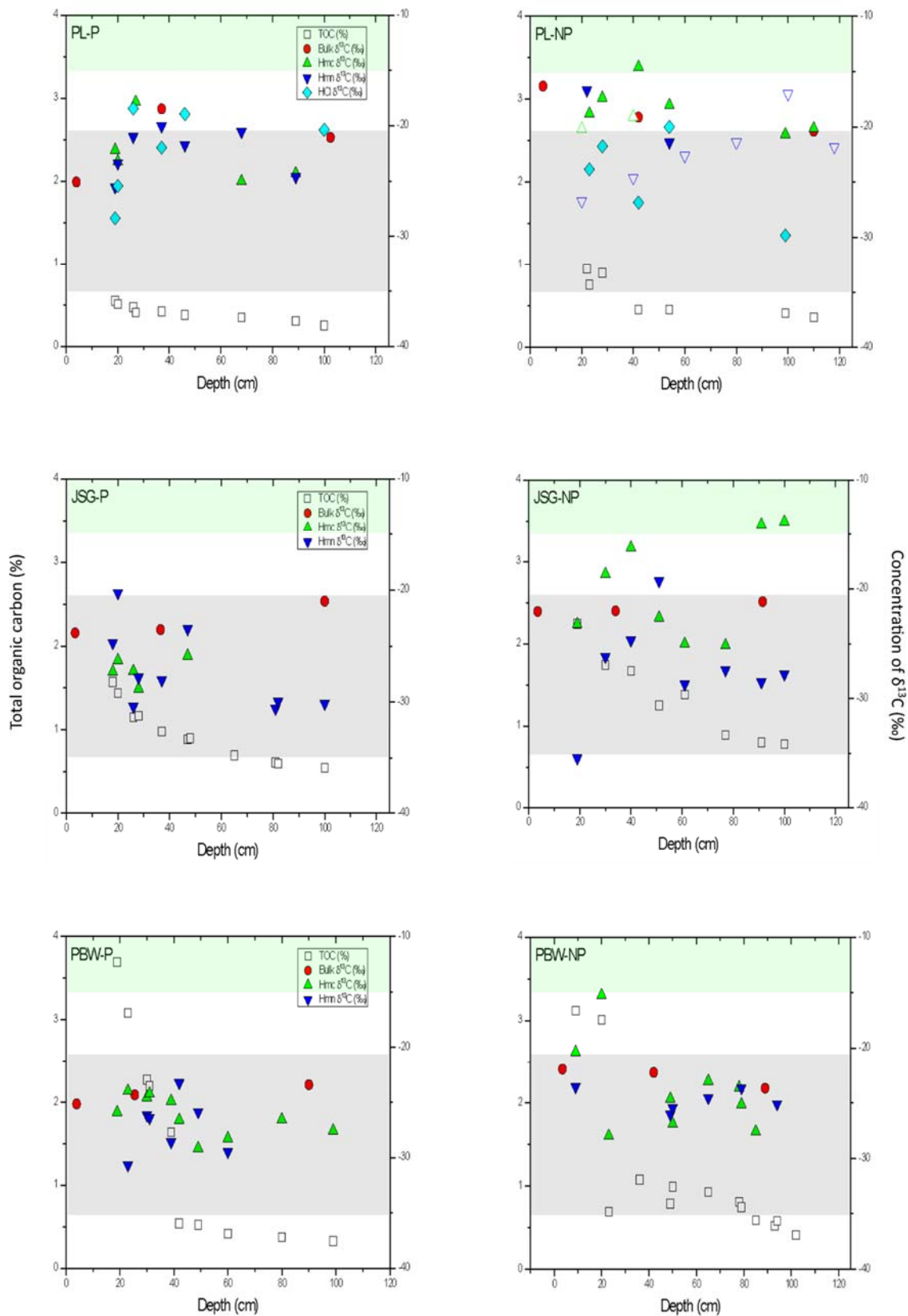


Figure. 4.5. Depth distribution of TOC and  $\delta^{13}\text{C}$  obtained from bulk, humic (hmc), humin (hmn), and conc. HCl extracted (only for PL) 2012 samples. Open marks in PL-NP represent samples from the garden plot. Grey and green shading represents  $\delta^{13}\text{C}$  range for  $\text{C}_3$  and  $\text{C}_4$  crop types according to Ehleringer (1991).

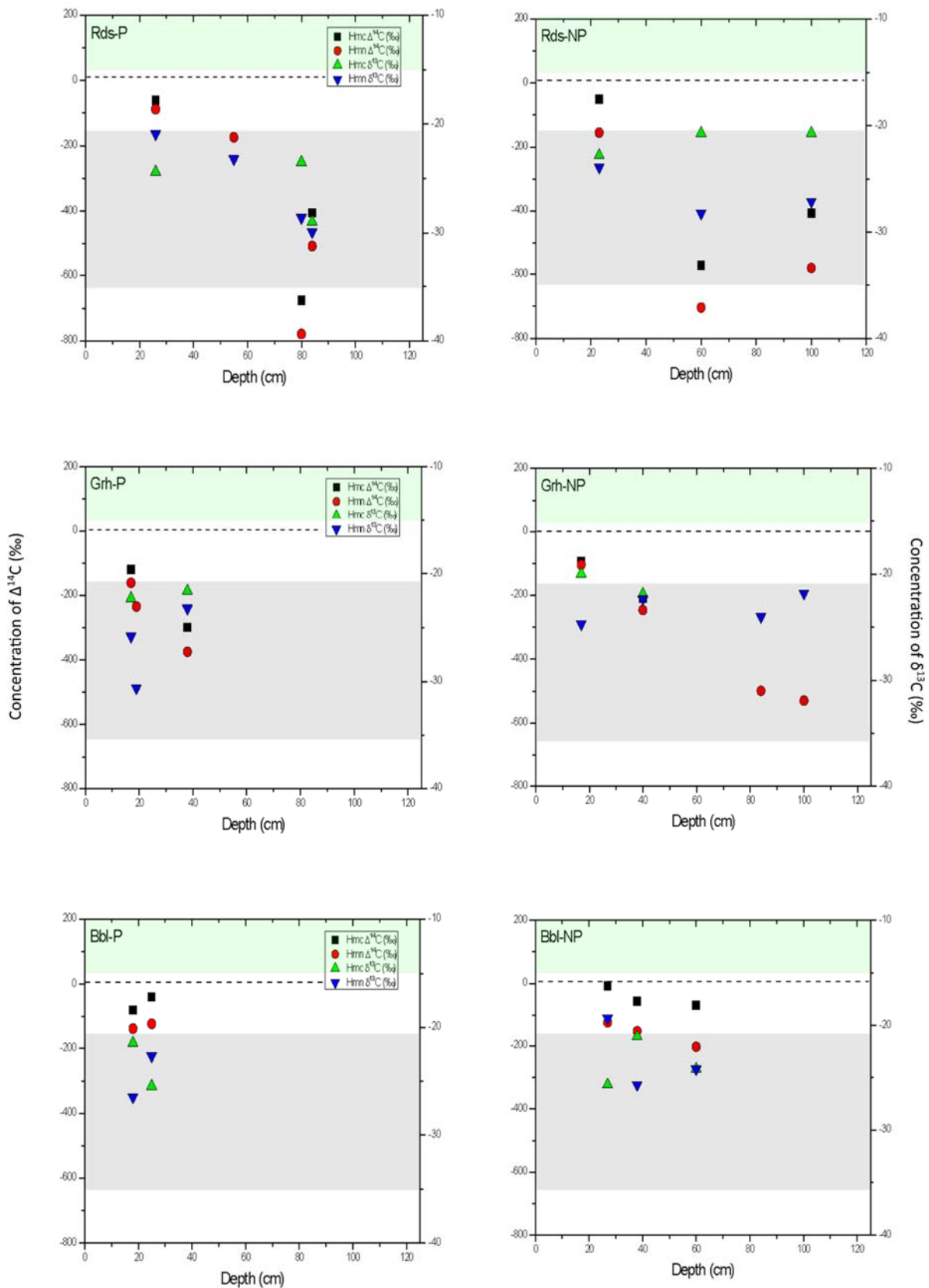


Figure. 4.6. Depth distribution of  $\Delta^{14}\text{C}$  and  $\delta^{13}\text{C}$  obtained from humic (hmc) and humin (hmn) 2016 samples. Grey and green shading represents  $\delta^{13}\text{C}$  range for  $\text{C}_3$  and  $\text{C}_4$  crop types according to Ehleringer (1991). Horizontal dotted lines indicate atmospheric level of  $\Delta^{14}\text{CO}_2$  in 2016 (~9‰) (Hammer and Levin, 2017; Levin et al., 2013).

Profile of PL is characterized by a less depleted subsoil  $\Delta^{14}\text{C}$ . At ca. 90-110 cm depth, the  $\Delta^{14}\text{C}$  show value ca. -300‰ in P (humic and humin) and ca. -200‰ in NP (humic), which are younger than other soils at the similar depth, e.g. ca. -400 to -600‰ in JSG and PBW, or ca. -500 to -800‰ in Rds and Grh. Given that smectite is a majority clay mineral in this soil (Winkler et al., 2016), the postulated argilli-pedoturbation may be responsible for the homogeneity of profile composition (section 4.2). Yet if compared to Grh profile with similar altitude on different slope of Mt. Lawu, which also exhibits a pedoturbation evidence, i.e. surface cracks and slickenside (Appendix 2.3), the level of subsoil  $\Delta^{14}\text{C}$  in PL is still significantly younger. This may lead to an assumption of the younger substrate, i.e. alluvial material, which may explain the younger subsoil  $\Delta^{14}\text{C}$  compared to other soils.

The concentration of  $\Delta^{14}\text{C}$  in the PL humin is higher than in the humic fractions in upper ca. 40 cm depth both at P and NP (Appendix 4.6). Below this point, the concentration of  $\Delta^{14}\text{C}$  in both fractions are quite similar (Fig. 4.7). As occurred in the top layers, the higher  $\Delta^{14}\text{C}$  content in the top layers humin may be related to the high abundance of root mass. The contribution of these materials may lead to a higher proportion of unextractable young carbon preserved in the humin. Conversely, in different soil types  $\Delta^{14}\text{C}$  content in the humin is lower than in the humic fractions. It is also occurred that humin in different soil types are older than PL humin (Appendix 4.6), (with excluding the anomalous sample of 35-40 cm depth in PBW-P). The bomb- $^{14}\text{C}$  enrichment to soil organic fractions are missing in P, but it is present in NP (both sugarcane and garden plot) as an enrichment in the humin fraction.

Different with other samples in PL profiles, the greenish-grey sample from Bik horizon at ca. 100 cm depth of garden plot shows a significantly older carbon with  $\Delta^{14}\text{C}$  content of ca. -440‰. This anomalous sample exhibits a pH of ca. 8.03 (Appendix 3.1), higher than the neighbouring layer with normal colour of Vertisol (dark) of ca. 7.72, which indicate the strong presence of alkaline minerals. As in alkaline soil condition carbon can be retained by Ca (Oades, 1988), therefore the low  $\Delta^{14}\text{C}$  content of sample with concomitant alkaline pH may be related to the preservation.

A regular depth distribution of  $^{14}\text{C}$  in JSG profiles may be related to the high homogeneity of layer compositions, as suggested by grain size and elemental compositions (section 3.1 and 3.2; Fig. 2.3). Coefficient of variation of clay shows a value below 15% which is quite low in variability (Table 3.2). The depth distribution of carbon may be interpreted as a result of typical carbon transport (section 4.1), and the increase in the apparent carbon ages with depth results from the increasingly limited fresh organic supply. As kaolinite is the majority of clay mineral in this soil (Winkler et al., 2016), thus the self-mixing activity may be low.

Deep radiocarbon enrichments are limited as a large difference of top-bottom  $^{14}\text{C}$  is observed (Fig. 4.6). The low level of enrichment is attributable to the limited supply of fresh carbon material from the soil surface. JSG is characterized by the consistent higher  $\Delta^{14}\text{C}$  content in the humic than in the humin fractions throughout soil columns. At ca. 20-25 cm depth bomb- $^{14}\text{C}$  enrichment to humic fraction is occurred at both P and NP.

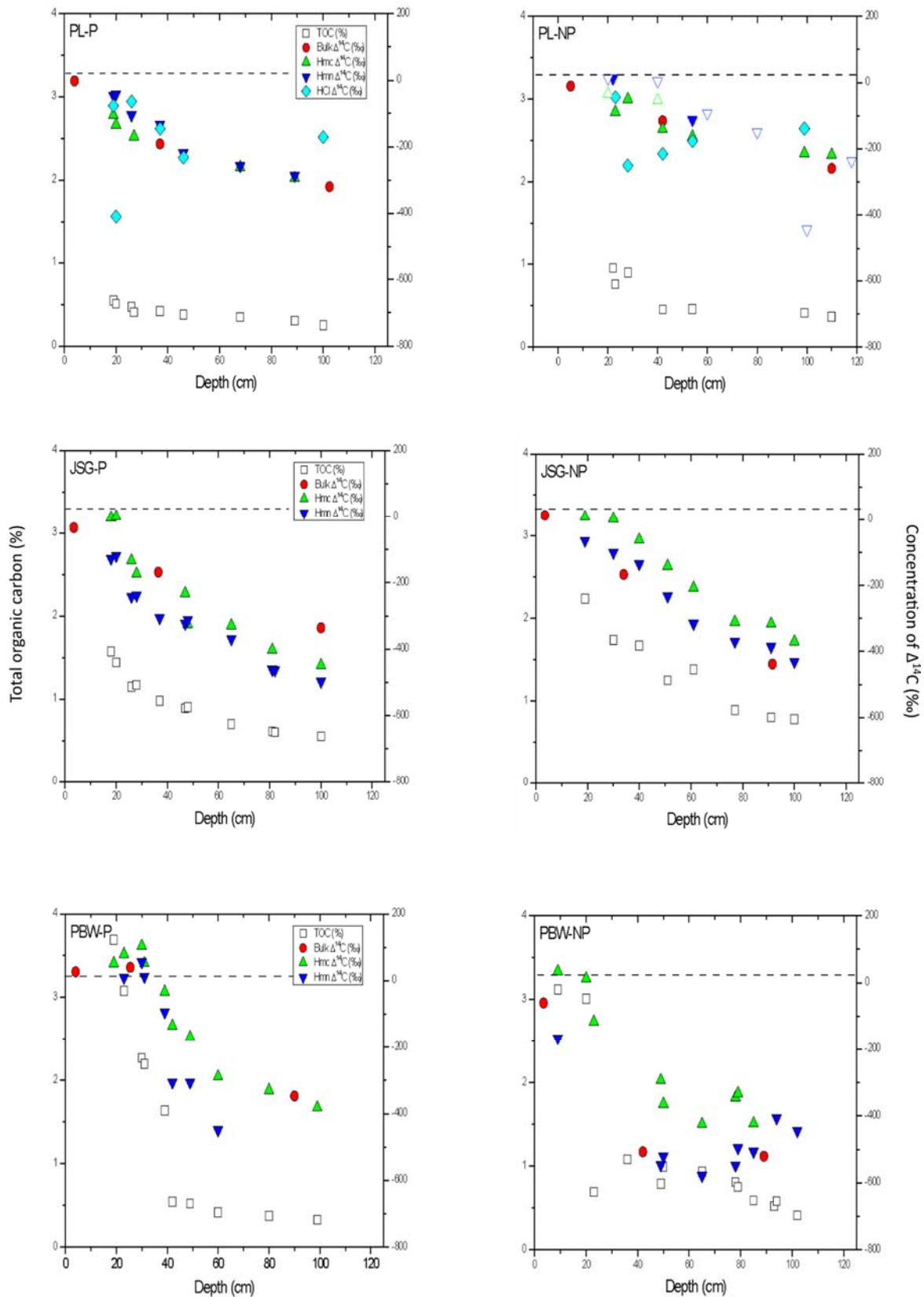


Figure. 4.7. Depth distribution of TOC and  $\Delta^{14}\text{C}$  obtained from bulk, humic (hmc), humin (hmn), and conc. HCl extracted (only for PL) samples. Open marks in PL-NP represent samples from the garden plot. Horizontal dotted lines indicate atmospheric level of  $\Delta^{14}\text{CO}_2$  in 2012 ( $\sim 31\text{‰}$ ) (Hammer and Levin, 2017; Levin et al., 2013).

PBW profiles are characterized by a high irregularity, or rather a discontinuity, of depth- $^{14}\text{C}$  values (Fig. 4.6), which may be attributable to the volcanic (lahar) nature of the parent materials (section 3.1; section 3.2). The difference in the amount of carbon preserved and in its  $^{14}\text{C}$  content in the soils above and below ca. 35 cm depth may, however, reflect an anthropogenic origin of the upper layers. Bomb- $^{14}\text{C}$  enrichment in soil organic matter fractions with  $\Delta^{14}\text{C}$  concentration up to ca. 102‰ (in humic fraction) were observed at upper 35 cm depth in the P column. This suggests a 1990s atmospheric composition of this material (Hua et al., 2013), which can be interpreted as the likely time of profile disturbance. These high  $^{14}\text{C}$  signals present in the soils imply a strong preservation of fresh material from that time buried below the puddled layer. Bomb- $^{14}\text{C}$  enrichment with lower extent also occurs at corresponding NP site with ca. 110 m higher altitude in the humic fraction. The  $\Delta^{14}\text{C}$  concentration was up to ca. 34‰ at above 20 cm layer depth.

Generally, the concentration of  $\Delta^{14}\text{C}$  is higher in the humic than in the humin fractions. The depth-distribution of humic is more regular than humin. From ca. 45 to 100 cm depth in PBW-NP while decreasing in humic the concentration of  $\Delta^{14}\text{C}$  in humin is conversely increasing. This may indicate a less depleted  $^{14}\text{C}$  in humin at deep layers.

Rds profile shows a high irregularity in the context of depth  $\Delta^{14}\text{C}$  distribution. With CV of clay is ca. 50% at both P and NP (Table 3.2), the variability in layer composition is high. A strongest preservation of  $^{14}\text{C}$  among other soil types occurs around in the middle of soil column (60-80 cm depth) up to almost -800‰ and -700‰ in humin fraction of P and NP. Below these layers, the concentration of  $\Delta^{14}\text{C}$  is decreasing. The increase in  $\Delta^{14}\text{C}$  concentration at 60-80 cm depth layers correspond with the drop of clay to less than 10% and increase in sand content to ca. 50% (Appendix 3.1). This may suggest a mineral associated of carbon preservation. The difference in pH of soil (pH of 7.27 in P and of 6.66 in NP samples) may indicate the difference in mineral responsible for this preservation. Data shows that humic fraction contains a higher  $^{14}\text{C}$  than humin (Appendix 4.6), as a typical of other soil types.

Bomb- $^{14}\text{C}$  enrichment signal was not observed in the top layers. The top soil  $\Delta^{14}\text{C}$  content (at ca. 23-28 cm depth) in humic fraction is younger in NP, but conversely in humin is younger in P. This may suggest the higher  $^{14}\text{C}$  preservation in NP top soil.

With CV of clay is around 20% (Table 3.2), profile in Grh has a quite homogeneous layer composition. Profile have two different layer where above ca. 84 cm depth the material is alluvial (dark) with an indication of soil development in progress. Below 84 cm depth (Bwkgc/Bwk horizon), the layer is a bit reddish with lower clay but higher in silt content (Appendix 3.1). In this layer,  $\Delta^{14}\text{C}$  content is down to ca. -530‰ (humin-NP) at 100 cm depth. While in the dark layer, the lowest  $\Delta^{14}\text{C}$  content is ca. 380‰ (humin-P) from the sample at 38 cm depth.

The concentration of  $\Delta^{14}\text{C}$  in humic is consistently higher than in the humin fraction throughout soil columns. The lower  $\Delta^{14}\text{C}$  content of top soil organic matter fractions than 2016 atmospheric level indicates a pre-bomb period derived carbon. With similar level of altitude, landuses, and soil properties (in this soil the surface crack and slickenside were also

observed) the  $^{14}\text{C}$  refreshment may show a different level compared to soil in PL. In this profiles, the concentration of  $\Delta^{14}\text{C}$  in the soil organic matter fraction is lower (Appendix 4.6).

A slight depth increase of  $^{14}\text{C}$  content in Bbl of P site may indicate a mixing of soil carbon on the top layers (Fig. 4.8). As situated in the depression area (section 2.1.2.6; Fig. 2.9), the site may be the sink for soil materials to deposit from different origins with various carbon compositions. The high moisture condition of shallow soil solum (with only ca. 30 cm thickness profile), due to the presence of underlying impermeable rock parent material (Fig. 2.10), may boost the carbon mixing through high mobility of dissolved organic carbon.

The concentration of  $\Delta^{14}\text{C}$  in humic is consistently higher than humin with observed bomb- $^{14}\text{C}$  enrichment on top layers. The radiocarbon is less depleted in the top soil organic matter fractions in NP (garden plot) at 18-29 cm depth. This may indicate the effect of agricultural practices in P plot to the faster cycling of carbon.

In general, it can be concluded that the highest  $^{14}\text{C}$  signals were obtained from NP sites (Fig. 4.7; Fig. 4.8; Appendix 4.4). Though the quantity of plant residues collected from some 2016 samples were not sufficient for analysis, results from 2012 samples indicated an association between  $^{14}\text{C}$  content in the humin and plant residues as in PL and JSG. Conversely in PBW samples, larger plant residue inputs are not likely contributed to the  $^{14}\text{C}$  enrichment in the humin. As results show that humin- $^{14}\text{C}$  sample from 9 cm depth in NP, with higher amount of plant residues (Appendix 4.1), showed smaller  $^{14}\text{C}$  content than the sample from 20 cm depth in P site with lower amount of plant residues. Different factor attributable to these signals that high plant residue inputs coupled with older carbon may indicate a high inaccessibility of organic carbon.

Below ca. 50 cm depth in the P profile of PBW,  $^{14}\text{C}$  may have decoupled according to the organic fractions (Fig. 4.7). As  $^{14}\text{C}$  in the humin fractions are getting smaller with depth, it may indicate the increase in the mineral preservation. The preservation is always associated with microbial inaccessibility (Gleixner, 2013), and in non-crystalline mineral dominant soil, as in PBW, it is because strong complexation of organic carbon to sesquioxides (Matus et al., 2014; Takahashi and Dahlgren, 2016).

#### 4.3.2.2. $^{14}\text{C}$ in the bulk and organic fractions

Three different sample types, i.e. bulk, humin and humic were used to evaluate the infiltration of  $^{14}\text{C}$  in different fractions. Though a direct comparison may not be fully appropriate due to the difference in sampling intervals, i.e. humic and humin acid fractions were obtained from 2 cm-thickness layers and bulk samples represented the complete averaged horizons (Appendix 4.6), this evaluation may lead to some insights into soil carbon cycling.

The high variability of carbon origins is evidenced by the variation in  $^{14}\text{C}$  values in the humic and humin fractions and in the corresponding bulk samples (Fig. 4.6). A previous report showed that bulk- $^{14}\text{C}$  consistently represents an average value for a younger fulvic- and humic- $^{14}\text{C}$ , and an older humin- $^{14}\text{C}$  in the subtropical Cambisols (Bräuer et al., 2013a). But in this study in tropical soils, bulk- $^{14}\text{C}$  values are closer to humic- $^{14}\text{C}$  than to humin- $^{14}\text{C}$  with exception of JSG-NP (Fig. 4.7; Appendix 4.6). These results may point out a similarity of  $^{14}\text{C}$  compositions between bulk and humic samples. Given that larger portion of carbon fixed in

the humin (section 4.2), however its carbon composition may be closer to bulk samples. Conversely, as mentioned before that in this study the composite bulk samples represent the interval of soil horizons.

In addition, the variability of  $\Delta^{14}\text{C}$  in bulk compared to  $\Delta^{14}\text{C}$  in humic and humin may be interpreted in different way in the context of carbon-mineral association. Different soil processes may be responsible to different stabilization that take places. As different soil horizons pose a different stabilizations, the efficiency of carbon extractions may be different for the same extractant used during AAA treatment (section 2.3.2) for humic and humin fractions. The variability carbon extracted is the result of difference in the efficiency of extractants (Wattel-Koekkoek et al., 2001). It is suggested a different binding mechanisms of organo-mineral responsible for different soil types. The variability in the mineral composition, and degree of crystallinity of soils from previous study in the Cambisol, and from current study (section 3.2) in the Vertisol, Alisol and Andosol has been discussed (Kölbl et al., 2014; Winkler et al., 2016).

The two groups, defined based on  $^{14}\text{C}$  composition, appeared as a result of organic matter fractionations. The first group has older carbon in the humic fractions mainly the first 40 cm depth from PL, and the second group has older carbon in the humin fractions, i.e. samples from JSG, PBW, Rds, Grh, and Bbl. Among soil types, the  $\Delta^{14}\text{C}$  content in PL humin is relatively higher in all samples (excluding the high level of bomb- $^{14}\text{C}$  enrichment in PBW top soil) (Appendix 4.6). But for humic, the younger carbon in PL occurs only for some samples below ca. 60 cm depth than humic samples from other soils.

Young carbon infiltrated in the humin fractions in PL is suggested as derived from acid-alkali-insoluble fine organic remains, e.g. cellulose, from litter, which is present in the humin fractions (Fabbri et al., 1996; Simpson et al., 2007). The observed gradual drop  $^{14}\text{C}$  in the humin towards humic sample at ca. 40 cm depth is related to both the reduced of fresh supply of carbon materials from the top and the increase in the  $^{14}\text{C}$  preservation. Provided that the clay composition is similar throughout the soil columns with CV  $\sim$  25% (Table 3.2), the increase in this preservation may be associated with the increase in the Ca concentrations (section 3.3). It means that the preservation of  $^{14}\text{C}$  occur due to the presence of organic complexes with Ca, i.e. Ca cation bridging (Mikutta et al., 2007; Oades, 1988), which may not be completely removed during AAA extraction. The cationic bridges have been proposed as a binding mechanisms of organo-mineral complexes in smectitic soils (Wattel-Koekkoek et al., 2001). The preservation of carbon in alkaline minerals, presumably Ca, was detected from greenish-grey sample from Bik horizon at ca. 100 cm depth of garden plot with  $\Delta^{14}\text{C}$  content of ca. -440‰, and with concomitant high pH of ca. 8.03.

With exception of the PBW profiles, the carbon in the organic fractions is consistently younger in the NP sites than P (section 4.3.1.1). As  $^{14}\text{C}$  concentration partly may associate with litter inputs (section 4.1), it is suggested that crop managements play an important role in the refreshment of carbon mainly in the top layers, as an earlier study reported (Bräuer et al., 2013b).

#### 4.3.2.3. <sup>14</sup>C in the particle size fractions

Carbon composition (total and <sup>14</sup>C) in relation to particle size distribution is discussed in this section. Fractions were isolated from bulk samples by wet sieving and sedimentation after ultrasonication (section 2.3.3). Special attention is given to the clay fraction (< 2 μm), as it is important in the context of soil carbon dynamics, e.g. controlling the supply of labile organic material, and the resistance of organic matter to microbial degradation (Anderson and Paul, 1984). Clay samples were prepared from different soil types (Table 4.4) to see if there is any influence of mineralogy composition on carbon ages.

Results show that carbon fixed in clay size fractions does not always associate with old carbon with low <sup>14</sup>C content (Table 4.4). The interaction of old carbon with clay (Eusterhues et al., 2005) is inconsistently appeared as in some samples from PL and PBW (Table 4.4). As some samples exhibit clays with modern carbon, ca. 40-50‰, e.g. JSG samples, there must be infiltration of fresh carbon into this fractions. The labile organic fractions may present in the clay as bacterial cells and colonies (Feller and Beare, 1997; Paul, 2016), and amino acid (Anderson and Paul, 1984). In special cases, however, microbes can also recycle stabilized carbon, even uptake fossil organic matter (Rethemeyer et al., 2004b; Trumbore, 2009).

Looking at the <sup>14</sup>C content in the clay and humin fractions obtained from the same bulk samples, the clays show a higher <sup>14</sup>C concentration, by ≈ 3 – 30%, than humin in JSG and PBW samples, but reduced, by ≈ 1 – 14%, in PL samples (Table 4.4; Appendix 4.6). As different stabilization mechanism may apply, i.e. in acid soils of JSG and PBW carbon fixed by Al/Fe (Al/Fe-carbon), and in alkaline condition as at PL carbon retained by Ca (Ca-carbon) (Oades, 1988), the variation of <sup>14</sup>C content among fractions may be the result of different mineral compositions. As humin samples were obtained from AAA extraction (section 2.3.2), the 1% HCl treatment prior to dispersion may have removed most of the Ca-carbon in the PL samples into solution. But 1% HCl may not significantly remove Al/Fe-carbon, since the higher concentration of HCl, i.e. 36% HCl, at high temperature is needed to dissolve them (Pansu and Gautheyrou, 2006). In contrast, sample preparation during clay extraction (section 2.3.3) did not apply any chemical treatment.

As a result, Ca-carbon may be retained in the clay more than humin samples. Therefore, it is suggested that carbon fixed by Ca is preserved, and responsible for lower <sup>14</sup>C content in clay than in humin of PL samples. Conversely, the sequence washing may not remove Al/Fe-carbon much more than 1% HCl extraction during AAA treatment. The higher <sup>14</sup>C content in the clay than in humin in JSG and PBW samples may be related to the infiltrated young carbon component that still remaining in clay which is probably eliminated for 1% HCl extraction.

The clay fractions obtained from deep layers of PL samples hold consistently older carbon than the clay extracted from top layers, ca. 20 cm depth (Table 4.4). The older carbon with depth may be associated with the increase of Ca-related stabilization and calcium carbonate (Appendix 3.2). In the top layers, young carbon enrichment may have occurred as contributed from high amount of plant debris, with concomitant high microbial activity.

Table. 4.4. Organic carbon and isotopic composition in the soil particle size fractions.

Site	Depth (cm)	Carbon	Particle size							
			250-2000 $\mu\text{m}$	63-250 $\mu\text{m}$	20-63 $\mu\text{m}$	6-20 $\mu\text{m}$	2-6 $\mu\text{m}$	<2 $\mu\text{m}$	Bulk < 63 $\mu\text{m}$	
PBW-P	39-40	TOC (%)	nd <sup>18</sup>	nd	nd	nd	nd	nd	2.41	1.85
		$\delta^{13}\text{C}$ (‰)	nd	nd	nd	nd	nd	nd	-22.9 $\pm$ 2.0	-25 $\pm$ 1.2
		$\Delta^{14}\text{C}$ (‰)	nd	nd	nd	nd	nd	nd	-60.67 $\pm$ 1.70	-65.83 $\pm$ 1.80
PBW-NP	49-50	TOC (%)	nd	nd	nd	nd	nd	nd	1.23	1.08
		$\delta^{13}\text{C}$ (‰)	nd	nd	nd	nd	nd	nd	-19.1 $\pm$ 2.3	-17.7 $\pm$ 1.9
		$\Delta^{14}\text{C}$ (‰)	nd	nd	nd	nd	nd	nd	-414.90 $\pm$ 1.60	-471.58 $\pm$ 1.20
JSG-P	18-20	TOC (%)	nd	nd	nd	nd	nd	nd	1.63	1.5
		$\delta^{13}\text{C}$ (‰)	nd	nd	nd	nd	nd	nd	-21.8 $\pm$ 1.1	-24.5 $\pm$ 1.1
		$\Delta^{14}\text{C}$ (‰)	nd	nd	nd	nd	nd	nd	0.67 $\pm$ 1.80	-19.68 $\pm$ 1.90
JSG-NP	19-20	TOC (%)	nd	nd	nd	nd	nd	nd	2.15	2.27
		$\delta^{13}\text{C}$ (‰)	nd	nd	nd	nd	nd	nd	-21 $\pm$ 2.1	-21.6 $\pm$ 2.5
		$\Delta^{14}\text{C}$ (‰)	nd	nd	nd	nd	nd	nd	9.16 $\pm$ 1.90	-2.91 $\pm$ 1.50
PL-P	19-20	TOC (%)	0.64	0.31	1.07	1.1	0.98	0.82	0.82	1.2
		$\delta^{13}\text{C}$ (‰)	-25.1 $\pm$ 3.60	-28.4 $\pm$ 1.90	-15.2 $\pm$ 1.50	-22.9 $\pm$ 1.80	-18.5 $\pm$ 1.60	-23.1 $\pm$ 1.70	-23.9 $\pm$ 1.80	
		$\Delta^{14}\text{C}$ (‰)	-34.27 $\pm$ 6.70	38.28 $\pm$ 2.20	-69.94 $\pm$ 2.30	-78.64 $\pm$ 3.60	-73.08 $\pm$ 1.90	-58.49 $\pm$ 2.20	-70.30 $\pm$ 1.90	
PL-P	100-101	TOC (%)	8.56	1.39	0.8	0.68	0.63	0.29	0.29	0.83
		$\delta^{13}\text{C}$ (‰)	-9.5 $\pm$ 2.20	-7.9 $\pm$ 2.60	-15.8 $\pm$ 2.80	-16.3 $\pm$ 2.10	-13.5 $\pm$ 1.80	-21.9 $\pm$ 2.70	-13.6 $\pm$ 2.40	
		$\Delta^{14}\text{C}$ (‰)	-427.01 $\pm$ 1.20	-618.37 $\pm$ 1.00	-482.30 $\pm$ 2.50	-469.20 $\pm$ 1.90	-441.31 $\pm$ 1.10	-329.45 $\pm$ 1.50	-553.06 $\pm$ 1.20	
PL-NP	22-23	TOC (%)	0.48	0.29	1.3	1.63	1.11	1.08	1.08	1.49
		$\delta^{13}\text{C}$ (‰)	-24.4 $\pm$ 3.80	-17.6 $\pm$ 1.50	-14.4 $\pm$ 1.20	-19.3 $\pm$ 1.40	-13.8 $\pm$ 1.40	-11.4 $\pm$ 2.20	-15 $\pm$ 2.30	
		$\Delta^{14}\text{C}$ (‰)	-407.46 $\pm$ 5.00	-25.83 $\pm$ 1.70	-62.95 $\pm$ 1.40	-73.47 $\pm$ 1.70	-118.93 $\pm$ 1.40	-121.31 $\pm$ 1.60	-60.37 $\pm$ 2.10	
PL-NP	110-111	TOC (%)	0.09	0.05	0.94	0.93	0.91	0.8	0.8	0.67
		$\delta^{13}\text{C}$ (‰)	-38.2 $\pm$ 0.10	-26 $\pm$ 1.20	-19.1 $\pm$ 1.80	-20 $\pm$ 1.70	-19.3 $\pm$ 1.50	-20.5 $\pm$ 2.50	-21.6 $\pm$ 1.90	
		$\Delta^{14}\text{C}$ (‰)	-166.18 $\pm$ 4.80	-212.33 $\pm$ 3.80	-237.34 $\pm$ 1.30	-218.09 $\pm$ 1.30	-234.56 $\pm$ 1.80	-233.07 $\pm$ 2.20	-232.28 $\pm$ 3.00	

<sup>18</sup> Not determined.

In this study, radiocarbon dating for six classes of soil particles was only performed for PL samples (Table 4.4). Results suggest no clear trends between soil size fractions and  $^{14}\text{C}$  contents. Coarse sand samples at depth of the P profile and the top layer in NP show older than the typical in this fraction. The older carbon at depth, ca. 100 cm, in P profile may be related to the limited fresh carbon supply from the top. In NP profile, top layer carbon shows significantly older ( $\approx -376\%$ ) than the same fraction from the depth ( $\approx -122\%$ ) (Table 4.4). As carbon in  $> 20 \mu\text{m}$  fractions are related to plant debris (Feller and Beare, 1997), the low  $^{14}\text{C}$  signal is likely derived from material with subject to high decomposition stage, and occluded in the aggregate.

In PL, the alkaline condition of soil shows to relate with the high distribution of carbonate minerals in the soil columns (section 3.3; Appendix 4.3). By the use  $\delta^{13}\text{C}$  as a tracer, the mobility of carbon through different soil fractions may be evaluated in combination with total inorganic carbon content (TIC) (Appendix 4.3). In PL-P TIC content is increasing with soil depth, but in PL-NP it tends to decrease.

Result shows that the high TIC in 100 cm depth sample of P (0.63%) provides a signal of enriched  $\delta^{13}\text{C}$  with values  $\leq -15\%$  in sand fractions. These values are tend to deplete towards the finer fractions. Conversely, with lower TIC in 110 cm depth sample of NP (0.12%), the signal of  $\delta^{13}\text{C}$  shows to deplete up to  $-38\%$  in sand fractions with a slightly enrichment towards fine fractions. The signal trends of  $\delta^{13}\text{C}$  vertically both in P and NP show to well-correlate with TIC content.

A poor correlation of  $^{14}\text{C}$  content and total organic carbon in the soil fractions ( $r = -0.068$ ) may indicate a random infiltration of  $^{14}\text{C}$ . This result is in contrast with the trend produced from bulk samples of, mainly, JSG and PL sites (section 4.2; Fig. 4.3), as they show high  $^{14}\text{C}$  content with total organic carbon. The high mobility of  $^{14}\text{C}$  in soil fractions may be related to different carbon compositions that associate with specific fractions, e.g. microbial cell wall, amino acid occurred in clay fractions (Anderson and Paul, 1984; Paul, 2016), highly humified plant, fungal debris in  $2 - 20 \mu\text{m}$  fractions, and plant debris in  $> 20 \mu\text{m}$  fractions (Feller and Beare, 1997). Conversely, values emerged from bulk samples are the average of overall components. Carbon materials infiltrated into fractions are likely facilitated by biotic and abiotic processes in the soil.

A better correlation of clay and bulk  $< 63\mu\text{m}$  samples (silt + clay associated carbon) in the context of  $^{14}\text{C}$  content and total organic carbon was observed ( $r=0.95$ ;  $r=0.87$ ). Bulk  $< 63\mu\text{m}$  is residual sample obtained after last withdraw for clay fractions (section 2.3.3). This result may have reflected similar carbon compositions regardless soil types and layers. Total organic carbon has typical increase in the clay fractions  $\approx 3 - 120\%$  from bulk samples, except in JSG-NP with observed 4% drop. The original texture of samples may be responsible to this variations. Sample with clay texture (section 3.1) show a small carbon enriched in clay fractions, e.g. JSG samples. It is suggested that in the originally clay texture soils, total organic carbon in bulk samples may represent carbon in the clay fractions. The signals of  $\delta^{13}\text{C}$  show consistently enriched in the clay ca. 10-40% from humin samples, except JSG sample in P site (section 4.3.1). This may be attributable to the higher heterogeneity of organic carbon compositions in humin samples.

## Conclusions

The collected plant remains at the profile assuming depth-distribution of plant residues may be fitted with an exponential model. Results show  $\mu$  values to vary with different soil types, i.e. 0.91 (PL-P), 0.93 (PL-NP), 0.96 (JSG-P), 0.96 (JSG-NP), 0.93 (PBW-P), and 0.85 (PBW-NP). This implies a higher carbon depth-distribution at JSG than other profiles. The most plant residues at top soils (0-20 cm depth) account for more than 50% of the total plant remains throughout the soil column. By comparing top soil carbon stock with the assumption made for total carbon inputs, the turnover time of carbon shows higher in PBW than in different sites.

Carbon dating of plant remains demonstrated no correlation between colours and the degree of decompositions. The dark roots do not reflect the old organic materials and light plant remains do not mean fresh residues. Colours may indicate the plant origins in combination with  $\delta^{13}\text{C}$  signals, as identified young dark roots were associated with sugarcane. The presence of modern plant residues at depth, ca. 100 cm depth, suggest a direct translocations. This is an option of carbon pathway into subsoils as shows to happen in all profiles, and likely soil type independent.

Total organic carbon (TOC) for 2012 samples varies within the range 0.25 to 0.55% in PL-P, 0.36 to 0.952% in PL-NP, 0.55 to 1.57% in JSG-P, 0.78 to 2.24% in JSG-NP, 0.33 to 3.69% in PBW-P, and 0.41 to 3.12% in PBW-NP. Coefficient of variation shows high variability of depth TOC distribution in PBW. The higher NP TOC content than P may indicate the association with plant litter inputs.

Samples with high organic carbon are consistently associated with high  $^{14}\text{C}$  content, which means that young carbon must have accounted for most of the bulk organic carbon. Conversely, samples with low total organic carbon content exhibit low  $^{14}\text{C}$  contents, which indicates a high proportion of old carbon. The organic carbon content shows higher in the humin than humic acid.

Soil  $^{13}\text{C}$  may be enriched or depleted in  $^{13}\text{C}$  as a result of carbon mixing due to the variation of carbon input in agricultural fields. The study shows a dominant of  $\text{C}_3$  type crops in the fields. Carbon enrichment is likely appeared to shift  $\delta^{13}\text{C}$  even from a monoculture field. This may indicate a different origin of some of the carbon, for instance from weeds, manure or irrigation water. By relating the concentration of  $\delta^{13}\text{C}$  and  $^{14}\text{C}$  from the same samples, analysis shows that there is no specific condition of crop types contributed to the  $^{14}\text{C}$  input but atmospheric compositions. Organic matter fractionation show the inconsistent variations in the  $\delta^{13}\text{C}$  signals compared to bulk samples.  $\delta^{13}\text{C}$ -bulks as mean values subject either to be enriched or depleted depending on the original carbon.

The concentration of  $\Delta^{14}\text{C}$  typically decreases gradually with increasing soil depth, with exception PBW and Rds profiles. In these two volcanic soils, the variability of depth- $\Delta^{14}\text{C}$  is higher. Profile of PL is characterized by a less depleted subsoil  $\Delta^{14}\text{C}$ . Given that smectite is a majority clay mineral in this soil, the postulated argilli-pedoturbation may be responsible for the homogeneity of profile composition. The higher  $\Delta^{14}\text{C}$  content in the PL top layers humin may be related to the high abundance of root mass that leads to a higher proportion of

unextractable young carbon preserved in the humin. A regular depth distribution of  $^{14}\text{C}$  in JSG profiles may be related to the high homogeneity of layer compositions. The low level of subsoil  $^{14}\text{C}$  enrichment is attributable to the limited supply of fresh carbon material from the soil surface. PBW profiles are characterized by a high irregularity, or rather a discontinuity, of depth- $^{14}\text{C}$  values which may be attributable to the volcanic (lahar) nature of the parent materials. The high  $^{14}\text{C}$  signals present in the soils imply a strong preservation of fresh material. Rds profile shows a high irregularity in the context of depth  $\Delta^{14}\text{C}$  distribution. A strong preservation of  $^{14}\text{C}$  occurs suggested as mineral associated. Profile of Grh has a quite homogeneous layer composition. The lower  $\Delta^{14}\text{C}$  content of top soil organic matter fractions than 2016 atmospheric level indicates a pre-bomb period derived carbon. In Bbl profiles, the radiocarbon is less depleted in the top soil organic matter fractions in NP indicating the effect of agricultural practices in P plot to the faster cycling of carbon.

In general, it can be concluded that the highest  $^{14}\text{C}$  signals were obtained from NP sites. With exception of the PBW profiles, the carbon in the organic fractions is consistently younger in the NP sites than P. As  $^{14}\text{C}$  concentration partly may associate with litter inputs, it is suggested that crop managements play an important role in the refreshment of carbon mainly in the top layers. The high variability of carbon origins is evidenced by the variation in  $^{14}\text{C}$  values in the humic and humin fractions and in the corresponding bulk samples. Results may point out a similarity of  $^{14}\text{C}$  compositions between bulk and humic samples. In this study the composite bulk samples represent the interval of soil horizons while humic and humin were obtained from point samples. The two groups, defined based on  $^{14}\text{C}$  composition, appeared as a result of organic matter fractionations. The first group has older carbon in the humic fractions mainly the first 40 cm depth from PL, and the second group has older carbon in the humin fractions, i.e. samples from JSG, PBW, Rds, Grh, and Bbl.

Results show that carbon fixed in clay size fractions does not always associate with old carbon with low  $^{14}\text{C}$  content. As some samples exhibit clays with modern carbon, there must be infiltration of fresh carbon into this fractions. The clays show a higher in  $^{14}\text{C}$  concentration, by  $\approx 3 - 30\%$ , than humin in JSG and PBW samples, but reduced, by  $\approx 1 - 14\%$ , in PL samples. The clay fractions obtained from deep layers of PL samples hold consistently older carbon than the clay extracted from top layers, ca. 20 cm depth. Results suggest no clear trends between soil size fractions and  $^{14}\text{C}$  contents. The signal trends shows a good association of  $\delta^{13}\text{C}$  in soil particles with TIC content.

A poor correlation of  $^{14}\text{C}$  content and total organic carbon in the soil fractions may indicate a random infiltration of  $^{14}\text{C}$ . The high mobility of  $^{14}\text{C}$  in soil fractions may be related to different carbon compositions that associate with specific soil fractions. A better correlation of clay and bulk  $< 63\mu\text{m}$  samples (silt + clay associated carbon) in the context of  $^{14}\text{C}$  content and total organic carbon may reflect a similar carbon compositions regardless soil types and layers. Bulk sample with clay texture show a small carbon enriched in clay fractions. It is suggested that in the originally clay texture soils, total organic carbon in bulk samples may represent carbon in the clay fractions.

## Chapter 5

### 5. Modelling carbon dynamics in agriculture soil in different soil types under different climate conditions

#### 5.1. Introduction

The formulation of a mathematical model to evaluate soil-process-related dynamics of soil carbon in the research areas in Java is discussed in this chapter. As presented earlier (section 4.2; section 4.3.2), the depth distribution of carbon may reflect the important processes in specific locations/soil types. These specific soil processes may have related to soil variability conditions, i.e. the origin of parent materials and topography, has been discussed previously (section 3.1; section 3.2).

Additionally, some factors that potentially influence soil carbon such as climate (section 3), quality and quantity of organic residues (section 3.3; section 4.1), and internal soil column properties, (e.g. penetrability and pedo-/bio-turbation), have also briefly been discussed. These factor have not been well quantified due to the different scope of research. Yet are, however, indispensable to soil carbon distribution with respect to specific locations/soil types. To fill this gap modelling could provide a faster way to unravel issues than direct experiments (Powlson, 1996).

The present model includes the processes of original carbon distribution into soil depth. Currently, the modelling of deep organic carbon is receiving broad attention (Ahrens et al., 2015; Bartsev and Pochekutov, 2016; Wells and Hancock, 2014), since its potential implication to the global carbon cycle has been recognized (Baisden and Parfitt, 2007; Jobbágy and Jackson, 2000; Rumpel and Kögel-Knabner, 2011). The ongoing modelling is still focused on deciphering the complex system of deep carbon to predict the impact of land management, to mitigate climate change, as well as policy related efforts (Campbell and Paustian, 2015).

Due to the high chemical complexity of soil organic matter, a model that reflects the heterogeneity, such as a multi-compartment model, is thought to provide more meaningful estimates than single-pool models (Schoor et al., 2016a). Every single conceptual soil organic fraction, e.g. active, passive, and slow (section 5.2.1.2) or humic/humin after acid-alkali-acid treatments (section 2.3.2), varies in residence time compared to the averaged bulk values (section 4.3.2.2). Furthermore, they have been reported to respond differently to temperature (Conant et al., 2008), and vary in the decomposition rate (Voroney et al., 1981). Therefore, the best soil organic matter evaluation may be made after taking into consideration the fraction levels.

In this model, we develop equations to describe the way top organic carbon goes down into deep layers, taking into account the processes in the top and subsoil, based on an assumption of steady-state conditions for simplification. Two different top soil environments, i.e. P and NP, determine the quantity of litter input and redox conditions. Model starts from the estimation of carbon introduced from plant litter. The capacity of the soil to store organic carbon is approached since different soil type may have different mechanisms, in relation of clay mineralogy composition to complex organic carbon (Singh et al., 2016; Winkler et al.,

2016). The quantity of organic fractions is estimated from <sup>13</sup>C-NMR analysis (section 2.4.4; section 3.3), taking into account the environmental variables, i.e. temperature, soil moisture, and oxygen availability to constrain their decomposition. The depth-distribution of carbon in soils is evaluated using two transport parameters, i.e. convection and diffusion (section 5.2.2).

## 5.2. Model formulation

In general, at least two processes may be responsible for carbon at depth, i.e. transformation and transportation. The fresh/residual carbon undergoes a microbial decomposition that brings about complex structural changes into different compounds as well as mineralization. Facilitated by soil processes, these decomposition products may be partly translocated down into sublayers. Under natural conditions, as a function of depth  $z$  and time  $t$ , carbon at depth mathematically can be expressed as  $C = C(z, t)$ . By taking into account these two processes, i.e. transformation and transportation, the basic understanding of depth carbon is expressed in eq. (5.1).

$$\frac{\partial C(z,t)}{\partial t} = \frac{\partial C_{transformation}}{\partial t} + \frac{\partial C_{transport}}{\partial z} \quad (5.1)$$

In eq. (5.1), the first term on the right hand side indicates carbon transformation, e.g. humification, as a result of microbial actions under control of organic compound quality, and environmental variables. The carbon input, excluding erosion, may come from litter and manure above the ground, and be derived from roots and exudate below ground. The carbon output is as gaseous loss through microbial respiration. Carbon fluxes within the soil column (in/outflux of a soil element) are determined by diffusion, transport through leaching, and bioturbation/pedoturbation (section 5.2.2). Based on eq. (5.1) above, the mathematical expression will be developed under assumption of steady state conditions. The carbon transformation will be discussed in section 5.2.1, and the carbon transport will be formulated in section 5.2.2.

### 5.2.1. Soil organic carbon transformation

The transformation of soil carbon is a continuous metabolic process in multiple pools with varying persistence through repeated synthesis from new organic inputs and re-synthesis of the older residual organic carbon (Gleixner, 2013). Once fresh/old organic residues have been deposited, the decomposition proceeds at a certain rate determined by driving factors, e.g. temperature, oxygen, soil moisture, and makes up a new synthesized organic carbon. This means that microbial activities always proceed with or without the addition of new organic material.

#### 5.2.1.1. Carbon inputs ( $C_{(i)}$ )

The stock of carbon in the layers,  $C$ , is assumed to be proportional with carbon influx,  $C = h * C_{influx}$  where  $h$  is the carbon storage coefficient, similar to the humification or carbon sequestration constant concept in different models (Kemanian and Stöckle, 2010; Taghizadeh-Toosi et al., 2014). The present model implements  $h$  to describe the extent of stabilized/sequestered carbon from total fresh residue entered in the soil. The  $h$  coefficient is not only a function of the clay content quantitatively as in the RothC (Coleman and

Jenkinson, 1999), C-TOOL (Taghizadeh-Toosi et al., 2014) and C-Farm model (Kemanian and Stöckle, 2010), but also a function of the mineral composition. The carbon sorption to different clay mineralogy may follow the order allophane > smectite > kaolinite (Singh et al., 2016). Therefore, the  $h$  coefficient will be assumed to follow this order.

Based on stability, the organic input into the soil as well as the organic material in the soil can be divided into decomposable, structural, and resistant. The proportion of the decomposable/fast/active ( $f\text{-fom}$ ), (ii) the structural/intermediate/passive ( $f\text{-iom}$ ), and (iii) the resistant/slow ( $f\text{-som}$ ) pools in organic material can be estimated through solid-state  $^{13}\text{C}$ -NMR analysis. Examples of  $f\text{-fom}$  materials are proteins, of  $f\text{-iom}$  cellulose and hemicellulose, and of  $f\text{-som}$  lignin-rich compounds. Relative contribution of molecular composition can be estimated from regions of the NMR spectrum using N:C ratio and signal intensity in a mixing model (Nelson and Baldock, 2005). The model assumes that  $f\text{-fom}$  attributes to protein, and microbial lipids,  $f\text{-iom}$  refers to carbohydrates, while  $f\text{-som}$  describes lignin, carbonyl, and lipid. The total soil lipids consist of an active pool to refer to microbial cell membranes and cell walls, and a slow pool for the remainder which is plant-derived. Microbial lipids account for 10% of total lipids in the soil (Dippold and Kuzyakov, 2016), therefore we cut-off 10% of total lipid for active pools.

Carbon input on the ground surface as a daily basis is estimated from references (Table 5.1), and partitioned for subsoil input at 20 cm depth by the formula below (Jackson et al., 1996):

$$Y = 1 - \mu^z \quad (5.2)$$

With:

- Y = cumulative root fraction (0 – 1)
- z = soil depth (cm)
- $\mu$  = fitted depth coefficient

Subsoil carbon input, at 20 cm depth, can be estimated by modifying eq. (5.2) as below:

$$C_t(z_i) = C_0 * (1 - Y) \quad (5.3)$$

With:

- $C_t(z_i)$  = carbon input at depth  $i$  cm,  $i = 20$  ( $\text{g C cm}^{-2} \text{d}^{-1}$ )
- $C_0$  = total carbon input at ground surface ( $\text{g C cm}^{-2} \text{d}^{-1}$ )

Results show (Appendix 5.1) that the  $\mu$  values obtained are 0.91 (PL-P), 0.93 (PL-NP), 0.96 (JSG-P), 0.96 (JSG-NP), 0.93 (PBW-P), and 0.85 (PBW-NP). The higher constant  $\mu$  indicates the more carbon distributed with depth.

### 5.2.1.2. Carbon decomposition ( $C_{(o)}$ )

Carbon losses are assumed to be through microbial respiration during organic fraction decompositions and, for  $^{14}\text{C}$ , through natural radioactive decay. First-order decomposition equation for bulk samples at time  $t$  can be expressed as  $\frac{dC(t)}{dt} = \Sigma k_i * C(t)$ , with  $k_i$  is the decomposition rate constant for carbon fractions (active, passive, and slow), or the decay constant for  $^{14}\text{C}$  which is equal to  $3.3 \times 10^{-7} \text{ d}^{-1}$ .

Unlike the natural  $^{14}\text{C}$  decay, the decomposition of organic carbon is controlled by environmental variables, such as temperature, soil moisture, and oxygen availability. Each variable will be included in the model formulation by a coefficient. The sensitivity of organic matter decomposition to temperature,  $f(t_s)$ , to organic matter decomposition is expressed by  $Q_{10}$  values, defined as a coefficient that indicates the increase in decomposition as a result of a temperature increase by  $10^\circ\text{C}$  (Dessureault-Rompré et al., 2010; Fierer et al., 2005; Leiros et al., 1999), as below:

$$f(t_s) = Q_{10}^{\frac{T_m - T_{ref}}{10}} \quad (5.4)$$

With:

$T_m$  = mean air annual temperature ( $^\circ\text{C}$ ), data from local climate stations

$T_{ref}$  = reference air temperature ( $20^\circ\text{C}$ )

Using  $Q_{10}$ , the interplay of temperature and the rate of decomposition is assumed to be exponential. In the large scale, a  $Q_{10}$  value of 2 is adequately used for modelling of temperature effects in the range  $5 - 40^\circ\text{C}$  (Kätterer et al., 1998). In this model, because individual organic fractions, i.e. active, passive, and slow, will be represented,  $Q_{10}$  values will vary, being higher for the more stable organic fractions, to indicate higher energy required to perform decomposition, and smaller for the more easily decomposable fractions (Conant et al., 2008). Due to the variability of  $Q_{10}$  with depth and soil texture (Graf et al., 2008; Juo and Franzluebbers, 2003), this model assumes the same top meter soil temperature at the ground surface for simplicity (Table 5.1; Appendix 5.2).

The effect of soil moisture in relation to soil organic matter decomposition,  $f(m_s)$ , is expressed as metric potential (Paul et al., 2003; Rawls et al., 1982). In principle, effective microbial metabolism can perform in the range  $-33 \text{ kPa}$  to  $-10 \text{ kPa}$  as soil is holding the maximum amount of water available (Juo and Franzluebbers, 2003), and optimum for net mineralization (Myers et al., 1982). It is suggested that air-filled pore space is sufficient for both microbial activity and plant growth in this range. As soil moisture increases to the saturation point ( $-0.1 \text{ kPa}$ ), or decreases to the permanent wilting point ( $-1500 \text{ kPa}$ ), the condition is less favorable for microbial activity.

As this model will include redox conditions in relation to soil organic matter decomposition, two conditions related to soil moisture will be defined: anoxic, typically corresponding to  $\text{Eh} < 300 \text{ mV}$ , and oxic, corresponding to  $300 > \text{Eh} > 600 \text{ mV}$  (Moorman and van Breemen, 1978).

During anoxic conditions the level of soil moisture may increase up to saturation point, while during oxic moisture is held around field capacity towards the permanent wilting point.

$$f(m_s) = \begin{cases} W_s - W_{fc} & \psi < -10 \text{ kPa} \\ 1 & -33 \leq \psi \leq -10 \text{ kPa} \\ W_{fc} - W_{pwp} & \psi > -33 \text{ kPa} \end{cases} \quad (5.5)$$

Remark:

$W_s$  = saturation point

$W_{fc}$  = field capacity

$W_{pwp}$  = permanent wilting point

As expressed in eq. (5.5), the optimum condition in the range -33 to -10 kPa will result in the  $f(m_s)$  value equal to 1. With the increase or decrease in soil moisture from this level, the coefficient  $f(m_s)$  will drop below one. This model assumes that under field conditions, neither the oxic, i.e. NP soil, P subsoil, nor the anoxic soil, i.e. P top soil, have the optimum moisture level. The  $m_s$  values for anoxic layers scale with the difference between potential saturation point,  $W_s$ , and field capacity  $W_{fc}$ , while for oxic layers the  $m_s$  value is designated as the difference between potential  $W_{fc}$  and  $W_{pwp}$ . This means that under oxic conditions, moisture status holds a value in between  $W_{pwp}$  and  $W_{fc}$ , and under anoxic in between  $W_{fc}$  and  $W_s$ .

As saturation point  $W_s$  indicates the level at which all soil pores are occupied by water (Juo and Franzluebbers, 2003), this value can be approached by the total porosity of the soil,  $n$ , defined as:

$$n = 1 - \frac{\rho_b}{\rho_p} \quad (5.6)$$

With:

$\rho_b$  = bulk density ( $\text{g cm}^{-3}$ )

$\rho_p$  = particle density (assumed  $2.65 \text{ g cm}^{-3}$ )

To estimate  $W_{fc}$  and  $W_{pwp}$ , which are the volumetric water contents at both -33 kPa and -1500 kPa, the formulas below are used (Rawls et al., 1982):

$$W_{fc} = 0.2576 - 0.0020 \cdot \text{sand}(\%) + 0.0036 \cdot \text{clay}(\%) + 0.0299 \cdot \text{OM}(\%) \quad (5.7)$$

$$W_{pwp} = 0.0260 + 0.0050 \cdot \text{clay}(\%) + 0.0158 \cdot \text{OM}(\%) \quad (5.8)$$

$$\text{OM} = \text{organic matter content, } 100/58 \cdot \text{organic C}(\%) \quad (5.9)$$

The results of the calculation are presented in the Table 5.1 taking into account top- and subsoil-layers. Under P management, layers are always assumed to be reduced in the top-, and oxidized in the sub-soil. This is consistent with profile observation in the field (section 2.2). Under NP, soil layers are all assumed to be in oxic condition.

The oxygen effect on the decomposition rate is implemented by the oxygen availability function,  $f(o_c)$ , following Monod type formula (Rubol et al., 2013). Under reduced oxygen conditions the aerobic microorganism activities may be limited, which leads to the slow-down of organic matter decomposition.

The oxygen coefficient is formulated in different way applies the condition as below:

$$f(o_c) = \begin{cases} 0 & o_i = 0 \\ \frac{o_i}{o_i + k_o} & 0 < o_c < 1 \\ 1 & o_i \gg k_o \end{cases} \quad (5.10)$$

With:

$o_c$  = oxygen coefficient (-)

$o_i$  = oxygen concentration for  $i$  = oxidized (o), and reduced (r) layers ( $\text{mg L}^{-1}$ )

$k_o$  = half saturation constant for oxygen uptake ( $\text{mg L}^{-1}$ )

Table. 5.1. General parameters used in model.

Description	Sub-description	Symbol	Unit	Value
Decomposition rate constant	sugars-amino acid	$k_{fom}$	$\text{d}^{-1}$	0.200
	cellulose-hemicellulose	$k_{iom}$	$\text{d}^{-1}$	0.051
	lignin	$k_{som}$	$\text{d}^{-1}$	0.003
$Q_{10}$	active organic fraction	$Q_{fom}$	(-)	2.100
	passive organic fraction	$Q_{iom}$	(-)	2.950
	slow organic fraction	$Q_{som}$	(-)	3.800
Total decay for C	active organic fraction	$k_{t-fom}$	$\text{d}^{-1}$	0.200
	passive organic fraction	$k_{t-iom}$	$\text{d}^{-1}$	0.051
	slow organic fraction	$k_{t-som}$	$\text{d}^{-1}$	0.003
Oxygen concentration	oxic layer	$O_{ox}$	$\text{mg L}^{-1}$	2.00E+06
	anoxic layer	$O_{anox}$	$\text{mg L}^{-1}$	2.00E+05
Half saturation constant for $O_2$ uptake	oxic layer	$k_{O_{ox}}$	$\text{mg L}^{-1}$	0.500
	anoxic layer	$k_{O_{anox}}$	$\text{mg L}^{-1}$	1.00E+05
$^{14}\text{CO}_2$ atmospheric level in 2012		-	$\text{Bq g}^{-1}\text{C}$	0.231
$^{14}\text{C}$ decay constant		$\lambda$	$\text{d}^{-1}$	3.30E-07

Oxygen concentrations both in the reduced and oxidized layers are estimated from redox potential, as it is providing a reasonable indication of soil aeration status (Megonigal et al., 1993; Reddy and DeLaune, 2008).

Table. 5.2. Specific parameters used in model.

Site	Layer	C input (mg C cm <sup>-2</sup> d <sup>-1</sup> )	<sup>14</sup> C input (Bq cm <sup>-2</sup> d <sup>-1</sup> )	SP (kPa)	FC (kPa)	PWP (kPa)	O <sub>2</sub> coeff (-)	C storage (-)	T sensitivity (-)			Org C fraction (-)		
Unit														
Symbol		C <sub>(t)</sub>	<sup>14</sup> C <sub>(t)</sub>	Ws	Wfc	Wpwp	Oc	h	Qfom	Qiom	Qsom	ffom	fiom	fsom
PL-P	Topsoil	0.7000	0.1617	0.61	0.52	0.38	0.194	0.754	1.63	2.04	2.41	0.32	0.10	0.57
	Subsoil	0.5929	0.1370	0.64	0.52	0.4	0.998	0.626	-	-	-	-	-	-
PL-NP	Topsoil	1.1400	0.2633	0.61	0.51	0.37	0.998	0.785	1.63	2.04	2.41	0.35	0.12	0.53
	Subsoil	0.8687	0.2007	0.64	0.51	0.4	0.998	0.718	-	-	-	-	-	-
JSG-P	Topsoil	0.9110	0.2104	0.62	0.46	0.27	0.194	0.731	1.53	1.87	2.17	0.38	0.21	0.41
	Subsoil	0.4819	0.1113	0.65	0.5	0.35	0.998	0.627	-	-	-	-	-	-
JSG-NP	Topsoil	0.1060	0.0245	0.61	0.47	0.28	0.998	0.777	1.53	1.87	2.17	0.43	0.27	0.29
	Subsoil	0.0568	0.0131	0.91	0.3	0.08	0.998	0.740	-	-	-	-	-	-
PBW-P	Topsoil	0.9220	0.4250	0.52	0.31	0.21	0.194	0.909	1.06	1.1	1.13	0.37	0.23	0.39
	Subsoil	0.4250	0.4089	0.58	0.31	0.21	0.998	0.909	-	-	-	-	-	-
PBW-NP	Topsoil	0.2130	0.0981	0.51	0.31	0.21	0.998	0.909	1.06	1.1	1.13	0.38	0.26	0.36
	Subsoil	0.1659	0.0944	0.68	0.31	0.21	0.998	0.909	-	-	-	-	-	-

(SP = saturation point; FC = field capacity, PWP = permanent wilting point)

The Eh value of top layer may drop to -100 mV within few weeks of flooding, and after drainage and aeration the the Eh rises to +600 mV as typical aerobic soils (Moorman and van Breemen, 1978). Below +300 mV the the  $O_2$  concentrations shows very little (Reddy and DeLaune, 2008), but organic matter can still proceed as microbes utilize electron acceptor elements like N, Mn, Fe and S.

Therefore, to facilitate the minimized decomposition under anoxic condition, model assumes the low concentration of  $O_2$  ca. 0.1% in the reduced top layers. While under oxic condition, soil  $O_2$  concentration ca. 20% equal to air composition. Both values are equal to 0.12 and 240  $mg L^{-1}$  by taking into account the density of air 1.20  $g L^{-1}$ . The calculation for oxygen coefficient  $O_c$  used  $k_o$  equal to 0.5  $mg L^{-1}$  (Sharifi et al., 2013), for both oxic and anoxic layers.

The oxygen coefficient,  $O_c$ , implies that the rate of decomposition is inhibited under low oxygen concentrations such as in the P top layers. The optimum condition, with coefficient 1, is reached under high oxygen concentrations (eq. 5.10), at which half-saturation constant  $k_o$  is negligible (Greenwood, 1961). But since the model assumes the maximum oxic condition 600 mV  $\approx$  20% oxygen concentration, the coefficients are below 1.

Organic matter build-up in the soil is simply the result of positive difference between total carbon inputs and outputs. Basically, as in eq. (5.12), the first term on the right hand side is the fresh litter supply into soil and the second term is the rate of carbon loss due to decomposition (Kemanian and Stöckle, 2010; Nieder and Benbi, 2008; Smith, 1982). The fresh litter is transformed into high molecular weight molecules through humification (MacCarthy, 2001; Saiz-Jimenez, 1996), and driving the storage of carbon in relation to soil clay (Coleman and Jenkinson, 1996; Hassink, 1997; Kemanian and Stöckle, 2010; Taghizadeh-Toosi et al., 2014; Wells and Hancock, 2014). Therefore, carbon storage capacity means the efficiency of soil to build-up carbon. The higher the efficiency, the higher soil carbon storage.

In this model, carbon storage efficiency  $E$  explains the amount of carbon that potentially will be sequestered through humification which is directly proportional to soil clay content. Therefore, the remaining carbon,  $R = 1 - E$ , will leave the system. In special cases, e.g. the coarse textured volcanic soil, the high carbon efficiency is possibly due to the presence of short range-ordered Al/Fe (Matus et al., 2014; Takahashi and Dahlgren, 2016). In this soil, routine analysis of grain size composition may not give an accurate indication of elementary particles, but rather of agglomerated particles (Legros, 2012). Therefore, this model assumes a 90% clay content to keep a highest efficiency in the simulation among soil types. Using this assumption, the problem of inaccurate soil texture analysis for soil with high content of short range-ordered Al/Fe may be reduced. The higher carbon efficiency in this soil has been confirmed through an adsorption capacity contributed by allophane, as a majority clay mineral in this soil, than montmorillonite and kaolinite (Singh et al., 2016). Although with low result of clay analysis  $\sim$  25%, this soil can contain high TOC up to more than 3% (Prastowo et al., 2017). Therefore, a direct application of clay analysis results to relate it with soil carbon storage capacity may not be appropriate.

A monod type rate limiting term (Soetaert and Herman, 2009), is applied to express the condition that the higher R (lower carbon efficiency) will result in a low of the carbon storage coefficient  $h$ , as the relationship below:

$$h = \frac{1}{1 + R} \quad (5.11)$$

$$\frac{dC(z,t)}{dt} = h \sum f_i C_t - \sum k_i C \quad (5.12)$$

With:

$C(z,t)$  : SOC formation at particular  $t$  and  $z$  ( $\text{g C.cm}^{-2}.\text{d}^{-1}$ )

$h$  : carbon storage coefficient (-)

$f_i$  : proportion of organic fractions (-)

$k_i$  : decomposition rate constant of organic fractions ( $\text{d}^{-1}$ ),  $i$  = active, passive, and slow

$C_t$  : total carbon inputs ( $\text{g C.cm}^{-2}.\text{d}^{-1}$ )

$C$  : the amount of carbon accumulated ( $\text{g C.cm}^{-2}.\text{d}^{-1}$ )

The first term on the right hand side of eq. (5.12) shows the total carbon input. Fresh litter is partitioned into three postulated organic fractions, active, passive, and slow. All these fractions are involved in making up carbon storage efficiency (eq. 5.11). For instance, the active easily decomposable fraction with fast turnover time (Schoor et al., 2016a), as first ingested preferentially by microbes, may also be stabilized in the clay particles as bacterial cells and colonies, amino acid, microbial cell wall (Anderson and Paul, 1984; Feller and Beare, 1997; Paul, 2016).

The second term implements a first order decomposition rate constant of organic carbon fractions (section 5.2.1.1). These constants reflect the progressive  $\text{CO}_2$  loss from stored organic compounds through time which is affected by litter quality and climate (Cotrufo et al., 2009; Smith, 1982; van Veen and Paul, 1981). Heterogeneity in the litter quality gives rise to a variety of decomposition constants where slow fractions, e.g. lignin, exhibit smallest values (Voroney et al., 1981). Climate effects through three variables, e.g. temperature, soil moisture, and oxygen availability have been discussed above. Under optimal conditions, all these variables will promote the decomposition of soil organic carbon.

By implementing temperature sensitivity  $f(t_s)$ , effective saturation  $f(m_s)$ , and oxygen limitation  $f(o_c)$ , for the decomposition rate of specific fractions,  $i$ , in eq. 5.12, the new formula becomes:

$$\frac{dC(z,t)}{dt} = h(f_{fom} + f_{iom} + f_{som})C_t - f(m_s)f(o_c)(f(t_s)k_{fom} + f(t_s)k_{iom} + f(t_s)k_{som})C \quad (5.13)$$

Equation (5.13) can be re-formulated for simplicity:

$$\frac{dC(z, t)}{dt} = h \sum f_i C_t - \beta C \quad (5.14)$$

Where,

$$\beta = f(m_s)f(o_c) \sum f(t_s)k_i, \beta = \text{decomposition coefficient}$$

Radiocarbon enters into the soil system following the movement of carbon. The average concentration of  $^{14}\text{C}$  in fresh litter is assumed to be equal to current atmospheric level, i.e. 103 pMC in 2012. Humification of litter will yield humified compounds. The composition of  $^{14}\text{C}$  in humified compound is assumed to be similar to humic fraction (section 2.3.2), as they pose a similarity in aromaticity (Stevenson, 1994). Therefore, this model uses  $^{14}\text{C}$  composition in the humic to represent the humified compounds.

Radiocarbon follows the same decay pattern of carbon. The natural decay of radiocarbon, with constant ( $\lambda$ ) equal to  $3.3 \times 10^{-7} \text{ d}^{-1}$  (based on an isotopic half-life of 5730 yr, (Godwin, 1962)), will proceed together with decomposition rate constant of organic fractions (Elzein and Balesdent, 1995). Therefore, a new constant,  $k_{t-i}$ , will be implemented into this model to represent organic fraction,  $k_i$ , and natural radiocarbon,  $\lambda$ , decays as below:

$$k_{t-i} = \lambda + k_i \quad (5.15)$$

Therefore, the eq. (5.12) can be re-formulated for radiocarbon model as following:

$$\frac{d^{14}C(z, t)}{dt} = h \sum f_i C_{(t)} - \alpha C \quad (5.16)$$

Where,

$$\alpha = f(t_s)f(m_s)f(o_c)k_{t-i}, \alpha = \text{decomposition coefficient}$$

To express  $^{14}\text{C}$  into unit  $\text{area}^{-1} \text{ time}^{-1}$  (carbon flow) or unit  $\text{area}^{-1}$  (carbon storage), that comparable with different carbon pool, the pMC will be converted into specific activity ( $\text{Bq g}^{-1} \text{ C}$ ) by assuming the absolute radiocarbon standard ( $A_{\text{abs}}$ ) equal to  $226 \text{ Bq kg}^{-1} \text{ C}$  (Mook and van der Plicht, 1999; Stenström et al., 2011). By applying this unit, the carbon input through litter can be converted into a daily basic  $^{14}\text{C}$  input, and it is more favorable in relation to the unit of transport parameter (section 5.2.2). The formula for unit conversion is as below:

$$A = \frac{\text{pMC}}{100} \cdot \left[ \frac{\left(1 + \frac{\delta^{13}\text{C}}{1000}\right)}{0.975} \right]^2 \cdot e^{(1950-y)/8267} \cdot 0.226 \text{ Bq g}^{-1} \text{ C} \quad (5.17)$$

With:

pMC : the  $^{14}\text{C}$  concentration (pMC) of samples

$\delta^{13}\text{C}$  : the  $^{13}\text{C}$  concentration ratio (‰) of samples

y : year of measurement

Using eq. (5.17), the  $^{14}\text{C}$  input through litter  $C_{(t-14)}$  is assumed as:

$$C_{(t-14)}(Bq\ cm^{-2}\ day^{-1}) = atm\ ^{14}CO_2(Bq\ g^{-1}\ C) \cdot C_{(t)}(g\ C\ cm^{-2}\ day^{-1}) \quad (5.18)$$

With:

atm  $^{14}CO_2$  : The  $^{14}C$  activity in 2012 atmosphere  $\approx 0.231\ Bq\ g^{-1}\ C$  (103 pMC, -25‰)

The unit of soil radiocarbon activity (Fig. 5.3) is obtained by taking into account total organic carbon ( $g\ g^{-1}$ ), bulk density ( $g\ cm^{-3}$ ), and sample interval (2 cm).

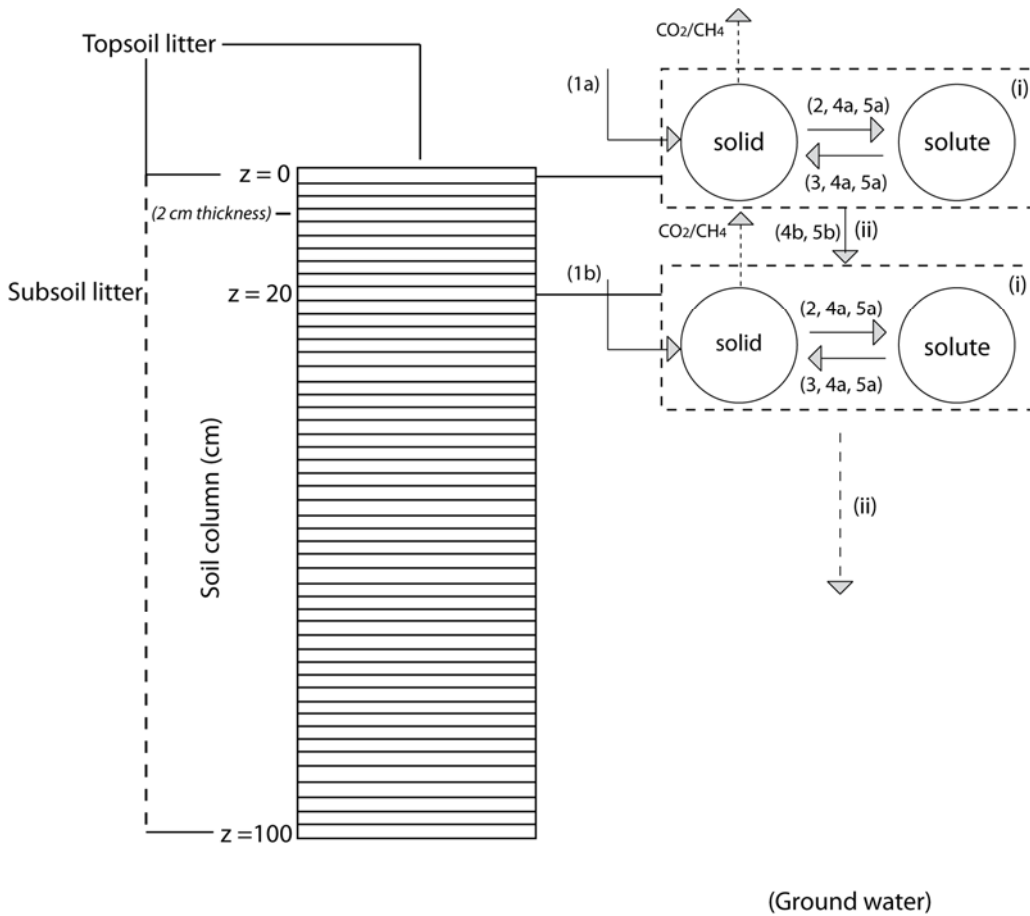


Figure. 5.1. Conceptual of soil carbon dynamics model (1a = topsoil litter at  $z=0$  cm depth; 1b = subsoil litter at  $z=20$  cm depth; 2 = desorption; 3 = adsorption; 4a = lateral diffusion; 4b = vertical diffusion; 5a = lateral convection; 5b = vertical convection; (i) = organic carbon transformation, (ii) = organic carbon transport).

### 5.2.2. Depth-transport of soil organic carbon

The model assumes that the downward carbon transport is not merely through the liquid phase, but also mechanical mixing of soil, i.e. pedoturbation, and the movement of soil fauna at depth, i.e. bioturbation. The movement of carbon in the liquid phase, i.e. dissolved organic carbon is characterized by a velocity, and called convective transport. It is expressed as

proportional to the first-order derivative of the soil carbon concentration in space  $z$  (Elzein and Balesdent, 1995) as below:

$$\frac{\partial C(z, t)}{\partial t} = -v \frac{\partial C}{\partial z} \quad (5.19)$$

The negative sign in eq. (5.19) means reducing the gradient. The transport of carbon analogous to pedo-/bio-turbation is more random, and called diffusive motion. The rate of displacement is proportional to the second derivative in space  $z$  (Elzein and Balesdent, 1995) as below:

$$\frac{\partial C(z, t)}{\partial t} = D \frac{\partial^2 C}{\partial z^2} \quad (5.20)$$

Combination of eq. (5.19) and (5.20) results in the formula:

$$\frac{\partial C(z, t)}{\partial t} = D \frac{\partial^2 C}{\partial z^2} - v \frac{\partial C}{\partial z} \quad (5.21)$$

With:

- D : diffusion coefficient ( $\text{cm}^2 \text{d}^{-1}$ ), fitting parameter
- V : convection coefficient ( $\text{cm d}^{-1}$ ), fitting parameter
- z : depth (cm)

### 5.2.3. Conceptual model

The model assumes two soil carbon pools namely solid and solute (Fig. 5.1). The solid pool is home for fresh to old organic carbon materials, as well as the microbial populations, while the solute pool is attributable to water dissolved organic matter. When carbon materials enter the soil, first of all they will be subject to transformation (section 5.2.1). Subsequently, they will be transported down into the soil column through either solution or pedo/bio-turbation (section 5.2.2). Two layers are partitioned, i.e. topsoil 0-20 cm depth, and subsoil 20-100 cm depth, to take into account carbon input from the ground surface, e.g. plant litter and manure, and from subsoil, e.g. root biomass in the rhizosphere. Additionally, topsoil is subject to temporary anoxic condition in the paddy soil which is assumed to create specific micro-environments differing from upland soil in the context of oxygen availability limitation.

Two state variables are applied to designate processes in the topsoil and subsoil, i.e. 1) top soil solid and solute pools, and 2) subsoil soil solid and solute pools (Fig. 5.1). The balance equation at both variables can be stated as:

$$\frac{dC_{solid}}{dt} = \left[ \frac{dC_{solid}}{dt} \right]_{topsoil} + \left[ \frac{dC_{solid}}{dt} \right]_{subsoil} \quad (5.22)$$

$$\begin{aligned} \frac{dC_{solid}}{dt} = & [((1a) + (3) + (4a)) - ((2) + (4b))]_{topsoil} \\ & + [((1b) + (3) + (4a) + (4b)) - ((2) + (4a))]_{subsoil} \end{aligned}$$

$$\frac{dC_{solid}}{dt} = (1a) + (3) + (4a) - (2) - (4b) + (1b) + (3) + (4b) - (2) \quad (5.23)$$

$$\frac{dC_{solute}}{dt} = \left[ \frac{dC_{solute}}{dt} \right]_{topsoil} + \left[ \frac{dC_{solute}}{dt} \right]_{subsoil} \quad (5.24)$$

$$\begin{aligned} \frac{dC_{solute}}{dt} = & [((2) + (5a)) - ((3) + (5b))]_{topsoil} \\ & + [((2) + (5a) + (5b)) - ((3) + (5a))]_{subsoil} \end{aligned}$$

$$\frac{dC_{solute}}{dt} = (2) - (3) + (2) + (5a) - (3) \quad (5.25)$$

The total carbon in the pools can be obtained by combining eq. (5.23) and eq. (5.25) as:

$$\frac{dC}{dt} = \frac{dC_{solid}}{dt} + \frac{dC_{solute}}{dt} \quad (5.26)$$

$$\frac{dC}{dt} = (1a) + (4a) + (1b) + (5a)$$

As (1a) and (1b) are carbon input, they are subject to carbon transformation which is formulated as in eq. (5.14). While (4a) and (5a) are the transport of carbon through diffusion (eq. 5.20) and convection (eq. 19). By substituting their equations, the formula becomes:

$$\frac{dC}{dt} = h \sum f_i C_{(top)} + h \sum f_i C_{(sub)} + D \frac{\partial^2 C}{\partial z^2} - v \frac{\partial C}{\partial z} - \beta C \quad (5.27)$$

Assuming steady state condition ( $\frac{dC}{dt} = 0$ ), and specify data quantity for carbon inputs the equation (5.27) can be re-arranged:

$$D \frac{\partial^2 C}{\partial z^2} - v \frac{\partial C}{\partial z} - \beta C + H(z) = 0 \quad (5.28)$$

Where  $H(z) = hf_i C_{(top)} + hf_i C_{(sub)}$

### 5.3. Finite element method

The ordinary differential equation (eq. 5.28) will be solved using one dimensional (1-D) finite element method (FEM) with boundary conditions applied for problem domain  $\Omega = (0, L)$ . Four steps would be taken to solve a governing equation using FEM, i.e. discretize the problem domain (Fig. 5.1), derive the approximating equations, develop and solve system of equations (Istok, 1989).

The distribution of carbon will be constrained by mixed type boundary condition (Robin type) (eq. 5.29) to define fluxes across the problem domain. The flux type (Neumann boundary) at the bottoms are applied (eq. 5.30) (Genuchten and Alves, 1982).

$$-\frac{\partial C(z)}{\partial z} + vC = vC_0 \quad (z = 0) \quad (5.29)$$

$$\frac{\partial C(z)}{\partial z} = 0, \quad (z = L) \quad (5.30)$$

The fluxes of external carbon are derived from litter, and possibly manure under agricultural practices (Table 5.1). The bottom condition is assumed to be zero at deep layer which means no more radiocarbon activity at this point (Bruun et al., 2007), and it is expressing the homogeneity of the soil column in the boundary area (Elzein and Balesdent, 1995) where no diffusive flux through it is present (Soetaert and Herman, 2009).

The problem domain,  $\Omega = (0, L)$ , is discretized into 2 cm of homogeneous finite elements (Fig. 5.1) with assumed 2 nodal points at both ends representing a linear system. The continuous variable  $C(z)$  is approximated to nodal variables  $C_i(z)$  by simple functions  $N_i(z)$  (eq. 5.35) in order to interpolate the solution over a finite element (Simpson, 2017).

$$C_{(z)} \approx \sum_{i=1}^m N_{i(z)} * C_{i(z)} \quad (5.31)$$

With:

$m$  = number of nodes within element

$N$  = interpolation function

$C_i$  = unknown values

Model assumes that the carbon variation in each elements can be expressed linearly between two nodes, therefore:

$$C_{(z)} \approx [N_{1(z)} \ N_{2(z)}] \begin{bmatrix} C_1 \\ C_2 \end{bmatrix} \quad (5.32)$$

Assuming a linear equation  $C_{(z)} = \alpha_0 + \alpha_1 \cdot z$  over the domain  $\Omega = (0, L)$  with  $C_0 = C_1$ , and  $C_L = C_2$ . When  $z = 0$ ,  $C_1 = \alpha_0$  and when  $z = L$ ,  $C_2 = \alpha_0 + \alpha_1 L$ . Solving the values  $\alpha_0$  and  $\alpha_1$ , and substituting to the linear equation above ends up with the following interpolation functions:

$$N_1 = 1 - \frac{z}{L}; \quad N_2 = \frac{z}{L} \quad (5.33)$$

Where  $L$  is the length of element, and  $z$  is depth variable which is 0 at node 1 and  $L$  at node 2 with  $N_1(z) + N_2(z) = 1$  over all elements.

Substituting the approximation (eq. 5.32) into the governing differential equation (eq. 5.28) in the single element results in the new formulation:

$$D \frac{d^2}{dz^2} [N_1 \ N_2] \begin{Bmatrix} C_1 \\ C_2 \end{Bmatrix} - v \frac{d}{dz} [N_1 \ N_2] \begin{Bmatrix} C_1 \\ C_2 \end{Bmatrix} - \beta [N_1 \ N_2] \begin{Bmatrix} C_1 \\ C_2 \end{Bmatrix} + H(z) = R \quad (5.34)$$

Where R is the residual or error introduced due to approximate solution which is occurred at each point of problem domain (Istok, 1989). The eq. (5.34) in the discretized variables of unknown  $C_1$  and  $C_2$  now have replaced the original equation (eq. 5.28). In order to find the unknown values,  $C_1$  and  $C_2$ , the residual R in eq. (5.34) must be minimized to close to zero by choosing n linearly independent weighting functions,  $W_i$  ( $i = 1, 2, \dots, n$ ) in each element (Luckner and Schestakow, 1991). Among weighted residuals methods, the Galerkin method is the most suitable to finite element applications (Huyakorn and Pinder, 1983).

$$\int_0^L R(z) W_i(z) dz = 0, i = 1, 2 \quad (5.35)$$

Where  $R(z)$  is the residual and  $W_i$  is the number of weighting functions, equal to the number of unknown coefficients, in this model is  $C_i$  ( $i = 2$ ).

$$\int_0^L W \left[ D \frac{d^2}{dz^2} [N_1 \ N_2] \begin{Bmatrix} C_1 \\ C_2 \end{Bmatrix} - v \frac{d}{dz} [N_1 \ N_2] \begin{Bmatrix} C_1 \\ C_2 \end{Bmatrix} - \beta [N_1 \ N_2] \begin{Bmatrix} C_1 \\ C_2 \end{Bmatrix} + H(z) \right] dz = 0 \quad (5.36)$$

In the Galerkin method, the weighting functions are equal to the interpolation function (Simpson, 2017). Therefore, substituting N into W in eq. (5.36) leads to the new formulation as below:

$$\begin{aligned} \int_0^L \begin{Bmatrix} N_1 \\ N_2 \end{Bmatrix} D \frac{d^2}{dz^2} [N_1 \ N_2] \begin{Bmatrix} C_1 \\ C_2 \end{Bmatrix} dz - \int_0^L \begin{Bmatrix} N_1 \\ N_2 \end{Bmatrix} v \frac{d}{dz} [N_1 \ N_2] \begin{Bmatrix} C_1 \\ C_2 \end{Bmatrix} dz - \\ \int_0^L \begin{Bmatrix} N_1 \\ N_2 \end{Bmatrix} \beta [N_1 \ N_2] \begin{Bmatrix} C_1 \\ C_2 \end{Bmatrix} dz + \int_0^L \begin{Bmatrix} N_1 \\ N_2 \end{Bmatrix} H(z) dz = \begin{Bmatrix} 0 \\ 0 \end{Bmatrix} \end{aligned} \quad (5.37)$$

The four terms on the left-hand side of eq. (5.37) come directly from the four respective terms in the governing equation (eq. 5.28). In this model the interpolation functions are assumed to be linear, double differentiation of these functions in term 2 would cause them to remove. This would result in physically unrealistic situation that the conduction term completely disappears (Simpson, 2017).

Therefore, the second derivative in the first term in eq (5.37) is then reduced to avoid this problem, and in order to form weak formula using Green's theorem (integration by parts).

The use of integration by part is actually to distribute differentiation equally between the dependent variable and the weight function  $W$ , and to implement the boundary terms (Reddy, 1993). In this case the boundary conditions will be imposed later when assembling the global system of equation. In one dimension, this yields:

$$\int_0^L \begin{Bmatrix} N_1 \\ N_2 \end{Bmatrix} D \frac{d^2}{dz^2} [N_1 \ N_2] \begin{Bmatrix} C_1 \\ C_2 \end{Bmatrix} dz = \left[ \begin{Bmatrix} N_1 \\ N_2 \end{Bmatrix} D \frac{dC(z)}{dz} \right]_0^L - \int_0^L D \frac{dC(z)}{dz} dz$$

Therefore eq (5.37) can be written as:

$$\begin{aligned} & \left[ \begin{Bmatrix} N_1 \\ N_2 \end{Bmatrix} D \frac{dC(z)}{dz} \right]_0^L \\ & - \int_0^L \frac{d}{dz} \begin{Bmatrix} N_1 \\ N_2 \end{Bmatrix} D \frac{d}{dz} [N_1 \ N_2] \begin{Bmatrix} C_1 \\ C_2 \end{Bmatrix} dz \\ & - \int_0^L \begin{Bmatrix} N_1 \\ N_2 \end{Bmatrix} v \frac{d}{dz} [N_1 \ N_2] \begin{Bmatrix} C_1 \\ C_2 \end{Bmatrix} dz \\ & - \int_0^L \begin{Bmatrix} N_1 \\ N_2 \end{Bmatrix} \beta [N_1 \ N_2] \begin{Bmatrix} C_1 \\ C_2 \end{Bmatrix} dz + \int_0^L \begin{Bmatrix} N_1 \\ N_2 \end{Bmatrix} H dz = \begin{Bmatrix} 0 \\ 0 \end{Bmatrix} \end{aligned} \quad (5.38)$$

Now the original integral involving twice differentiable interpolation functions is converted into a boundary term (the first term on the right hand side of eq. 5.38). It is implicitly introduced the Neumann boundary condition as in eq. (5.30).

Rearranging eq (5.38):

$$\begin{aligned} & \left[ - \int_0^L \frac{d}{dz} \begin{Bmatrix} N_1 \\ N_2 \end{Bmatrix} D \frac{d}{dz} [N_1 \ N_2] \begin{Bmatrix} C_1 \\ C_2 \end{Bmatrix} dz \right. \\ & \quad \left. - \int_0^L \begin{Bmatrix} N_1 \\ N_2 \end{Bmatrix} v \frac{d}{dz} [N_1 \ N_2] \begin{Bmatrix} C_1 \\ C_2 \end{Bmatrix} dz - \int_0^L \begin{Bmatrix} N_1 \\ N_2 \end{Bmatrix} \beta [N_1 \ N_2] \begin{Bmatrix} C_1 \\ C_2 \end{Bmatrix} dz \right] \\ & = - \int_0^L \begin{Bmatrix} N_1 \\ N_2 \end{Bmatrix} H(z) dz - \left[ [N_1 \ N_2] D \frac{d}{dz} [N_1 \ N_2] \begin{Bmatrix} C_1 \\ C_2 \end{Bmatrix} \right]_0^L \end{aligned} \quad (5.39)$$

The eq. (5.39) can be written as following:

$$\begin{aligned} & - \int_0^L D \begin{bmatrix} \frac{dN_1}{dz} \frac{dN_1}{dz} & \frac{dN_1}{dz} \frac{dN_2}{dz} \\ \frac{dN_2}{dz} \frac{dN_1}{dz} & \frac{dN_2}{dz} \frac{dN_2}{dz} \end{bmatrix} \begin{Bmatrix} C_1 \\ C_2 \end{Bmatrix} dz - \int_0^L v \begin{bmatrix} N_1 N_1 & N_1 N_2 \\ N_2 N_1 & N_2 N_2 \end{bmatrix} \frac{d}{dz} \begin{Bmatrix} C_1 \\ C_2 \end{Bmatrix} dz \\ & - \int_0^L \beta \begin{bmatrix} N_1 N_1 & N_1 N_2 \\ N_2 N_1 & N_2 N_2 \end{bmatrix} dz \begin{Bmatrix} C_1 \\ C_2 \end{Bmatrix} \\ & = \int_0^L \begin{Bmatrix} N_1 \\ N_2 \end{Bmatrix} H(z) dz - \left[ [N_1 \ N_2] D \frac{d}{dz} [N_1 \ N_2] \begin{Bmatrix} C_1 \\ C_2 \end{Bmatrix} \right]_0^L \end{aligned} \quad (5.40)$$

One now has two equations for the two unknowns  $C_1$  and  $C_2$ . To evaluate the integrals the  $N$  defined in eq. (5.33) is used to the element stiffness matrix for the left hand side of eq. (5.40) to yield:

$$[K] = -D \begin{bmatrix} \frac{1}{L} & -\frac{1}{L} \\ -\frac{1}{L} & \frac{1}{L} \end{bmatrix} \begin{Bmatrix} C_1 \\ C_2 \end{Bmatrix} - v \begin{bmatrix} -\frac{1}{2} & \frac{1}{2} \\ -\frac{1}{2} & \frac{1}{2} \end{bmatrix} \frac{d}{dz} \begin{Bmatrix} C_1 \\ C_2 \end{Bmatrix} - \beta \begin{bmatrix} \frac{L}{3} & \frac{L}{6} \\ \frac{L}{6} & \frac{L}{3} \end{bmatrix} \begin{Bmatrix} C_1 \\ C_2 \end{Bmatrix} \quad (5.41)$$

Reformulate eq. (5.41), with  $L = \Delta z$  which is the length of element size, results in the following equation:

$$[K] = -\frac{D}{\Delta z} \begin{bmatrix} 1 & -1 \\ -1 & 1 \end{bmatrix} - \frac{v}{2} \begin{bmatrix} -1 & 1 \\ -1 & 1 \end{bmatrix} - \frac{\beta \Delta z}{6} \begin{bmatrix} 2 & 1 \\ 1 & 2 \end{bmatrix} \quad (5.42)$$

The element load vector for the right hand side equations, by substituting  $D \frac{dC}{dz} \Big|_{z=0} = Q_0$ ;

$D \frac{dC}{dz} \Big|_{z=L} = Q_L$ , is:

$$\{F\} = - \int_0^L \begin{Bmatrix} N_1 \\ N_2 \end{Bmatrix} H(z) dz - \begin{bmatrix} N_1 Q_L \\ N_2 Q_0 \end{bmatrix} \quad (5.43)$$

The first term in eq. (5.43), specifies  $H(z)$  for carbon and radiocarbon (with applying eq. 5.33) becomes:

$$F_c = -h \frac{\Delta z}{2} \begin{Bmatrix} f_i C(t) \\ f_i C(t) \end{Bmatrix} \quad (5.44)$$

The derivative boundary conditions (eq. 5.29 and eq. 5.30) will be imposed in the second term on the right side (eq. 5.43). They are assumed to be the natural type so that they can be included in the statements (Reddy, 1993).

The bottom constraint,  $Q_L$ , in (eq. 5.30) will cancel out because the derivative condition equal to zero. The re-arrangement of eq. (5.29) results in  $Q_0 = vC_0 - vC_1$ . This condition can be imposed in the global stiffness matrix and forcing vector (Hafez and Awad, 2016), as the following:

$$\begin{bmatrix} k_{11} + v & k_{12} \\ k_{21} & k_{22} \\ & & k_{nn} \end{bmatrix} \begin{Bmatrix} C_1 \\ C_2 \\ C_n \end{Bmatrix} = \begin{Bmatrix} f_1 + vC_0 \\ f_2 \\ f_n \end{Bmatrix} \quad (5.45)$$

The term  $C_0$  is assumed as the flux of external carbon into the boundary at  $z=0$  (Wells and Hancock, 2014) which is the total input of carbon per day (Table 5.1), while  $C_1$  is carbon concentration at soil surface. The simplification of the final general linear system of equations ends up with the following equation:

$$[K]\{C\} = \{F\} \quad (5.46)$$

Where vector {C} is the unknowns to be solved using MATLAB R2014a (Kwon and Bang, 2000).

#### 5.4. Model validation

The model is validated using data sets from first field campaign (section 2.1.1). The TOC data was obtained by analysis of bulk soil samples performed using C/N analyzer while <sup>14</sup>C measurements for humic samples were done by AMS (section 2.3.2). To evaluate the performance of the model the efficiency (EF) is calculated (Smith et al., 1996):

$$EF = \frac{\sum_{i=1}^n (O_i - \bar{O})^2 - \sum_{i=1}^n (P_i - O_i)^2}{\sum_{i=1}^n (O_i - \bar{O})^2} \quad (5.47)$$

With:

- O<sub>i</sub> : the observed values
- P<sub>i</sub> : the predicted values
- $\bar{O}$  : mean of observed data

The EF is calculated by comparing the variance of predicted from observed values to the variance of observed values from the mean of the observations. If the predicted values exactly match the measured values, then the EF reach the maximum value at 1 but otherwise if less than 0 the simulated values are worse.

#### 5.5. Result and discussion

Two models are formulated in attempt to simulate the depth distribution of total organic carbon (TOC<sub>M</sub>), and radiocarbon activity (R<sub>M</sub>) in different soil types. Model validation shows a a wide range of values in different soil profiles (Table. 5.3).

Table. 5.3. The efficiency of model (EF).

Sites	TOC <sub>M</sub>	R <sub>M</sub>
PL-P	0.72	0.76
PL-NP	0.60	0.58
JSG-P	0.90	0.83
JSG-NP	0.82	0.95
PBW-P	0.93	0.58
PBW-NP	0.56	0.65

Field heterogeneity, i.e. layer composition, may be partly responsible to the response of model to data observations, as some profiles in study areas show a high heterogeneity of

layer composition (section 3.1; section 3.2). In the PBW-P,  $TOC_M$  model shows a better performance than  $R_M$ . The high depth variability in carbon isotope composition (section 4.3.2.1) more than the total organic carbon may be responsible for the lower  $EF$  in  $R_M$  than in  $TOC_M$ . Conversely, the simulation of both models in JSG profiles yield a higher  $EF$  which is associated with the higher homogeneity of layer composition than the other sites. In different case, two profiles in the same soil type in PL with similar compositions generate a different  $EF$ , with P is better than NP (Table 5.3). This may lead to an assumption of the presence of additional factor that influence the depth carbon distribution. The lower of  $EF$  in NP profile suggests a larger depth-carbon variation.

### 5.5.1. TOC-model ( $TOC_M$ )

The coefficient of diffusion  $D$  may be interpreted as a soil mechanical mixing (Elzein and Balesdent, 1995). The higher  $D$  value means that the greater carbon is distributed into subsoil. As presented in Table 5.4,  $D$  values range from 0.014 in PBW-NP to 0.060  $cm^2 d^{-1}$  in JSG-P. The significant difference in  $D$  values between P and NP of JSG profile may reflect the difference in depth-distribution of carbon (Fig. 5.2). The diffusive movement of subsoil carbon may be more dominant in JSG-NP.

Table. 5.4. Estimated parameter of models.

	$TOC_M$		$R_M$	
	$D$ ( $cm^2 d^{-1}$ )	$v$ ( $cm d^{-1}$ )	$D$ ( $cm^2 d^{-1}$ )	$v$ ( $cm d^{-1}$ )
PL-P	0.020	-0.0040	0.020	-0.0184
PL-NP	0.020	-0.0050	0.020	-0.0040
JSG-P	0.060	-0.0080	0.060	-0.0100
JSG-NP	0.012	-0.0005	0.070	-0.0100
PBW-P	0.018	-0.0090	0.080	-0.0150
PBW-NP	0.014	-0.0040	0.095	-0.0160

Similarly, subsoil convective  $v$  also likely plays an important role for transport of carbon. The values of  $v$  range from -0.0005 in JSG-NP to -0.009  $cm d^{-1}$  in PBW-P. The  $v$  values are significantly different between P and NP sites in JSG. The significantly lower  $v$  in JSG-NP may indicate that mechanisms that resulting in convective movement of carbon may be not dominant. The depth-transport of carbon through convective may be an inseparable process with diffusion, as their coefficient values may pose a similar trend (Table 5.4).

In general, it is suggested that profile composition may explain the transport of carbon in the soil column. Soil types may strongly affect the diffusive and convective mechanisms of carbon movement at depth. These two parameter coefficients obtained from this modelling show ca. 10 times lower of values than the data obtained from field measurements.

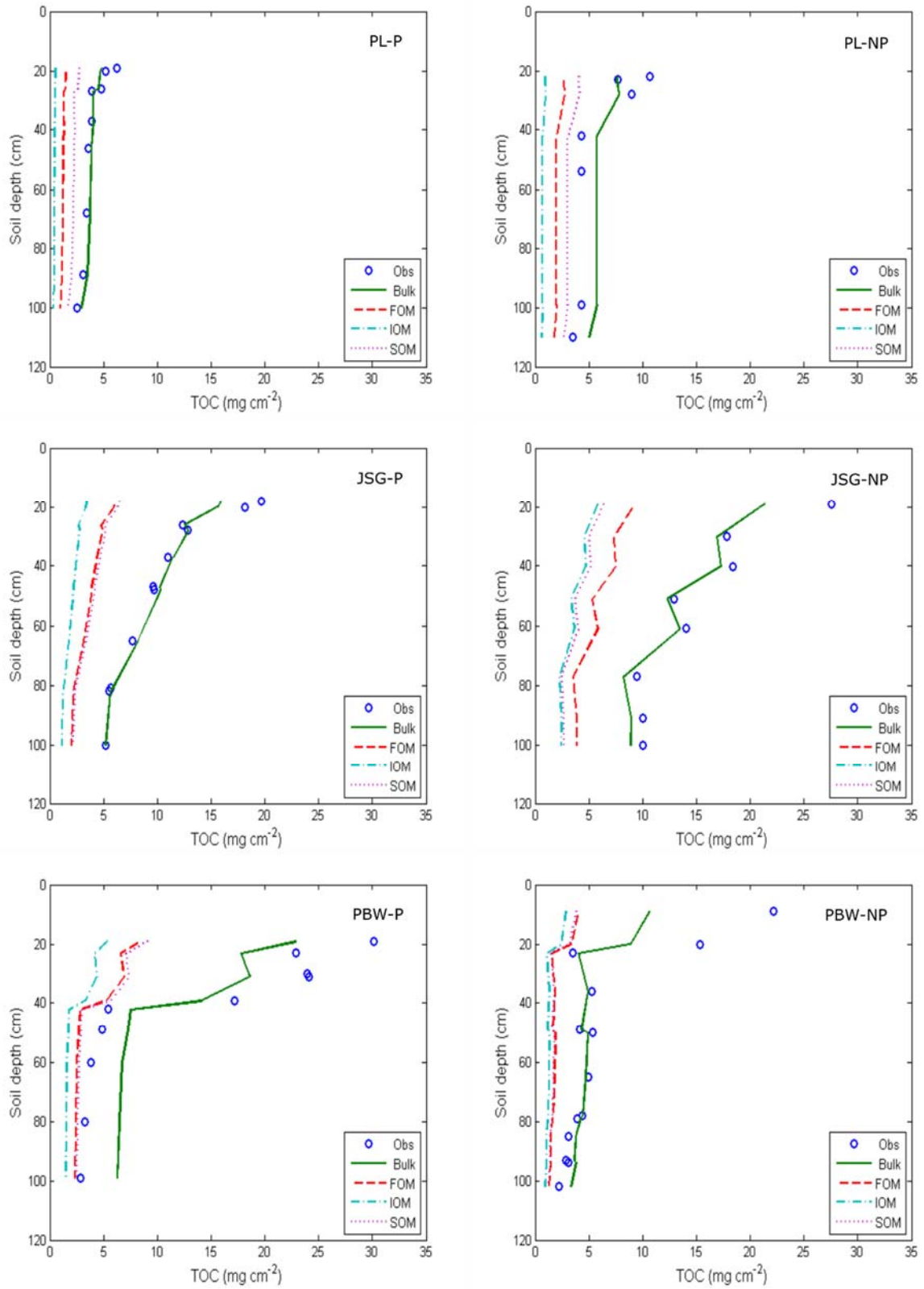


Figure. 5.2. Simulated depth distribution of TOC and organic fractions in different soil types and crop managements (Obs: data measured, Bulk: total organic fractions, FOM: active fractions, IOM: passive fractions, SOM: slow fractions).

The typical values of  $D$  for aqueous solution in clay and soil materials are ca.  $0.08\text{-}1.66\text{ cm}^2\text{ d}^{-1}$  (Leij and van Genuchten, 2002), while the hydraulic conductivity of clay is ca.  $0.08\text{ cm d}^{-1}$  (Miyazaki, 2006). This difference, however, may be related to the high complexity of field condition, and to the limited assumptions used to develop this model.

In this model, soil moisture  $f(m_s)$  and oxygen availability  $f(O_c)$  are set to adjust the anoxic condition in the top layer of P profiles (Table 5.1), i.e. to reduce the carbon losses. With  $f(O_c)$  ca. 9 times smaller in top soil P, however, no clear evidence was found in the context of their effect to diffusion and convection in comparison to NP. As the variation of  $D$  and  $\nu$  are apparently inconsistent between P and NP (Table 5.3), it is suggested that the anoxic condition simulated in this model may not significantly influence the subsoil transport of carbon.

The implementation of climate variables through temperature sensitivity  $f(t_s)$ , and in combination with moisture sensitivity  $f(m_s)$  and oxygen availability  $f(O_c)$  through decomposition efficiency  $\beta$  (section 5.2.1.2) are actually to evaluate of their effects to soil organic matter decomposition.

A higher  $\beta$  value (Appendix 5.8), suggested an optimum environment for organic matter breakdown as in JSG and PL. The favourable condition in JSG-NP, as indicated by the highest  $\beta$  up to 0.05, may be related to the majority of clay fractions (section 3.1) that providing a more moisture. In contrast, the combination of high  $f(m_s)$  with concomitant low  $f(t_s)$ , as in PBW, may not provide a favourable condition for organic matter decomposition. Consequently, organic matter tends to accumulate (section 4.1; section 4.2) as indicated by the lower  $\beta$  values ca. 0.01.

The high  $\beta$  value in PL, reflecting the higher carbon loss (eq. 5.14), may explain the lower organic carbon stock despite the higher litter input in this soil. The high organic biomass derived from sugarcane (NP site) (Appendix 5.6) may not produce the higher carbon stock than different soils. The more intensive organic matter decomposition in this soil may be confirmed by the high level of organic compound aromaticity (section 3.3).

The carbon storage capacity  $h$  was simulated according to clay content/mineralogy composition, and litter quantity input  $C(t)$  based on the identified crops operated in the field (Appendix 5.6; Appendix 5.7; Appendix 5.8). As indicated in eq. (5.14), the first term to the right hand side includes soil factor  $h$  and quantity of litter  $C(t)$  as important factors to carbon storage. The smaller variation of  $h$  values among soil types compared to the variation of  $C(t)$ , which is up to a factor of 20, for instance between sugarcane (PL-NP) and maize (PBW-NP), may show the important of  $C(t)$  to contribute to soil carbon storage.

The small variation of  $h$  simulated in this model, i.e. PBW ca. 0.9, JSG ca. 0.7-0.8, and PL 0.8, are assumed to be related to the bulk composition, which is made up by mixing of multi-composition of clay minerals, which is more practicable for field condition. In the pure clay, the variation of carbon adsorption capacity ( $Q_{\max}$ ) may be by a factor of ca. 2 between allophane > smectite, and > kaolinite (Singh et al., 2017), which is not quite different with the assumption made in this model.

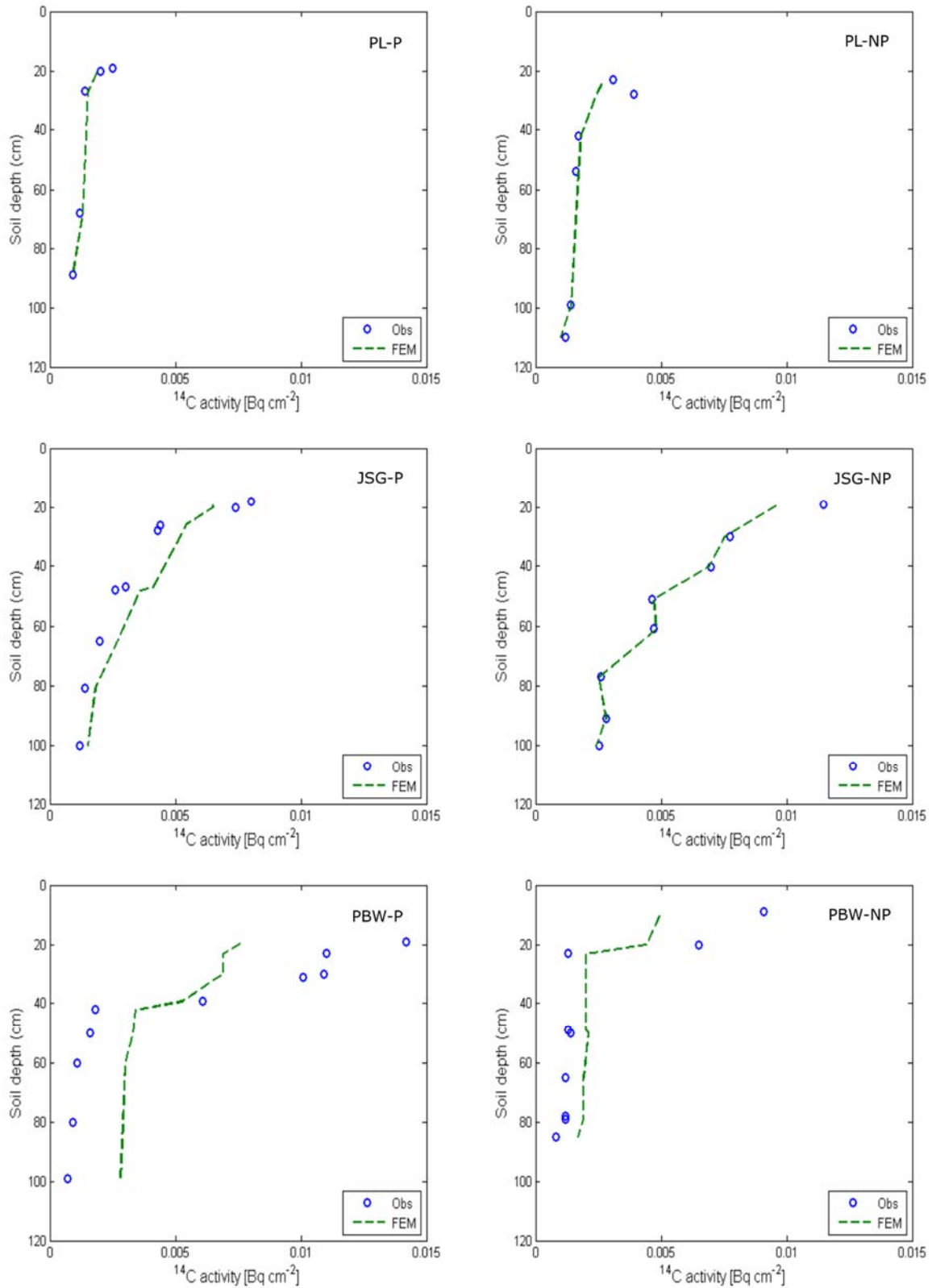


Figure. 5.3. Simulated depth distribution of  $^{14}\text{C}$  activity in different soil types and crop managements.

Partitioning organic compound into individual organic fractions (Fig. 5.2), may show a more coincidence of bulk organic matter with slow organic fractions (SOM) than to different fractions. The fast organic fractions (FOM) or SOM exist in the space closer to bulk TOC than

IOM (Fig. 5.2). This may indicate a higher contribution of these components to bulk TOC. The use of only single coefficient for organic fractions in this model (Table 5.1; section 2.4.4) may have resulted in a consistent trends of organic fractions distribution at depth. Consequently, it may have limited the relative variation of organic fractions across the soil columns.

### 5.5.2. Radiocarbon-model ( $R_M$ )

The lower  $EF$  in PBW profiles (Table 5.3) is clearly reflected in the plots (Fig. 5.3). The high heterogeneity of profile composition in PBW may limit the application of  $R_M$  model.

The continuous model used in this study with assuming a homogeneous of soil profiles may not explain the layer composition variability. The values of  $D$  range from 0.020 in PL to 0.095  $\text{cm}^2 \text{d}^{-1}$  in PBW-P which does not show highly different values between P and NP. The lower  $D$  in PL compared to different soil types may indicate a less depth-gradient of  $^{14}\text{C}$ .

The convection  $v$  is not significantly different among soil types (Table 5.3), ranging from -0.018 in PL-P to -0.004  $\text{cm d}^{-1}$  in PL-NP. The convective transport of  $^{14}\text{C}$  may not be dominant in PL-NP, as  $v$  value shows significantly smaller than different soil types. Compared to the P profile, the model is more deviated in NP mainly at 20-40 cm depth. Similar to  $\text{TOC}_M$  model, both  $D$  and  $v$  may associate each other as data indicates a similar trends (Table 5.3).

In  $R_M$  model, carbon input  $C(t)$  through litter has apparently a great contribution to the level of  $^{14}\text{C}$  enrichment. The higher  $C(t)$  has increased the  $^{14}\text{C}$  activity (Appendix 5.6; Appendix 5.7; Appendix 5.8). The clear example as observed in PL sites where plant litter input in NP is significantly higher than in P profile. With the increase of total  $C(t)$  almost 6 times, simulated at both top- and subsoil, the increase in  $^{14}\text{C}$  activity in NP shows to have ca. 5 times (Appendix 5.6; Fig. 5.3).

As the decay constant of organic material is obtained from the total constant of organic fractions and natural decay of radioactive (section 5.2.1.2), therefore all environmental variables, i.e. temperature, soil moisture condition, and oxygen availability, will be assumed to influence depth transport of  $^{14}\text{C}$  activity as for total organic carbon. The decomposition efficiency  $\beta$  poses the same condition as  $\text{TOC}_M$  model. However, results show no clear indication of these variables to affect to  $^{14}\text{C}$  activity among soil types.

## 5.6. Conclusions

A single model formula is attempted to explain the depth-distribution of total organic carbon, and  $^{14}\text{C}$ . Field heterogeneity is suggested being responsible to the response of field observation to models. The transport parameters,  $D$  and  $v$ , vary among different soil types indicating a different mechanisms responsible for the movement of subsoil carbon.

As governing equation used in this modelling is based on the assumption that soil column composition is homogeneous, therefore, it gives a large deviation from the data observations mainly in PBW profiles, which is disturbed. However, the application of this model may be limited to continuous soil columns.

The coefficient of transport parameters resulted from this modelling may not be realistic, as they show lower values compared to the data obtained from field measurements.

Nevertheless, models are able to show the variety in the dynamic transport of carbon at depth in different soil types.

The application of environment variables in  $TOC_M$  and  $R_M$  model may not give a pronounced effect to carbon transport parameters. Decomposition efficiency  $\beta$  indicates a favourable condition for organic matter decomposition in JSG and PL sites. The lower  $\beta$  value in PBW may provide unfavourable condition that allowing organic carbon to accumulate. In contrast, the increase in  $\beta$  in PL may indicate a better condition for soil organic matter decomposition.

## Chapter 6

### 6. Synthesis

The interplay of soil carbon with soil processes and climate is complex processes (Goudie and Viles, 2012). As mineral compositions vary with different soil types, the stabilization of carbon through organo-mineral complex may exhibit a specific processes as results of parent material and environmental conditions (Feller and Beare, 1997; Han et al., 2016; Matus et al., 2014; Paul, 2016; Rumpel and Kögel-Knabner, 2011; Takahashi and Dahlgren, 2016; Wattel-Koekkoek et al., 2001). Temperature and moisture condition as derivatives of climate may play a role as drivers to the cycling of carbon (Davidson and Janssens, 2006; Guntiñas et al., 2012; Leiros et al., 1999; Lützow and Kögel-knabner, 2009). With sizes variably change according to landuses (Batjes, 1996; Detwiler, 1986), the dynamics of soil carbon in terms of influx, outflux, and sequestration may vary across different regions (Janzen, 2004; Lal, 2011, 2004). Therefore, it is suggested that different region may apply different important soil processes to control the dynamics of carbon.

Based on the widely accepted concept about some factors in relation to soil carbon dynamics, as mentioned above, the study of carbon dynamics in different tropical soils under different climate and crop managements were performed in Java, Indonesia. A detailed sampling with 2-3 intervals in main horizons aimed at getting a closer look about the important soil processes posed in every soil types. The research information was obtained by incorporating both field and laboratory analysis, to get a comprehensive knowledge in the context of study areas.

In this study, the dynamics of carbon in combination with important soil processes were evaluated through natural carbon isotopic tracer. Carbon isotopes, i.e.  $^{13}\text{C}$  and  $^{14}\text{C}$ , have been applied broadly to identify specific processes in the soil. The make use of  $\delta^{13}\text{C}$  signals allow us to identify the origin of carbon in the context of plant material (Balesdent et al., 1990, 1987; Nissenbaum and Schallinger, 1974). While the application of  $^{14}\text{C}$  is more extended with multi-purposes for instance to trace the infiltration of carbon through soil fractions (Anderson and Paul, 1984), to track the mobility of young carbon in the soil column through dissolved organic carbon (Gandois et al., 2014; Hagedorn et al., 2015), to trace the outflux of carbon through soil respiration (Gaudinski et al., 2000), or to trace the flow of carbon through the microbial system (Rethemeyer et al., 2004a).

In this section, the essential finding obtained from this study will be extracted to build up a proposed concept in relation to the implications of environmental variables to the dynamics of soil carbon. In the first part (section 6.1), the role of physical environment to the current standing of soil carbon in different soil types will be discussed. In the second part (section 6.2), the effect of specific condition, i.e. quantity of litter inputs, to the dynamics of soil carbon will be presented.

#### 6.1. Field variability controls of soil organic carbon dynamics

Though the complexity of field conditions, at least four factors may have been observed to control the dynamics of carbon in the study areas, i.e. soil types, topography, temperature,

and crop managements (Fig. 6.1). All factors are in principle indispensable to create a specific condition for soil carbon. Soil types relate, mainly, soil carbon with the mineralogy compositions that lead to the variety in the carbon storing capacity and losses through leaching into deep layers. As three different dominant clay mineralogy composition have been identified in the study areas (Winkler et al., 2016), i.e. allophanic in Andosol (PBW), kaolinitic in Alisol (JSG), and smectitic in Vertisol (PL), the carbon storing capacity may pose different mechanisms in each soil types. Andosol (PBW) with majority mineral composition is short range-ordered minerals may pose a strongest complex with organic carbon resulting in the high preservation of  $^{14}\text{C}$  (section 4.3.2.1). The inaccessibility of organic carbon to microbial decomposition may have exhibited the presence of carbon signals originated from different atmospheric composition at the subsoil (ca. 30-40 cm depth) which is extremely higher than current level.

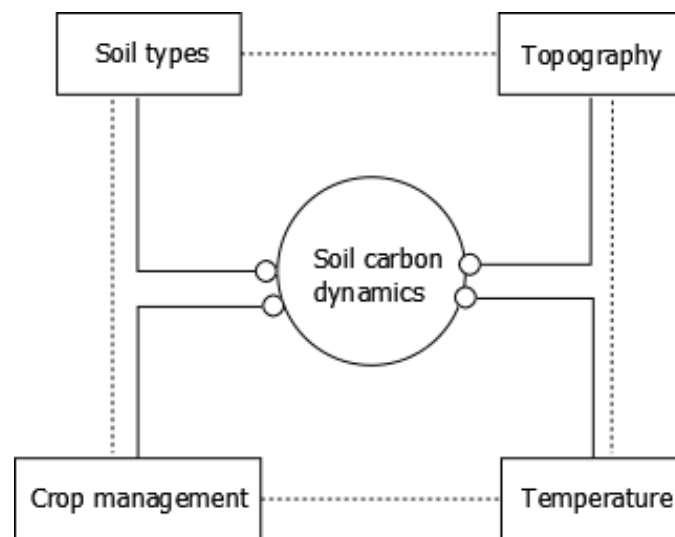


Figure. 6.1. Field variability controls the dynamics of soil carbon in the study areas.

The implication of topography factors are through the parent material origins, climate conditions, and water table positions. The area situated at the upper slope of volcanic regions, i.e. Andosol (PBW), may have showed a high heterogeneity of parent materials, in the context of grain size compositions (section 3.1) and elemental compositions (section 3.3). Provided that temperature is quite low in this area at ca. 21°C (Table 2.1), it is less favourable for soil organic matter decomposition resulting in the increasing of organic carbon storage (section 4.2). Down to lowest slope in Vertisol (PL), the total carbon storage is decreasing with correspond to the increasing in the, presumably, decomposition rate (section 3.4) as the result of warmer environment (section 2.1.1). The effect of shallow water table may have noticed through the accumulation of salt minerals in the layers close to water table, most probably is going up through capillarity (section 3.3; Appendix 4.3).

The temperature effect to the soil carbon mineralization has been well recognized (Davidson and Janssens, 2006; Lützow and Kögel-knabner, 2009). As it increases with decreases altitude,

the higher mineralization rate in Vertisol (PL), at ca. 80 m a.s.l, is as theoretically expected. The carbon rich in the aromatic compounds seems to be dominant in Vertisol (PL), and with the increase in aliphatic compounds towards higher altitude in Andosol (PBW) and Alisol (JSG) along the decrease in temperatures (section 3.4). Temperature may provide an extra condition for carbon storage, beside the soil fixing capacity, where controls the influx/outflux of carbon in the soil system. The favourable condition for organic carbon accumulation may provide a higher potential of top soil carbon to transport down into subsoil, as indicated by simple modelling (section 5.5.1; section 5.5.2).

The association of carbon stored in the soils with plant residue quantities may have roughly been observed in this study (section 4.1; section 4.2). Crop managements, i.e. crop types, and annual rotations, may influence soil carbon level. The application of C<sub>4</sub> crop types may tend to contribute land with more organic carbon than C<sub>3</sub> crop types. However, the postulated organic carbon preservation related to anoxic condition during rice cultivations (Kögel-Knabner et al., 2010) were not observed in this research by carbon isotope study, first because the object of study in this research is subsoil which is not directly influenced by waterlogging, second the anoxic condition during rice management is not constant. The alternating oxic-anoxic condition existed due to crop rotations (section 4.2).

## 6.2. Plant litter control to carbon refreshments

The type of crops may not implicate any condition to the level of <sup>14</sup>C in the soil but organic biomass produced during growing season. By converting the concentration of <sup>14</sup>C (pMC) into specific activity (Bq cm<sup>-2</sup>) in modelling (section 5.5.2), this idea is likely confirmed. The quantity of plant litter input may play a significant role to the level of carbon enrichment. As simulation showed that the increase of organic carbon through litter 6 times results in the increase in <sup>14</sup>C activity ca. 5 times.

As the plant litter input is generally higher in NP than P sites (section 4.1), a comparative analysis is made on the top layer at which direct input of plant residues is located. Result shows, with exception the anomalous condition in PBW, the consistent higher <sup>14</sup>C content in the humin of top NP than P samples (section 4.3.2.2). Assuming the same atmospheric origins (in 2012), the increase in <sup>14</sup>C content in the humin up to > 100 pMC in Vertisol (PL) shows the highest level among the other sites. Yet, being sugarcane as majority crop in this site, the higher level of top <sup>14</sup>C is likely related to the different <sup>14</sup>CO<sub>2</sub> origins. As biennial crop, sugarcane can develop new structure using carbon fixed in the previous 1-2 years (Gaudinski et al., 2001).

Given this condition, it is suggested that plant residue quantities may associate with the level of carbon enrichment. This assumption may have been confirmed by previous study in the soil chronosequence in China (Bräuer et al., 2013a, 2013b). Crop managements both in rice and non-rice paddies have promoted the <sup>14</sup>C concentration of the original parent materials to the values close to current atmospheric level.

## Conclusions

Four factors may have been identified to control the dynamics of carbon in the study areas, i.e. soil types, topography, temperature, and crop managements which indispensable each

other. Soil types relate, mainly, soil carbon with the mineralogy compositions that lead to the variety in the carbon storing capacity and losses through leaching into deep layers. The implication of topography factors are likely through the parent material origins, climate conditions, and water table positions. The temperature effect to the soil carbon mineralization is related to the mineralization rate. The association of carbon stored in the soils with plant residue quantities may be related to crop managements, i.e. crop types, and annual rotations, as different field operational may result in different litter produced.

The quantity of plant litter input may play a significant role to the level of carbon enrichment. The largest quantity of litter input identified in the study areas, under sugarcane in Vertisol (PL), shows to increase the  $^{14}\text{C}$  content in the humin fraction up to more than 100 pMC.

## References

- Ahmad, R., Nelson, P.N., Kookana, R.S., 2006. The molecular composition of soil organic matter as determined by  $^{13}\text{C}$  NMR and elemental analyses and correlation with pesticide ... The molecular composition of soil organic matter as determined by  $^{13}\text{C}$  NMR and elemental analyses and correlation with pesti 57, 883–893. doi:10.1111/j.1365-2389.2005.00784.x
- Ahr, S.W., Nordt, L.C., Driese, S.G., 2012. Assessing lithologic discontinuities and parent material uniformity within the Texas sandy mantle and implications for archaeological burial and preservation potential in upland settings. *Quat. Res.* 78, 60–71. doi:10.1016/j.yqres.2012.03.013
- Ahrens, B., Braakhekke, M.C., Guggenberger, G., Schrumpf, M., Reichstein, M., 2015. Contribution of sorption, DOC transport and microbial interactions to the 14 C age of a soil organic carbon profile : Insights from a calibrated process model. *Soil Biol. Biochem.* 88, 390–402. doi:10.1016/j.soilbio.2015.06.008
- Amelung, W., Zech, W., Zhang, X., Follett, R.F., Tiessen, H., Knox, E., Flach, K.-W., 1998. Carbon, Nitrogen, and Sulfur Pools in Particle-Size Fractions as Influenced by Climate. *Soil Sci. Soc. Am. J.* 62, 172. doi:10.2136/sssaj1998.03615995006200010023x
- Amien, P.R., Pramudia, A., Susanti, E., 1996. Effects of interannual climate variability and climate change on rice yield in Java, Indonesia. *Water. Air. Soil Pollut.* 92, 29–39.
- Anderson, D.W., Paul, E.A., 1984. Organo-mineral complexes and their study by radiocarbon dating. *Soil Sci Soc Am J* 48, 298–301.
- Baisden, W.T., Parfitt, R.L., 2007. Bomb  $^{14}\text{C}$  enrichment indicates decadal C pool in deep soil? *Biogeochemistry* 85, 59–68. doi:10.1007/s10533-007-9101-7
- Baldock, J.A., Oades, J.M., Nelson, P.N., Skene, T.M., Golchin, A., Clarke, P., 1997. Assessing the extent of decomposition of natural organic materials using solid-state  $^{13}\text{C}$  NMR spectroscopy. *Aust. J. Soil Res.* 35, 1061–1083.
- Balesdent, J., Balabane, M., 1996. Major contribution of roots to soil carbon storage inferred from maize cultivated soils. *Soil Biol. Biochem.* 28, 1261–1263. doi:10.1016/0038-0717(96)00112-5
- Balesdent, J., Mariotti, A., Boisgontier, D., 1990. Effect of tillage on soil organic carbon mineralization estimated from  $^{13}\text{C}$  abundance in maize fields. *J. Soil Sci.* 41, 587–596. doi:10.1111/j.1365-2389.1990.tb00228.x
- Balesdent, J., Mariotti, A., Guillet, B., 1987. Natural  $^{13}\text{C}$  abundance as a tracer for studies of soil organic matter dynamics. *Soil Biol. Biochem.* 19, 25–30. doi:10.1016/0038-0717(87)90120-9
- Bandyopadhyay, K.K., Mohanty, M., Painuli, D.K., Misra, A.K., Hati, K.M., Mandal, K.G., Ghosh, P.K., Chaudhary, R.S., Acharya, C.L., 2003. Influence of tillage practices and nutrient

- management on crack parameters in a Vertisol of central India. *Soil Tillage Res.* 71, 133–142. doi:10.1016/S0167-1987(03)00043-6
- Bartsev, S.I., Pochekutov, A.A., 2016. The vertical distribution of soil organic matter predicted by a simple continuous model of soil organic matter transformations. *Ecol. Modell.* 328, 95–98. doi:10.1016/j.ecolmodel.2016.02.020
- Batjes, N.H., 1996. Total carbon and nitrogen in the soils of the world. *Eur. J. Soil Sci.* 47, 151–163. doi:10.1111/j.1365-2389.1996.tb01386.x
- Belousov, A., Belousova, M., Krimer, D., Costa, F., Prambada, O., Zaennudin, A., 2015. Volcaniclastic stratigraphy of Gede Volcano, West Java, Indonesia: How it erupted and when. *J. Volcanol. Geotherm. Res.* 301, 238–252. doi:10.1016/j.jvolgeores.2015.05.018
- Benbi, D.K., Boparai, A.K., Brar, K., 2014. Decomposition of particulate organic matter is more sensitive to temperature than the mineral associated organic matter. *Soil Biol. Biochem.* 70, 183–192. doi:10.1016/j.soilbio.2013.12.032
- Beyaert, R.P., Voroney, R.P., 2011. Estimation of decay constants for crop residues measured over 15 years in conventional and reduced tillage systems in a coarse-textured soil in southern Ontario. *Can. J. Soil Sci.* 91, 985–995. doi:10.4141/CJSS2010-055
- Bhagwat, A.S., 2005. Photosynthesis Carbon Assimilation of C3, C4, and CAM Pathways, in: Pessaraki, M. (Ed.), *Handbook of Photosynthesis*. CRC Press, Boca Raton.
- Birkeland, P.W., 1999. *Soils and Geomorphology*. Oxford University Press, Oxford.
- Boutton, T.W., 1991. Stable Carbon Isotope Ratios of Natural Materials: II. Atmospheric, Terrestrial, Marine, and Freshwater Environments, in: *Carbon Isotop Technique*. Academic Press, Inc, San Diego.
- Bowman, S., 1990. *Radiocarbon Dating*. University of California Press, Berkeley.
- Bräuer, T., Grootes, P.M., Nadeau, M.-J., 2013a. Origin of Subsoil Carbon in a Chinese Paddy Soil Chronosequence. *Radiocarbon* 55, 1058–1070. doi:10.1017/S0033822200058197
- Bräuer, T., Grootes, P.M., Nadeau, M.-J., Andersen, N., 2013b. Downward carbon transport in a 2000-year rice paddy soil chronosequence traced by radiocarbon measurements. *Nucl. Instruments Methods Phys. Res. Sect. B Beam Interact. with Mater. Atoms* 294, 584–587. doi:10.1016/j.nimb.2012.07.012
- Bruun, S., Christensen, B.T., Thomsen, I.K., Jensen, E.S., Jensen, L.S., 2007. Modeling vertical movement of organic matter in a soil incubated for 41 years with <sup>14</sup>C labeled straw. *Soil Tillage Res.* 39, 368–371. doi:10.1016/j.soilbio.2006.07.003
- Buurman, P., 2004. Stratification of parent material in European volcanic and related soils studied by laser-diffraction grain-sizing and chemical analysis 56, 127–144. doi:10.1016/j.catena.2003.10.007
- Buurman, P., Amézquita, M.C., Ramirez, H.F., 2008. Factors Affecting Soil C Stocks: A

- Multivariate Analysis Approach, in: Mannetje, 't, Amézquita, M.C., Buurman, P., Ibrahim, M.A. (Eds.), *Carbon Sequestration in Tropical Grassland Ecosystems*. Wageningen Academic Publishers, Wageningen.
- Campbell, E.E., Paustian, K., 2015. Current developments in soil organic matter modeling and the expansion of model applications : a review. *Environ. Res. Lett* 10.
- Chapman, S.L., Horn, M., 1968. Parent material uniformity and origin of silty soils in Northwest Arkansas based on zirconium-titanium contents. *Soil Sci Soc Am J* 32, 265–271.
- Christensen, B.T., 2001. Physical fractionation of soil and structural and functional complexity in organic matter turnover. *Eur. J. Soil Sci.* 52, 345–353. doi:10.1046/j.1365-2389.2001.00417.x
- Coleman, K., Jenkinson, D.S., 1999. RothC-26.3. A Model for the Turnover of Carbon in Soil: Model Description and Windows Users Guide.
- Coleman, K., Jenkinson, D.S., 1996. RothC-26.3 - A Model For the Turnover of Carbon in Soil, in: Powlson, D.S., Smith, P., Smith, J.U. (Eds.), *Evaluation of Soil Organic Matter Models. Using Existing Long-Term Datasets*. Springer, Berlin, pp. 237–246.
- Conant, R.T., Drijber, R.A., Haddix, M.L., Parton, W.J., Paul, E.A., Plante, A.F., Six, J., Steinweg, M., 2008. Sensitivity of organic matter decomposition to warming varies with its quality. *Glob. Chang. Biol.* 14, 868–877. doi:10.1111/j.1365-2486.2008.01541.x
- Conklin, A.R., 2005. *Introduction to Soil Chemistry. Analysis and Instrumentation*. John Wiley & Sons, Inc, New Jersey.
- Cotrufo, M.F., Galdo, I, D., Piermatteo, D., 2009. Litter Decomposition: Concepts, Methods and Future Perspectives, in: Kutsch, W.L., Bahn, M., Heinemeyer, A. (Eds.), *Soil Carbon Dynamics. An Integrated Methodology*. Cambridge University Press, New York, pp. 76–90.
- Craig, H., 1953. The geochemistry of the stable carbon isotopes. *Geochim. Cosmochim. Acta* 3, 53–92. doi:10.1016/0016-7037(53)90001-5
- Dames, T.W.G., 1955. *The Soils of East Central Java*. Indonesian Soil Research Institute, Bogor.
- Davidson, E.A., Janssens, I.A., 2006. Temperature sensitivity of soil carbon decomposition and feedbacks to climate change. *Nature* 440, 165–173. doi:10.1038/nature04514
- Davidson, E.A., Trumbore, S.E., Amundson, R., 2000. Soil warming and organic carbon content. *Nature* 408, 789–790. doi:10.1038/35048672
- Dell'Abate, M.T., Benedetti, A., Trinchera, A., Dazzi, C., 2002. Humic substances along the profile of two Typic Haploxerert. *Geoderma* 107, 281–296. doi:10.1016/S0016-7061(01)00153-7
- Dessureault-Rompré, J., Zebarth, B.J., Georgallas, A., Burton, D.L., Grant, C.A., Drury, C.F., 2010. Temperature dependence of soil nitrogen mineralization rate : Comparison of

- mathematical models , reference temperatures and origin of the soils. *Geoderma* 157, 97–108. doi:10.1016/j.geoderma.2010.04.001
- Detwiler, R., 1986. Land use change and the global carbon cycle: the role of tropical soils. *Biogeochemistry* 2, 67–93. doi:10.1007/BF02186966
- Dieterich, U., 2012. Description of 18 Profiles of Andosols, Ferralsols, and Vertisols Under Paddy and Non-Paddy Use in Java (Indonesia). Technische Universität München.
- Dippold, M.A., Kuzyakov, Y., 2016. Direct incorporation of fatty acids into microbial phospholipids in soils : Position-specific labeling tells the story. *Geochim. Cosmochim. Acta* 174, 211–221. doi:10.1016/j.gca.2015.10.032
- Dreibrodt, S., Furholt, M., Hofmann, R., Hinz, M., Cheben, I., 2017. P-ed-XRF-geochemical signatures of a 7300 year old Linear Band Pottery house ditch fill at Vráble-Ve'lké Lehemy, Slovakia-House inhabitation and post-depositional processes. *Quat. Int.* 438, 131–143.
- Ehleringer, J.R., 1991.  $^{13}\text{C}/^{12}\text{C}$  Fractionation and Its Utility in Terrestrial Plant Studies, in: Coleman, D.C., Fry, B. (Eds.), *Carbon Isotop Technique*. Academic Press, Inc, San Diego.
- Elzein, A., Balesdent, J., 1995. Mechanistic simulation of vertical distribution of carbon concentrations and residence times in soils. *Soil Sci Soc Am J* 59, 1328–1335.
- Essington, M.E., 2005. *Soil and Water Chemistry. An Integrative Approach*. CRC Press, Boca Raton.
- Eusterhues, K., Rumpel, C., Kögel-Knabner, I., 2007. Composition and radiocarbon age of HF-resistant soil organic matter in a Podzol and a Cambisol. *Org. Geochem.* 38, 1356–1372. doi:10.1016/j.orggeochem.2007.04.001
- Eusterhues, K., Rumpel, C., Kögel-Knabner, I., 2005. Stabilization of soil organic matter isolated via oxidative degradation. *Org. Geochem.* 36, 1567–1575. doi:10.1016/j.orggeochem.2005.06.010
- Everitt, B., Hothorn, T., 2011. *An Introduction to Applied Multivariate Analysis with R*. Publisher, New York.
- Fabbri, D., Chiavari, G., Galletti, G.C., 1996. Characterization of soil humin by pyrolysis(/methylation)-gas chromatography/mass spectrometry: structural relationships with humic acids. *J. Anal. Appl. Pyrolysis* 37, 161–172. doi:10.1016/0165-2370(96)00943-6
- Faithfull, N.T., 2002. *Methods In Agricultural Chemical Analysis. A Practical Handbook*. CABI Publishing, Oxon.
- FAO, 2006. *Guidelines for Soil Description*, 4th ed. Rome.
- Feller, C., Beare, M.H., 1997. Physical control of soil organic matter dynamics in the tropics. *Geoderma* 79, 69–116.

- Fierer, N., Craine, J.M., McLauchlan, K., Schimel, J.P., 2005. Litter quality and the temperature sensitivity of decomposition. *Ecology* 86, 320–326.
- Gandois, L., Teisserenc, R., Cobb, A.R., Chieng, H.I., Lim, L.B.L., Kamariah, A.S., Hoyt, A., Harvey, C.F., 2014. Origin, composition, and transformation of dissolved organic matter in tropical peatlands. *Geochim. Cosmochim. Acta* 137, 35–47. doi:10.1016/j.gca.2014.03.012
- Gaudinski, J.B., Trumbore, S.E., Davidson, E. a, Cook, a C., Markewitz, D., Richter, D.D., 2001. The age of fine-root carbon in three forests of the eastern United States measured by radiocarbon. *Oecologia* 104, 420–429. doi:10.1007/s004420100746
- Gaudinski, J.B., Trumbore, S.E., Davidson, E.A., Zheng, S., 2000. Soil carbon cycling in a temperate forest: radiocarbon-based estimates of residence times, .... *Biogeochemistry* 51, 33–69.
- Genuchten, M.T. Van, Alves, W.J., 1982. Analytical Solutions of the One-Dimensional Convective-Dispersive Solute Transport Equation (No. No. 1661).
- Gillespie, R., 1984. Radiocarbon User's Handbook. Oxford University Press, Oxford.
- Gleixner, G., 2013. Soil organic matter dynamics: A biological perspective derived from the use of compound-specific isotopes studies. *Ecol. Res.* 28, 683–695. doi:10.1007/s11284-012-1022-9
- Godwin, H., 1962. Half-life of Radiocarbon. *Nature* 195, 984.
- Goh, K.M., 1991. Carbon Dating, in: Carbon Isotope Techniques. Academic Press, Inc, California, pp. 125–143.
- Goudie, A.S., Viles, H.A., 2012. Weathering and the global carbon cycle: Geomorphological perspectives. *Earth-Science Rev.* 113, 59–71. doi:10.1016/j.earscirev.2012.03.005
- Graf, A., Weihermüller, L., Huisman, J.A., Herbst, M., Vereecken, H., 2008. Measurement depth effects on the apparent temperature sensitivity of soil respiration in field studies. *Biogeosciences* 5, 1175–1188.
- Greenwood, D.J., 1961. The effect of oxygen concentration on the decomposition of organic materials in soil. *Plant Soil* 14, 360–376.
- Grootes, P.M., 1977. Thermal Diffusion Isotopic Enrichment and Radiocarbon Dating Beyond 50.000 Years BP. PhD Thesis. Rijkuniversiteit Groningen.
- Grootes, P.M., Nadeau, M.-J., Rieck, A., 2004. 14C-AMS at the Leibniz-Labor: Radiometric dating and isotope research. *Nucl. Instruments Methods Phys. Res. Sect. B Beam Interact. with Mater. Atoms* 223–224, 55–61. doi:10.1016/j.nimb.2004.04.015
- Gutiñas, M.E., Leirós, M.C., Trasar-Cepeda, C., Gil-Sotres, F., 2012. Effects of moisture and temperature on net soil nitrogen mineralization: A laboratory study. *Eur. J. Soil Biol.* 48, 73–80. doi:10.1016/j.ejsobi.2011.07.015

- Hafez, Y.I., Awad, E., 2016. Finite element modeling of radon distribution in natural soils of different geophysical regions. *Cogent Phys.* 41, 1–16. doi:10.1080/23311940.2016.1254859
- Hagedorn, F., Bruderhofer, N., Ferrari, A., Niklaus, P.A., 2015. Tracking litter-derived dissolved organic matter along a soil chronosequence using <sup>14</sup>C imaging: Biodegradation, physico-chemical retention or preferential flow? *Soil Biol. Biochem.* 88, 333–343. doi:10.1016/j.soilbio.2015.06.014
- Hammer, S., Levin, I., 2017. Monthly mean atmospheric D<sup>14</sup>CO<sub>2</sub> at Jungfraujoch and Schauinsland from 1986 to 2016 [WWW Document]. <https://heidata.uni-heidelberg.de/>. doi:<https://doi.org/10.11588/data/10100>
- Han, L., Sun, K., Jin, J., Xing, B., 2016. Some concepts of soil organic carbon characteristics and mineral interaction from a review of literature. *Soil Biol. Biochem.* 94. doi:10.1016/j.soilbio.2015.11.023
- Harrison, K.G., Broecker, S., Bonani, G., 1993. The effect of changing land use on soil radiocarbon. *Science (80-. )*. 262, 725–726.
- Hassink, J., 1997. The capacity of soils to preserve organic C and N by their association with clay and silt particles. *Plant Soil* 191, 77–87. doi:10.2136/sssaj1997.03615995006100010020x
- Hayes, M.H.B., Himes, F.L., 1986. Nature and Properties of Humus-Mineral Complexes, in: Huang, P.M., Schnitzer, M. (Eds.), *Interactions of Soil Minerals with Natural Organics and Microbes*. SSSA Special Publication Number 17, Wisconsin, pp. 103–158.
- Hellborg, R., Skog, G., 2008. Accelerator mass spectrometry. *Mass Spectrom. Rev.* 27, 398–427. doi:10.1002/mas.20172
- Heymann, C., Nelle, O., Dör, W., Zagana, H., Nowaczyk, N., Xue, J., Unkel, I., 2013. Late Glacial to mid-Holocene palaeoclimate development of Southern Greece inferred from the sediment sequence of Lake. *Quat. Int.* 302, 42–60. doi:10.1016/j.quaint.2013.02.014
- Hillel, D., 2004. *Introduction to Environmental Soil Physics*. Academic Press, Inc, San Diego.
- Houghton, R.A., 2007. Balancing the global carbon budget. *Annu. Rev. Earth Planet. Sci.* 35, 313–347. doi:DOI 10.1146/annurev.earth.35.031306.140057
- Houghton, R.A., Davidson, E.A., Woodwell, G.M., 1998. Missing sinks, feedbacks, and understanding the role of terrestrial ecosystems in the global carbon balance. *Global Biogeochem. Cycles* 12, 25–34. doi:10.1029/97GB02729
- Hua, Q., Barbetti, M., Rakowski, A.Z., 2013. Atmospheric radiocarbon for the period 1950–2010. *Radiocarbon* 55, 2059–2072. doi:10.2458/azu\_js\_rc.v55i2.16177
- Hulugalle, N.R., Weaver, T.B., Finlay, L.A., Luelf, N.W., Tan, D.K.Y., 2009. Potential contribution by cotton roots to soil carbon stocks in irrigated vertosols. *Aust. J. Soil Res.* 47, 243–252.

doi:10.1071/SR08180

- Hütsch, B.W., Augustin, J., Merbach, W., 2002. Plant rhizodeposition - an important source for carbon turnover in soils. *J. Plant Nutr. Soil Sci.* 165, 479–486. doi:10.1002/1522-2624(200208)165
- Huyakorn, P.S., Pinder, G.F., 1983. *Computational Methods In Subsurface Flow*. Academic Press, Inc, London.
- Istok, J., 1989. *Groundwater Modeling by the Finite Element Method*. American Geophysical Union, Florida.
- Jackson, R.B., Canadell, J., Ehleringer, J.R., Mooney, H.A., Sala, O.E., Schulze, E.D., 1996. A global analysis of root distributions for terrestrial biomes. *Oecologia* 108, 389–411.
- Janzen, H.H., 2004. Carbon cycling in earth systems—a soil science perspective. *Agric. Ecosyst. Environ.* 104, 399–417. doi:10.1016/j.agee.2004.01.040
- Jobbágy, E.G., Jackson, R.B., 2000. The vertical distribution of soil organic carbon and its relation to climate and vegetation. *Ecol. Appl.* 10, 423–436. doi:10.1890/1051-0761(2000)010[0423:TVDOSO]2.0.CO;2
- Juo, A.S.R., Franzluebbers, K., 2003. *Tropical Soils: Properties and Management for Sustainable Agriculture*. Oxford University Press, Oxford.
- Kalbitz, K., Schmerwitz, J., Schwesig, D., Matzner, E., 2003. Biodegradation of soil-derived dissolved organic matter as related to its properties 113, 273–291. doi:10.1016/S0016-7061(02)00365-8
- Kätterer, T., Reichstein, M., Andrén, O., Lomander, A., 1998. Temperature dependence of organic matter decomposition : a critical review using literature data analyzed with different models. *Biol. Fertil. Soils* 27, 258–262.
- Kemanian, A.R., Stöckle, C.O., 2010. C-Farm : A simple model to evaluate the carbon balance of soil profiles. *Eur. J. Agron.* 32, 22–29. doi:10.1016/j.eja.2009.08.003
- Kimura, M., Murase, J., Lu, Y., 2004. Carbon cycling in rice field ecosystems in the context of input , decomposition and translocation of organic materials and the fates of their end products ( CO<sub>2</sub> and CH<sub>4</sub> ). *Soil Biol. Biochem.* 36, 1399–1416. doi:10.1016/j.soilbio.2004.03.006
- Kirk, G., 2004. *The Biogeochemistry of Submerged Soils*. John Wiley & Sons, Inc, Chichester.
- Klein, M.G., Mous, D.J.W., Gott dang, A., 2006. A compact 1MV multi-element AMS system. *Nucl. Instruments Methods Phys. Res. Sect. B Beam Interact. with Mater. Atoms* 249, 764–767. doi:10.1016/j.nimb.2006.03.135
- Kögel-Knabner, I., 1997. <sup>13</sup>C and <sup>15</sup>N NMR spectroscopy as a tool in soil organic matter studies. *Geoderma* 80, 243–270.

- Kögel-Knabner, I., Amelung, W., Cao, Z., Fiedler, S., Frenzel, P., Jahn, R., Kalbitz, K., Kölbl, A., Schloter, M., 2010. Biogeochemistry of paddy soils. *Geoderma* 157, 1–14. doi:10.1016/j.geoderma.2010.03.009
- Kölbl, A., Kögel-Knabner, I., 2004. Content and composition of free and occluded particulate organic matter in a differently textured arable Cambisol as revealed by solid-state <sup>13</sup>C NMR spectroscopy. *J. Plant Nutr. Soil Sci.* 167, 45–53. doi:10.1002/jpln.200321185
- Kölbl, A., Schad, P., Jahn, R., Amelung, W., Bannert, A., Cao, Z.H., Fiedler, S., Kalbitz, K., Lehndorff, E., Müller-Niggemann, C., Schloter, M., Schwark, L., Vogelsang, V., Wissing, L., Kögel-Knabner, I., 2014. Accelerated soil formation due to paddy management on marshlands (Zhejiang Province, China). *Geoderma* 228–229, 67–89. doi:10.1016/j.geoderma.2013.09.005
- Kothwala, D.N., Moore, T.R., Hendershot, W.H., 2008. Soil properties controlling the adsorption of dissolved organic carbon to mineral soils. *Soil Sci Soc Am J* 73, 1831–1842. doi:10.2136/sssaj2008.0254
- Kramer, C., Gleixner, G., 2008. Soil organic matter in soil depth profiles: Distinct carbon preferences of microbial groups during carbon transformation. *Soil Biol. Biochem.* 40, 425–433. doi:10.1016/j.soilbio.2007.09.016
- Kuzyakov, Y., Domanski, G., 2000. Carbon input by plants into the soil. Review. *Zeitschrift für Pflanzenernährung und Bodenk.* 163, 421–431. doi:10.1002/1522-2624(200008)163:4<421::aid-jpln421>3.0.co;2-r
- Kwon, Y.W., Bang, H., 2000. *The Finite Element Method Using MATLAB*. CRC Press, Boca Raton.
- Kylander, M.E., Ampel, L., Wohlfarth, B., Veres, D., 2011. High-resolution X-ray fluorescence core scanning analysis of Les Echets ( France ) sedimentary sequence : new insights from chemical proxies 26, 109–117. doi:10.1002/jqs.1438
- Lal, R., 2011. Sequestering carbon in soils of agro-ecosystems. *Food Policy* 36, S33–S39. doi:10.1016/j.foodpol.2010.12.001
- Lal, R., 2004. Agricultural activities and the global carbon cycle. *Nutr Cycl Agroecosys* 70, 103–116.
- Legros, J.-P., 2012. *Major Soil Groups of the World. Ecology, Genesis, Properties and Classification*. CRC Press, Boca Raton.
- Lehndorff, E., Houtermans, M., Winkler, P., Kaiser, K., Kölbl, A., Romani, M., Said-pullicino, D., Utami, S.R., Zhang, G.L., Cao, Z.H., Mikutta, R., Guggenberger, G., Amelung, W., 2016. Black carbon and black nitrogen storage under long-term paddy and non-paddy management in major reference soil groups. *Geoderma* 284, 214–225. doi:10.1016/j.geoderma.2016.08.026
- Leij, F.J., van Genuchten, M.T., 2002. Solute Transport, in: Warrick, A.W. (Ed.), *Soil Physics*

Companion. CRC Press, Boca Raton.

- Leiros, M.C., Trasar-Cepeda, C., Seoane, S., Gil-Sotres, F., 1999. Dependence of mineralization of soil organic matter on temperature and moisture. *Soil Biol. Biochem.* 31, 327–335.
- Levin, I., Kromer, B., Hammer, S., 2013. Atmospheric  $\delta^{14}\text{C}$  trend in Western European background air from 2000 to 2012. *Tellus B* 65, 1–7. doi:10.3402/tellusb.v65i0.20092
- Liang, Y., Bai, C., Mu, L., Zhou, M., 2014. Soil respiration in cucumber field under crop rotation in solar greenhouse. *Sci. Agric.* 71, 337–341.
- Luckner, L., Schestakow, W.M., 1991. *Migration Processes in the Soil and Groundwater Zone.* Lewis Publisher, Inc, Michigan.
- Lugo, A.E., Sanchez, M.J., Brown, S., 1986. Land use and organic carbon content of some subtropical soils. *Plant Soil* 96, 185–196. doi:10.1007/BF02374763
- Lützow, M. Von, Kögel-knabner, I., 2009. Temperature sensitivity of soil organic matter decomposition — what do we know ? *Biol. Fertil. Soils* 46, 1–15. doi:10.1007/s00374-009-0413-8
- MacCarthy, P., 2001. The principle of humic substances. *Soil Sci.* 166, 738–751.
- Maie, N., Watanabe, A., Kimura, M., 2004a. Chemical characteristics and potential source of fulvic acids leached from the plow layer of paddy soil 120, 309–323. doi:10.1016/j.geoderma.2004.02.007
- Maie, N., Watanabe, A., Kimura, M., 2004b. Chemical characteristics and potential source of fulvic acids leached from the plow layer of paddy soil. *Geoderma* 120, 309–323. doi:10.1016/j.geoderma.2004.02.007
- Mann, W.B., 1983. An international reference material for radiocarbon dating. *Radiocarbon* 25, 519–527. doi:10.1017/S0033822200005816
- Mathieu, J.A., Hatté, C., Balesdent, J., Parent, É., 2015. Deep soil carbon dynamics are driven more by soil type than by climate: a worldwide meta-analysis of radiocarbon profiles. *Glob. Chang. Biol.* 21, 4278–4292. doi:10.1111/gcb.13012
- Matus, F., Rumpel, C., Neculman, R., Panichini, M., Mora, M.L., 2014. Soil carbon storage and stabilisation in andic soils: A review. *Catena* 120, 102–110. doi:10.1016/j.catena.2014.04.008
- Mayes, M.A., Heal, K.R., Brandt, C.C., Phillips, J.R., Jardine, P.M., 2011. Relation between soil order and sorption of dissolved organic carbon in temperate subsoils. *Soil Sci Soc Am J* 76, 1027–1037. doi:10.2136/sssaj
- McKillup, S., Dyar, M.D., 2010. *Geostatistics Explained.* Cambridge University Press, Cambridge.
- Megonigal, J.P., Patrick, J.W.H., Faulkner, S.P., 1993. *Wetland identification in seasonally*

- flooded forest soils: Soil morphology and redox dynamics. *Soil Sci Soc Am J* 57, 140–149.
- Mikutta, R., Kleber, M., Jahn, R., 2005. Poorly crystalline minerals protect organic carbon in clay subfractions from acid subsoil horizons. *Geoderma* 128, 106–115. doi:10.1016/j.geoderma.2004.12.018
- Mikutta, R., Kleber, M., Torn, M.S., Jahn, R., 2006. Stabilization of soil organic matter: Association with minerals or chemical recalcitrance? *Biogeochemistry* 77, 25–56. doi:10.1007/s10533-005-0712-6
- Mikutta, R., Mikutta, C., Kalbitz, K., Scheel, T., Kaiser, K., Jahn, R., 2007. Biodegradation of forest floor organic matter bound to minerals via different binding mechanisms 71, 2569–2590. doi:10.1016/j.gca.2007.03.002
- Miyazaki, T., 2006. *Water Flows in Soils*, Second Edi. ed. CRC Press, Boca Raton.
- Mook, W.G., van der Plicht, J., 1999. Reporting <sup>14</sup>C activities and concentrations. *Radiocarbon* 41, 227–239. doi:10.1017/S0033822200057106
- Moorman, F.R., van Breemen, N., 1978. *Rice: Soil, Water, Land*. International Rice Research Institute, Manila.
- Morra, M.J., Blank, R.R., Freeborn, L.L., Shafii, B., 1991. Size fractionation of soil organo-mineral complexes using ultrasonic dispersion. *Soil Sci.*
- Myers, R.J.K., Campbell, C.A., Weier, K.L., 1982. Quantitative relationship between net nitrogen mineralization and moisture content of soils. *Can. J. Soil Sci.* 62, 111–124.
- Nadeau, M.J., Vaernes, E., Svarva, H.L., Larsen, E., Gulliksen, S., Klein, M., Mous, D.J.W., 2015. Status of the “new” AMS facility in Trondheim. *Nucl. Instruments Methods Phys. Res. Sect. B Beam Interact. with Mater. Atoms* 361, 149–155. doi:10.1016/j.nimb.2015.06.002
- Nelson, P.N., Baldock, J.A., 2005. Estimating the molecular composition of a diverse range of natural organic materials from solid-state <sup>13</sup>C NMR and elemental analyses. *Biogeochemistry* 72, 1–34. doi:10.1007/s10533-004-0076-3
- Nelson, P.N., Baldock, J.A., Clarke, P., Oades, J.M., Churchman, G.J., 1999. Dispersed clay and organic matter in soil: their nature and associations. *Aust. J. Soil Res.* 37, 289–315. doi:10.1071/S98076
- Nicoullaud, B., King, D., Tardieu, F., 1994. Vertical distribution of maize roots in relation to permanent soil characteristics. *Plant Soil* 159, 245–254. doi:10.1007/BF00009287
- Nieder, R., Benbi, D.K., 2008. *Carbon and Nitrogen in the Terrestrial Environment*. Springer.
- Nishimura, S., Yonemura, S., Sawamoto, T., Shirato, Y., Akiyama, H., Sudo, S., Yagi, K., 2008. Effect of land use change from paddy rice cultivation to upland crop cultivation on soil carbon budget of a cropland in Japan 125, 9–20. doi:10.1016/j.agee.2007.11.003

- Nishio, T., Sekiya, H., Toriyama, K., Kogano, K., 1994. Changes in gross rates of nitrogen transformations in soils caused by conversion of paddy fields to upland fields. *Soil Sci. Plant Nutr.* 40, 301–309.
- Nissenbaum, A., Schallinger, K.M., 1974. The distribution of the stable carbon isotope ( $^{13}\text{C}/^{12}\text{C}$ ) in fractions of soil organic matter. *Geoderma* 11, 137–145.
- North, P.F., 1976. Towards an absolute measurement of soil structural stability using ultrasound. *J. Soil Sci.* doi:10.1111/j.1365-2389.1976.tb02014.x
- O’Leary, M.H., 1988. Carbon isotopes in photosynthesis. Fractionation techniques may reveal new aspects of carbon dynamics in plants. *Bioscience* 38, 328–336.
- O’Leary, M.H., 1981. Carbon isotope fractionation in plants. *Phytochemistry* 20, 553–567. doi:http://dx.doi.org/10.1016/0031-9422(81)85134-5
- Oades, J.M., 1988. The retention of organic matter in soils. *Biogeochemistry* 70, 35–70.
- Ono, S., 1989. Nitrogen mineralization from paddy and upland soils under flooded and non flooded incubation. *Soil Sci. Plant Nutr.* 35, 417–426.
- Oorts, K., Vanlauwe, B., Recous, S., Merckx, R., 2005. Redistribution of particulate organic matter during ultrasonic dispersion of highly weathered soils. *Eur. J. Soil Sci.* 56, 77–91. doi:10.1111/j.1365-2389.2004.00654.x
- Pansu, Gautheyrou, J., 2006. *Handbook of Soil Analysis. Mineralogical, Organic and Inorganic Methods.* Springer Berlin Heidelberg.
- Park, R., Epstein, S., 1960. Carbon isotope fractionation during photosynthesis. *Geochim. Cosmochim. Acta* 21, 110–126. doi:10.1016/S0016-7037(60)80006-3
- Paul, E.A., 2016. The nature and dynamics of soil organic matter: Plant inputs, microbial transformations, and organic matter stabilization. *Soil Biol. Biochem.* 98, 109–126. doi:http://dx.doi.org/10.1016/j.soilbio.2016.04.001
- Paul, K.I., Polglase, P.J., O’Connell, A.M., Carlyle, J.C., Smethurst, P.J., Khanna, P.K., 2003. Defining the relation between soil water content and net nitrogen mineralization. *Eur. J. Soil Sci.* 54, 39–47.
- Pausch, J., Tian, J., Riederer, M., Kuzyakov, Y., 2013. Estimation of rhizodeposition at field scale: upscaling of a  $^{14}\text{C}$  labeling study. *Plant Soil* 364, 273–285. doi:10.1007/s11104-012-1363-8
- Poeplau, C., Don, A., 2014. Effect of ultrasonic power on soil organic carbon fractions. *J. Plant Nutr. Soil Sci.* 177, 137–140. doi:10.1002/jpln.201300492
- Powlson, D.S., 1996. Why Evaluate Soil Organic Matter Models, in: Powlson, D.S., Smith, P., Smith, J.U. (Eds.), *Evaluation of Soil Organic Matter Models. Using Existing Long-Term Datasets.* Springer, Berlin, pp. 3–12.

- Prasetyo, B.H., 2007. Differentiation in Properties of Vertisol From Various Parent Materials. *J. Ilmu-Ilmu Pertan. Indones.* 9, 20–31.
- Prasetyo, B.H., Suganda, H., Kasno, A., 2007. Pengaruh Bahan Volkan pada Sifat Tanah Sawah. *J. Tanah dan Iklim* 25, 45–58.
- Prastowo, E., Grootes, P.M., Nadeau, M.-J., Utami, S.R., 2017. Subsoil 14C Dynamics in Different Types of Tropical and Subtropical Soils under Different Crop Management. *Radiocarbon* 59, 1021–1034. doi:10.1017/RDC.2016.81
- Prastowo, E., Purwanto, B, H., Hanudin, E., Sukristyonubowo, De Neve, S., 2013. Balance of carbon and sustainable index of rice field managed organically and conventionally in Sawangan, Magelang, Indonesia, in: Suwardi, Nurcholis, M., Agus, F., Anwar, S., Setiawan, B.I., Ardi, D. (Eds.), *Proceeding of the 11th International Conference of the East and Southeast Asia Federation of Soil Science Societies*. Indonesian Society of Soil Science, pp. 278–279.
- Preston, C.M., Nault, J.R., Trofymow, J.A., 2009. Chemical changes during 6 years of decomposition of 11 litters in some Canadian forest sites C. Part 2. 13C abundance , solid-state 13C NMR spectroscopy and the meaning of “lignin .” *Ecosystem* 12, 1078–1102. doi:10.1007/s10021-009-9267-z
- Raine, S., So, H., 1994. Ultrasonic dispersion of soil in water - the effect of suspension properties on energy dissipation and soil dispersion. *Aust. J. Soil Res.* doi:10.1071/SR9941157
- Rapp, G., Hill, C.L., 2006. *Geoarchaeology. The Earth Science Approach to Archaeological Interpretation*, Second Edi. ed. Yale University Press, New Haven and London.
- Rawls, W.J., Brakensiek, D.L., Saxton, K.E., 1982. Estimation of soil water properties. *Trans. ASAE* 25, 1316–1320.
- Reddy, J.N., 1993. *An Introduction to Finite Element Method*. McGraw-Hill Companies, Inc, New York.
- Reddy, K.R., DeLaune, R.D., 2008. *Biogeochemistry of Wetlands. Science and Applications*. CRC, Boca Raton.
- Reimer, P.J., Bard, E., Bayliss, A., Beck, J.W., Blackwell, P.G., Ramsey, C.B., Buck, C.E., Cheng, H., Edwards, R.L., Friedrich, M., Grootes, P.M., Guilderson, T.P., Hafliadason, H., Hajdas, I., Hatté, C., Heaton, T.J., Hoffmann, D.L., Hogg, A.G., Hughen, K.A., Kaiser, K.F., Kromer, B., Manning, S.W., Niu, M., Reimer, R.W., Richards, D.A., Scott, E.M., Southon, J.R., Staff, R.A., Turney, C.S.M., van der Plicht, J., 2013. IntCal13 and Marine13 Radiocarbon Age Calibration Curves 0–50,000 Years cal BP. *Radiocarbon* 55, 1869–1887. doi:10.2458/azu\_js\_rc.55.16947
- Reimer, P.J., Brown, T. a, Reimer, R.W., 2004. Discussion: Reporting and Calibration of Post-Bomb 14C Data. *Radiocarbon* 46, 1299–1304. doi:10.2458/azu\_js\_rc.46.4183

- Rethemeyer, J., Grootes, P.M., Bruhn, F., Andersen, N., Nadeau, M.J., Kramer, C., Gleixner, G., 2004a. Age heterogeneity of soil organic matter. *Nucl. Instruments Methods Phys. Res. Sect. B Beam Interact. with Mater. Atoms* 223–224, 521–527. doi:10.1016/j.nimb.2004.04.098
- Rethemeyer, J., Kramer, C., Gleixner, G., John, B., Yamashita, T., Flessa, H., Andersen, N., Nadeau, M.J., Grootes, P.M., 2005. Transformation of organic matter in agricultural soils: Radiocarbon concentration versus soil depth. *Geoderma* 128, 94–105. doi:10.1016/j.geoderma.2004.12.017
- Rethemeyer, J., Kramer, C., Gleixner, G., Wiesenberg, G.L.B., Schwark, L., Andersen, N., Nadeau, M.-J., Grootes, P.M., 2004b. Complexity of soil organic matter: AMS 14C analysis of soil lipid fractions and individual compounds. *Radiocarbon* 46, 1111–1150.
- Rubol, S., Manzoni, S., Bellin, A., Porporato, A., 2013. Modeling soil moisture and oxygen effects on soil biogeochemical cycles including dissimilatory nitrate reduction to ammonium (DNRA). *Adv. Water Resour.* 62, 106–124.
- Rumpel, C., Kögel-Knabner, I., 2011. Deep soil organic matter—a key but poorly understood component of terrestrial C cycle. *Plant Soil* 338, 143–158. doi:10.1007/s11104-010-0391-5
- Sage, R.F., Zhu, X.-G., 2011. Exploiting the engine of C4 photosynthesis. *J. Exp. Bot.* 62, 2989–3000.
- Saggar, S., Parshotam, A., Sparling, G.P., Feltham, C.W., Hart, P.B.S., 1997. 14C-Labelled ryegrass turnover and residence times in soils varying in clay content and mineralogy. *Soil Biol. Biochem.* 28, 1677–1686.
- Saiz-Jimenez, C., 1996. The Chemical Structure of Humic Substances: Recent Advances, in: Piccolo, A. (Ed.), *Humic Substances in Terrestrial Ecosystems*. Elsevier Science B. V, Amsterdam, pp. 1–44.
- Schlesinger, W.H., Andrews, J.A., 2000. Soil respiration and the global carbon cycle. *Biogeochemistry* 48, 7–20. doi:10.1023/a:1006247623877
- Schmidt, M.W.I., Rumpel, C., Kögel-Knabner, I., 1999. Evaluation of an ultrasonic dispersion procedure to isolate primary organomineral complexes from soils. *Eur. J. Soil Sci.* 50, 87–94. doi:10.1046/j.1365-2389.1999.00211.x
- Schuur, E.A.G., Carbone, M.S., Pries, C.E.H., Hopkins, F.M., Natali, S.M., 2016a. Radiocarbon in Terrestrial Systems, in: *Radiocarbon and Climate Change. Mechanisms, Applications and Laboratory Techniques*. Springer International Publishing Switzerland, pp. 167–220.
- Schuur, E.A.G., Trumbore, S.E., Druffel, E.F.M., Southon, J.R., Steinhof, A., Taylor, R.E., Turnbull, J.C., 2016b. Radiocarbon and Global Carbon Cycle, in: *Radiocarbon and Climate Change. Mechanisms, Applications and Laboratory Techniques*. Springer International Publishing Switzerland, pp. 1–20.

- Sharifi, A., Kalin, L., Hantush, M.M., Isik, S., Jordan, T.E., 2013. Carbon dynamics and export from flooded wetlands: A modeling approach. *Ecol. Modell.* 263, 196–210. doi:10.1016/j.ecolmodel.2013.04.023
- Shirato, Y., Paisancharoen, K., Sangtong, P., Nakviro, C., Yokozawa, M., Matsumoto, N., 2005. Testing the Rothamsted Carbon Model against data from long-term experiments on upland soils in Thailand. *Eur. J. Soil Biol.* 179–188. doi:10.1111/j.1365-2389.2004.00659.x
- Simpson, A.J., Song, G., Smith, E., Lam, B., Novotny, E.H., Hayes, M.H.B., 2007. Unraveling the structural components of soil humin by use of solution-state nuclear magnetic resonance spectroscopy. *Environ. Sci. Technol.* 41, 876–883. doi:10.1021/es061576c
- Simpson, G., 2017. *Practical Finite Element Modelling in Earth Science Using Matlab*. Willey Blackwell, Geneva.
- Singh, M., Sarkar, B., Biswas, B., Bolan, N.S., Jock, G., 2017. Relationship between soil clay mineralogy and carbon protection capacity as influenced by temperature and moisture. *Soil Biol. Biochem.* 109, 95–106. doi:10.1016/j.soilbio.2017.02.003
- Singh, M., Sarkar, B., Biswas, B., Churchman, J., Bolan, N.S., 2016. Adsorption-desorption behavior of dissolved organic carbon by soil clay fractions of varying mineralogy. *Geoderma* 280, 47–56. doi:10.1016/j.geoderma.2016.06.005
- Slota, P.J., Jull, A.J.T., Linick, T.W., Toolin, I.J., 1987. Preparation of small samples for <sup>14</sup>C accelerator targets by catalytic reduction fo CO. *Radiocarbon* 29, 303–306.
- Smith, J., Smith, P., Addiscot, T., 1996. Quantitative Methods to Evaluate and Compare Soil Organic Matter Models, in: *Evaluation of Soil Organic Matter Models. Using Existing Long-Term Datasets*. Springer, Berlin, pp. 181–200.
- Smith, O.L., 1982. *Soil Microbiology: A Model of Decomposition and Nutrient Cycling*. CRC Press, Boca Raton.
- Soetaert, K., Herman, P.M.J., 2009. *A Practical Guide to Ecological Modelling. Using R as a Simulation Platform*. Springer.
- Steinhof, A., 2016. Accelerator Mass Spectrometry of Radiocarbon, in: Schuur, E.A.G., Druffel, E.R.M., Trumbore, S.E. (Eds.), *Radiocarbon and Climate Change. Mechanisms, Applications and Laboratory Techniques*. Springer International Publishing Switzerland, pp. 253–278.
- Stenström, K.E., Skog, G., Georgiadou, E., Genberg, J., Johansson, A., 2011. *A guide to radiocarbon units and calculations*. Lund.
- Stevenson, F.J., 1994. *Humus Chemistry. Genesis, Composition, Reactions, Second Edi.* ed. John Wiley & Sons, Inc, New York.
- Stuiver, M., Polach, H.A., 1977. Discussion Reporting of <sup>14</sup>C Data. *Radiocarbon* 19, 355–363.

doi:10.1017/S0033822200003672

Suess, H.E., 1965. Secular variations of the cosmic-ray-produced carbon 14 in the atmosphere and their interpretations. *J. Geophys. Res.* 70, 5937–5952. doi:10.1029/JZ070i023p05937

Taghizadeh-Toosi, A., Christensen, B.T., Hutchings, N.J., Vejlin, J., Kätterer, T., Glendining, M., Olesen, J.E., 2014. C-TOOL : A simple model for simulating whole-profile carbon storage in temperate agricultural soils. *Ecol. Modell.* 292, 11–25.

Takahashi, T., Dahlgren, R.A., 2016. Nature, properties and function of aluminum – humus complexes in volcanic soils. *Geoderma* 263, 110–121. doi:10.1016/j.geoderma.2015.08.032

Tan, K.H., 2008. *Soils in the Humid Tropics and Monsoon Region of Indonesia*. CRC Press, Boca Raton.

Tavares, R.L.M., de Souza, Z.M., Siqueira, D.S., La Scala Júnior, N., Panosso, A.R., Campos, M.C.C., 2015. Soil CO<sub>2</sub> emission in sugarcane management systems. *Acta Agric. Scand. Sect. B — Soil Plant Sci.* 65, 755–762. doi:10.1080/09064710.2015.1061048

Taylor, R.E., Bar-Yosef, O., 2014. *Radiocarbon Dating. An Archaeological Perspective*. Left Coast Press, Inc, California.

Tipping, E., 2004. *Cation Binding by Humic Substances*. Cambridge University Press, Cambridge.

Tirado-Corbalá, R., Anderson, R., Wang, D., Ayars, J., 2015. Soil carbon and nitrogen stocks of different Hawaiian sugarcane cultivars. *Agronomy* 5, 239–261. doi:10.3390/agronomy5020239

Torn, M.S., Trumbore, S.E., Chadwick, O. a, Vitousek, P.M., Hendricks, D.M., 1997. Mineral control of soil organic carbon storage and turnover. *Nature* 389, 3601–3603. doi:10.1038/38260

Trumbore, S., 2009. Radiocarbon and soil carbon dynamics. *Annu. Rev. Earth Planet. Sci.* 37, 47–66. doi:10.1146/annurev.earth.36.031207.124300

Trumbore, S.E., Chadwick, O. a., Amundson, R., 1996. Rapid Exchange Between Soil Carbon and Atmospheric Carbon Dioxide Driven by Temperature Change. *Science* (80-. ). doi:10.1126/science.272.5260.393

Trumbore, S.E., Sierra, C.A., Pries, C.E.H., 2016. Radiocarbon Nomenclature, Theory, Models, and Interpretation: Measuring Age, Determining Cycling Rates, and Tracing Source Pools, in: Schuur, E.A.G., Druffel, E.R.M., Trumbore, S.E. (Eds.), *Radiocarbon and Climate Change. Mechanisms, Applications and Laboratory Techniques*. Springer International Publishing Switzerland.

Trumbore, S.E., Vogel, J.S., Southon, J.R., 1989. AMS 14C measurements of fractionated soil

- organic matter: An approach to deciphering the soil carbon cycle. *Radiocarbon* 31, 644–654.
- Tuniz, C., Bird, J.R., Fink, D., Herzog, G.F., 1998. *Accelerator Mass Spectrometry. Ultrasensitive Analysis for Global Science*. CRC Press, Boca Raton.
- van Bemmelen, R.W., 1949. *The Geology of Indonesia. General Geology of Indonesia and Adjacent Archipelagoes*.
- van Reeuwijk, L.P., 2002. *Procedures for Soil Analysis*. International Soil Reference and Information Centre, Wageningen.
- van Veen, J.A., Paul, E.A., 1981. Organic carbon dynamics in grassland soils. I. Background information and computer simulation. *Can. J. Soil Sci.* 61, 185–201.
- Voroney, R.P., van Veen, J.A., Paul, E.A., 1981. Organic matter dynamics in grassland soils. 2. Model validation and simulation of the long-term effects of cultivation and rainfall erosion. *Can. J. Soil Sci.* 61, 211–224.
- Wang, Y., Amundson, R., Trumbore, S., 1996. Radiocarbon Dating of Soil Organic Matter. *Quat. Res.* 45, 282–288. doi:10.1006/qres.1996.0029
- Warren, G.P., Meredith, J.A., 1998. Isotopic Composition of Organic Carbon in Some Soils of Semiarid Africa, in: Bergström, L., Kirchmann, H. (Eds.), *Carbon and Nutrient Dynamics in Natural and Agricultural Tropical Ecosystems*. CAB International, Oxon.
- Wassmann, R., Neue, H.U., Lantin, R.S., Makarim, K., Chareonsilp, N., Buendia, L. V, Rennenberg, H., 2000. Characterization of methane emissions from rice fields in Asia . II . Differences among irrigated , rainfed , and deepwater rice. *Nutr. Cycl. Agroecosystems* 58, 13–22.
- Wattel-Koekkoek, E.J.W., van Genuchten, P.P.L., Buurman, P., van Lagen, B., 2001. Amount and composition of clay-associated soil organic matter in a range of kaolinitic and smectitic soils. *Geoderma* 99, 27–49.
- Wells, T., Hancock, G., 2014. Comparison of vertical transport of <sup>137</sup>Cs and organic carbon in agricultural cracking soils. *Geoderma* 214–215, 228–238. doi:10.1016/j.geoderma.2013.09.007
- Wibisono, G.W., Sudarsono, Darmawan, 2016. Characterisrics of andisols of northeast Gunung Gede, West Java with breccia and volcanic mudflow parent materials. *J. Tanah dan Iklim* 40, 61–70.
- Wilson, M.A., Goh, K.M., Collin, P.J., Greenfield, P.J., 1986. Origin of Humus Variations. *Org. Geochem.* 9, 225–231.
- Winkler, P., Kaiser, K., Kölbl, A., Kühn, T., Schad, P., Urbanski, L., Fiedler, S., Lehndorff, E., Kalbitz, K., Utami, S.R., Cao, Z., Zhang, G., Jahn, R., Kögel-Knabner, I., 2016. Response of Vertisols, Andosols, and Alisols to paddy management. *Geoderma* 261, 23–35.

doi:10.1016/j.geoderma.2015.06.017

- Wissing, L., Kölbl, A., Häusler, W., Schad, P., Cao, Z.H., Kögel-Knabner, I., 2013. Management-induced organic carbon accumulation in paddy soils: The role of organo-mineral associations. *Soil Tillage Res.* 126, 60–71. doi:10.1016/j.still.2012.08.004
- Wissing, L., Kölbl, A., Schad, P., Bräuer, T., Cao, Z.-H., Kögel-Knabner, I., 2014. Organic carbon accumulation on soil mineral surfaces in paddy soils derived from tidal wetlands. *Geoderma* 228–229, 90–103. doi:10.1016/j.geoderma.2013.12.012
- Wissing, L., Kölbl, A., Vogelsang, V., Fu, J.-R., Cao, Z.-H., Kögel-Knabner, I., 2011. Organic carbon accumulation in a 2000-year chronosequence of paddy soil evolution. *Catena* 87, 376–385. doi:10.1016/j.catena.2011.07.007
- Wood, C.W., Edwards, J.H., 1992. Agroecosystem management effects on soil carbon and nitrogen. *Agric. Ecosyst. Environ.* 39, 123–138. doi:10.1016/0167-8809(92)90048-G
- Zech, W., Senesi, N., Guggenberger, G., Kaiser, K., Lehmann, J., Miano, T.M., Miltner, A., Schroth, G., 1997. Factors controlling humification and mineralization of soil organic matter in the tropics. *Geoderma* 79, 117–161.
- Zhu, Z.L., Minasny, B.B., Field, D.J., 2009. Measurement of aggregate bond energy using ultrasonic dispersion. *Eur. J. Soil Sci.* 60, 695–705. doi:10.1111/j.1365-2389.2009.01146.x



Appendix 2.1. Farm questionnaires

Date: 20.07.2016

Locality: Randusongo village, Gerih sub-district

Farmer/Land owner: Djumadi

Crops: Rice (*Oryza sativa*)-Rice-Soybean (*Glycine max*)

1. *How long have you been farming here?*

Since 1958.

2. *What is the area of the farm?*

3000 m<sup>2</sup>.

3. *What do you know happened before you were on the farm?*

The farm had already been there.

4. *How is land use and rotation history of your farming system? How many times do you plant rice?*

Since 1965 crop rotations were rice-soybean-bare before converted into rice-rice-soybean in 1970 up to now.

5. *How do you maintain the fertility of soil? Fertilizer history, green manure?*

Mineral fertilizers are applied twice during rice seasons, of which 2 bags of @50 kg Phonska, 1 bag of 50 kg Urea and extra 4 bags of @40 kg Petroganik (organic fertilizer) at 15 days post-planting, and 1 bag @50 kg Phonska and ½ bag of 50 kg Urea at 25 days post-planting are applied. They are applied in the dry land after inundation. During soybean seasons, plants are fertilized with Gandasil (foliar fertilizer) during each vegetative (Gandasil D) and generative (Gandasil B) phase by diluting 1 small bag (100 g) into 15 liter water.

6. *How have you used herbicide?*

Herbicide is not applied, but pesticide during pest outbreak event by mixing 2 bottle cap of Matador or Sidor per 15 liter of water.

7. *How do you work the farm, by tillage type buffalo or hand tractor? When is it?*

During dry season after soybean, soil fork is applied to overturn top soils through the cracks. Hand tractor is applied in the rainy season.

8. *How did you build terraces (if applicable)?*

No terraces

9. *How do you irrigate farm? (How often, how much)*

Water is obtained from irrigation canal. Flooding for 2-3 cm depth is done pre- and post-planting.

10. *What rice variety do you grow or crops name? Does it have a name? Is it an old or modern variety?*

Modern: Ciherang, Pertiwi; local: Sri Kuning, Sri Putih.

11. *What are your yields?*

Depending on the variety, 18-20 quintal/season if Sri Putih and can up to 34 quintal/season for Sri Kuning.

12. *What are your soil types like and what are their limitations for you in your management of the land?*

There is nothing problem for tilling. Leaves turned into yellowish on soybean was visible in last cropping season.

Date: 21.07.2016

Locality: Randusongo village, Gerih sub-district

Farmer/Land owner: Djumadi

Crops: Teak (*Tectona grandis*)-existing; cassava (*Manihot utilissima*), groundnut (*Arachis hypogaea*)-past

1. *How long have you been farming here?*  
Since 1958
2. *What is the area of the farm?*  
2000 m<sup>2</sup>
3. *What do you know happened before you were on the farm?*  
The farm had already been there
4. *How is landuse and rotation history of your farming system?*  
Since 1960's land was planted with cassava and groundnut, since 4 years ago it was changed into teak. The land partially was subjected to fire at 2014.
5. *How do you maintain the fertility of soil? Fertilizer history, green manure?*  
During cassava and groundnut the management was poor, the fertilization schedules was not clear. In the beginning of teak trees, urea was applied once with particular doses (out of memory).
6. *How have you used herbicide?*  
No herbicide, no pesticide.
7. *How do you work the farm, by tillage type buffalo or hand tractor? When is it?*  
No tillage
8. *How did you build terraces (if applicable)?*  
No terraces
9. *How do you irrigate farm? (How often, how much)*  
Irrigation only from rainwater
10. *What rice variety do you grow or crops name? Does it have a name? Is it an old or modern variety?*  
The variety used is Jati plus
11. *What are your yields?*  
Existing plants are first growing season.
12. *What are your soil types like and what are their limitations for you in your management of the land?*  
Lots of stone and coarse materials in the soil. Tilling is no minor undertaking.

Date: 22.07.2016

Locality: Gerih village, Gerih sub-district

Farmer/Land owner: Tukiman

Crops: Rice monoculture

1. *How long have you been farming here?*  
Since 1990's
2. *What is the area of the farm?*  
2500 m<sup>2</sup>
3. *What do you know happened before you were on the farm?*  
They were there from a long history of farming
4. *How is landuse and rotation history of your farming system? How many times do you plant rice?*  
Rice-rice-rice
5. *How do you maintain the fertility of soil? Fertilizer history, green manure?*  
Any kind of green manure is not applied. Mineral fertilizers are 1.50 kg Urea, 150 kg Phonska, 150 kg TS, 300 kg ZA, 390 kg Petroganik (organic fertilizer).
6. *How have you used herbicide?*

Pesticide is applied by combining 250 cc PPC per 15 liter of water

7. *How do you work the farm, by tillage type buffalo or hand tractor? When is it?*  
Hand tractor.
8. *How did you build terraces (if applicable)?*  
No terraces.
9. *How do you irrigate farm? (How often, how much)*  
Irrigation using well pump water.
10. *What rice variety do you grow or crops name? Does it have a name? Is it an old or modern variety?*  
Varieties are Ciherang, IR 64, and Pertiwi.
11. *What are your yields?*  
15 quintal
12. *What are your soil types like and what are their limitations for you in your management of the land?*  
There is no problem

Date: 21.07.2016

Locality: Gerih village, Gerih sub-district

Farmer/Land owner: Tukiman

Crops: Teak-existing, Sunn hemp (*Crotalaria juncea*)-past

1. *How long have you been farming here?*  
Since 1960
2. *What is the area of the farm?*  
1500 m<sup>2</sup>
3. *What do you know happened before you were on the farm?*  
He took over land from someone else, so he did not know exactly what the land was.
4. *How is land use and rotation history of your farming system?*  
8 years teak trees
5. *How do you maintain the fertility of soil? Fertilizer history, green manure?*  
Manure (doses do not quantified) and 100 kg urea.
6. *How have you used herbicide?*  
No herbicide
7. *How do you work the farm, by tillage type buffalo or hand tractor? When is it?*  
Manual tilling with hoe, soil fork whenever necessary.
8. *How did you build terraces (if applicable)?*  
No terraces
9. *How do you irrigate farm? (How often, how much)*  
Irrigation water coming from the rain
10. *What rice variety do you grow or crops name? Does it have a name? Is it an old or modern variety?*  
Local teak.
11. *What are your yields?*  
Have not been harvested yet.
12. *What are your soil types like and what are their limitations for you in your management of the land?*  
There is no problem

Date: 23.07.2016

Locality: Pojok village, Kwadungan sub-district

Farmer/Land owner: Darminto

Crops: Rice-existing since 2 years ago, Sugarcane-in the past 2009-2014

1. *How long have you been farming here?*

Since 1960's

2. *What is the area of the farm?*

2500 m<sup>2</sup>

3. *What do you know happened before you were on the farm?*

Farms were there since he was child so he did not understand about it

4. *How is landuse and rotation history of your farming system? How many times do you plant rice?*

Rice-rice-rice. Rice was interrupted by sugarcane for 5 years (2009-2014).

5. *How do you maintain the fertility of soil? Fertilizer history, green manure?*

Green manure is not applied. Mineral fertilizers are 50 kg Urea, 50 kg Phonska, 25 kg TS, 40 kg Petroganik.

6. *How have you used herbicide?*

PPC

7. *How do you work the farm, by tillage type buffalo or hand tractor? When is it?*

Hand tractor

8. *How did you build terraces (if applicable)?*

Terraces were built manually by hoe

9. *How do you irrigate farm? (How often, how much)*

Irrigation water is from well pump.

10. *What rice variety do you grow or crops name? Does it have a name? Is it an old or modern variety?*

Ciherang, IR-64

11. *What are your yields?*

15 quintal.

12. *What are your soil types like and what are their limitations for you in your management of the land?*

There is no problem.

Date: 23.07.2016

Locality: Pojok village, Kwadungan sub-district

Farmer/Land owner: Darminto

Crops: Bamboo (*Bambusoideae*)

1. *How long have you been farming here?*

Since 1957

2. *What is the area of the farm?*

3000 m<sup>2</sup>

3. *What do you know happened before you were on the farm?*

Land was there since he was child

4. *How is landuse and rotation history of your farming system? How many times do you plant rice?*

Bamboo and some Teak trees as border of area.

5. *How do you maintain the fertility of soil? Fertilizer history, green manure?*

Mineral fertilizer "mutiara hijau" is applied 500 kg.

6. *How have you used herbicide?*  
No herbicide
7. *How do you work the farm, by tillage type buffalo or hand tractor? When is it?*  
No tillage
8. *How did you build terraces (if applicable)?*  
No terraces
9. *How do you irrigate farm? (How often, how much)*  
Irrigation from rain
10. *What rice variety do you grow or crops name? Does it have a name? Is it an old or modern variety?*
11. *What are your yields?*
12. *What are your soil types like and what are their limitations for you in your management of the land?*

Date: 24.07.2016

Locality: Danguk village, Karangjati sub-district

Farmer/Land owner: Hadi Sudarno

Crops: Rice-rice-rice

1. *How long have you been farming here?*  
More than 100 years
2. *What is the area of the farm?*  
1400 m<sup>2</sup>
3. *What do you know happened before you were on the farm?*  
He did not know because the farm was there before he was born.
4. *How is land use and rotation history of your farming system? How many times do you plant rice?*  
Rice-rice-rice
5. *How do you maintain the fertility of soil? Fertilizer history, green manure?*  
Mineral fertilizers are 25 kg Urea, 50 kg Phonska, 25 kg ZA, 25 kg TSP. Green manure is not applied.
6. *How have you used herbicide?*  
Herbicide is not applied
7. *How do you work the farm, by tillage type buffalo or hand tractor? When is it?*  
Hand tractor.
8. *How did you build terraces (if applicable)?*  
No terraces
9. *How do you irrigate farm? (How often, how much)*  
Water comes through irrigation canal from Sangiran dam. Land is watered thrice per season of rice. Water level is kept 2 cm during flooding.
10. *What rice variety do you grow or crops name? Does it have a name? Is it an old or modern variety?*  
Rice Ciherang
11. *What are your yields?*  
1200 kg
12. *What are your soil types like and what are their limitations for you in your management of the land?*  
Fertilizer dosis is increasing from time to time.

Date: 24.07.2016

Locality: Danguk village, Karangjati sub-district

Farmer/Land owner: Hadi Sudarno  
Crops: Banana (*Musaceae*)

1. *How long have you been farming here?*  
63 years
2. *What is the area of the farm?*  
400 m<sup>2</sup>
3. *What do you know happened before you were on the farm?*  
He did not know because the farm was there before he was born.
4. *How is landuse and rotation history of your farming system? How many times do you plant rice?*  
Banana garden
5. *How do you maintain the fertility of soil? Fertilizer history, green manure?*  
Manure
6. *How have you used herbicide?*  
No herbicide
7. *How do you work the farm, by tillage type buffalo or hand tractor? When is it?*  
Soil tilling is manually by hoe
8. *How did you build terraces (if applicable)?*  
No terraces
9. *How do you irrigate farm? (How often, how much)*  
Water irrigation is coming from rain
10. *What rice variety do you grow or crops name? Does it have a name? Is it an old or modern variety?*  
The name of variety is "Raja".
11. *What are your yields?*
12. *What are your soil types like and what are their limitations for you in your management of the land?*

Date: 22.07.2016  
Locality: Ploso lor village, Karangjati sub-district  
Farmer/Land owner: Gugup  
Crops: Mixed garden with grass, banana etc  
Note: Non-agriculture area, interview was not conducted.

Date: 23.07.2016  
Locality: Bobol village, Sekar sub-district  
Farmer/Land owner: Suroso  
Crops: Rice-rice-soybean

1. *How long have you been farming here?*  
Since 1980's
2. *What is the area of the farm?*  
5000 m<sup>2</sup>
3. *What do you know happened before you were on the farm?*  
Farm was there since he was child
4. *How is landuse and rotation history of your farming system? How many times do you plant rice?*  
Rice-rice-soybean

5. *How do you maintain the fertility of soil? Fertilizer history, green manure?*  
Fertilizers are 100 kg of Urea, 200 kg of Phonska, 100 kg of Petroganik (Organic fertilizer).
6. *How have you used herbicide?*  
Insecticide "Sankill" is applied 250 g per 15 liter water
7. *How do you work the farm, by tillage type buffalo or hand tractor? When is it?*  
Hand tractor is applied.
8. *How did you build terraces (if applicable)?*  
Terraces were built manually by hoe
9. *How do you irrigate farm? (How often, how much)*  
Irrigation uses rain water.
10. *What rice variety do you grow or crops name? Does it have a name? Is it an old or modern variety?*  
Varieties are Ciherang, IR-64, Cibogo, Situ Bagendit.
11. *What are your yields?*  
3000 kg
12. *What are your soil types like and what are their limitations for you in your management of the land?*  
Irrigation water is rain-dependent, so pump system that can take up groundwater is needed.

Date: 24.07.2016

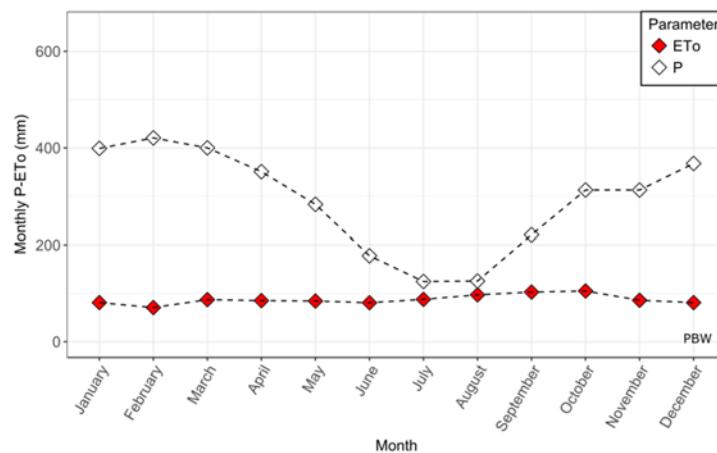
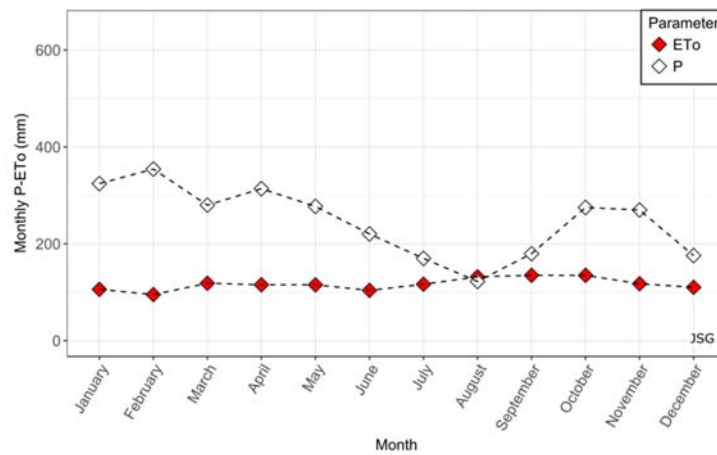
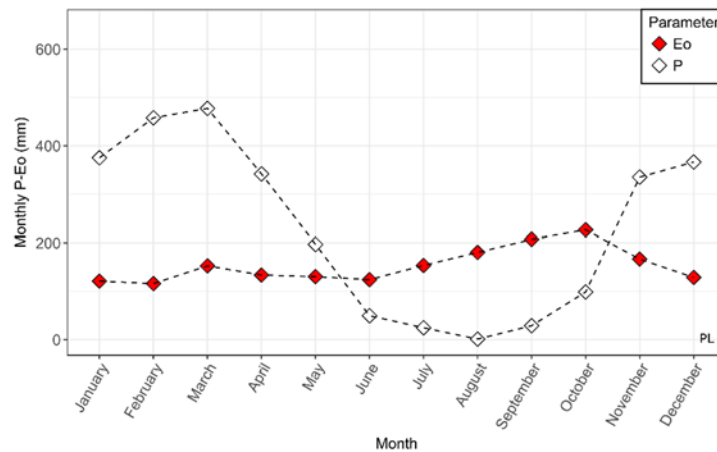
Locality: Bobol village, Sekar sub-district

Farmer/Land owner: Suroso

Crops: Mixed garden, bare land

Note: Non-agriculture area, interview was not conducted.

### Appendix 2.2. Distribution of P, Eo and ETo in some research areas



The monthly precipitations were obtained from the average data of 2006 – 2014 (PL), and 2001 – 2010 (JSG and PBW). The actual evaporation (Eo) was measured by open pan evaporation method using the average data of 2012 – 2014. The potential evapotranspiration (ETo) was estimated by Penman-Monteith method (CROPWAT 8.0) using the average data of 1975 – 2013 (Source of all primary data: Indonesian Agency for Meteorology, Climatology, and Geophysics). P = precipitation, Eo = actual evaporation, ETo = potential evaporation.

### Appendix 2.3. Soil profile descriptions of 2016 field campaign

#### **Randusongo village-Paddy (P)**



Date: 20.07.2016

Location: Randusongo village, Gerih sub-district.

Crops: Rice (*Oryza sativa*)-rice-soybean (*Glycine max*)

Map reference: WGS 1984 UTM Zone 49S, Lat -7.5705, Long 111.3454

Altitude: 197 m a.s.l

Physiography: Lower slope of Mt. Lawu. Parent material is lahar consisting of various size of andesite, basalt mixing with tuff volcanic.

Soil type (tentative): Endostagnic Regosol

Surface characteristics: Surface disturbed and puddled by hand-tractor prior to rice seasons. Soil moisture status: moist.

Soil description:

Ap1 0-24 cm

Dark brown (7.5 YR 3/2). Sandy loam. Strong pedality. Thin to thick platy (1-10 mm). Very few (0-2%) of sub-rounded fine to medium gravel (2-10 mm) tuff volcanic fragments. Very fine (<0.5 mm) to fine (0.5-2 mm) roots 15 per dm<sup>2</sup>. Wavy. Clear (2-5 cm) boundary to...

Ap2 24-42 cm

Brown (7.5 YR 5/3). Sandy loam. Strong pedality. Very thin to thick platy (1-10 mm). Very few (0-2%) of sub-rounded fine to medium gravel (2-10 mm) tuff volcanic fragments. Medium (2-5 mm) to coarse (> 5 mm) roots 1-2 per dm<sup>2</sup>. Wavy. Gradual (5-15 cm) boundary to...

ACI 42-55 cm

Light brown (7.5 YR 6/3). Loamy sand. Weak to moderate pedality. Very thin to thick platy (1-10 mm). Many (15-40%) reddish-brown mottles (2.5 YR 4/4). Many (15-40%) of sub-rounded fine to medium gravel (2-10 mm) tuff volcanic fragments. Wavy. Diffuse (> 15 cm) boundary to...

CI 55-108+ cm

Strong brown (7.5 YR 5/6). Loamy sand. Weak to moderate pedality. Very thin to thick platy (1-10 mm). Many (15-40%) reddish-brown mottles (2.5 YR 4/4). High (>10 cm) dendritic tubular grey-clay channel (7.5 YR 8/6). ). Many (15-40%) of sub-rounded fine to medium gravel (2-10 mm) tuff volcanic fragments.

**Randusongo village-Non Paddy (NP)**



Date: 21.07.2016

Location: Randusongo village, Gerih sub-district.

Crops: Teak (*Tectona grandis*)

Map reference: WGS 1984 UTM Zone 49S, Lat -7.5728, Long 111.3416

Altitude: 204 m a.s.l

Physiography: Lower slope of Mt. Lawu. Parent material is lahar consisting of various size of andesite, basalt mixing with tuff volcanic.

Soil type (tentative): Leptic Regosol

Soil surface: Surface disturbed and not frequently cultivated but once before planting by hand. Soil moisture status: wet. Many fine to coarse gravels, few stones to boulders.

Soil description:

Ah1 0-10 cm

Dark brown (7.5 YR 3/2). Loamy sand. Weak to moderate pedality. Fine to coarse granular (1-10 mm). Many (5-14%) of sub-rounded fine to coarse gravel (2-60 mm) tuff volcanic + andesite. Fine (0.5-2 mm) and coarse (>5 mm) roots 4 per dm<sup>2</sup>. Smooth. Gradual (5-15 cm) boundary to...

Ah2 10-25 cm

Dark brown (7.5 YR 3/3). Loamy sand. Weak to moderate pedality. Medium to very coarse granular (2->10 mm). Many (5-14%) of sub-rounded medium to coarse gravel (6-60 mm) tuff volcanic + andesite. Fine (0.5-2 mm) and coarse (>5 mm) roots 4 per dm<sup>2</sup>. Smooth. Diffuse (> 15cm) boundary to...

C > 25 cm

Yellow (10YR 7/8). No observed roots. Dominant (>80%) andesite stones and boulders.

**Gerih village – Paddy (P)**

Date: 22.07.2016

Location: Gerih village, Gerih sub-district.

Crops: Rice-rice-rice (*Oryza sativa*)

Map reference: WGS 1984 UTM Zone 49S, Lat -7.5295, Long 111.3999

Altitude: 81 m a.s.l

Physiography: Footslope of Mt. Lawu. Area is floodplain of Bemu River to the west. Parent material is alluvial deposits.

Soil type (tentative): Vertic Pantostagnic Cambisol (Protocalcic)

Soil surface: Surface disturbed and frequently cultivated by hand-tractor. Soil moisture status: very wet.

Soil description:

Apg 0-19 cm

Gray (7.5 YR 6/1). Clay loam. Moderate to strong pedality. Fine to

medium angular blocky (5-20 mm). Very few (0-2%) of sub-rounded fine gravel (2-6 mm) tuff volcanic fragments. Very fine (0.5-2 mm) to fine (< 0.5 mm) roots 20 per dm<sup>2</sup>. Smooth. Gradual (5-15 cm) boundary to...

Big 19-40 cm

Gray (7.5 YR 5/1). Clay. Strong pedality. Fine to medium angular blocky (5-20 mm). Very few (0-2%) of sub-rounded fine gravel (2-6 mm) tuff volcanic fragments. Faint to distinct slickensides abundant. Fine roots (<0.5 mm) 5 per dm<sup>2</sup>. Smooth. Gradual (5-15 cm) boundary to...

Bkg 40-60 cm

Gray (7.5 YR 5/1). Silty clay. Moderate to strong pedality. Fine to medium angular blocky (5-20 mm). Abundant (40-80%) of irregularly shaped fine to medium (2-20 mm) secondary hard carbonate nodules (7.5 YR 8/2), extremely strong reaction, hard. Smooth. Diffuse (> 15 cm) boundary to...

Bwkgc 60-83+ cm

Brown (7.5 YR 5/4). Silty clay. Moderate pedality. Fine to medium subangular blocky (5-20 mm). Very few (0-2%) of sub-rounded fine gravel (2-6 mm) tuff volcanic fragments. Few (2-5%) of rounded fine Fe-Mn concretions (2-6 mm). Abundant (40-80%) of irregularly shaped fine to medium (2-20 mm) secondary hard carbonate nodules (7.5 YR 8/2), extremely strong reaction, hard.

**Gerih village – Non Paddy (NP)**

Date: 21.07.2016

Location: Gerih village, Gerih sub-district.

Crops: Teak (*Tectona grandis*)

Map reference: WGS 1984 UTM Zone 49S, Lat -7.5297, Long 111.3997

Altitude: 81 m a.s.l

Physiography: Footslope of Mt. Lawu. Footslope of Mt. Lawu. Area is floodplain of Bemu River to the west. Parent material is alluvial deposits.

Soil type (tentative): Vertic Endostagnic Cambisol (Protocalcic)

Soil surface: surface disturbed and not frequently cultivated by hand. Soil moisture status: moist.

Soil description:

Ah 0-19 cm

Dark brown (7.5 YR 3/3). Clay loam. Moderate to strong pedality. Fine to

medium angular blocky (5-20 mm). Very few (0-2%) of sub-rounded fine gravel (2-6 mm) tuff volcanic fragments. Very fine (0.5-2 mm) to fine (<0.5 mm) roots 12 per dm<sup>2</sup>. Wavy. Gradual (5-15 cm) boundary to...

Bil 19-63 cm

Very dark gray (7.5 YR 3/1). Clay. Strong pedality. Medium to coarse wedge-shaped (20-100 mm). Very few (0-2%) of sub-rounded fine gravel (2-6 mm) tuff volcanic fragments. Prominent slickensides abundant. Very fine (0.5-2 mm) to fine (<0.5 mm) roots 7 per dm<sup>2</sup>. Smooth. Clear (2-5 cm) boundary to...

Bkl 63-84 cm

Gray (7.5 YR 5/1). Silty clay. Moderate to strong pedality. Fine to medium angular blocky (5-20 mm). Abundant (40-80%) of irregularly shaped fine to medium (2-20 mm) secondary hard carbonate nodules (7.5 YR 8/2), extremely strong reaction, hard. Very fine (0.5-2 mm) to fine (<0.5 mm) roots 13 per dm<sup>2</sup>. Wavy. Clear (2-5 cm) boundary to...

Bwk 84-110+ cm

Brown (7.5 YR 5/4). Silty clay. Moderate to strong pedality. Fine to medium angular blocky (5-20 mm). Many (15-40%) of irregularly shaped fine to medium (2-20 mm) secondary carbonate nodules (7.5 YR 8/2)-only on the top 10 cm, extremely strong reaction, hard. Very fine (0.5-2 mm) to fine (<0.5 mm) roots 3 per dm<sup>2</sup>.

**Pojok village - Paddy**

Date: 23.07.2016

Location: Pojok village, Kwadungan sub-district.

Crops: Rice-rice-rice (*Oryza sativa*)

Map reference: WGS 1984 UTM Zone 49S, Lat -7.4933, Long 111.4809

Altitude: 52 m a.s.l

Physiography: Toe slope of Mt. Lawu. Active alluvial plain which continuously receives deposits from Madiun River.

Soil type (tentative): Fluvisol (Protocalcic)

Soil surface: Surface disturbed and frequently puddled by hand-tractor. Soil moisture status: moist. Observed cracks width 1-2 cm, depth 2-10 cm.

Soil description:

Ap 0-45 cm

Gray (7.5 YR 5/1). Clay loam. Moderate to strong pedality. Fine to medium angular blocky (5-20 mm). Fine (0.5-2 mm) and medium (2-5 mm) roots > 50/dm<sup>2</sup>. Smooth. Diffuse (> 15 cm) boundary to...

Bk1 45-100 cm

Gray (7.5 YR 5/1). Silty clay loam. Moderate to strong pedality. Fine to medium angular blocky (5-20 mm). Few (2-5%) of irregularly shaped fine to medium (2-20 mm) secondary hard carbonate concretions (7.5 YR 8/2), extremely strong reaction, soft. Very fine roots 5-10/dm<sup>2</sup>. Smooth. Diffuse (> 15 cm) boundary to...

Bk2 >100 cm

Dark brown (7.5 YR 3/2). Sandy loam. Weak to moderate pedality. Fine to coarse granular (1-10 mm). Few (2-5%) of irregularly shaped fine to medium (2-20 mm) secondary hard carbonate concretions (7.5 YR 8/2), extremely strong reaction, soft.

**Pojok village – Non Paddy**

Date: 23.07.2016

Location: Pojok village, Kwadungan sub-district.

Crops: Bamboo (*Bambusoideae*)

Map reference: WGS 1984 UTM Zone 49S, Lat -7.4929,  
Long 111.4808

Altitude: 51 m a.s.l

Physiography: Active alluvial plain which continuously receives deposits from Madiun River.

Soil type (tentative): Katostagnic Fluvisol (Protocalcic, Protovertic)

Soil surface: Surface disturbed, not frequently cultivated. Soil moisture status: moist.

Soil description:

Ah 0-20 cm

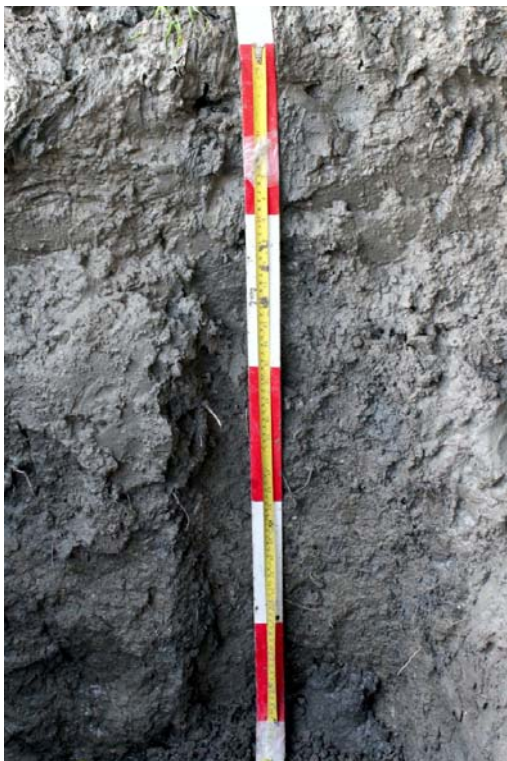
Brown (7.5 YR 4/2). Sandy clay loam. Weak to moderate pedality. Thin to very coarse granular (1 to >20 mm). Fine (0.5-2 mm) to medium (2-5 mm) roots 15-30 per dm<sup>2</sup>. Smooth. Diffuse (>15 cm) boundary to...

Bkl 20-56 cm

Gray (7.5 YR 5/1). Clay loam. Weak to moderate pedality. Fine to very coarse granular (1 to >20 mm). Few (2-5%) of irregularly shaped fine to medium (2-20 mm) carbonate concretions (7.5 YR 8/2), extremely strong reaction, soft. Many (15-40%) reddish-brown mottles (2.5 YR 4/4). Fine roots (0.5-2 mm) 5 per dm<sup>2</sup>. Smooth. Diffuse (>15 cm) boundary to...

Bil 56-120+ cm

Gray (7.5 YR 5/1). Sandy loam. Weak pedality. Fine to very coarse granular (1 to >20 mm). Distinct slickensides abundant.

**Danguk village - Paddy**

Date: 24.07.2016

Location: Danguk village, Karangjati sub-district.

Crops: Rice-rice-rice (*Oryza sativa*)

Map reference: WGS 1984 UTM Zone 49S, Lat -7.4847, Long 111.5637

Altitude: 63 m a.s.l

Physiography: Non active meander alluvial plain.

Soil type (tentative): Pantostagnic Fluvisol (Protocalcic)

Soil surface: Surface disturbed and frequently puddled by hand-tractor. Soil moisture status: very wet.

Soil description:

Apg 0-15 cm

Dark gray (Gley I 4/N). Silt loam. Weak to moderate pedality. Fine to very coarse granular (1 to >20 mm). Many (15-40%) reddish-brown mottles (2.5 YR 4/4). Smooth. Diffuse (>15 cm) boundary to...

ABkg 15-90+ cm

Dark gray (Gley I 4/N). Silty clay loam. Moderate to strong pedality. Fine to very coarse granular (1 to >20 mm). Many (15-40%) reddish-brown mottles (2.5 YR 4/4). Few (2-5%) of irregularly shaped fine to medium (2-6 mm) carbonate concretions (7.5 YR 8/2), extremely strong reaction, hard.

**Danguk village – Non Paddy**

Date: 24.07.2016

Location: Danguk village, Karangjati sub-district.

Crops: Banana (*Musaceae*)

Map reference: WGS 1984 UTM Zone 49S, Lat -7.4839, Long 111.5631

Altitude: 64 m a.s.l

Physiography: Non active meander alluvial plain.

Soil type (tentative): Endostagnic Fluvisol

Soil surface: Surface disturbed, not frequently cultivated. Soil moisture status: moist.

Soil description:

Ah 0-8 cm

Very dark gray (7.5 YR 3/1). Very fine (<0.5 mm) and fine roots (0.5-2 mm) 15-20 per dm<sup>2</sup>. Smooth. Gradual (5-15 cm) boundary to...

A1 8-17 cm

Dark gray (7.5 YR 4/1). Sandy loam. Weak pedality. Fine to very course granular (1 to >20 mm). Smooth. Very fine roots (<0.5 mm) 5 per dm<sup>2</sup>. Wavy. Clear (2-5 cm) boundary to...

A2 17-46 cm

Brown (7.5 YR 5/2). Sandy loam. Weak pedality. Fine to very course granular (1 to >20 mm). Smooth. Clear (2-5 cm) boundary to...

A'1 46-60 cm

Dark gray (7.5 YR 4/1). Sandy loam. Weak pedality. Fine to very course granular (1 to >20 mm). Smooth. Clear (2-5 cm) boundary to...

A'2 60-70 cm

Brown (7.5 YR 5/2). Sandy loam. Weak pedality. Fine to very course granular (1 to >20 mm). Smooth. Gradual (5-15 cm) boundary to...

A13 70-105 cm

Gray (7.5 YR 6/1). Sandy loam. Weak pedality. Fine to very course granular (1 to >20 mm). Many (15-40%) reddish-brown mottles (2.5 YR 4/4). Smooth. Gradual (5-15 cm) boundary to...

ABI >105 cm

Brown (7.5 YR 5/2). Silt loam. Weak to moderate pedality. Fine to very course granular (1 to >20 mm). Gray mottles (Gley I 4/N).

**Ploso Lor village– Non Paddy**

Date: 22.07.2016

Location: Ploso Lor village, Karangjati sub-district.

Crops: Non-agriculture area

Map reference: WGS 1984 UTM Zone 49S, Lat -7.4441,  
Long 111.6114

Altitude: 79 m a.s.l

Physiography: Non active meander alluvial plain.

Soil type (tentative): Protocalcic Pellic Vertisols (Endostagnic)

Soil surface: Surface disturbed, non-cultivated grounds. Soil moisture status: moist.

Soil description:

Ah 0-6 cm

Black (7.5 YR 2.5/1). Silty clay. Strong pedality. Fine to coarse angular blocky (5-50 mm). Medium roots (2-5 mm) >20 per dm<sup>2</sup>. Smooth. Diffuse (>15 cm) boundary to...

Bik 6-120 cm

Very dark gray (7.5 YR 3/1). Clay. Strong pedality. Fine to coarse angular blocky (5-50 mm). Prominent slickensides abundant. Abundant (40-80%) of irregularly shaped fine to medium (2-20 mm) secondary hard carbonate concretions (7.5 YR 8/2), extremely strong reaction, hard. Coarse (>5 mm) roots 1-2 per dm<sup>2</sup>. Irregular. Clear (2-5 cm) boundary to...

Bkl > 120 cm

Light brown (7.5 YR 6/3). Silty clay. Strong pedality. Few (2-5%) of irregularly shaped fine to medium (2-20 mm) secondary hard carbonate concretions (7.5 YR 8/2), extremely strong reaction, hard. Gray mottles (Gley I 4/N).

**Bobol village - Paddy**

Date: 23.07.2016

Location: Bobol village, Sekar sub-district.

Crops: Rice-rice-soybean

Map reference: WGS 1984 UTM Zone 49S, Lat -7.3842, Long 111.6694

Altitude: 151 m a.s.l

Physiography: Valley zone of Kendeng anticlinorium on the Kerek formation. The position is at lower slope of highest top at Mt. Pandan to the southeast. Soil is derived from colluvium materials containing sandstone, claystone, and tuff volcanic.

Soil type (tentative): Leptic Epistagnic Regosol

Soil surface: Surface disturbed, frequently puddle by hand. Soil moisture status: very wet.

Soil description:

Apl1 0-20 cm

Gray (7.5 YR 5/1). Silt loam. Moderate pedality. Fine to coarse granular (1-10 mm). Many (15-40%) red mottles (2.5 YR 3/4). Very few (0-2%) of sub-rounded fine to medium gravel (2-10 mm) sedimentary rock fragments (i.e. claystone). Very fine (<0.5 mm) and fine roots (0.5-2 mm) 20-50 per dm<sup>2</sup>. Smooth. Diffuse (> 15 cm) boundary to...

Apl2 20-27 cm

Very dark gray (7.5 YR 3/1). Sandy loam. Low to moderate pedality. Many (15-40%) red mottles (2.5 YR 3/4). Many (15-40%) of sub-rounded fine to medium gravel (2-10 mm) sedimentary rock fragments. Very fine (<0.5 mm) and fine roots (0.5-2 mm) 8-10 per dm<sup>2</sup>. Smooth. Abrupt (0.5-2 cm) boundary to...

R > 27 cm

Claystone

**Bobol village – Non Paddy**

Date: 24.07.2016

Location: Bobol village, Sekar sub-district.

Crops: Non-agriculture area.

Map reference: WGS 1984 UTM Zone 49S, Lat -7.3847, Long 111.6686

Altitude: 152 m a.s.l

Physiography: Valley zone of Kendeng anticlinorium on the Kerek formation. The position is at lower slope of highest top at Mt. Pandan to the southeast. Soil is derived from colluviums materials containing sandstone, claystone, and tuff volcanic.

Soil type (tentative): Endostagnic Regosols

Soil surface: Surface disturbed, non-cultivated grounds. Soil moisture status: moist.

Soil description:

A1 0-29 cm

Brown (7.5 YR 5/3). Sandy loam. Weak pedality. Fine to coarse granular (1-10 mm). Medium (0.5-2 mm) to coarse (2-5 mm) roots 6 per dm<sup>2</sup>. Wavy. Clear (2-5 cm) boundary to...

A2 29-40 cm

Brown (7.5 YR 5/2). Sandy clay loam. Weak to moderate pedality. Fine to coarse granular (1-10 mm). Fine

roots (0.5-2 mm) 3 per dm<sup>2</sup>. Smooth. Diffuse (>15 cm) boundary to...

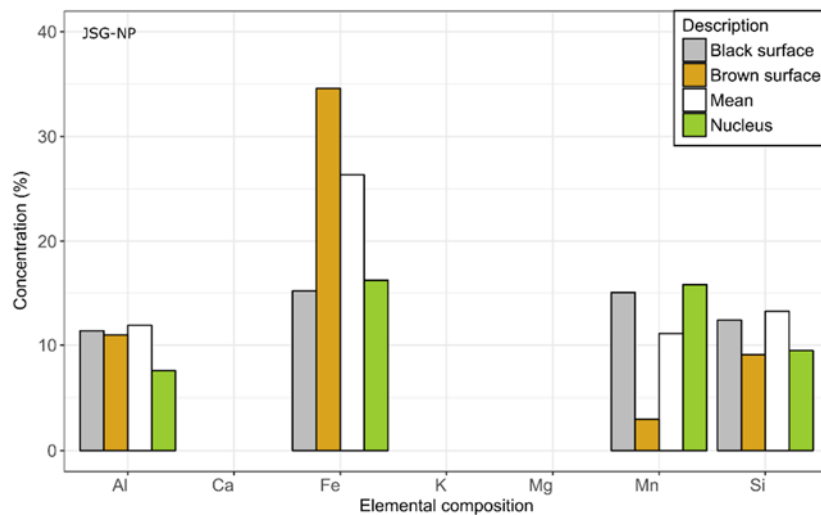
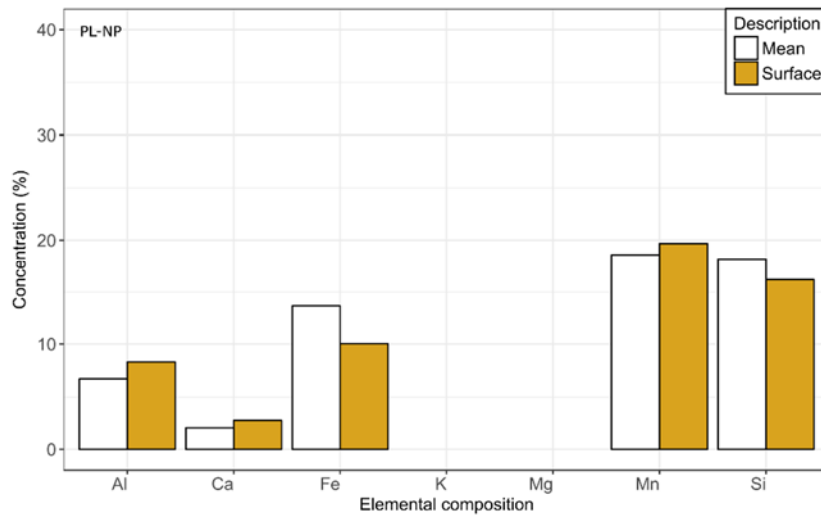
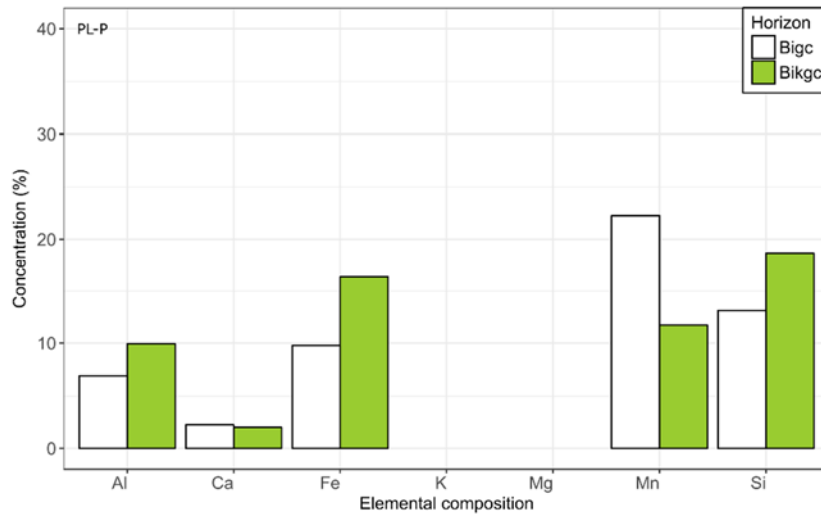
Al 40-80+ cm

Gray (7.5 YR 5/1). Clay loam. Weak to moderate pedality. Fine to coarse granular (1-10 mm). Many (15-40%) red mottles (2.5 YR 3/4). Very few (0-2%) of sub-rounded fine to medium gravel (2-10 mm) sedimentary rock fragments (i.e. claystone).

## Appendix 2.4. Weight proportion of concretions

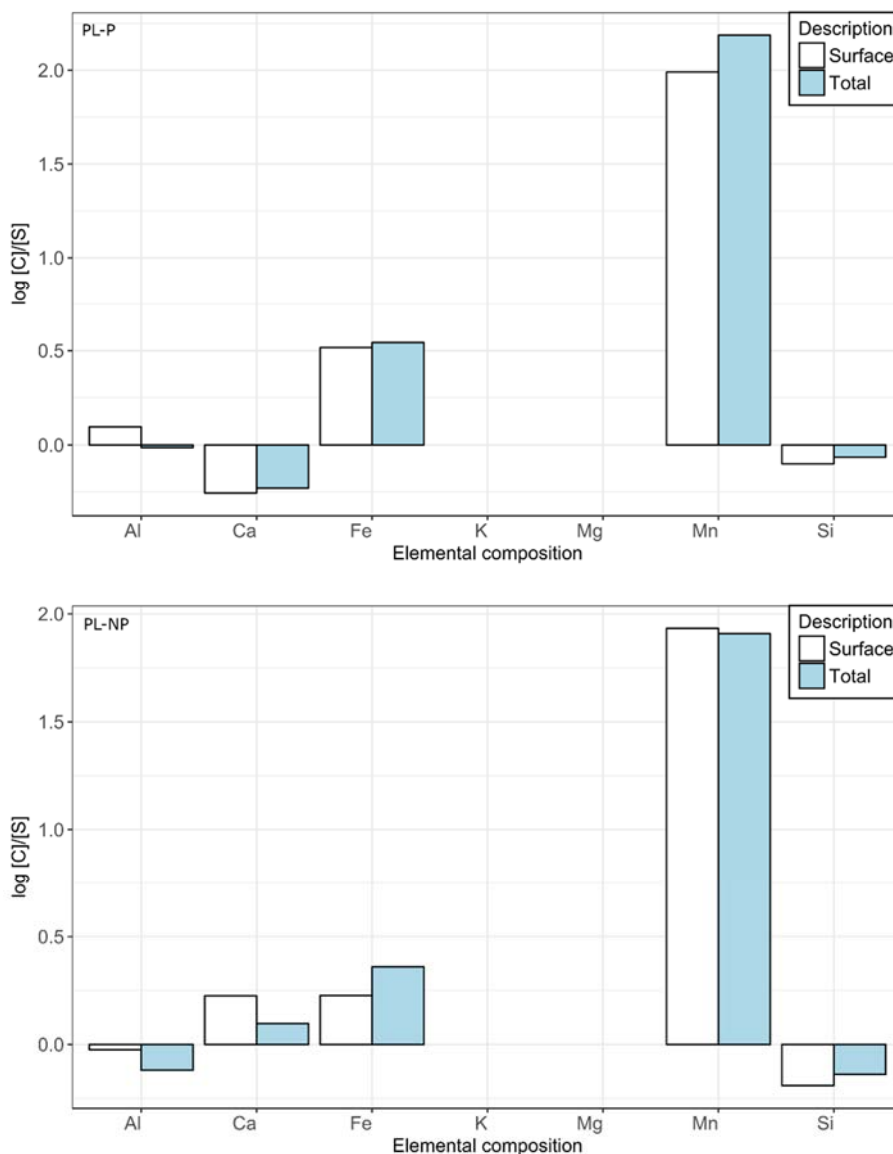
Code	Landuse	Horison	$\phi > 2 \text{ mm}$			$\phi 1 - 2 \text{ mm}$			$\phi 0,37 - 1 \text{ mm}$			Total weight (g)	Weight soil (g)		Relative proportion to soil (%)	
			w0 (g)	w1 (g)	w1-w0 (g)	w0 (g)	w1 (g)	w1-w0 (g)	w0 (g)	w1 (g)	w1-w0 (g)		> 2 mm	Total air-dried	By > 2 mm	By total air-dried
			$\Sigma =$			$\Sigma =$			$\Sigma =$							
<b>PL</b>																
119	P	Aidp	0.6	3	2.4	9.51	9.68	0.17	9.54	10.73	1.19	3.76	3.5	5788.8	68.57	0.065
120	P	Bwi	0.6	6.7	6.1	9.51	11.32	1.81	9.6	12.03	2.43	10.34	6.9	5110	88.41	0.202
121	P	Bigc	0.6	12.9	12.3	9.55	12.54	2.99	9.43	12.64	3.21	18.5	14.9	5207.1	82.55	0.355
122	P	Bigc	1.3	13.3	12	9.56	11.28	1.72	9.56	11.27	1.71	15.43	26.4	5718.9	45.45	0.270
123	P	Bikgc	0.6	34.2	33.6	9.47	12.78	3.31	9.59	11.52	1.93	38.84	140.2	5039.4	23.97	0.771
				$\Sigma =$	66.4		$\Sigma =$	10		$\Sigma =$	10.47	86.87	0.50602	26864.2		
124	NP	Ah2	0.6	0.9	0.3	9.55	10.54	0.99	9.6	9.66	0.06	1.35	2.2	4496.3	13.64	0.030
125	NP	Bwi1	0.6	0.8	0.2	9.48	9.73	0.25	9.6	10.07	0.47	0.92	3.7	6303.3	5.41	0.015
126	NP	Bwi2	0.5	0.7	0.2	9.68	9.97	0.29	9.46	9.79	0.33	0.82	0.8	4914.4	25.00	0.017
127	NP	Bwi2	0.6	1.1	0.5	9.59	10.34	0.75	9.45	11.29	1.84	3.09	0.9	5031.4	55.56	0.061
128	NP	Bwi2	0.6	2.2	1.6	9.37	13.33	3.96	9.56	14.5	4.94	10.5	2.2	5110.7	72.73	0.205
129	NP	Bwi3	0.6	2.7	2.1	9.62	11.74	2.12	9.57	13.93	4.36	8.58	2.2	5196	95.45	0.165
				$\Sigma =$	4.9		$\Sigma =$	7.37		$\Sigma =$	11.94	23.91	0.42857	31052.1		
<b>JSG</b>																
109	P	Alcdp	0.6	0.7	0.1							0.1	10.9	6013.3	0.92	0.002
110	P	B(t)gc1	0.5	0.6	0.1							0.1	0.7	6198.6	14.29	0.002
111	P	B(t)gc2	0.5	0.6	0.1							0.1	0.7	5257.5	14.29	0.002
112	P	B(t)gc3	0.6	0.7	0.1							0.1	1.4	4662	7.14	0.002
113	P	B(t)gc3	0.6	1.4	0.8							0.8	3.5	4587	22.86	0.017
				$\Sigma =$	1.2						$\Sigma =$	1.2				
114	NP	B(t)o1	0	0	0							0	21.7	4971.1	0.00	0.000
115	NP	B(t)o2	0.5	0.6	0.1							0.1	5.3	5625	1.89	0.002
116	NP	B(t)o3	0.5	0.6	0.1							0.1	0.7	5139.4	14.29	0.002
117	NP	B(t)o4	0.5	1	0.5							0.5	2.1	4597.7	23.81	0.011
118	NP	B(t)o5	0.5	1	0.5							0.5	2.6	4536.6	19.23	0.011
119	NP	B(t)o4-5	0.6	15.6	15							15	29.8	4134.9	50.34	0.363
				$\Sigma =$	16.2						$\Sigma =$	16.2				

### Appendix 2.5. Some important mineral content in concretions



Concretions were scanned by XRF right on the surface collected from Bigc and Bikgc horizons (PL-P, top); on the surface and ground samples (mean) collected from Bwi3 horizon (PL-NP, middle); and on the black/brown surface, nucleus and ground samples collected from B(t)o4-o5 horizon (JSG-NP, bottom).

### Appendix 2.6. Mineral enrichment in PL samples

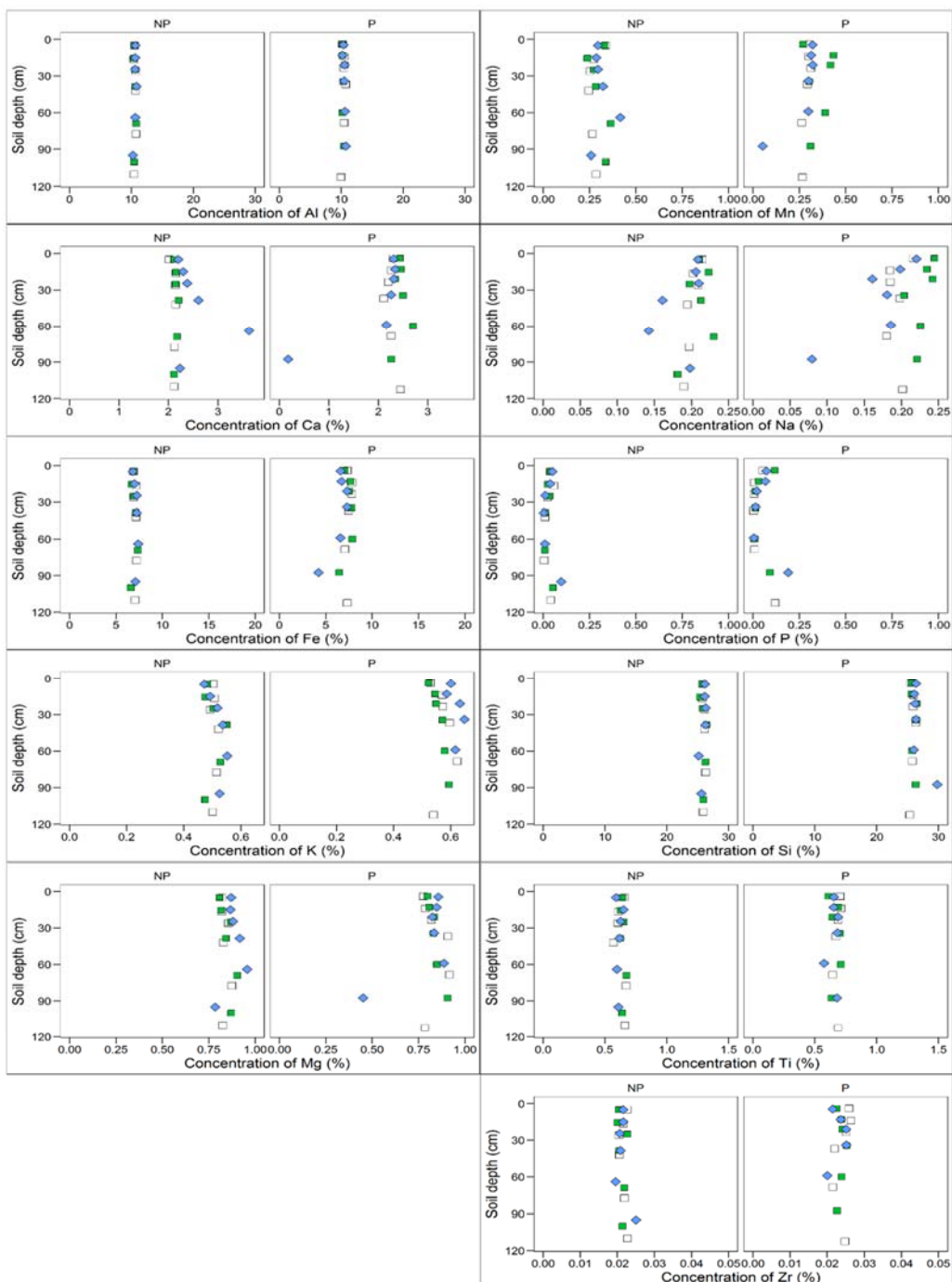


The enrichment factor (EF) was calculated according to Dawson et al., (1985):  $EF = \log \frac{[C]}{[S]}$  where [C] is concentration of elements in the either surface or grounded concretion samples, and [S] is concentration of elements in the surrounding soil matrix. The positive values point out the mineral enrichment, while the negative values mean depletion. The EF was not calculated for JSG samples (Appendix 2.5) because the data of elemental composition of surrounding soil matrix was not available.

Appendix 2.7. Elemental composition of some soil inorganic fractions<sup>19</sup> from point samples

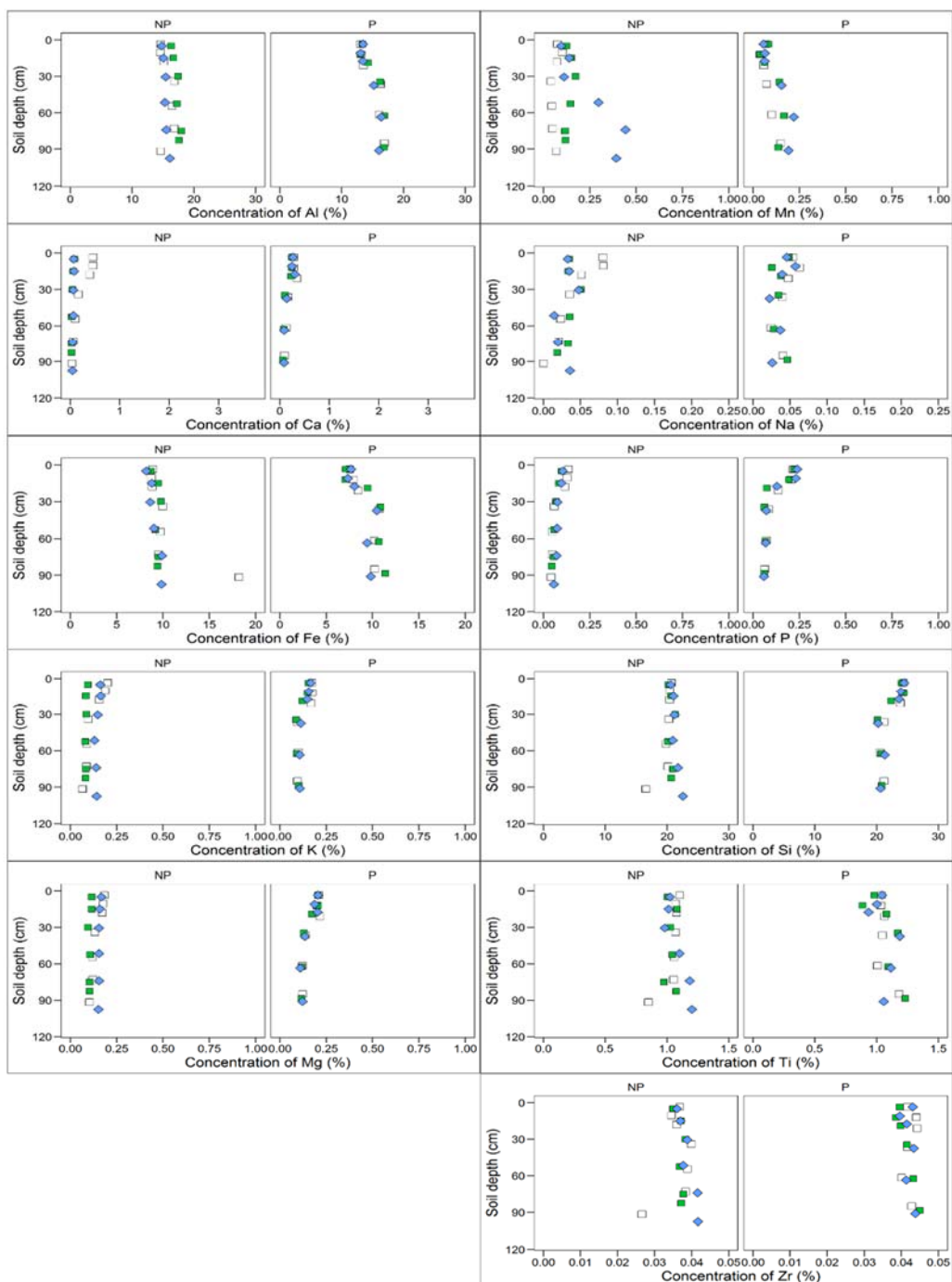
Sam- ple	φ	Depth (cm)	Zr	Zr (E)	Sr	Sr (E)	Rb	Rb (E)	Fe	Fe (E)	Mn	Mn (E)	Ti	Ti (E)	Ca	Ca (E)	K	K (E)	Al	Al (E)	Si	Si (E)	Mg	Mg (E)
PL-P	1	37-38	3.16 E+01	2.92 E+00	5.75 E+02	5.85 E+00	nd	4.14 E+00	5.61 E+04	3.48 E+02	1.80 E+04	1.84 E+02	6.09 E+03	1.05 E+03	5.92 E+04	6.57 E+02	5.43 E+03	2.84 E+02	7.09 E+04	7.43 E+02	2.92 E+05	1.25 E+03	5.07 E+03	1.08 E+03
PL-P	2	37-38	2.93 E+01	2.34 E+00	4.84 E+02	4.41 E+00	nd	3.83 E+00	2.64 E+04	1.85 E+02	1.39 E+04	1.45 E+02	1.24 E+03	6.57 E+02	5.16 E+04	4.96 E+02	3.58 E+03	1.84 E+02	5.80 E+04	5.14 E+02	2.14 E+05	8.95 E+02	2.88 E+03	6.75 E+02
PL-P	3	37-38	1.20 E+02	2.50 E+00	9.22 E+01	1.76 E+00	5.52 E+01	3.00 E+00	5.67 E+04	3.05 E+02	7.20 E+02	4.52 E+01	4.90 E+03	6.52 E+02	1.27 E+04	2.73 E+02	3.67 E+03	2.01 E+02	5.06 E+04	4.28 E+02	1.53 E+05	7.17 E+02	3.66 E+03	5.22 E+02
PL- NP	1	42-43	2.51 E+01	2.72 E+00	6.43 E+02	5.75 E+00	nd	3.61 E+00	3.10 E+04	2.20 E+02	6.43 E+02	4.71 E+01	2.86 E+03	5.66 E+02	7.33 E+04	6.11 E+02	3.05 E+03	1.66 E+02	8.47 E+04	7.78 E+02	2.77 E+05	1.10 E+03	7.26 E+03	9.81 E+02
PL- NP	2	42-43	6.52 E+01	2.55 E+00	4.17 E+02	4.10 E+00	7.62 E+00	2.55 E+00	2.87 E+04	1.99 E+02	1.42 E+03	5.66 E+01	2.88 E+03	4.67 E+02	4.69 E+04	4.42 E+02	3.93 E+03	1.50 E+02	4.93 E+04	4.56 E+02	2.24 E+05	8.90 E+02	4.51 E+03	6.63 E+02
PL- NP	3	42-43	1.32 E+02	2.60 E+00	8.80 E+01	1.72 E+00	6.24 E+01	3.06 E+00	5.54 E+04	3.00 E+02	1.74 E+03	5.78 E+01	6.77 E+03	7.37 E+02	1.25 E+04	2.77 E+02	4.01 E+03	2.21 E+02	5.11 E+04	4.34 E+02	1.61 E+05	7.87 E+02	3.39 E+03	5.39 E+02
JSG- P	1	18-20	1.93 E+02	2.99 E+00	2.41 E+01	1.00 E+00	5.71 E+00	2.61 E+00	6.50 E+04	3.35 E+02	5.43 E+01	3.44 E+01	5.42 E+03	5.96 E+02	2.30 E+03	1.19 E+02	4.79 E+02	1.68 E+02	4.71 E+04	4.12 E+02	1.90 E+05	8.65 E+02	nd	7.68 E+02
JSG- P	2	18-20	3.80 E+02	4.41 E+00	3.63 E+01	1.17 E+00	nd	5.63 E+00	5.95 E+04	3.22 E+02	5.05 E+02	4.28 E+01	9.48 E+03	7.45 E+02	5.47 E+03	1.83 E+02	1.70 E+03	2.15 E+02	3.85 E+04	4.15 E+02	2.95 E+05	1.20 E+03	1.37 E+03	7.13 E+02
JSG- P	3	18-20	2.24 E+02	3.30 E+00	1.23 E+01	1.00 E+00	1.04 E+01	2.66 E+00	7.49 E+04	3.76 E+02	nd	6.96 E+01	7.13 E+03	7.54 E+02	2.43 E+03	1.40 E+02	4.53 E+02	2.09 E+02	7.42 E+04	5.66 E+02	1.45 E+05	7.08 E+02	1.35 E+03	5.06 E+02
JSG- NP	1	19-20	2.25 E+02	3.49 E+00	1.52 E+01	1.00 E+00	1.26 E+01	2.85 E+00	8.40 E+04	4.31 E+02	1.09 E+03	5.13 E+01	6.92 E+03	7.09 E+02	1.11 E+03	9.78 E+01	1.16 E+03	2.02 E+02	6.69 E+04	5.43 E+02	1.34 E+05	6.93 E+02	nd	9.08 E+02
JSG- NP	2	19-20	2.99 E+02	4.21 E+00	2.51 E+01	1.11 E+00	nd	4.59 E+00	1.01 E+05	5.08 E+02	1.42 E+03	5.65 E+01	1.25 E+04	9.92 E+02	3.85 E+03	1.83 E+02	1.81 E+03	2.77 E+02	6.25 E+04	5.82 E+02	2.09 E+05	1.00 E+03	1.38 E+03	7.12 E+02
JSG- NP	3	19-20	2.32 E+02	3.38 E+00	4.90 E+00	1.00 E+00	7.98 E+00	2.76 E+00	7.63 E+04	3.85 E+02	4.88 E+02	4.20 E+01	8.44 E+03	8.05 E+02	6.69 E+02	8.58 E+01	4.03 E+02	2.22 E+02	8.02 E+04	6.08 E+02	1.31 E+05	6.75 E+02	1.07 E+03	5.04 E+02
PBW -P	1	39-40	1.12 E+02	2.67 E+00	8.34 E+01	1.85 E+00	2.40 E+01	3.02 E+00	8.80 E+04	4.54 E+02	7.55 E+02	4.76 E+01	5.05 E+03	7.22 E+02	8.84 E+03	2.54 E+02	3.72 E+03	2.23 E+02	6.89 E+04	5.82 E+02	1.37 E+05	7.13 E+02	8.00 E+03	6.61 E+02
PBW -P	2	39-40	8.52 E+01	2.46 E+00	9.14 E+01	1.96 E+00	1.43 E+01	2.98 E+00	9.00 E+04	4.70 E+02	1.11 E+03	5.30 E+01	4.93 E+03	7.40 E+02	1.94 E+04	3.72 E+02	3.80 E+03	2.25 E+02	7.92 E+04	6.73 E+02	1.66 E+05	8.30 E+02	1.01 E+04	7.69 E+02
PBW -P	3	39-40	1.57 E+02	2.77 E+00	1.06 E+02	1.86 E+00	1.07 E+01	2.57 E+00	6.57 E+04	3.28 E+02	nd	4.68 E+01	6.23 E+03	7.42 E+02	3.26 E+03	1.53 E+02	1.52 E+03	2.13 E+02	8.35 E+04	6.13 E+02	1.15 E+05	5.90 E+02	nd	1.14 E+03
PBW -NP	1	36-38	1.58 E+02	2.87 E+00	5.03 E+01	1.38 E+00	3.28 E+01	2.99 E+00	7.30 E+04	3.75 E+02	2.12 E+03	6.22 E+01	5.51 E+03	6.89 E+02	1.06 E+04	2.54 E+02	1.94 E+03	1.98 E+02	7.46 E+04	5.92 E+02	9.87 E+04	5.38 E+02	5.39 E+03	5.74 E+02
PBW -NP	2	36-38	1.13 E+02	2.53 E+00	3.50 E+01	1.21 E+00	8.94 E+00	2.83 E+00	8.58 E+04	4.31 E+02	3.06 E+03	7.19 E+01	5.18 E+03	7.75 E+02	9.14 E+03	2.58 E+02	1.26 E+03	2.18 E+02	9.94 E+04	7.50 E+02	1.03 E+05	5.61 E+02	7.61 E+03	6.31 E+02
PBW -NP	3	36-38	1.87 E+02	2.84 E+00	1.96 E+01	1.00 E+00	4.65 E+00	2.52 E+00	6.41 E+04	3.19 E+02	1.57 E+03	5.31 E+01	5.49 E+03	7.04 E+02	6.54 E+02	8.05 E+01	nd	4.32 E+02	9.95 E+04	6.81 E+02	8.33 E+04	4.65 E+02	nd	8.81 E+02

<sup>19</sup> Unit in ppm, (1) 250 – 2000 μm, (2) 63 – 250 μm, (3) <2 μm (Nd = undetected during XRF scanning).

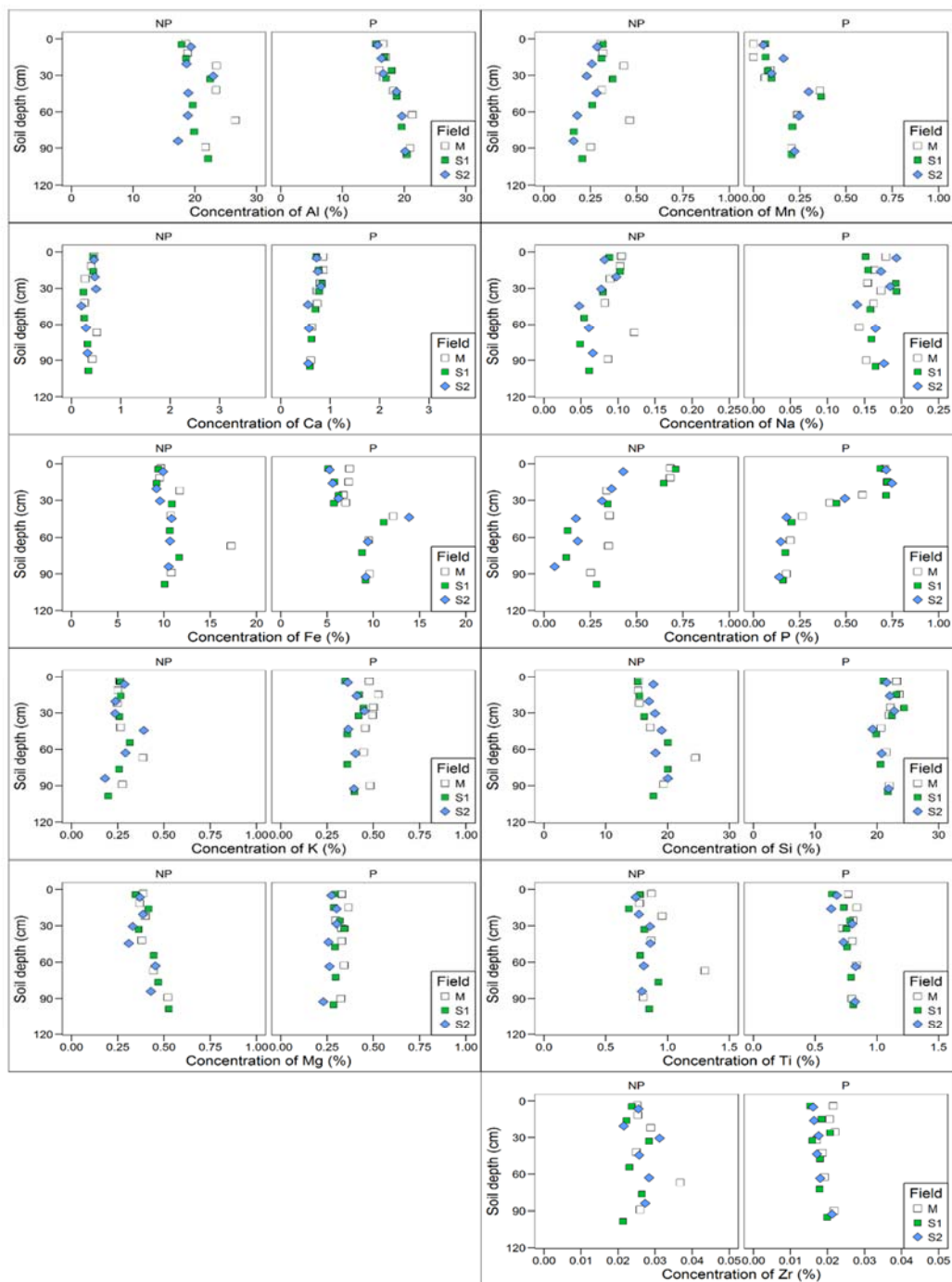
Appendix 2.8. Elemental composition of 2012 bulk soil samples<sup>20</sup>

(Mineral distributions from 3 soil profiles of PL-Vertisol under P and NP)

<sup>20</sup> Source of primary data: Pauline Winkler, Pers. Comm (Group P1)



(Mineral distributions from 3 soil profiles of JSG-Alisol under P and NP)



(Mineral distributions from 3 soil profiles of PBW-Andosol under P and NP)

Appendix 3.1. Grain size composition, TOC (%), pH (H<sub>2</sub>O) and EC of point samples<sup>21</sup>

Site	Depth (cm)	LU	Soil fractions (%)						TOC (%)	pH (H <sub>2</sub> O) (1:2.5)	EC (μS cm <sup>-1</sup> )	Fractions (% soil weight)		Proportion to TOC (%)	
			C	FSi	MSi	CSi	FS	MCS				C-humic	C-humin	C-humic	C-humin
PL	19-20	P	39.7	25.0	17.9	11.8	3.2	2.3	0.55	nd	nd	nd	nd	nd	nd
PL	20-21	P	19.9	25.1	30.3	20.7	3.9	0.0	0.51	nd	nd	nd	nd	nd	nd
PL	26-27	P	43.3	28.9	15.0	8.9	1.8	2.2	0.47	nd	nd	nd	0.18	nd	39
PL	27-28	P	32.5	24.2	19.4	12.3	4.6	7.0	0.41	nd	nd	nd	nd	nd	nd
PL	37-38	P	41.3	30.5	15.3	8.3	1.8	2.8	0.42	nd	nd	nd	nd	nd	nd
PL	46-47	P	28.9	25.3	24.2	16.4	3.8	1.3	0.38	nd	nd	nd	nd	nd	nd
PL	68-69	P	36.8	32.0	16.7	9.7	1.9	2.9	0.35	nd	nd	nd	nd	nd	nd
PL	89-90	P	23.4	25.1	27.2	19.3	4.5	0.6	0.30	nd	nd	0.23	nd	77	nd
PL	100-101	P	26.5	25.8	26.1	17.1	3.3	1.2	0.25	nd	nd	nd	nd	nd	nd
PL	22-23	NP	22.3	24.3	26.2	16.9	6.3	3.9	0.95	nd	nd	nd	nd	nd	nd
PL	23-24	NP	24.6	24.8	25.5	15.4	6.3	3.4	0.76	nd	nd	nd	nd	nd	nd
PL	28-29	NP	22.1	24.2	26.3	19.1	7.1	1.3	0.89	nd	nd	nd	nd	nd	nd
PL	42-43	NP	42.7	26.9	15.4	9.1	3.1	2.9	0.46	nd	nd	nd	nd	nd	nd
PL	54-55	NP	25.9	24.3	23.9	15.3	6.2	4.4	0.46	nd	nd	nd	0.17	nd	36
PL	99-100	NP	23.8	27.3	28.9	16.8	3.1	0.1	0.41	nd	nd	nd	nd	nd	nd
PL	110-111	NP	23.9	22.9	27.7	18.7	5.4	1.5	0.36	nd	nd	0.01	nd	1	nd
PBW	9-10	NP	22.3	21.7	20.8	14.7	8.2	12.3	3.12	nd	nd	0.26	0.79	8	25
PBW	20-23	NP	21.9	20.9	20.9	14.3	7.4	14.6	3.01	nd	nd	nd	nd	nd	nd
PBW	23-24	NP	22.2	24.3	20.1	12.5	6.9	13.9	0.69	nd	nd	nd	nd	nd	nd
PBW	36-38	NP	18.9	17.6	20.2	15.3	9.1	18.9	1.08	nd	nd	nd	nd	nd	nd
PBW	49-50	NP	22.2	23.5	22.2	12.9	6.8	12.5	0.79	nd	nd	nd	nd	nd	nd
PBW	50-52	NP	17.4	17.7	19.9	15.1	9.2	20.7	0.99	nd	nd	0.04	0.18	4	18

<sup>21</sup> LU = landuse; (b) = sample collected from brown layer, (g) = sample collected from grey layer; C= clay; FSi = fine silt; MSi = medium silt; CSi = coarse silt; FS = fine sand; MC = total medium and coarse sized particles; PL = Ploso lor, Vertisol; PBW = Perbawati, Andosol; JSG = Jasinga, Alisol; Cixi = Cixi, Cambisol; Rds = Randusongo, Regosol; Grh = Gerih, Cambisol; Pjk = Pojok, Fluvisol; Dgk = Danguk, Fluvisol; PL.G = Ploso lor garden plot, Vertisol; Bbl = Bobol, Regosol

Site	Depth (cm)	LU	Soil fractions (%)						TOC (%)	pH (H <sub>2</sub> O) (1:2.5)	EC ( $\mu\text{S cm}^{-1}$ )	Fractions (% soil weight)		Proportion to TOC (%)	
			C	FSi	MSi	CSi	FS	MCS				C-humic	C-humin	C-humic	C-humin
PBW	65-66	NP	20.0	18.5	19.4	14.0	9.2	18.9	0.93	nd	nd	0.08	0.17	9	18
PBW	78-79	NP	18.4	18.9	20.4	14.7	9.2	18.4	0.81	nd	nd	nd	nd	nd	nd
PBW	79-80	NP	18.9	18.8	20.8	15.5	9.2	16.8	0.75	nd	nd	nd	nd	nd	nd
PBW	85-87	NP	18.9	18.9	20.5	14.7	9.0	17.9	0.59	nd	nd	nd	nd	nd	nd
PBW	93-94	NP	11.7	11.9	13.6	14.7	16.1	31.9	0.52	nd	nd	nd	nd	nd	nd
PBW	94-95	NP	10.3	12.5	14.7	16.5	16.9	29.0	0.58	nd	nd	nd	nd	nd	nd
PBW	102-103	NP	7.9	14.7	22.9	22.5	16.4	15.6	0.41	nd	nd	nd	nd	nd	nd
PBW	19-20	P	5.4	13.7	24.3	21.2	17.7	17.9	3.69	nd	nd	nd	nd	nd	nd
PBW	23-24	P	6.7	16.1	22.5	16.7	15.5	22.6	3.08	nd	nd	nd	nd	nd	nd
PBW	30-31	P	10.8	15.4	23.5	24.6	12.8	12.9	2.27	nd	nd	nd	nd	nd	nd
PBW	31-32	P	15.1	15.8	18.2	22.6	16.1	12.2	2.20	nd	nd	nd	nd	nd	nd
PBW	39-40	P	12.2	17.1	22.8	24.5	14.4	9.0	1.64	nd	nd	nd	nd	nd	nd
PBW	42-45	P	9.5	15.2	21.8	22.8	15.9	14.8	0.54	nd	nd	nd	nd	nd	nd
PBW	49-51	P	10.4	14.8	20.6	21.2	16.4	16.4	0.53	nd	nd	nd	nd	nd	nd
PBW	60-62	P	22.9	19.2	20.9	17.5	10.3	9.2	0.42	nd	nd	nd	nd	nd	nd
PBW	80-81	P	28.9	20.0	18.6	13.8	7.9	10.8	0.38	nd	nd	nd	nd	nd	nd
PBW	99-101	P	36.9	24.5	19.0	10.9	4.7	3.9	0.33	nd	nd	nd	nd	nd	nd
JSG	18-20	P	32.3	24.3	22.1	14.8	4.5	2.0	1.57	nd	nd	0.18	1.16	12	73
JSG	20-21	P	32.5	23.4	20.9	13.7	4.9	4.6	1.44	nd	nd	nd	nd	nd	nd
JSG	26-27	P	47.6	18.2	16.9	12.2	4.4	0.8	1.15	nd	nd	nd	nd	nd	nd
JSG	28-29	P	37.5	21.9	19.2	13.3	4.9	3.1	1.17	nd	nd	0.03	0.53	2	45
JSG	37-38	P	50.0	18.7	16.7	10.6	3.8	0.2	0.98	nd	nd	nd	nd	nd	nd
JSG	47-48	P	50.7	18.5	16.6	10.3	3.7	0.3	0.89	nd	nd	nd	nd	nd	nd
JSG	48-49	P	46.2	18.7	17.9	11.5	4.6	1.1	0.90	nd	nd	nd	nd	nd	nd
JSG	65-66	P	49.5	19.1	17.4	10.4	3.5	0.2	0.70	nd	nd	nd	nd	nd	nd
JSG	81-82	P	48.2	22.9	17.9	8.8	2.2	0.1	0.61	nd	nd	nd	nd	nd	nd

Site	Depth (cm)	LU	Soil fractions (%)						TOC (%)	pH (H <sub>2</sub> O) (1:2.5)	EC (μS cm <sup>-1</sup> )	Fractions (% soil weight)		Proportion to TOC (%)	
			C	FSi	MSi	CSi	FS	MCS				C-humic	C-humin	C-humic	C-humin
JSG	82-83	P	46.5	19.1	17.9	11.1	4.4	1.0	0.60	nd	nd	nd	nd	nd	nd
JSG	100	P	46.7	19.5	17.8	10.8	4.2	0.9	0.55	nd	nd	nd	nd	nd	nd
JSG	19-20	NP	38.2	22.9	19.9	12.4	4.0	2.6	2.24	nd	nd	nd	nd	nd	nd
JSG	30-31	NP	38.8	22.3	19.3	12.3	4.6	2.8	1.74	nd	nd	0.06	0.63	4	36
JSG	40-41	NP	48.3	18.6	16.9	10.9	4.9	0.4	1.67	nd	nd	nd	nd	nd	nd
JSG	51-52	NP	42.6	22.1	17.6	11.6	4.6	1.5	1.25	nd	nd	nd	nd	nd	nd
JSG	61-62	NP	42.1	22.4	18.3	11.8	4.6	0.9	1.11	nd	nd	0.03	0.4	3	36
JSG	77-78	NP	41.8	22.3	17.6	11.8	4.7	1.8	0.89	nd	nd	nd	nd	nd	nd
JSG	91-92	NP	41.9	22.1	17.5	11.7	4.6	2.1	0.80	nd	nd	0.02	0.41	2	45
JSG	100-101	NP	39.6	22.5	18.4	12.4	4.5	2.6	0.78	nd	nd	nd	nd	nd	nd
Cixi	0-7	P	29.0	13.7	38.4	15.1	1.0	2.8	1.20	nd	nd	nd	nd	nd	nd
Cixi	7-14	P	29.7	13.7	37.1	14.5	1.0	4.0	1.13	nd	nd	nd	nd	nd	nd
Cixi	14-23	P	32.1	18.9	36.5	8.7	1.0	2.8	0.49	nd	nd	nd	nd	nd	nd
Cixi	23-38	P	28.3	13.5	39.9	16.0	0.8	1.5	0.17	nd	nd	nd	nd	nd	nd
Cixi	38-50	P	22.0	12.9	44.7	17.4	0.8	2.2	0.19	nd	nd	nd	nd	nd	nd
Cixi	50-70	P	29.8	15.5	40.3	11.0	0.8	2.6	0.15	nd	nd	nd	nd	nd	nd
Cixi	70-100	P	31.4	16.4	38.2	10.9	0.8	2.3	0.13	nd	nd	nd	nd	nd	nd
Cixi	0-9	NP	20.8	10.8	46.4	18.5	2.4	1.1	0.67	nd	nd	nd	nd	nd	nd
Cixi	9-17	NP	23.2	11.7	45.0	17.1	1.4	1.6	0.54	nd	nd	nd	nd	nd	nd
Cixi	17-24	NP	24.1	11.0	45.2	17.2	1.0	1.5	0.27	nd	nd	nd	nd	nd	nd
Cixi	24-45	NP	22.6	10.3	43.4	15.7	3.8	4.2	0.18	nd	nd	nd	nd	nd	nd
Cixi	45-70	NP	26.8	12.1	42.3	15.5	1.8	1.5	0.15	nd	nd	nd	nd	nd	nd
Cixi	70-100	NP	22.3	10.1	46.3	19.0	0.6	1.7	0.15	nd	nd	nd	nd	nd	nd
Rds	10-12	P	24.6	26.2	23.2	14.7	6.5	4.8	nd	6.76	32	0.13	0.24	nd	nd
Rds	26-28	P	22.7	26.1	22.8	12.8	8.6	7.0	nd	6.64	29	nd	nd	nd	nd
Rds	55-57	P	11.2	18.4	18.3	12.4	16.5	23.2	nd	7.01	40	nd	0.15	nd	nd

Site	Depth (cm)	LU	Soil fractions (%)						TOC (%)	pH (H <sub>2</sub> O) (1:2.5)	EC (μS cm <sup>-1</sup> )	Fractions (% soil weight)		Proportion to TOC (%)	
			C	FSi	MSi	CSi	FS	MCS				C-humic	C-humin	C-humic	C-humin
Rds	57-60 (b)	P	8.2	16.5	18.2	11.8	15.5	29.7	nd	7.11	33	nd	nd	nd	nd
Rds	80-82	P	8.4	15.3	17.4	10.9	16.1	31.8	nd	7.27	28	0.01	0.05	nd	nd
Rds	82-100	P	8.2	19.1	23.3	11.4	12.9	25.2	nd	7.15	25	nd	nd	nd	nd
Rds	84-86	P	9.3	22.1	19.5	10.0	12.2	27.0	nd	7.54	39	0.03	0.06	nd	nd
Rds	98-100 (g)	P	10.6	26.8	31.6	17.5	7.2	6.3	nd	7.01	34	nd	nd	nd	nd
Rds	100-102	P	7.4	18.6	27.7	13.1	13.6	19.8	nd	7.15	27	nd	nd	nd	nd
Rds	0-2	NP	10.3	13.6	16.1	15.5	22.7	21.8	nd	7.29	136	nd	nd	nd	nd
Rds	10-12	NP	18.7	18.6	18.5	14.1	14.1	16.1	nd	6.29	71	nd	nd	nd	nd
Rds	23-25	NP	16.8	18.9	16.8	11.0	13.6	22.9	nd	6.38	46	0.11	0.17	nd	nd
Rds	40-42	NP	6.6	16.8	22.3	13.3	9.4	31.7	nd	6.82	29	nd	nd	nd	nd
Rds	60-62	NP	5.9	12.2	17.2	12.9	12.3	39.5	nd	6.66	29	0.01	0.01	nd	nd
Rds	80-82	NP	4.1	8.8	11.8	9.6	14.5	51.2	nd	6.72	39	nd	nd	nd	nd
Rds	100-102	NP	4.9	9.5	12.3	10.4	16.3	46.5	nd	6.73	28	0.01	0.05	nd	nd
Grh	17-19	P	18.5	27.9	21.1	14.1	11.1	7.4	nd	7.37	113	0.08	0.13	nd	nd
Grh	19-21	P	20.5	33.8	21.4	12.2	7.9	4.2	nd	7.34	111	nd	0.09	nd	nd
Grh	38-40	P	21.4	35.3	22.4	10.9	5.5	4.5	nd	7.35	106	0.06	0.09	nd	nd
Grh	46-48	P	15.9	35.7	26.1	11.8	6.4	4.0	nd	7.98	166	nd	nd	nd	nd
Grh	58-60	P	18.3	32.3	24.2	12.9	7.3	4.9	nd	7.85	163	nd	nd	nd	nd
Grh	80-82	P	11.9	26.7	25.3	18.6	12.1	5.4	nd	7.9	161	nd	nd	nd	nd
Grh	17-19	NP	18.8	29.7	21.4	14.2	9.8	6.3	nd	6.8	48	0.13	0.19	nd	nd
Grh	19-21	NP	21.1	32.1	21.8	12.8	7.4	4.8	nd	6.75	48	nd	nd	nd	nd
Grh	40-42	NP	21.9	34.9	21.4	10.8	6.8	4.2	nd	7.13	38	0.06	0.11	nd	nd
Grh	61-63	NP	24.2	38.5	20.9	8.5	4.9	3.1	nd	7.33	74	nd	nd	nd	nd
Grh	63-65	NP	21.8	36.2	20.6	10.9	6.1	4.4	nd	7.98	129	nd	nd	nd	nd
Grh	83-84	NP	12.1	24.5	30.5	22.7	6.8	3.4	nd	8.2	106	nd	nd	nd	nd
Grh	84-86	NP	17.6	30.4	22.8	13.1	8.7	7.4	nd	7.97	127	nd	nd	nd	nd

Site	Depth (cm)	LU	Soil fractions (%)						TOC (%)	pH (H <sub>2</sub> O) (1:2.5)	EC ( $\mu\text{S cm}^{-1}$ )	Fractions (% soil weight)		Proportion to TOC (%)	
			C	FSi	MSi	CSi	FS	MCS				C-humic	C-humin	C-humic	C-humin
Grh	100-102	NP	13.5	26.6	23.3	15.8	11.9	8.8	nd	7.99	99	nd	nd	nd	nd
Pjk	18-20	P	22.0	31.2	24.4	11.3	7.8	3.3	nd	6.46	67	nd	nd	nd	nd
Pjk	43-45	P	22.9	29.2	21.9	11.5	9.6	4.8	nd	6.98	59	nd	nd	nd	nd
Pjk	45-47	P	21.9	27.0	20.9	10.9	10.9	8.4	nd	6.95	54	nd	nd	nd	nd
Pjk	74-76	P	17.8	24.6	15.2	11.3	17.1	14.1	nd	8.03	143	nd	nd	nd	nd
Pjk	98-100	P	14.7	18.0	11.1	7.7	17.3	31.1	nd	8.14	124	nd	nd	nd	nd
Pjk	18-20	NP	23.6	35.8	26.8	9.4	3.1	1.3	nd	8.06	130	nd	nd	nd	nd
Pjk	38-40	NP	15.9	33.5	34.2	14.0	2.3	0.0	nd	8.29	96	nd	nd	nd	nd
Pjk	54-56	NP	21.9	33.6	24.5	13.6	4.5	1.9	nd	8.35	109	nd	nd	nd	nd
Pjk	78-80	NP	23.6	28.7	23.9	15.8	5.8	2.2	nd	8.42	124	nd	nd	nd	nd
Pjk	98-100	NP	15.9	32.6	26.6	14.7	6.1	4.1	nd	8.49	116	nd	nd	nd	nd
Pjk	118-120	NP	16.8	32.6	25.2	15.2	6.7	3.5	nd	8.61	119	nd	nd	nd	nd
Dgk	18-20	P	26.5	33.0	22.3	11.2	5.3	1.8	nd	7.88	288	nd	nd	nd	nd
Dgk	38-40	P	26.9	34.7	23.8	8.9	3.6	1.9	nd	7.92	402	nd	nd	nd	nd
Dgk	58-60	P	26.1	34.2	25.4	11.2	3.1	0.2	nd	8.08	329	nd	nd	nd	nd
Dgk	78-80	P	22.0	27.9	22.9	18.5	7.8	0.8	nd	8.14	366	nd	nd	nd	nd
Dgk	18-20	NP	21.0	24.3	24.1	15.0	8.4	7.2	nd	8.24	201	nd	nd	nd	nd
Dgk	38-40	NP	24.8	27.1	20.1	13.1	12.0	2.8	nd	8.49	300	nd	nd	nd	nd
Dgk	58-60	NP	24.6	26.4	19.1	12.9	12.7	4.3	nd	8.61	266	nd	nd	nd	nd
Dgk	65-69	NP	15.8	23.3	18.4	14.2	22.6	5.7	nd	8.71	203	nd	nd	nd	nd
Dgk	78-80	NP	21.0	24.6	20.0	15.3	12.9	6.2	nd	8.61	225	nd	nd	nd	nd
Dgk	78-80	NP	21.0	24.6	20.0	15.3	12.9	6.2	nd	8.61	225	nd	nd	nd	nd
Dgk	98-100	NP	14.9	20.9	16.5	17.9	27.1	2.6	nd	8.65	208	nd	nd	nd	nd
PL.G	20-22	NP	18.1	23.7	21.2	14.5	11.0	11.6	nd	nd	nd	0.18	0.33	nd	nd
PL.G	40-42	NP	19.4	27.4	21.6	13.5	10.4	7.7	nd	7.55	101	0.15	0.26	nd	nd
PL.G	60-62	NP	20.8	30.9	20.8	11.5	8.1	7.9	nd	7.63	168	nd	0.15	nd	nd

Site	Depth (cm)	LU	Soil fractions (%)						TOC (%)	pH (H <sub>2</sub> O) (1:2.5)	EC (μS cm <sup>-1</sup> )	Fractions (% soil weight)		Proportion to TOC (%)	
			C	FSi	MSi	CSi	FS	MCS				C-humic	C-humin	C-humic	C-humin
PL.G	80-82	NP	19.8	24.8	21.6	13.5	10.9	9.2	nd	7.37	271	nd	0.12	nd	nd
PL.G	80-90 (g)	NP	20.3	25.1	18.5	10.7	11.9	13.5	nd	8.01	243	nd	nd	nd	nd
PL.G	100-102	NP	19.7	31.6	22.2	11.2	7.7	7.6	nd	7.72	602	nd	0.29	nd	nd
PL.G	100-102(g)	NP	17.8	24.1	18.8	10.3	12.3	16.8	nd	8.03	417	nd	nd	nd	nd
PL.G	120-122	NP	19.6	30.7	21.0	10.6	8.1	9.9	nd	7.67	802	nd	0.09	nd	nd
PL.G	120-122(g)	NP	16.1	24.2	20.2	11.1	11.6	16.8	nd	7.87	791	nd	nd	nd	nd
PL.G	140-142	NP	19.9	23.6	18.7	10.6	10.6	16.5	nd	7.8	950	nd	nd	nd	nd
PL.G	140-142(g)	NP	19.5	23.9	18.5	10.8	11.7	15.7	nd	7.85	904	nd	nd	nd	nd
Bbl	18-20	P	20.3	24.3	20.2	14.6	12.9	7.8	nd	7.32	83	0.10	0.20	nd	nd
Bbl	25-27	P	10.2	17.6	16.8	14.8	13.0	27.6	nd	7.30	69	0.06	0.13	nd	nd
Bbl	27-29	NP	16.3	21.2	18.8	16.1	16.4	11.2	nd	6.85	35	0.07	0.17	nd	nd
Bbl	29-31	NP	15.2	21.8	19.9	16.3	16.1	10.7	nd	6.97	37	nd	nd	nd	nd
Bbl	38-40	NP	19.2	24.9	21.1	15.1	11.6	8.1	nd	6.95	49	0.24	0.19	nd	nd
Bbl	40-42	NP	21.5	24.8	20.3	16.7	10.9	5.8	nd	7.05	44	nd	nd	nd	nd
Bbl	60-62	NP	12.4	19.5	17.6	16.2	14.9	19.1	nd	7.17	86	nd	nd	nd	nd
Bbl	78-80	NP	11.8	18.8	18.0	18.8	15.8	16.8	nd	7.21	62	0.08	0.04	nd	nd

Appendix 3.2. Data from analysis of bulk samples used for PCA<sup>22</sup> (excl. EC)

Site	Profile	Depth (cm)	LU	Si	Al	Fe	Mn	P	Ti	Zr	Na	Mg	K	Ca	TOC	TON	pH (H <sub>2</sub> O)	EC (μS cm <sup>-1</sup> )
				(%)														
PBW	M	0-7	NP	15.3	18.5	9.6	0.3	0.7	0.9	0.0	0.1	0.4	0.3	0.5	3.52	0.35	4.8	160
PBW	M	7-16	NP	15.2	18.8	9.5	0.3	0.7	0.8	0.0	0.1	0.4	0.3	0.4	3.32	0.33	4.8	120
PBW	M	16-28	NP	15.4	23.5	11.7	0.4	0.3	1.0	0.0	0.1	0.4	0.3	0.3	1.74	0.18	5.4	24
PBW	M	28-56	NP	17.2	23.4	10.7	0.3	0.4	0.9	0.0	0.1	0.4	0.3	0.3	1.35	0.13	5.6	14
PBW	M	56-78	NP	24.5	26.6	17.2	0.5	0.4	1.3	0.0	0.1	0.4	0.4	0.5	1.38	0.14	6.2	20
PBW	M	78-100+	NP	19.3	21.7	10.8	0.3	0.3	0.8	0.0	0.1	0.5	0.3	0.4	0.88	0.08	6.4	15
PBW	S1	0-9	NP	15.2	17.8	9.4	0.3	0.7	0.8	0.0	0.1	0.4	0.3	0.4	4.09	0.42	4.8	230
PBW	S1	9-23	NP	15.5	18.6	9.2	0.3	0.7	0.7	0.0	0.1	0.4	0.3	0.4	3.62	0.37	4.7	199
PBW	S1	23-43	NP	16.2	22.5	10.8	0.4	0.3	0.8	0.0	0.1	0.4	0.3	0.3	1.92	0.22	4.9	82
PBW	S1	43-66	NP	20.1	19.7	10.6	0.3	0.1	0.8	0.0	0.1	0.4	0.3	0.3	0.93	0.11	5.6	51
PBW	S1	66-87	NP	20.0	19.9	11.6	0.2	0.1	0.9	0.0	0.1	0.5	0.3	0.3	0.75	0.08	5.9	34
PBW	S1	87-110+	NP	17.7	22.1	10.1	0.2	0.3	0.9	0.0	0.1	0.5	0.2	0.4	0.89	0.08	5.8	6
PBW	S2	0-13	NP	17.7	19.4	9.9	0.3	0.4	0.7	0.0	0.1	0.4	0.3	0.5	3.57	0.37	5.2	174
PBW	S2	13-28	NP	17.0	18.6	9.2	0.3	0.4	0.8	0.0	0.1	0.4	0.2	0.5	3.44	0.35	5.3	111
PBW	S2	28-33	NP	18.0	23.0	9.6	0.2	0.3	0.9	0.0	0.1	0.3	0.2	0.5	1.72	0.17	6.4	18
PBW	S2	33-56	NP	19.0	18.9	10.8	0.3	0.2	0.9	0.0	0.1	0.3	0.4	0.2	1.28	0.16	5.7	28
PBW	S2	56-70	NP	18.0	18.9	10.6	0.2	0.2	0.8	0.0	0.1	0.5	0.3	0.3	0.82	0.09	5.9	28
PBW	S2	70-105+	NP	20.1	17.3	10.5	0.2	0.1	0.8	0.0	0.1	0.4	0.2	0.3	0.63	0.07	5.8	10
PBW	M	0-8	P	23.2	16.6	7.4	0.0	0.7	0.8	0.0	0.2	0.3	0.5	0.9	3.95	0.42	5.4	200
PBW	M	8-22	P	23.6	17.0	7.3	0.0	0.7	0.8	0.0	0.2	0.4	0.5	0.9	4.44	0.45	5.4	230
PBW	M	22-29	P	22.2	15.9	6.7	0.1	0.6	0.8	0.0	0.2	0.3	0.5	0.8	4.00	0.41	5.5	210
PBW	M	29-35	P	22.0	16.6	7.0	0.1	0.4	0.7	0.0	0.2	0.3	0.5	0.7	2.46	0.25	6.0	110

<sup>22</sup> Elemental composition measured by ICP-OES (obtained from Pauline Winkler, group P1), total organic carbon (TOC), total organic nitrogen (TON), pH and EC (obtained from Angelika Kölbl, group P2) of bulk soil samples of 2012 sampling year. PBW = Perbawati, Andosol; JSG = Jasinga, Alisol; PL = Ploso lor, Vertisol; M = main-site samples, S1 = sub-site-1 samples, S2 = sub-site-2 samples; LU = landuse.

PBW	M	35-50	P	20.7	18.3	12.1	0.4	0.3	0.8	0.0	0.2	0.3	0.5	0.7	1.64	0.16	6.6	93
PBW	M	50-75	P	21.5	21.3	9.5	0.2	0.2	0.8	0.0	0.1	0.3	0.5	0.6	1.00	0.09	7.1	63
PBW	M	75-105	P	22.0	21.0	9.6	0.2	0.2	0.8	0.0	0.2	0.3	0.5	0.6	0.62	0.06	7.1	44
PBW	S1	0-8	P	21.0	15.4	5.1	0.1	0.7	0.6	0.0	0.2	0.3	0.4	0.7	4.25	0.44	5.6	160
PBW	S1	8-22	P	23.2	16.8	5.8	0.1	0.7	0.7	0.0	0.2	0.3	0.4	0.8	4.29	0.44	5.5	270
PBW	S1	22-30	P	24.4	18.0	6.2	0.1	0.7	0.8	0.0	0.2	0.3	0.5	0.8	3.75	0.39	5.7	240
PBW	S1	30-35	P	22.4	17.0	5.7	0.1	0.5	0.8	0.0	0.2	0.3	0.4	0.8	2.45	0.25	5.9	110
PBW	S1	35-60	P	19.9	18.8	11.1	0.4	0.2	0.8	0.0	0.2	0.3	0.4	0.7	1.07	0.10	6.7	70
PBW	S1	60-85	P	20.6	19.6	8.8	0.2	0.2	0.8	0.0	0.2	0.3	0.4	0.6	0.52	0.05	7.0	57
PBW	S1	85-105+	P	21.8	20.4	9.1	0.2	0.2	0.8	0.0	0.2	0.3	0.4	0.6	0.42	0.04	7.1	52
PBW	S2	0-10	P	21.6	15.7	5.3	0.1	0.7	0.7	0.0	0.2	0.3	0.4	0.7	4.41	0.44	5.3	100
PBW	S2	10-22	P	22.1	16.3	5.6	0.2	0.8	0.6	0.0	0.2	0.3	0.4	0.8	3.95	0.40	5.4	240
PBW	S2	22-35	P	22.8	16.6	6.2	0.1	0.5	0.8	0.0	0.2	0.3	0.5	0.8	2.68	0.29	5.9	150
PBW	S2	35-52	P	19.3	18.7	13.8	0.3	0.2	0.7	0.0	0.1	0.3	0.4	0.6	0.74	0.08	6.5	90
PBW	S2	52-75	P	20.8	19.6	9.4	0.3	0.2	0.8	0.0	0.2	0.3	0.4	0.6	0.46	0.04	6.6	100
PBW	S2	75-110+	P	21.9	20.1	9.2	0.2	0.1	0.8	0.0	0.2	0.2	0.4	0.6	0.44	0.04	6.7	80
JSG	M	0-7	NP	20.7	14.6	8.9	0.1	0.1	1.1	0.0	0.1	0.2	0.2	0.5	2.00	0.18	5.9	95
JSG	M	7-14	NP	20.5	14.6	8.8	0.1	0.1	1.1	0.0	0.1	0.2	0.2	0.5	1.85	0.16	6.0	70
JSG	M	14-22	NP	20.4	15.1	8.8	0.1	0.1	1.1	0.0	0.1	0.2	0.2	0.4	1.72	0.16	6.1	60
JSG	M	22-46	NP	20.3	16.8	10.0	0.0	0.1	1.1	0.0	0.0	0.1	0.1	0.2	0.94	0.09	5.3	24
JSG	M	46-63	NP	19.8	16.5	9.7	0.0	0.1	1.1	0.0	0.0	0.1	0.1	0.1	0.78	0.07	5.4	14
JSG	M	63-83	NP	20.1	16.8	9.5	0.1	0.1	1.1	0.0	0.0	0.1	0.1	0.1	0.68	0.07	5.3	15
JSG	M	83-100+	NP	16.6	14.6	18.2	0.1	0.0	0.9	0.0	0.0	0.1	0.1	0.0	0.42	0.05	5.2	14
JSG	S1	0-10	NP	20.2	16.3	8.7	0.1	0.1	1.0	0.0	0.0	0.1	0.1	0.1	2.54	0.25	4.3	530
JSG	S1	10-20	NP	20.7	16.7	9.5	0.2	0.1	1.1	0.0	0.0	0.1	0.1	0.1	2.05	0.19	4.5	170
JSG	S1	20-40	NP	21.3	17.4	9.8	0.2	0.1	1.0	0.0	0.1	0.1	0.1	0.0	1.81	0.15	4.7	54
JSG	S1	40-65	NP	20.1	17.2	9.2	0.2	0.1	1.0	0.0	0.0	0.1	0.1	0.0	1.37	0.12	4.9	29
JSG	S1	65-85	NP	21.0	18.0	9.5	0.1	0.1	1.0	0.0	0.0	0.1	0.1	0.0	0.99	0.09	4.9	17
JSG	S1	85-100+	NP	20.7	17.6	9.4	0.1	0.1	1.1	0.0	0.0	0.1	0.1	0.0	0.75	0.08	4.9	18
JSG	S2	0-10	NP	20.6	14.8	8.2	0.1	0.1	1.0	0.0	0.0	0.2	0.2	0.1	2.61	0.25	4.1	430

JSG	S2	10-20	NP	21.0	15.0	8.8	0.1	0.1	1.0	0.0	0.0	0.2	0.2	0.1	2.43	0.24	4.2	420
JSG	S2	20-41	NP	21.2	15.4	8.6	0.1	0.1	1.0	0.0	0.1	0.2	0.2	0.1	1.70	0.16	4.4	160
JSG	S2	41-62	NP	20.9	15.3	9.0	0.3	0.1	1.1	0.0	0.0	0.2	0.1	0.1	1.26	0.13	4.5	140
JSG	S2	62-92	NP	21.7	15.5	9.9	0.4	0.1	1.2	0.0	0.0	0.2	0.1	0.1	0.95	0.10	4.6	80
JSG	S2	92-103+	NP	22.6	16.1	9.8	0.4	0.1	1.2	0.0	0.0	0.2	0.1	0.0	0.76	0.08	4.9	24
JSG	M	0-7	P	24.3	13.0	7.5	0.1	0.2	1.0	0.0	0.1	0.2	0.2	0.3	1.86	0.19	5.1	75
JSG	M	7-17	P	24.2	13.2	7.9	0.0	0.2	1.0	0.0	0.1	0.2	0.2	0.3	1.79	0.18	5.3	53
JSG	M	17-25	P	23.9	13.5	8.4	0.1	0.1	1.1	0.0	0.1	0.2	0.2	0.3	1.37	0.14	5.4	60
JSG	M	25-48	P	21.2	16.3	10.7	0.1	0.1	1.1	0.0	0.0	0.1	0.1	0.2	1.10	0.11	5.3	38
JSG	M	48-75	P	20.6	16.1	10.2	0.1	0.1	1.0	0.0	0.0	0.1	0.1	0.1	0.99	0.10	5.2	51
JSG	M	75-95+	P	21.2	16.9	10.2	0.2	0.1	1.2	0.0	0.0	0.1	0.1	0.1	0.70	0.07	5.0	42
JSG	S1	0-7	P	24.1	13.3	7.1	0.1	0.2	1.0	0.0	0.1	0.2	0.2	0.2	2.09	0.21	5.2	49
JSG	S1	7-17	P	24.4	13.0	7.1	0.0	0.2	0.9	0.0	0.0	0.2	0.2	0.2	1.91	0.19	5.3	43
JSG	S1	17-21	P	22.4	14.2	9.5	0.1	0.1	1.1	0.0	0.0	0.2	0.1	0.2	1.22	0.12	5.4	35
JSG	S1	21-48	P	20.2	16.2	10.9	0.1	0.1	1.2	0.0	0.0	0.1	0.1	0.1	0.99	0.09	5.4	23
JSG	S1	48-77	P	20.7	16.9	10.7	0.2	0.1	1.1	0.0	0.0	0.1	0.1	0.1	0.74	0.08	5.2	25
JSG	S1	77-100	P	20.8	16.8	11.4	0.1	0.1	1.2	0.1	0.1	0.1	0.1	0.1	0.60	0.07	5.1	25
JSG	S2	0-7	P	24.4	13.4	7.7	0.1	0.2	1.0	0.0	0.1	0.2	0.2	0.3	2.07	0.21	5.3	57
JSG	S2	7-15	P	23.9	13.1	7.3	0.1	0.2	1.0	0.0	0.1	0.2	0.2	0.2	1.76	0.18	5.2	47
JSG	S2	15-20	P	23.6	13.4	8.0	0.1	0.1	0.9	0.0	0.0	0.2	0.2	0.3	1.30	0.13	5.4	38
JSG	S2	20-55	P	20.2	15.2	10.5	0.2	0.1	1.2	0.0	0.0	0.1	0.1	0.1	1.07	0.10	5.3	25
JSG	S2	55-72	P	21.3	16.4	9.4	0.2	0.1	1.1	0.0	0.0	0.1	0.1	0.1	0.84	0.09	5.2	23
JSG	S2	72-90	P	20.6	16.0	9.8	0.2	0.1	1.1	0.0	0.0	0.1	0.1	0.1	0.77	0.08	5.1	24
PL	M	0-10	NP	25.8	10.5	6.9	0.3	0.0	0.7	0.0	0.2	0.8	0.5	2.0	1.44	0.12	5.8	187
PL	M	10-23	NP	25.8	10.4	7.2	0.3	0.1	0.6	0.0	0.2	0.8	0.5	2.2	1.42	0.11	6.8	143
PL	M	23-29	NP	26.1	10.7	6.9	0.3	0.0	0.6	0.0	0.2	0.9	0.5	2.1	0.90	0.07	7.3	218
PL	M	29-55	NP	26.1	10.7	7.2	0.3	0.0	0.6	0.0	0.2	0.8	0.5	2.2	0.71	0.05	7.8	204
PL	M	55-100	NP	26.3	10.7	7.2	0.3	0.0	0.7	0.0	0.2	0.9	0.5	2.1	0.58	0.05	8.0	237
PL	M	100-120+	NP	25.9	10.4	7.1	0.3	0.0	0.7	0.0	0.2	0.8	0.5	2.1	0.48	0.04	8.3	345
PL	S1	0-10	NP	25.7	10.5	6.9	0.3	0.0	0.6	0.0	0.2	0.8	0.5	2.1	1.41	0.11	6.7	170

PL	S1	10-21	NP	25.3	10.4	6.7	0.2	0.0	0.6	0.0	0.2	0.8	0.5	2.1	1.35	0.10	6.8	201
PL	S1	21-29	NP	25.8	10.6	6.9	0.3	0.0	0.7	0.0	0.2	0.9	0.5	2.1	1.27	0.09	7.4	379
PL	S1	29-48	NP	26.4	10.6	7.1	0.3	0.0	0.6	0.0	0.2	0.8	0.6	2.2	1.07	0.08	7.6	215
PL	S1	48-90	NP	26.2	10.8	7.4	0.4	0.0	0.7	0.0	0.2	0.9	0.5	2.2	0.57	0.04	8.1	257
PL	S1	90-110+	NP	25.9	10.5	6.6	0.3	0.1	0.6	0.0	0.2	0.9	0.5	2.1	0.48	0.04	7.9	387
PL	S2	0-10	NP	26.1	10.6	6.8	0.3	0.1	0.6	0.0	0.2	0.9	0.5	2.2	1.68	0.13	5.7	303
PL	S2	10-20	NP	26.1	10.6	7.0	0.3	0.0	0.7	0.0	0.2	0.9	0.5	2.3	1.32	0.10	6.6	145
PL	S2	20-29	NP	26.3	10.6	7.2	0.3	0.0	0.6	0.0	0.2	0.9	0.5	2.4	1.13	0.09	7.0	136
PL	S2	29-48	NP	26.2	10.8	7.2	0.3	0.0	0.6	0.0	0.2	0.9	0.5	2.6	0.69	0.06	7.7	196
PL	S2	48-80	NP	25.1	10.6	7.4	0.4	0.0	0.6	0.0	0.1	1.0	0.6	3.6	0.57	0.04	8.3	233
PL	S2	80-110+	NP	25.6	10.2	7.1	0.3	0.1	0.6	0.0	0.2	0.8	0.5	2.2	0.79	0.04	8.5	274
PL	M	0-8	P	25.5	10.2	7.3	0.3	0.1	0.7	0.0	0.2	0.8	0.5	2.3	1.59	0.15	7.0	590
PL	M	8-20	P	26.0	10.4	7.8	0.3	0.0	0.7	0.0	0.2	0.8	0.6	2.3	0.96	0.09	7.4	375
PL	M	20-27	P	25.9	10.4	7.8	0.3	0.0	0.7	0.0	0.2	0.8	0.6	2.2	0.65	0.06	8.0	332
PL	M	27-47	P	26.3	10.7	7.5	0.3	0.0	0.7	0.0	0.2	0.9	0.6	2.1	0.52	0.05	8.1	360
PL	M	47-90	P	25.8	10.5	7.1	0.3	0.0	0.6	0.0	0.2	0.9	0.6	2.3	0.48	0.04	8.3	396
PL	M	90-115+	P	25.4	10.0	7.3	0.3	0.1	0.7	0.0	0.2	0.8	0.5	2.5	0.46	0.03	8.4	376
PL	S1	0-8	P	25.7	10.2	7.0	0.3	0.1	0.6	0.0	0.2	0.8	0.5	2.4	1.53	0.14	7.4	700
PL	S1	8-18	P	25.6	10.2	7.7	0.4	0.0	0.7	0.0	0.2	0.8	0.6	2.5	1.36	0.12	7.6	635
PL	S1	18-24	P	26.5	10.5	7.5	0.4	0.0	0.6	0.0	0.2	0.8	0.6	2.4	0.78	0.06	8.1	336
PL	S1	24-45	P	26.4	10.4	7.8	0.3	0.0	0.7	0.0	0.2	0.8	0.6	2.5	0.58	0.04	8.3	262
PL	S1	45-75	P	25.7	10.2	7.9	0.4	0.0	0.7	0.0	0.2	0.9	0.6	2.7	0.51	0.04	8.5	350
PL	S1	75-100+	P	26.3	10.4	6.4	0.3	0.1	0.6	0.0	0.2	0.9	0.6	2.3	0.55	0.04	8.3	552
PL	S2	0-9	P	26.4	10.3	6.6	0.3	0.1	0.7	0.0	0.2	0.9	0.6	2.3	1.35	0.12	7.7	463
PL	S2	9-17	P	26.0	10.2	6.7	0.3	0.1	0.7	0.0	0.2	0.9	0.6	2.3	1.27	0.11	7.7	465
PL	S2	17-25	P	26.2	10.5	7.3	0.3	0.0	0.7	0.0	0.2	0.8	0.6	2.3	1.04	0.09	7.8	339
PL	S2	25-43	P	26.3	10.5	7.3	0.3	0.0	0.7	0.0	0.2	0.8	0.7	2.3	0.72	0.06	8.0	176
PL	S2	43-75	P	26.0	10.6	6.6	0.3	0.0	0.6	0.0	0.2	0.9	0.6	2.2	0.66	0.05	8.0	145
PL	S2	75-100+	P	29.8	10.7	4.2	0.1	0.2	0.7	0.1	0.1	0.5	1.4	0.2	0.53	0.04	8.0	285

Appendix 3.3. Data used for principal component analysis<sup>23</sup>

Soil	Type	alkyl-C	O-alkyl-C	aryl-C	carboxyl-C	A-OA	TOC	TON	C	FSi	MSi	CoSi	FS	MS	CS	Carbohyd rate	Protein	Lignin	Lipid	Carbonyl	Char
Alisol	P	28.8	37.4	16.9	16.8	0.77	1.57	0.17	32.34	24.32	22.12	14.76	4.45	2.02	0	0.214	0.361	0.089	0.199	0.029	0.109
Alisol	NP	24.4	42.9	16.8	15.9	0.57	2.24	0.23	38.17	22.87	19.97	12.36	4.03	2.60	0	0.272	0.421	0.071	0.114	0.008	0.115
Andosol	P	27.3	43.1	13.4	16.2	0.63	3.69	0.44	5.36	13.68	24.27	21.15	17.66	13.22	4.65	0.264	0.362	0.143	0.171	0.028	0.033
Andosol	NP	27.9	40.9	15.8	15.3	0.68	3.12	0.33	22.25	21.72	20.83	14.74	8.21	8.40	3.84	0.234	0.352	0.157	0.183	0.017	0.057
Vertisol	P	22.6	25.4	34.8	17.2	0.89	0.82	0.06	39.67	25.02	17.94	11.82	3.23	2.32	0.00	0.105	0.307	0.058	0.141	0.026	0.364
Vertisol	NP	22.0	26.1	35.5	16.4	0.85	1.44	0.11	22.33	24.29	26.16	16.99	6.30	2.58	1.35	0.121	0.336	0	0.128	0.011	0.405

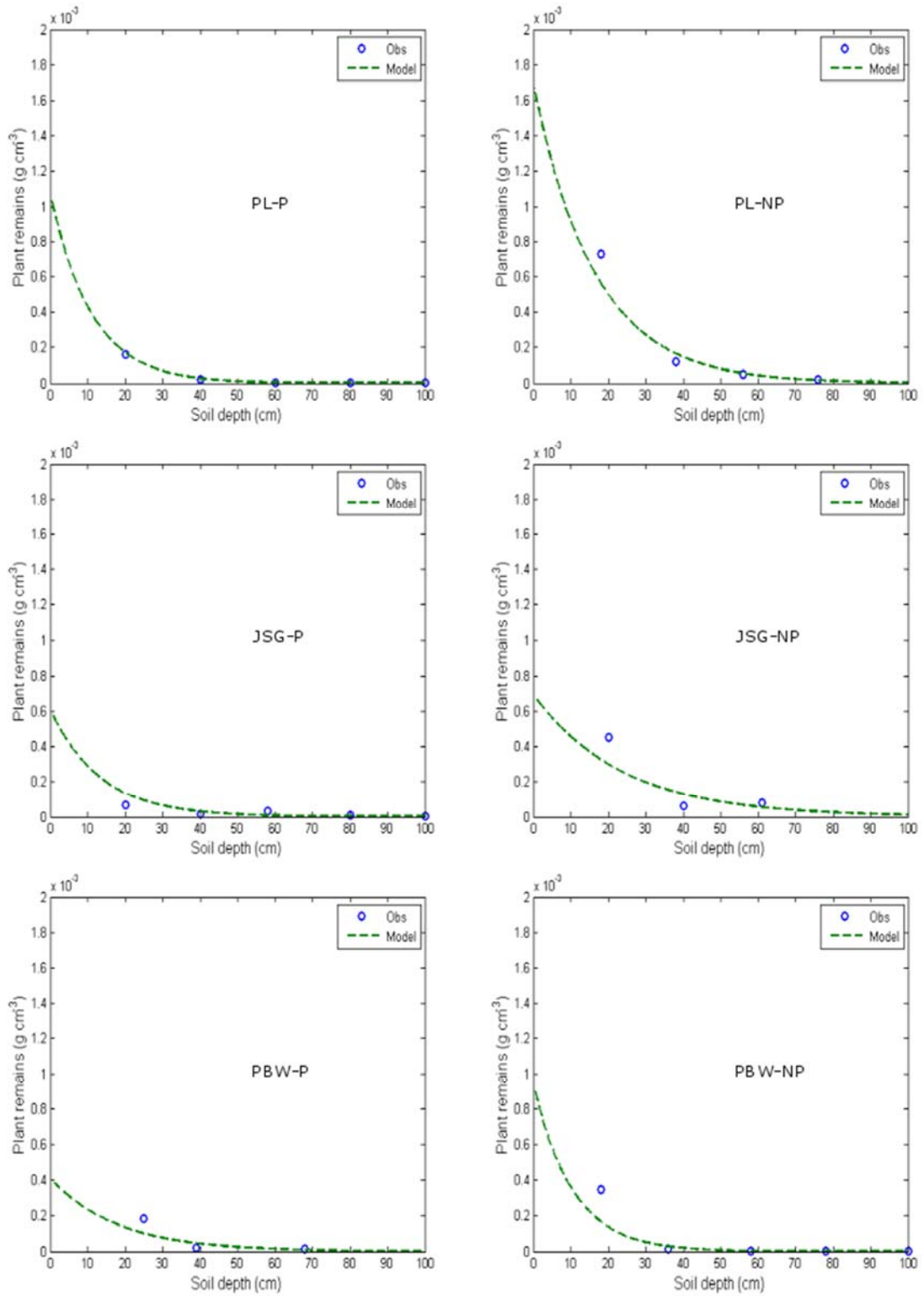
<sup>23</sup> Molecular compounds obtained from <sup>13</sup>C NMR and grain size compositions, A-OA = ratio of alkyl-C to O-alkyl-C, TOC = total organic carbon, TON = total organic nitrogen, C = clay, FSi = fine silt, MSi = medium silt, CoSi = coarse silt, FS = fine sand, MS = medium sand, CS = coarse sand. Molecular composition of organic compound was predicted according to Nelson and Baldock (2005).

Appendix 3.4. <sup>13</sup>C NMR integral of samples

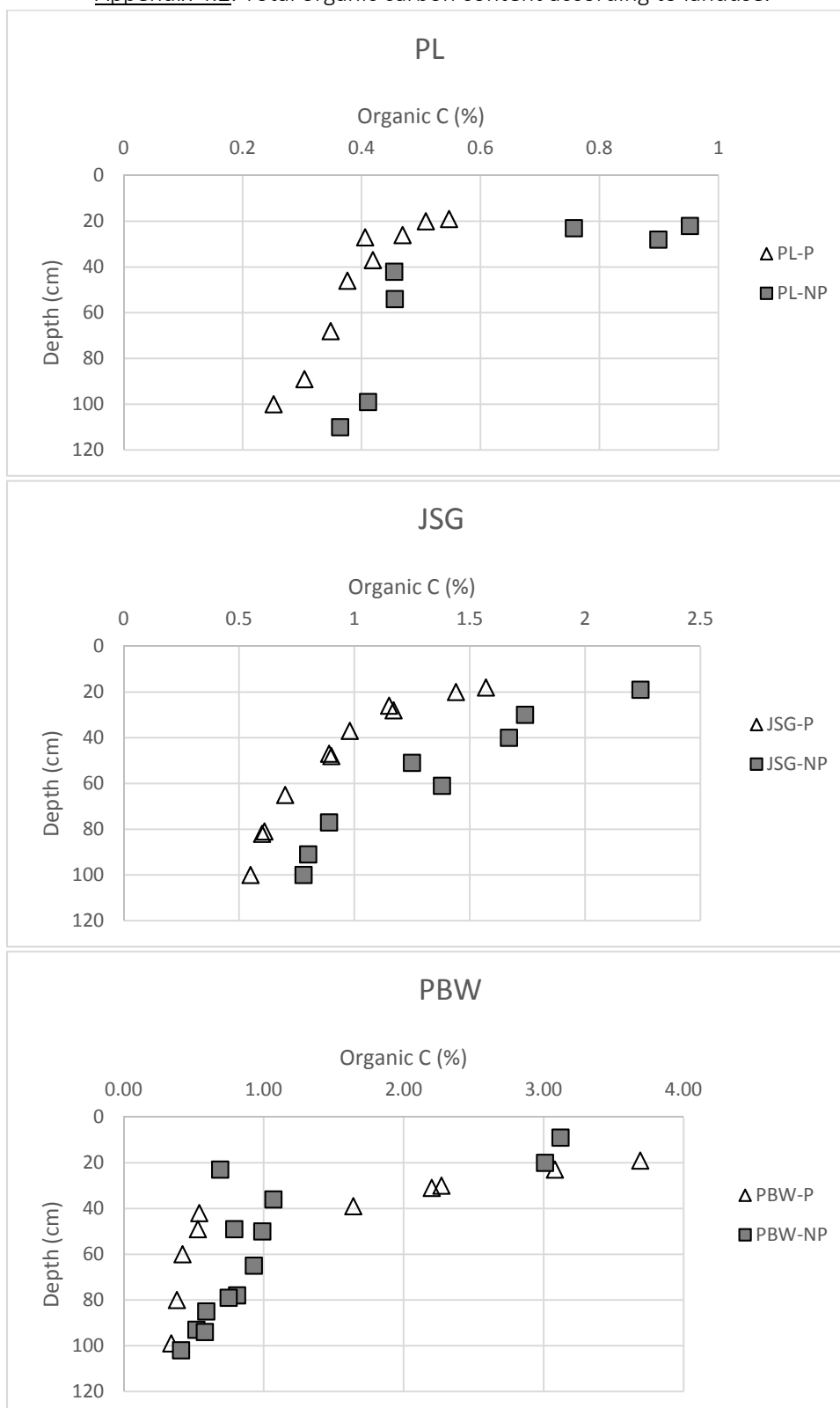
Site	Object	Integral [abs]	Integral [rel]	Peaks	Range (F1) from	Range (F1) to	v(F1) [ppm]	Concentration (Eretic)	Atoms (Eretic)	Intensity [abs]
PL-P	Integral 1	163825808.1	17.19763963	1	220	160	190	n/a	n/a	
	Integral 2	59042199.94	6.197964102	0	160	145	152.5	n/a	n/a	
	Integral 3	272661689.7	28.6227032	1	145	110	127.5	n/a	n/a	
	Integral 4	41321339.97	4.337714077	0	110	95	102.5	n/a	n/a	
	Integral 5	200964364.4	21.09626534	2	95	45	70	n/a	n/a	
	Integral 6	214790791.7	22.54769669	1	45	0	22.5	n/a	n/a	
PL-NP	Integral 1	852903039.4	16.42434701	1	220	160	190	n/a	n/a	
	Integral 2	299409924.9	5.765734528	0	160	145	152.5	n/a	n/a	
	Integral 3	1542589330	29.70563039	1	145	110	127.5	n/a	n/a	
	Integral 4	235540240.2	4.53579652	0	110	95	102.5	n/a	n/a	
	Integral 5	1117669235	21.52294752	2	95	45	70	n/a	n/a	
	Integral 6	1144807914	22.04555684	1	45	0	22.5	n/a	n/a	
JSG-P	Integral 1	252336949.1	16.80438437	1	220	160	190	n/a	n/a	
	Integral 2	49389195.42	3.289074496	0	160	145	152.5	n/a	n/a	
	Integral 3	205478081.5	13.68381711	1	145	110	127.5	n/a	n/a	
	Integral 4	73501741.11	4.894849978	1	110	95	102.5	n/a	n/a	
	Integral 5	488196973.8	32.51148763	2	95	45	70	n/a	n/a	
	Integral 6	432710827.7	28.81638657	1	45	0	22.5	n/a	n/a	
JSG-NP	Integral 1	418512841.1	15.87409965	1	220	160	190	n/a	n/a	
	Integral 2	79631992.91	3.020423908	0	160	145	152.5	n/a	n/a	
	Integral 3	363296069.7	13.77973971	1	145	110	127.5	n/a	n/a	
	Integral 4	148830628.6	5.64511288	1	110	95	102.5	n/a	n/a	
	Integral 5	983352892.9	37.2983581	2	95	45	70	n/a	n/a	
	Integral 6	642826438.2	24.38226486	2	45	0	22.5	n/a	n/a	
PBW-P	Integral 1	145790480.6	16.21082656	1	220	160	190	n/a	n/a	
	Integral 2	27697421.6	3.079749074	1	160	145	152.5	n/a	n/a	

	Integral 3	93012423.39	10.34229572	2	145	110	127.5	n/a	n/a	
	Integral 4	49486139.75	5.502493889	1	110	95	102.5	n/a	n/a	
	Integral 5	338050079.5	37.58867646	2	95	45	70	n/a	n/a	
	Integral 6	245303655.7	27.27595793	1	45	0	22.5	n/a	n/a	
PBW-NP	Integral 1	212504490.1	15.31842255	1	220	160	190	n/a	n/a	
	Integral 2	48585777.66	3.502314101	1	160	145	152.5	n/a	n/a	
	Integral 3	170402750.3	12.28351143	1	145	110	127.5	n/a	n/a	
	Integral 4	77453732.51	5.583265568	1	110	95	102.5	n/a	n/a	
	Integral 5	490196941.5	35.33593045	2	95	45	70	n/a	n/a	
	Integral 6	388104359	27.97656916	1	45	0	22.5	n/a	n/a	

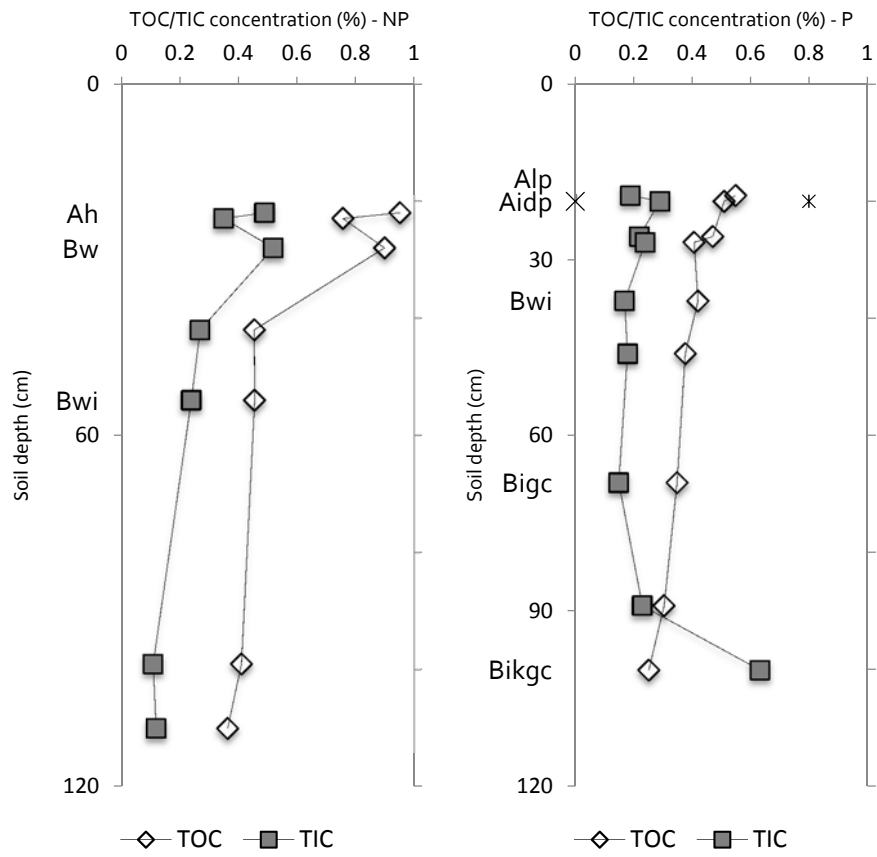
Appendix 4.1. Model of depth distribution of litter



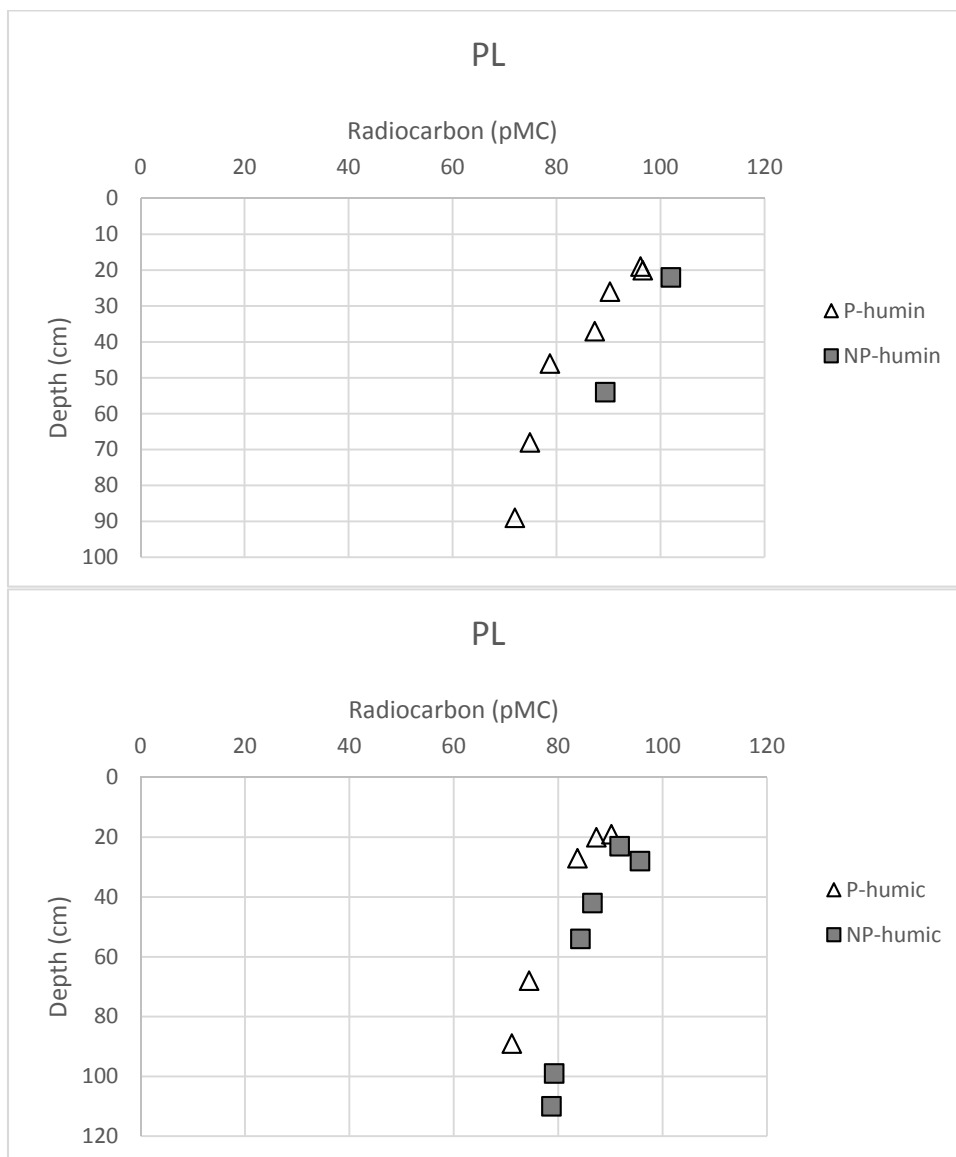
Appendix 4.2. Total organic carbon content according to landuse.

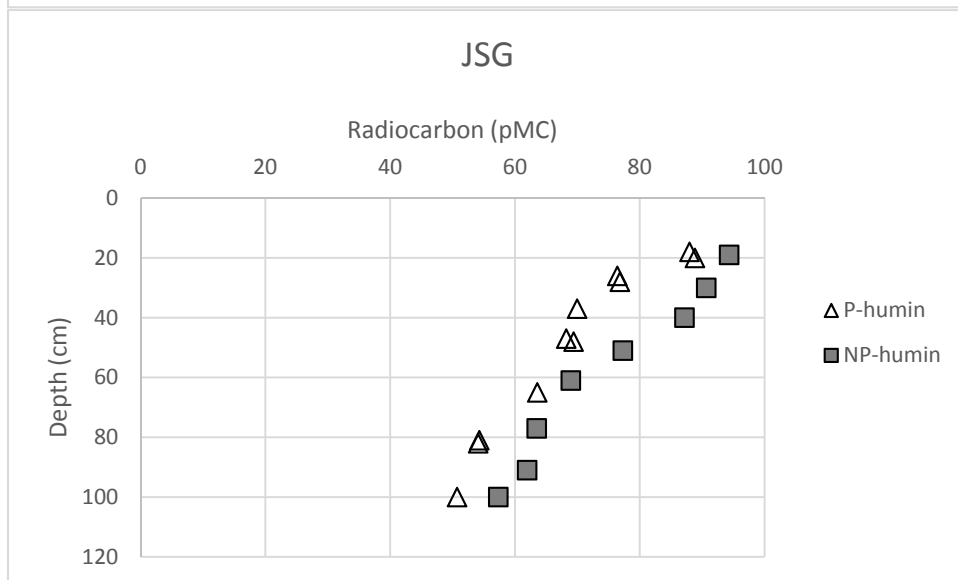
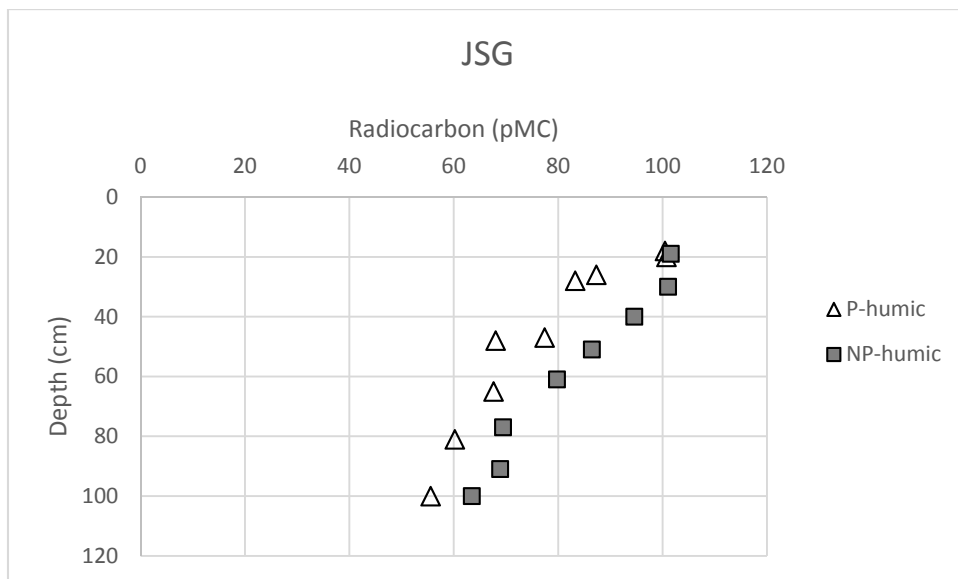


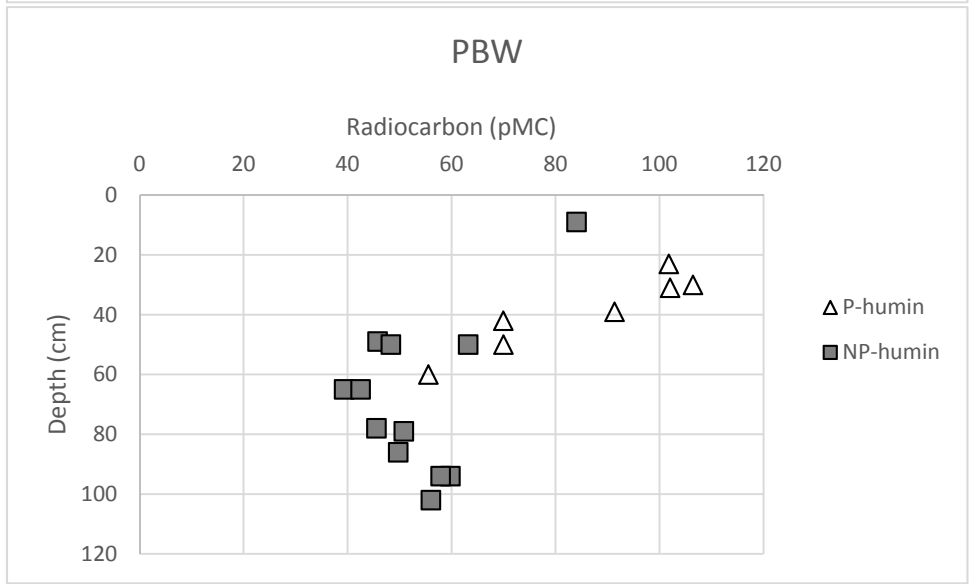
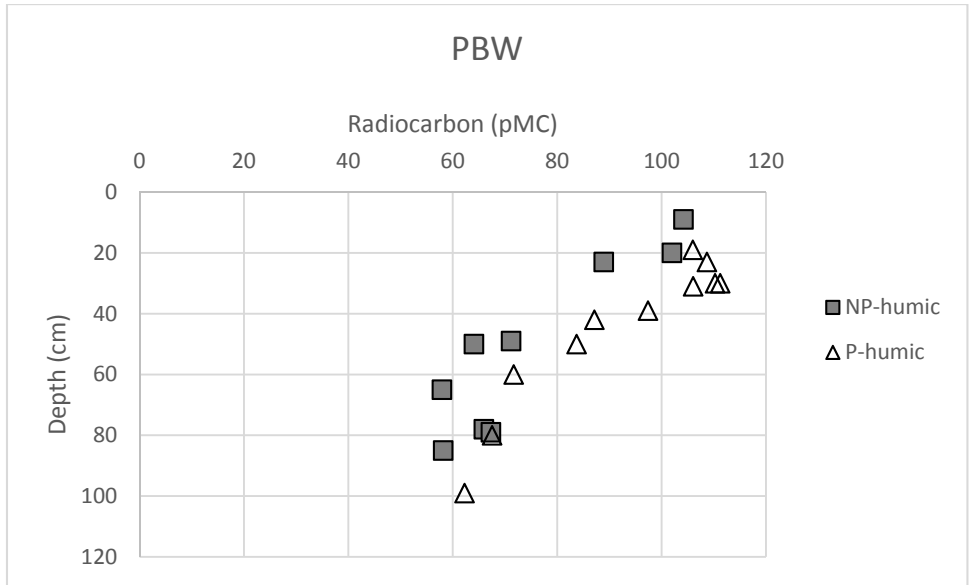
Appendix 4.3. TOC and TIC (%) in Vertisol (PL).



Appendix 4.4. Radiocarbon content according to landuses.







## Appendix 4.5. Plant remains collected from soil profiles.

Site	Depth	Plant remains (g)	Proportion (%)	Soil weight (g)	Plant remain/soil (%)	BD	Layer	Total plant remains		C tissue	Plant remains g C cm <sup>-3</sup>	Proportion (%)
						g.cm <sup>-3</sup>		cm	g.cm <sup>-2</sup>	g.cm <sup>-3</sup>		
<i>PL-P</i>												
119	20	0.9200	85.67	5788.8	0.015893	1	5	0.000795	0.000159	0.44	6.99281E-05	0.85
120	40	0.1200	11.17	5110	0.002348	0.93	5	0.000109	2.18E-05	0.44	9.60939E-06	0.12
121	60	0.0227	2.11	5207.1	0.000436	0.99	5	2.16E-05	4.32E-06	0.44	1.89897E-06	0.02
122	80	0.0109	1.01	5718.9	0.000191	0.99	5	9.43E-06	1.89E-06	0.44	8.30237E-07	0.01
123	100	0.0003	0.03	5039.4	0.000006	0.94	5	2.8E-07	5.6E-08	0.44	2.4622E-08	0.00
		1.0739	100.00								8.22914E-05	1.00
<i>PL-NP</i>												
124	18	2.9700	68.28	4496.3	0.066054	1.1	5	0.003633	0.000727	0.48	0.000348767	0.76
125	38	0.8100	18.62	6303.3	0.012850	0.92	5	0.000591	0.000118	0.48	5.67474E-05	0.12
126	56	0.2500	5.75	4914.4	0.005087	0.98	5	0.000249	4.99E-05	0.48	2.39297E-05	0.05
127	76	0.1000	2.30	5031.4	0.001988	0.98	5	9.74E-05	1.95E-05	0.48	9.34929E-06	0.02
128	96	0.1200	2.76	5110.7	0.002348	0.94	5	0.00011	2.21E-05	0.48	1.05942E-05	0.02
129	110	0.1000	2.30	5196	0.001925	0.94	5	9.05E-05	1.81E-05	0.48	8.6836E-06	0.02
		4.3500	100.00								0.000458071	1.00
<i>JSG-P</i>												
109	20	0.3700	53.60	6013.3	0.006153	1.14	5	0.000351	7.01E-05	0.53	3.71766E-05	0.56
110	40	0.1000	14.49	6198.6	0.001613	0.98	5	7.91E-05	1.58E-05	0.53	8.37931E-06	0.13
111	58	0.1700	24.63	5257.5	0.003233	0.93	5	0.00015	3.01E-05	0.53	1.59378E-05	0.24
112	80	0.0500	7.24	4662	0.001073	0.84	5	4.5E-05	9.01E-06	0.53	4.77477E-06	0.07
113	100	0.0003	0.04	4587	0.000007	0.84	5	2.75E-07	5.49E-08	0.53	2.91171E-08	0.00
		0.6903	100.00	4971.1					0.000125		6.62976E-05	1.00
<i>JSG-NP</i>												
114	20	2.2800	46.81	5625	0.040533	1.12	5	0.00227	0.000454	0.46	2.09E-04	0.64

115	40	0.3100	6.36	5139.4	0.006032	0.97	5	0.000293	5.85E-05	0.46	2.6914E-05	0.08
116	61	0.3900	8.01	4597.7	0.008483	0.95	5	0.000403	8.06E-05	0.46	3.70685E-05	0.11
117	80	0.3300	6.78	4536.6	0.007274	0.94	5	0.000342	6.84E-05	0.46	3.14535E-05	0.10
118	100	0.1800	3.70	4134.9	0.004353	1.11	5	0.000242	4.83E-05	0.46	2.22274E-05	0.07
		4.8706	71.65						0.00071		3.26E-04	1.00
<i>PBW-P</i>												
105	25	1.1200	85.50	4454.1	0.025145	0.73	5	0.000918	0.000184	0.46	8.44382E-05	0.85
106	39	0.1500	11.45	6451	0.002325	0.85	5	9.88E-05	1.98E-05	0.46	9.09161E-06	0.09
107	68	0.0400	3.05	2622.8	0.001525	0.82	5	6.25E-05	1.25E-05	0.46	5.75263E-06	0.06
108	98	0.0000	0.00	5801.9	0.000000	0.75	5	0	0	0.46	0	0.00
		1.3100	100.00								9.92824E-05	1.00
<i>PBW-NP</i>												
100	18	4.3400	94.96	5701.6	0.076119	0.46	5	0.001751	0.00035	0.44	1.54E-04	0.95
101	36	0.1800	3.94	5922.4	0.003039	0.47	5	7.14E-05	1.43E-05	0.44	6.28529E-06	0.04
102	58	0.0100	0.22	5780.5	0.000173	0.51	5	4.41E-06	8.82E-07	0.44	3.88202E-07	0.00
103	78	0.0400	0.88	5186.6	0.000771	0.51	5	1.97E-05	3.93E-06	0.44	1.73061E-06	0.01
104	100	0.0003	0.01	4587	0.000007	0.51	5	1.67E-07	3.34E-08	0.44	1.46763E-08	0.00
		4.5703	100.00								1.62E-04	1.00

Appendix 4.6. TOC, TON,  $\Delta^{14}\text{C}$ , and  $\delta^{13}\text{C}$  content of selected bulk soil, humic, fulvic, and conc. HCl extracted samples<sup>24</sup> (only for PL samples).

Site	Depth	Hor	Sample point	TOC	TN	$\Delta^{14}\text{C}$				$\delta^{13}\text{C}$			
						Bulk	Humic	Humin	HCl	Bulk	Humic	Humin	HCl
	[cm]		[cm]	[%]	[%]	[%]				[%]			
PL-P	0 - 8	Alp1				50.20 ± 2.30	nd	nd	nd	-25.08 ± 0.13			
	8 - 20	Alp2	19 - 20	0.82	0.06		-57.72 ± 2.20	4.54 ± 2.30	-27.74 ± 1.90		-22.20 ± 0.08	-25.54 ± 0.12	-28.37 ± 0.26
	20 - 27	Aidp	20 - 21	0.81	0.11		-87.92 ± 3.0	9.04 ± 2.40	-378.05 ± 2.70		-23.24 ± 0.31	-23.38 ± 0.82	-25.46 ± 0.59
			26 - 27	0.69	0.06		nd	-57.20 ± 2.80	-14.79 ± 1.60		nd	-20.99 ± 0.23	-18.47 ± 0.21
	27 - 47	Bwi	27 - 28	0.66	0.06	-149.14 ± 2.20	-125.84 ± 3.60	nd	nd	-18.48 ± 0.11	-17.85 ± 0.92	nd	nd
			37 - 38	0.59	0.05		nd	-87.71 ± 2.30	-100.87 ± 1.40		nd	-20.04 ± 0.61	-21.98 ± 0.96
			46 - 47	0.56	0.05		nd	-177.66 ± 2.60	-191.14 ± 1.60		nd	-21.76 ± 0.77	-18.95 ± 0.52
	47 - 90	Bigc	68 - 69	0.51	0.07		-222.69 ± 5.80	-217.89 ± 2.50	nd		-25.04 ± 0.97	-20.55 ± 0.89	nd
			89 - 90	0.52	0.03		-257.07 ± 4.10	-248.19 ± 2.70	nd		nd	-24.36 ± 0.45	nd
	90 - 115+	Bikgc	100 - 101	0.93	0.05	-283.92 ± 2.60	nd	nd	-126.78 ± 1.60	-21.06 ± 0.27	-24.32 ± 0.5	nd	-20.37 ± 0.65
PL-NP	0 - 10	Ah1				41.01 ± 2.80				-16.32 ± 0.23			
	10 - 23	Ah2											
			22 - 23	1.44	0.11		nd	65.56 ± 0.17	nd		nd	-16.68 ± 0.35	nd
	23 - 29	Bw	23 - 24	1.16	0.18		-41.32 ± 2.60	nd	-44.35 ± 1.60		-18.81 ± 0.60	nd	-23.83 ± 0.5
			28 - 29	1.41	0.11		-0.68 ± 2.20	nd	-250.28 ± 1.70		-17.38 ± 0.48	nd	-21.75 ± 0.44
	29 - 55	Bwi1	42 - 43	0.71	0.05	-69.32 ± 3.10	-95.65 ± 5.20	nd	-215.38 ± 2	-19.13 ± 0.21	-14.60 ± 2.44	nd	-26.83 ± 0.26
			54 - 55	0.70	0.05		-119.58 ± 2.60	-66.29 ± -0.21	-176.72 ± 1.50		-18.05 ± 1.1	-21.4 ± 0.63	-20.01 ± 0.2
	55 - 100	Bwi2	99 - 100	0.52	0.08		-172.34 ± 3.10	nd	-138.80 ± 2.50		-20.67 ± 0.19	nd	-29.8 ± 0.37
	100 - 120	Bwi3	110 - 111	0.51	0.04	-220.29 ± 2.50	-177.66 ± 2.90	nd	nd	-20.4 ± 0.19	-20.15 ± 1.04	nd	nd
PL-NP	0 - 6	Ah	20 - 22	nd	nd		16.77 ± 1.80	66.81 ± 3.80			-20.2 ± 0.4	-26.7 ± 2.5	
(Garden)	6 - 120	Bik	40 - 42	nd	nd		-4.44 ± 1.40	56.47 ± 2.60			-19.1 ± 0.4	-24.6 ± 2	
			60 - 62	nd	nd		nd	-92.10 ± 2			nd	-22.6 ± 1.9	

<sup>24</sup> from different soil types. Hor = horizon, PL = Ploso Lor, JSG = Jasinga, PBW = Perbawati, Rds = Randusongo, Grh = Gerih, Bbl = Bobol. (\*) = samples with grey colour in the profile.



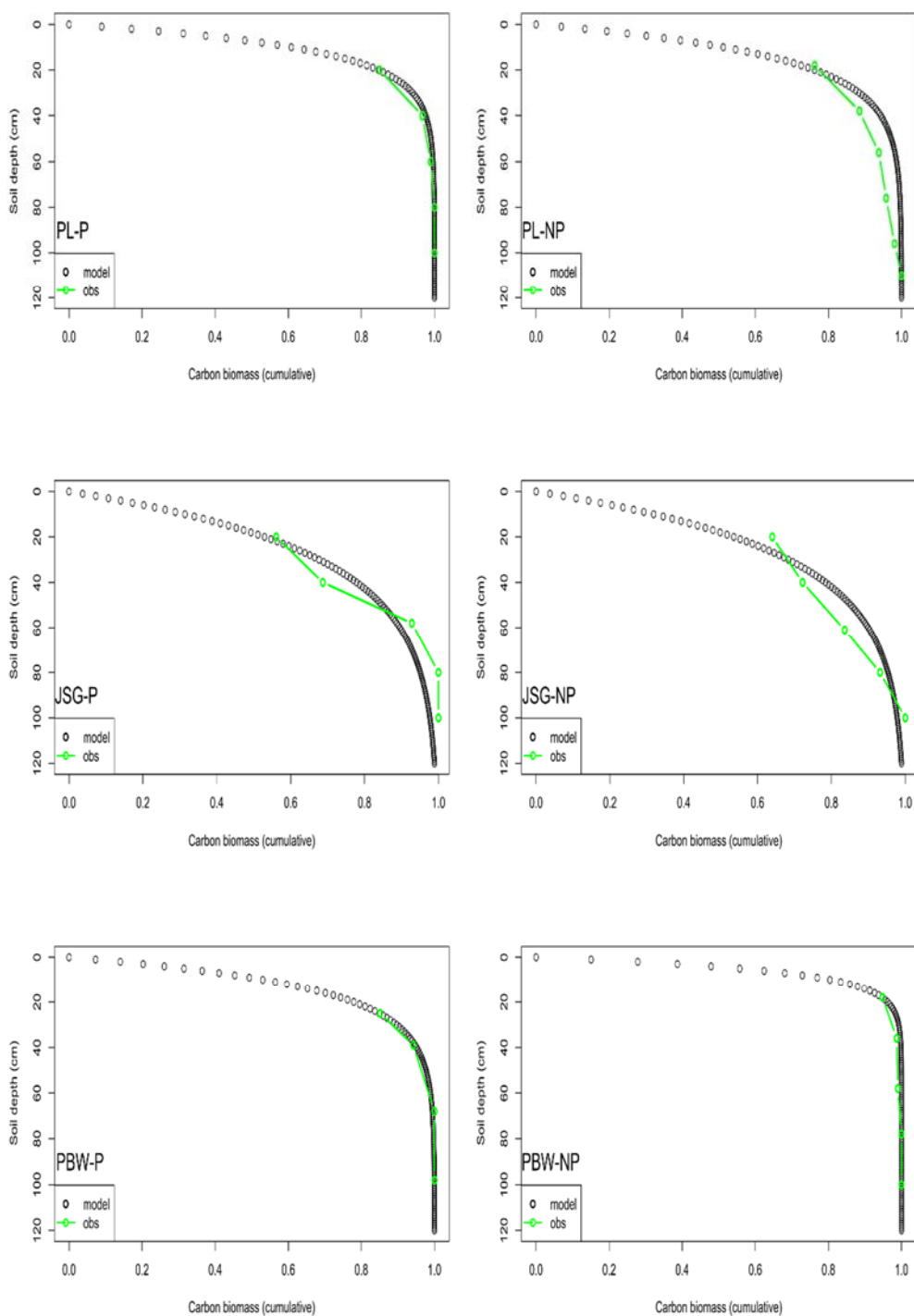
(continued)

Site	Depth	Hor	Sample point	TOC	TN	$\Delta^{14}\text{C}$				$\delta^{13}\text{C}$			
						Bulk	Humic	Humic	HCl	Bulk	Humic	Humic	HCl
	[cm]					[cm]	[%]	[%]	[‰]				[‰]
			61 - 62	0.80	0.12		-166.38 ± 4.0	-279.63 ± 1.70			-25.03 ± 0.37	-28.7 ± 0.30	
	65 - 85	B(t)o3	77 - 78	0.78	0.11		-274.41 ± 9.40	-336.57 ± 1.70			-25.17 ± 1.06	-27.24 ± 0.11	
	85 - 100+	B(t)o4	91 - 92			-408.98 ± 2.60	-280.26 ± 12.60	-352.87 ± 1.90		-21.17 ± 0.23	-14.09 ± 2.32	-28.52 ± 0.36	
			100 - 101				-336.78 ± 9.30	-400.93 ± 1.60			-13.82 ± 2.25	-27.79 ± 0.14	
PBW-P	0 - 10	Alp1				81.23 ± 3.20				-25.15 ± 0.25			
	10 - 22	Alp2	19 - 20	3.69	0.44		107.24 ± 1.40	nd			-25.30 ± 0.33	-25.91 ± 0.23	
	22 - 35	Aldp	23 - 24	3.08	0.45	94.39 ± 2.90	135.45 ± 1.40	63.36 ± 3.30		-24.34 ± 0.25	-24 ± 0.31	-23.98 ± 0.16	
			30 - 31	2.27	0.26		161.78 ± 1.80	111.84 ± 1.80			-24.55 ± 0.42	-24.58 ± 0.22	
			31 - 32	2.20	0.3		107.87 ± 1.30	65.98 ± 1.40			-23.1 ± 0.27	-24.24 ± 0.46	
	35 - 52	Bgc1	39 - 40	1.64	0.27		17.39 ± 1.90	-45.92 ± 1.20			-24.4 ± 0.1	-24.89 ± 0.14	
			42 - 45	0.54	0.09		-89.90 ± 3.10	-269.29 ± 2			-26.62 ± 0.81	-26.62 ± 0.81	
			50 - 51	0.53	0.06		-125.43 ± 3.20	-269.08 ± 1.80			-29.16 ± 0.17	-29.16 ± 0.17	
	52 - 75	Bgc2	60 - 62	0.41	0.09		-251.32 ± 2.30	-419.95 ± 1.10			-28.28 ± 0.52	-28.28 ± 0.52	
	75 - 110+	Bw	80 - 81	0.38	0.06	-312.44 ± 2.70	-294.57 ± 3.40	nd		-23.43 ± 0.22	-26.57 ± 0.97	-26.57 ± 0.97	
			99 - 101	0.33	0.11		-349.74 ± 1.90	nd			-27.74 ± 0.08	-27.58 ± 0.22	
PBW-NP	0 - 7	Ah1				-11.13 ± 2.90				-21.93 ± 0.33			
	7 - 16	Ah2	9 - 10	3.12	0.33		88.54 ± 2.30	-121.87 ± 1.30			-20.35 ± 0.39	-23.53 ± 0.25	
	16 - 28	BwAh	20 - 23	3.01	0.36		65.35 ± 2.20	nd			-15.22 ± 1.08	nd	
			23 - 24	0.69	0.07		-70.89 ± 2.90	nd			-27.97 ± 2.02	nd	
	28 - 56	Bw1	36 - 38	1.08	0.16	-481.48 ± 2.10	nd	nd		-22.23 ± 0.21	nd	nd	
			49 - 50	0.79	0.10		-256.65 ± 2	-521.91 ± 1.90			-24.63 ± 0.72	-26.02 ± 0.11	
			50 - 52	0.99	0.15		-330.83 ± 2.90	-495.06 ± 3.20			-26.89 ± 0.16	-26.18 ± 0.41	
	56 - 78	Bw2	65 - 66	0.93	0.13		-394.87 ± 2.20	-555.97 ± 1.10			-23.02 ± 0.09	-24.52 ± 0.44	
	78 - 100	Bw3	78 - 79	0.81	0.16	-495.48 ± 2.90	-311.08 ± 3.20	-524.11 ± 3.40		-23.66 ± 0.11	-23.61 ± 0.52	-69.22 ± 0.71	
			79 - 80	0.75	0.19		-296.98 ± 3.70	-469.05 ± 2.10			-25.14 ± 0.35	-23.62 ± 0.94	
			86 - 87	0.59	0.07		-392.36 ± 3.40	-480.44 ± 1.60			-27.58 ± 0.16	-49.79 ± 1.76	





Appendix 5.1. Model litter distribution in the soil columns.



## Appendix 5.2. Temperature sensitivity coefficient.

Site	Type	Fraction	Q10	Tm	Tref	f(ts)
			[1]	[2]	[3]	$[1]^{\frac{[2]-[3]}{10}}$
PL	P	Active	2.1	26.6	20	1.63
		Passive	2.95	26.6	20	2.04
		Slow	3.8	26.6	20	2.41
		Bulk	2	26.6	20	1.58
	NP	Active	2.1	26.6	20	1.63
		Passive	2.95	26.6	20	2.04
		Slow	3.8	26.6	20	2.41
		Bulk	2	26.6	20	1.58
JSG	P	Active	2.1	25.5	20	1.50
		Passive	2.95	25.5	20	1.81
		Slow	3.8	25.5	20	2.08
		Bulk	2	25.5	20	1.46
	NP	Active	2.1	25.5	20	1.50
		Passive	2.95	25.5	20	1.81
		Slow	3.8	25.5	20	2.08
		Bulk	2	25.5	20	1.46
PBW	P	Active	2.1	20.4	20	1.03
		Passive	2.95	20.4	20	1.04
		Slow	3.8	20.4	20	1.05
		Bulk	2	20.4	20	1.03
	NP	Active	2.1	20.4	20	1.03
		Passive	2.95	20.4	20	1.04
		Slow	3.8	20.4	20	1.05
		Bulk	2	20.4	20	1.03

## Appendix 5.3. Soil moisture sensitivity coefficient.

Sites	Type	Depth (cm)	Sand	Clay	OM	BD	Ws	Wfc	Wpw	f(m <sub>s</sub> )
			(%)	(%)	(%)	(g cm <sup>-3</sup> )	(-)	(-)	(-)	(-)
PL	P	0-20	14.84	64.68	1.85	1.04	0.61	0.52	0.38	0.09
	P	20-115+	10.46	73.39	0.74	0.96	0.64	0.52	0.40	0.12
	NP	0-23	21.85	62.83	2.18	1.03	0.61	0.51	0.37	0.13
	NP	23-120+	14.35	71.42	0.92	0.96	0.64	0.51	0.40	0.12
JSG	P	0-25	8.27	40.34	2.62	1.01	0.62	0.46	0.27	0.20
	P	25-95+	4.89	60.54	1.30	0.92	0.65	0.50	0.35	0.15
	NP	0-14	14.75	40.55	3.07	1.03	0.61	0.47	0.28	0.19
	NP	14-100+	1.73	10.9	0.28	0.23	0.91	0.30	0.08	0.22
PBW	P	0-22	nd	nd	4.51	1.26	0.52	0.31	0.21	0.21
	P	22-110+	nd	nd	1.12	1.29	0.51	0.31	0.21	0.20
	NP	0-16	nd	nd	4.66	1.10	0.58	0.31	0.21	0.27
	NP	16-100+	nd	nd	1.43	0.84	0.68	0.31	0.21	0.37

## Appendix 5.4. Soil oxygen coefficient.

Sites	Type	Depth	Status	[O <sub>2</sub> ]	k <sub>o</sub>	O <sub>c</sub>
		(cm)		(mg/L)	(mg/L)	(-)
PL	P	0-20	anoxic	0.12	0.50	0.1935
	P	20-115+	oxic	240.00	0.50	0.9979
	NP	0-23	oxic	240.00	0.50	0.9979
	NP	23-120+	oxic	240.00	0.50	0.9979
JSG	P	0-25	anoxic	0.12	0.50	0.1935
	P	25-95+	oxic	240.00	0.50	0.9979
	NP	0-14	oxic	240.00	0.50	0.9979
	NP	14-100+	oxic	240.00	0.50	0.9979
PBW	P	0-22	anoxic	0.12	0.50	0.1935
	P	22-110+	oxic	240.00	0.50	0.9979
	NP	0-16	oxic	240.00	0.50	0.9979
	NP	16-100+	oxic	240.00	0.50	0.9979

## Appendix 5.5. Soil carbon storage coefficient.

Sites	Type	Depth	%Clay	R	C storage (h)
		(cm)	(1)	$1 - ((1)/100)$	$1/(R+1)$
PL	P	0-25	67.36	0.326	0.754
	P	25-105+	72.63	0.274	0.785
	NP	0-21	40.27	0.597	0.626
	NP	21-113+	60.79	0.392	0.718
JSG	P	0-22	63.29	0.367	0.731
	P	22-95+	71.27	0.287	0.777
	NP	0-18	40.50	0.595	0.627
	NP	18-101+	64.95	0.351	0.740
PBW	P	0-22	90.00	0.100	0.909
	P	22-107+	90.00	0.100	0.909
	NP	0-22	90.00	0.100	0.909
	NP	22-103+	90.00	0.100	0.909

## Appendix 5.6. Soil carbon transformation-PL.

Type	Top soil C load (mg C cm <sup>-2</sup> d <sup>-1</sup> )	Sub soil C load (mg C cm <sup>-2</sup> d <sup>-1</sup> )	Carbon storage (h) topsoil	Carbon storage (h) subsoil	Fraction fi	hfiC <sub>0i</sub>			q10	Tm	Tref	f(ts)	ws		wfc		wpwp		f(ms)		O <sub>i</sub>		k <sub>o</sub>	f(O <sub>c</sub> )		k <sub>i</sub>	β			C <sub>o</sub>	C <sub>1</sub>		
						(top)	(sub)	(total)					(top)	(sub)	(top)	(sub)	(top)	(sub)	(top)	(sub)	(top)	(sub)		(top)	(sub)		(top)	(sub)	(total)				
<i>Carbon model</i>																																	
P	0.7	0.5929	0.754	0.626	Active	0.32068	0.1693	0.1190	0.2883	2.1	26.6	20	1.63	0.61	0.64	0.52	0.52	0.38	0.40	0.09	0.12	0.12	240	0.5	0.1935	0.9979	0.2	0.0057	0.0391	0.0448	0.7	0.12	
					Passive	0.1049	0.0554	0.0389	0.0943	2.95	26.6	20	2.04														0.051	0.0018	0.0125	0.0143			
					Slow	0.57472	0.3033	0.2133	0.5166	3.8	26.6	20	2.41														0.003	0.0001	0.0009	0.0010			
					Bulk	1	0.5278	0.3712	0.8990	2	26.6	20	1.58														0.084667	0.0023	0.0160	0.0184			
NP	1.14	0.86868	0.785	0.718	Active	0.34876	0.3121	0.2175	0.5296	2.1	26.6	20	1.63	0.61	0.64	0.51	0.51	0.37	0.40	0.14	0.11	240	240	0.5	0.9979	0.9979	0.2	0.0456	0.0358	0.0814			
					Passive	0.1205	0.1078	0.0752	0.1830	2.95	26.6	20	2.04															0.051	0.0146	0.0114	0.0260	1.14	0.136
					Slow	0.53044	0.4747	0.3308	0.8055	3.8	26.6	20	2.41															0.003	0.0010	0.0008	0.0018		
					Bulk	1	0.8949	0.6237	1.5186	2	26.6	20	1.58															0.084667	0.0187	0.0147	0.0334		
<i>Radiocarbon model</i>																																	
P	0.0002	0.0001	0.754	0.626	Active	0.32068	0.0000	0.0000	0.0001	2.1	26.6	20	1.63	0.61	0.64	0.52	0.52	0.38	0.40	0.09	0.12	0.12	240	0.5	0.1935	0.9979	0.2	0.0057	0.0391	0.0448	0.0002	0.231	
					Passive	0.1049	0.0000	0.0000	0.0000	2.95	26.6	20	2.04															0.051	0.0018	0.0125	0.0143		
					Slow	0.57472	0.0001	0.0000	0.0001	3.8	26.6	20	2.41															0.003	0.0001	0.0009	0.0010		
					Bulk	1	0.0001	0.0001	0.0002	2	26.6	20	1.58															0.084667	0.0023	0.0160	0.0184		
NP	0.0002633	0.0002	0.785	0.718	Active	0.34876	0.0001	0.0001	0.0001	2.1	26.6	20	1.63	0.61	0.64	0.51	0.51	0.37	0.40	0.14	0.11	240	240	0.5	0.9979	0.9979	0.2	0.0456	0.0358	0.0814			
					Passive	0.1205	0.0000	0.0000	0.0000	2.95	26.6	20	2.04															0.051	0.0146	0.0114	0.0260	0.000263	0.231
					Slow	0.53044	0.0001	0.0000	0.0002	3.8	26.6	20	2.41															0.003	0.0010	0.0008	0.0018		
					Bulk	1	0.0002	0.0001	0.0003	2	26.6	20	1.58															0.084667	0.0187	0.0147	0.0334		

## Appendix 5.7. Soil carbon transformation-PBW.

Type	Top soil C load (mg C cm <sup>-2</sup> d <sup>-1</sup> )	Sub soil C load (mg C cm <sup>-2</sup> d <sup>-1</sup> )	Carbon storage (h) topsoil	Carbon storage (h) subsoil	Fraction	fi	hfC <sub>0</sub>			q10	Tm	Tref	f(ts)	ws		wfc		wpwp		f(ms)		O <sub>i</sub>		k <sub>o</sub>	f(Oc)		k <sub>i</sub>	β			C <sub>o</sub>	C <sub>1</sub>	
							(top)	(sub)	(total)					(top)	(sub)	(top)	(sub)	(top)	(sub)	(top)	(sub)	(top)	(sub)		(top)	(sub)		(top)	(sub)	(total)			
<i>Carbon model</i>																																	
P	0.922	0.7182	0.91	0.91	Active	0.3703	0.3103	0.2418	0.5521	2.1	20.4	20	1.03	0.52	0.51	0.31	0.31	0.21	0.21	0.21	0.10	0.12	240	0.5	0.1935	0.9979	0.2	0.0084	0.0206	0.0289	0.922	0.265	
					Passive	0.2336	0.1958	0.1525	0.3483	2.95	20.4	20	1.04													0.051	0.0022	0.0053	0.0075				
					Slow	0.396	0.3319	0.2585	0.5904	3.8	20.4	20	1.05													0.003	0.0001	0.0003	0.0004				
					Bulk	1	0.8381	0.6529	1.4910	2	20.4	20	1.03													0.084667	0.0035	0.0087	0.0122				
NP	0.425	0.4089	0.91	0.91	Active	0.37954	0.1466	0.1411	0.2877	2.1	20.4	20	1.03	0.58	0.68	0.31	0.31	0.21	0.21	0.10	0.10	240	240	0.5	0.9979	0.9979	0.2	0.0206	0.0206	0.0411			
					Passive	0.2639	0.1020	0.0981	0.2000	2.95	20.4	20	1.04														0.051	0.0053	0.0053	0.0106	0.425	0.153	
					Slow	0.35796	0.1383	0.1330	0.2713	3.8	20.4	20	1.05														0.003	0.0003	0.0003	0.0006			
					Bulk	1	0.3863	0.3716	0.7580	2	20.4	20	1.03														0.084667	0.0087	0.0087	0.0174			
<i>Radiocarbon model</i>																																	
P	0.0002	0.0002	0.91	0.91	Active	0.3703	0.0001	0.0001	0.0001	2.1	20.4	20	1.03	0.52	0.51	0.31	0.31	0.21	0.21	0.21	0.10	0.12	240	0.5	0.1935	0.9979	0.2	0.0084	0.0206	0.0289	0.0002	0.231	
					Passive	0.2336	0.0000	0.0000	0.0001	2.95	20.4	20	1.04														0.051	0.0022	0.0053	0.0075			
					Slow	0.396	0.0001	0.0001	0.0001	3.8	20.4	20	1.05														0.003	0.0001	0.0003	0.0004			
					Bulk	1	0.0002	0.0002	0.0003	2	20.4	20	1.03														0.084667	0.0035	0.0087	0.0122			
NP	0.000098175	0.0001	0.91	0.91	Active	0.37954	0.0000	0.0000	0.0001	2.1	20.4	20	1.03	0.58	0.68	0.31	0.31	0.21	0.21	0.10	0.10	240	240	0.5	0.9979	0.9979	0.2	0.0206	0.0206	0.0411			
					Passive	0.2639	0.0000	0.0000	0.0001	2.95	20.4	20	1.04															0.051	0.0053	0.0053	0.0106	0.0001	0.231
					Slow	0.35796	0.0000	0.0001	0.0001	3.8	20.4	20	1.05															0.003	0.0003	0.0003	0.0006		
					Bulk	1	0.0001	0.0002	0.0002	2	20.4	20	1.03															0.084667	0.0087	0.0087	0.0174		

Appendix 5.8. Soil carbon transformation-JSG.

Type	Top soil C load (mg C cm <sup>-2</sup> d <sup>-1</sup> )	Sub soil C load (mg C cm <sup>-2</sup> d <sup>-1</sup> )	Carbon storage (h) topsoil	Carbon storage (h) subsoil	Fraction	fi	hf(C <sub>t</sub> )			q10	Tm	Tref	f(ts)	ws		wfc		wpwp		f(ms)		Oi		ko	f(Oc)		ki	β			Co	C1	
							(top)	(sub)	(total)					(top)	(sub)		(top)	(sub)		(top)	(sub)	(total)											
<b>Carbon model</b>																																	
P	0.911	0.4819	0.73	0.63	Active	0.38079	0.2536	0.1151	0.3686	2.1	25.5	20	1.50	0.62	0.65	0.46	0.50	0.27	0.35	0.16	0.15	0.12	240	0.5	0.1935	0.9979	0.2	0.0093	0.0450	0.0543	0.911	0.118	
					Passive	0.2143	0.1427	0.0648	0.2075	2.95	25.5	20	1.81													0.051	0.0029	0.0138	0.0167				
					Slow	0.40521	0.2698	0.1224	0.3923	3.8	25.5	20	2.08													0.003	0.0002	0.0009	0.0011				
					Bulk	1	0.6659	0.3022	0.9681	2	25.5	20	1.46													0.084667	0.0038	0.0186	0.0224				
NP	0.106	0.0568	0.777	0.74	Active	0.4325	0.0356	0.0182	0.0538	2.1	25.5	20	1.50	0.61	0.91	0.47	0.30	0.28	0.08	0.19	0.22	240	240	0.5	0.9979	0.9979	0.2	0.0570	0.0660	0.1231			
					Passive	0.2716	0.0224	0.0114	0.0338	2.95	25.5	20	1.81														0.051	0.0175	0.0203	0.0378	0.106	0.103	
					Slow	0.2967	0.0244	0.0125	0.0369	3.8	25.5	20	2.08														0.003	0.0012	0.0014	0.0026			
					Bulk	1	0.0824	0.0420	0.1244	2	25.5	20	1.46														0.084667	0.0235	0.0272	0.0507			
<b>Radiocarbon model</b>																																	
P	0.0002	0.0001	0.73	0.63	Active	0.38079	0.0001	0.0000	0.0001	2.1	25.5	20	1.50	0.62	0.65	0.46	0.50	0.27	0.35	0.16	0.15	0.12	240	0.5	0.1935	0.9979	0.2	0.0093	0.0450	0.0543	0.0002	0.231	
					Passive	0.2143	0.0000	0.0000	0.0000	2.95	25.5	20	1.81														0.051	0.0029	0.0138	0.0167			
					Slow	0.40521	0.0001	0.0000	0.0001	3.8	25.5	20	2.08														0.003	0.0002	0.0009	0.0011			
					Bulk	1	0.0002	0.0001	0.0002	2	25.5	20	1.46														0.084667	0.0038	0.0186	0.0224			
NP	0.00024486	0.0000	0.777	0.74	Active	0.4325	0.0000	0.0000	0.0000	2.1	25.5	20	1.50	0.61	0.91	0.47	0.30	0.28	0.08	0.19	0.22	240	240	0.5	0.9979	0.9979	0.2	0.0570	0.0660	0.1231			
					Passive	0.2716	0.0000	0.0000	0.0000	2.95	25.5	20	1.81															0.051	0.0175	0.0203	0.0378	2.45E-05	0.231
					Slow	0.2967	0.0000	0.0000	0.0000	3.8	25.5	20	2.08														0.003	0.0012	0.0014	0.0026			
					Bulk	1	0.0000	0.0001	0.0001	2	25.5	20	1.46														0.084667	0.0235	0.0272	0.0507			

Appendix 5.9. FEM modelling MATLAB script.

```
function [kk,ff]=feaplyc2(kk,ff,bcdof,bcval)

%-----
% Purpose:
%   Apply constraints to matrix equation [kk]{x}={ff}
%
% Synopsis:
%   [kk,ff]=feaplybc(kk,ff,bcdof,bcval)
%
% Variable Description:
%   kk - system matrix before applying constraints
%   ff - system vector before applying constraints
%   bcdof - a vector containing constrained d.o.f
%   bcval - a vector containing contained value
%
%-----

n=length(bcdof);
sdof=size(kk);

for i=1:n
    c=bcdof(i);
    for j=1:sdof
        kk(c,j)=0;
    end

    kk(c,c)=1;
    ff(c)=bcval(i);
end

function [kk,ff]=feasmb12(kk,ff,k,f,index)

%-----
% Purpose:
%   Assembly of element matrices into the system matrix &
%   Assembly of element vectors into the system vector
%
% Synopsis:
%   [kk,ff]=feasmb12(kk,ff,k,f,index)
%
% Variable Description:
%   kk - system matrix
%   ff - system vector
%   k - element matrix
%   f - element vector
%   index - d.o.f. vector associated with an element
%-----

edof = length(index);
for i=1:edof
    ii=index(i);
    ff(ii)=ff(ii)+f(i);
    for j=1:edof
```

```

    jj=index(j);
    kk(ii,jj)=kk(ii,jj)+k(i,j);
end
end

```

```
function [index]=feeldof1(iel,nnel,ndof)
```

```

%-----
% Purpose:
%   Compute system dofs associated with each element in one-
%   dimensional problem
%
% Synopsis:
%   [index]=feeldof1(iel,nnel,ndof)
%
% Variable Description:
%   index - system dof vector associated with element "iel"
%   iel - element number whose system dofs are to be determined
%   nnel - number of nodes per element
%   ndof - number of dofs per node

```

```
%-----
```

```

edof = nnel*ndof;
start = (iel-1)*(nnel-1)*ndof;

```

```

for i=1:edof
    index(i)=start+i;
end

```

```
function [f]=fef1l(xl,xr,lc,bcoef,flux)
```

```

%-----
% Purpose:
%   element vector for  $f(x)=1$ 
%   using linear element
%
% Synopsis:
%   [f]=fef1l(xl,xr)
%
% Variable Description:
%   f - element vector (size of 2x1)
%   xl - coordinate value of the left node
%   xr - coordinate value of the right node
%-----

```

```

% element vector
eleng=xr-xl;          % element length
f=[ -(eleng/2)*lc+bcoef*flux; -(eleng/2)*lc];
function [k]=feode2l(acoef,bcoef,ccoef,eleng)

```

```

%-----
% Purpose:
%   element matrix for  $(a u'' + b u' + c u)$ 
%   using linear element
%
% Synopsis:

```

```

% [k]=feode2l(acoef,bcoef,ccoef,eleng)
%
% Variable Description:
% k - element matrix (size of 2x2)
% acoef - coefficient of the second order derivative term
% bcoef - coefficient of the first order derivative term
% ccoef - coefficient of the zero-th order derivative term
% eleng - element length
%-----

% element matrix

a1=-(acoef/eleng); a2=-(bcoef/2); a3=-(ccoef*eleng/6);
k=[ a1-a2+2*a3+bcoef  -a1+a2+a3;...
   -a1-a2+a3  a1+a2+2*a3];

%-----

% to solve the ordinary differential equation given as
% a u'' - b u' - c u = -g(x) - Q0
%
% using 100 linear elements
%
% Variable descriptions
% k = element matrix
% f = element vector
% kk = system matrix
% ff = system vector
% index = a vector containing system dofs associated with each element
% bcdof = a vector containing dofs associated with boundary conditions
% bcval = a vector containing boundary condition values associated with
%         the dofs in 'bcdof'
%-----

%-----
% input data for control parameters
%-----

clear
nel=100;          % number of elements
nnel=2;          % number of nodes per element
ndof=1;          % number of dofs per node
nnode=101;       % total number of nodes in system
sdof=nnode*ndof; % total system dofs

%-----

% input data for nodal coordinate values
%-----

gcoord(1) = 0.0; gcoord(2) = 0.01; gcoord(3) = 0.02; gcoord(4) = 0.03; gcoord(5) = 0.04;
gcoord(6) = 0.05; gcoord(7) = 0.06; gcoord(8) = 0.07; gcoord(9) = 0.08; gcoord(10) = 0.09;
gcoord(11) = 0.1; gcoord(12) = 0.11; gcoord(13) = 0.12; gcoord(14) = 0.13; gcoord(15) = 0.14;
gcoord(16) = 0.15; gcoord(17) = 0.16; gcoord(18) = 0.17; gcoord(19) = 0.18; gcoord(20) = 0.19;
gcoord(21) = 0.2; gcoord(22) = 0.21; gcoord(23) = 0.22; gcoord(24) = 0.23; gcoord(25) = 0.24;
gcoord(26) = 0.25; gcoord(27) = 0.26; gcoord(28) = 0.27; gcoord(29) = 0.28; gcoord(30) = 0.29;
gcoord(31) = 0.30; gcoord(32) = 0.31; gcoord(33) = 0.32; gcoord(34) = 0.33; gcoord(35) = 0.34;
gcoord(36) = 0.35; gcoord(37) = 0.36; gcoord(38) = 0.37; gcoord(39) = 0.38; gcoord(40) = 0.39;
gcoord(41) = 0.4; gcoord(42) = 0.41; gcoord(43) = 0.42; gcoord(44) = 0.43; gcoord(45) = 0.44;

```

```

gcoord(46) = 0.45; gcoord(47) = 0.46; gcoord(48) = 0.47; gcoord(49) = 0.48; gcoord(50) = 0.49;
gcoord(51) = 0.50; gcoord(52) = 0.51; gcoord(53) = 0.52; gcoord(54) = 0.53; gcoord(55) = 0.54;
gcoord(56) = 0.55; gcoord(57) = 0.56; gcoord(58) = 0.57; gcoord(59) = 0.58; gcoord(60) = 0.59;
gcoord(61) = 0.60; gcoord(62) = 0.61; gcoord(63) = 0.62; gcoord(64) = 0.63; gcoord(65) = 0.64;
gcoord(66) = 0.65; gcoord(67) = 0.66; gcoord(68) = 0.67; gcoord(69) = 0.68; gcoord(70) = 0.69;
gcoord(71) = 0.70; gcoord(72) = 0.71; gcoord(73) = 0.72; gcoord(74) = 0.73; gcoord(75) = 0.74;
gcoord(76) = 0.75; gcoord(77) = 0.76; gcoord(78) = 0.77; gcoord(79) = 0.78; gcoord(80) = 0.79;
gcoord(81) = 0.80; gcoord(82) = 0.81; gcoord(83) = 0.82; gcoord(84) = 0.83; gcoord(85) = 0.84;
gcoord(86) = 0.85; gcoord(87) = 0.86; gcoord(88) = 0.87; gcoord(89) = 0.88; gcoord(90) = 0.89;
gcoord(91) = 0.90; gcoord(92) = 0.91; gcoord(93) = 0.92; gcoord(94) = 0.93; gcoord(95) = 0.94;
gcoord(96) = 0.95; gcoord(97) = 0.96; gcoord(98) = 0.97; gcoord(99) = 0.98; gcoord(100) = 0.99;
gcoord(101) = 1;

```

```

%-----
% input data for nodal connectivity for each element
%-----

```

```

nodes(1,1) = 1; nodes(1,2) = 2; nodes(2,1) = 2; nodes(2,2) = 3; nodes(3,1) = 3; nodes(3,2) = 4;
nodes(4,1) = 4; nodes(4,2) = 5; nodes(5,1) = 5; nodes(5,2) = 6; nodes(6,1) = 6; nodes(6,2) = 7;
nodes(7,1) = 7; nodes(7,2) = 8; nodes(8,1) = 8; nodes(8,2) = 9; nodes(9,1) = 9; nodes(9,2) = 10;
nodes(10,1) = 10; nodes(10,2) = 11; nodes(11,1) = 11; nodes(11,2) = 12; nodes(12,1) = 12;
nodes(12,2) = 13;
nodes(13,1) = 13; nodes(13,2) = 14; nodes(14,1) = 14; nodes(14,2) = 15; nodes(15,1) = 15;
nodes(15,2) = 16;
nodes(16,1) = 16; nodes(16,2) = 17; nodes(17,1) = 17; nodes(17,2) = 18; nodes(18,1) = 18;
nodes(18,2) = 19;
nodes(19,1) = 19; nodes(19,2) = 20; nodes(20,1) = 20; nodes(20,2) = 21; nodes(21,1) = 21;
nodes(21,2) = 22;
nodes(22,1) = 22; nodes(22,2) = 23; nodes(23,1) = 23; nodes(23,2) = 24; nodes(24,1) = 24;
nodes(24,2) = 25;
nodes(25,1) = 25; nodes(25,2) = 26; nodes(26,1) = 26; nodes(26,2) = 27; nodes(27,1) = 27;
nodes(27,2) = 28;
nodes(28,1) = 28; nodes(28,2) = 29; nodes(29,1) = 29; nodes(29,2) = 30; nodes(30,1) = 30;
nodes(30,2) = 31;
nodes(31,1) = 31; nodes(31,2) = 32; nodes(32,1) = 32; nodes(32,2) = 33; nodes(33,1) = 33;
nodes(33,2) = 34;
nodes(34,1) = 34; nodes(34,2) = 35; nodes(35,1) = 35; nodes(35,2) = 36; nodes(36,1) = 36;
nodes(36,2) = 37;
nodes(37,1) = 37; nodes(37,2) = 38; nodes(38,1) = 38; nodes(38,2) = 39; nodes(39,1) = 39;
nodes(39,2) = 40;
nodes(40,1) = 40; nodes(40,2) = 41; nodes(41,1) = 41; nodes(41,2) = 42; nodes(42,1) = 42;
nodes(42,2) = 43;
nodes(43,1) = 43; nodes(43,2) = 44; nodes(44,1) = 44; nodes(44,2) = 45; nodes(45,1) = 45;
nodes(45,2) = 46;
nodes(46,1) = 46; nodes(46,2) = 47; nodes(47,1) = 47; nodes(47,2) = 48; nodes(48,1) = 48;
nodes(48,2) = 49;
nodes(49,1) = 49; nodes(49,2) = 50; nodes(50,1) = 50; nodes(50,2) = 51; nodes(51,1) = 51;
nodes(51,2) = 52;
nodes(52,1) = 52; nodes(52,2) = 53; nodes(53,1) = 53; nodes(53,2) = 54; nodes(54,1) = 54;
nodes(54,2) = 55;
nodes(55,1) = 55; nodes(55,2) = 56; nodes(56,1) = 56; nodes(56,2) = 57; nodes(57,1) = 57;
nodes(57,2) = 58;
nodes(58,1) = 58; nodes(58,2) = 59; nodes(59,1) = 59; nodes(59,2) = 60; nodes(60,1) = 60;
nodes(60,2) = 61;
nodes(61,1) = 61; nodes(61,2) = 62; nodes(62,1) = 62; nodes(62,2) = 63; nodes(63,1) = 63;
nodes(63,2) = 64;

```

```

nodes(64,1) = 64; nodes(64,2) = 65; nodes(65,1) = 65; nodes(65,2) = 66; nodes(66,1) = 66;
nodes(66,2) = 67;
nodes(67,1) = 67; nodes(67,2) = 68; nodes(68,1) = 68; nodes(68,2) = 69; nodes(69,1) = 69;
nodes(69,2) = 70;
nodes(70,1) = 70; nodes(70,2) = 71; nodes(71,1) = 71; nodes(71,2) = 72; nodes(72,1) = 72;
nodes(72,2) = 73;
nodes(73,1) = 73; nodes(73,2) = 74; nodes(74,1) = 74; nodes(74,2) = 75; nodes(75,1) = 75;
nodes(75,2) = 76;
nodes(76,1) = 76; nodes(76,2) = 77; nodes(77,1) = 77; nodes(77,2) = 78; nodes(78,1) = 78;
nodes(78,2) = 79;
nodes(79,1) = 79; nodes(79,2) = 80; nodes(80,1) = 80; nodes(80,2) = 81; nodes(81,1) = 81;
nodes(81,2) = 82;
nodes(82,1) = 82; nodes(82,2) = 83; nodes(83,1) = 83; nodes(83,2) = 84; nodes(84,1) = 84;
nodes(84,2) = 85;
nodes(85,1) = 85; nodes(85,2) = 86; nodes(86,1) = 86; nodes(86,2) = 87; nodes(87,1) = 87;
nodes(87,2) = 88;
nodes(88,1) = 88; nodes(88,2) = 89; nodes(89,1) = 89; nodes(89,2) = 90; nodes(90,1) = 90;
nodes(90,2) = 91;
nodes(91,1) = 91; nodes(91,2) = 92; nodes(92,1) = 92; nodes(92,2) = 93; nodes(93,1) = 93;
nodes(93,2) = 94;
nodes(94,1) = 94; nodes(94,2) = 95; nodes(95,1) = 95; nodes(95,2) = 96; nodes(96,1) = 96;
nodes(96,2) = 97;
nodes(97,1) = 97; nodes(97,2) = 98; nodes(98,1) = 98; nodes(98,2) = 99; nodes(99,1) = 99;
nodes(99,2) = 100;
nodes(100,1) = 100; nodes(100,2) = 101;

```

```

%-----
% input data for coefficients of the ODE
%-----

```

```

acoef= 0.02;          % D
bcoef= -0.004;       % v
ccoef= 0.0184;      % β, from calculation table
Ic = 0.899; % total carbon load (mg C/cm2/d) - hfiC(t)
flux= 0.7; % topsoil C load (mg C cm-2 d-1) - litter

```

```

%-----
% input data for boundary conditions
%-----

```

```

bcdof(1) = 1;          % first node is constrained
bcval(1) = 5.83;      % carbon at z=0

```

```

%-----
% initialization of matrices and vectors
%-----

```

```

ff=zeros(s dof,1);    % initialization of system force vector
kk=zeros(s dof,s dof); % initialization of system matrix
index=zeros(nnel*ndof,1); % initialization of index vector

```

```

%-----
% computation of element matrices and vectors and their assembly
%-----

```

```

for iel=1:nel          % loop for the total number of elements

```

```

    nl=nodes(iel,1); nr=nodes(iel,2); % extract nodes for (iel)-th element

```

```

xl=gcoord(nl); xr=gcoord(nr);% extract nodal coord values for the element
eleng=xr-xl;          % element length
index=feeldof1(iel,nnel,ndof);% extract system dofs associated with element

k=feode2l(acoef,bcoef,ccoef,eleng); % compute element matrix
f=fef1l(xl,xr,lc, bcoef, flux);      % compute element vector
[kk,ff]=feasmb12(kk,ff,k,f,index); % assemble element matrices and vectors

end

%-----
%  apply boundary condition at the last node
%-----

ff(nnode)=ff(nnode)-0;

%-----
%  apply boundary conditions
%-----
[kk,ff]=feaplyc2(kk,ff,bcdof,bcval);

%-----
%  solve the matrix equation
%-----

fsol=kk\ff;

%-----
%  print fem solutions (example for PL-P)
%-----

length=0:2:200;

Cstock = [6.2, 5.2, 4.8, 3.9, 3.9, 3.6, 3.4, 3.1, 2.5]; %mg cm-2
depth=[19, 20, 26, 27, 37, 46, 68, 89, 100];

plot(Cstock, -depth, 'o');

hold on
plot(fsol, -length, 'green')
hold off

xlabel ('TOC [mg.cm^{-2}]')
ylabel ('Soil depth [cm]')
legend (' Obs ', ' FEM ', 'location', 'northeast')
xlim([0 8])
ylim([-120 0])
%-----

```



## List of Publications

### Scientific paper

1. Prastowo, E., P. Grootes., M.-J. Nadeau, Utami, S. R. 2017. Subsoil  $^{14}\text{C}$  dynamics in different types of tropical and subtropical soils under different crop management. *Radiocarbon*. 59 (3), 1021-1034.

### Poster presentation

1. Prastowo, E., P. Grootes., M.-J. Nadeau, Utami, S. R, Unkel, I. Transport of C and  $^{14}\text{C}$ , and elemental composition and distribution of Fe-Mn concretions in a Vertisol profile on Jawa, Indonesia. International workshop on "Biogeochemistry of submerged agroecosystem: properties, processes, cycles and functions", München, 21-25 September, 2014.
2. Prastowo, E., P. Grootes., M.-J. Nadeau, Utami, S. R, Unkel, I. Subsoil C dynamics in a vertisol profile under different crop management on Jawa, Indonesia – Accelerator Mass Spectrometry (AMS)  $^{14}\text{C}$  study. 5<sup>th</sup> International symposium on Soil Organic Matter, 20-24.09.2015, Göttingen, Germany.
3. Prastowo, E., P. Grootes., M.-J. Nadeau. Carbon and  $^{14}\text{C}$  distribution in tropical and subtropical agricultural soils. International Conference, European Geoscience Union General Assembly, 17-22 April 2016, Vienna, Austria.
4. Prastowo, E., P. Grootes., M.-J. Nadeau. Subsoil C dynamics in tropical soils under different crop management on Jawa, Indonesia. International Conference, European Geoscience Union General Assembly, 17-22 April 2016, Vienna, Austria.
5. Prastowo, E., P. Grootes., M.-J. Nadeau. Field variability controls soil depth-distribution of radiocarbon in a tropical environment. 23<sup>rd</sup> International Radiocarbon Conference, 17-22 June 2018, Trondheim, Norway.

## Erklärung

Hiermit erkläre ich, dass ich die vorliegende Dissertation nach den Regeln guter wissenschaftlicher Praxis der Deutschen Forschungsgemeinschaft selbst verfasst habe. Dabei habe ich keine Hilfe, außer der wissenschaftlichen Beratung durch meine Betreuer in Anspruch genommen. Es wurden keine weiteren als die angegebenen Hilfsmittel und Quellen verwendet. Des Weiteren erkläre ich, dass diese Arbeit weder ganz noch zum Teil einer anderen Stelle im Rahmen eines Prüfungsverfahrens vorgelegt wurde. Ich habe bisher keinen anderen Promotionversuch unternommen.

Teile dieser Arbeit wurden bereits veröffentlicht oder zur Publikation vorbereitet.

Kiel, den 12. 09. 2018

Erwin Prastowo